Significance of Methylthioadenosine Metabolism to Plant Growth and Development

by

Chammika Ishari Waduwara-Jayabahu

A thesis
presented to the University of Waterloo
in fulfillment of the
thesis requirement for the degree of
Doctor of Philosophy
in
Biology

Waterloo, Ontario, Canada, 2011

Author's Declaration

I hereby declare that I am the sole author of this thesis. This is a true copy of the thesis, including any required final revisions, as accepted by my examiners.

I understand that my thesis may be made electronically available to the public.

Abstract

Arabidopsis thaliana contains two genes annotated as methylthioadenosine nucleosidases (*MTN*): *MTN1*, At4g38800 and *MTN2*, At4g34840. This enzyme activity hydrolyzes the methylthioadenosine (MTA) produced by nicotianamine (NA), polyamine (PA), and ethylene biosynthesis to methylthioribose (MTR) within the Yang cycle. Comprehensive analysis of the *mtn1-1mtn2-1* mutant line with 14 % residual MTN activity revealed a complex phenotype that includes male and female infertility and abnormal vascular development. Based on metabolite profiling, *mtn1-1mtn2-1* has a reduced NA content, altered PA profiles with higher putrescine (Put) and lower spermidine (Spd) and spermine (Spm) levels, disrupted metal ion profiles, and abnormal auxin distribution. The modeling of Arabidopsis PA synthases developed by comparison with the crystal structures of human Spd and spermine synthases complexed with MTA suggests that Arabidopsis PA synthases are product inhibited by MTA. Thus, these pleiotropic mutant phenotypes possibly are the result of one metabolite directly inhibiting numerous pathways.

By creating and analyzing a series of mutants and transgenic lines with moderate levels of MTN activity the complex phenotype of *mtn1-1mtn2-1* was dissected in order to determine the fundamental trait associated with MTN deficiency. Two double mutants were identified by crossing single T-DNA mutants, and an artificial micro RNA (amiRNA) line was generated by transforming *mtn1-1* with amiRNA specific to *MTN2*. The T-DNA double mutants, *mtn1-4mtn2-1,* and *mtn1-1mtn2-5* had 98 % and 28 % MTN activity, respectively, whereas the amiRNA line has 16 % MTN activity. The growth, development, and metabolite analysis of these mutants revealed that their delayed bolting, correlated with an increased number of leaves, was the common trait observed across all lines. Xylem proliferation defects and increased number of vascular bundles per unit area were shared in all lines except *mtn1-4mtn2-1*. Based on these

results, auxin distribution is proposed as the key target of the accumulated MTA that results from MTN deficiency.

The infertility related to MTN-deficiency was restored by supplying 100 µM of Spd to the *mtn1-1mtn2-1* seedlings over 14 days. The data presented in this thesis reveals two potential links that work synergistically to recover fertility in this *mtn1-1mtn2-1* line. Based on a detailed analysis of the female gynoecia morphology, transcript, hormone and metabolite profiles, it is proposed that the Spd partially reverses the mutant phenotypes through the recovery of auxin distribution and /or vascular development. Interestingly, the Spd effect seems to be transgenerational: they give rise to plants that are genotypically *mtn1-1mtn2-1* but phenotypically WT over generations. Taken together, all of the results suggest that *MTN*-deficient mutants provide the potential for unraveling the molecular mechanism associated with nicotianamine, polyamines, auxin, and vascular development with respect to enhancing the efficiency of nutrient use and yields in plants.

Acknowledgements

First, I would like to thank my supervisor, Prof. Barb Moffatt. Barb, I am without the words to express how thankful I am to you. You have stood by me, encouraged me, guided me, and helped me develop in to a confident scientist. I know that sometimes I was difficult to handle, but you always managed me with great patience. You have been a model for me in many ways and have also played many roles in my life, from tough master to comforting soul. For all of your contributions to the person I have become, not only in a scientific context but also in day-to-day life situations, I owe you the greatest possible gratitude.

To my committee members, Dr. Susan Lolle, Dr Frederique Guinel, and Dr. Simon Chuong (not in a particular order), I am indebted to all three of you for the invaluable expertise, suggestions, and guidance you provided during the committee meetings what have made this project a success. I would also like to thank each of you individually for inspiring me in your own special ways:

- Susan, you always had an encouraging word for me even when I met you in the hallway for a quick question. I especially thank you for supervising my work during Barb's sabbatical. Your suggestions were always valuable, but particularly in the case of my proposal for the NSERC-summer-Japan scholarship, they helped to make my application outstanding.
- Dr. Guinel, you have inspired me in many ways especially with respect to your meticulous method of editing scientific writing. You have been there to discuss scientific issues or how to focus on writing a paper, and you have gone even beyond expectations to lend me your literature collection when needed it.
- Simon, I feel very fortunate to have had your "gentle" criticism throughout my graduate career: you were there as a committee member when I defended my MSc thesis in 2007, and four years later you were in the same position at my PhD defense. It was

because of your advice, that I hold my basic knowledge of plant anatomy and physiology as a source of pride.

I would also like to thank my external supervisors, Prof. Jim Mattson and Dr. Betsy Daub, for devoting their precious time to the reading of my thesis and for critically evaluating my current knowledge.

I give special thanks to all who contributed toward the success of this project. I would certainly not have been able to progress as far as I have without all of your hard work.

- Our collaborators Prof. Rudiger Hell and Dr. Markus Wirtz from the University of Heidelberg, Germany; Prof. Margret Sauter and Yasmin Oppermann from Universität Kiel, Germany; Prof. Hitoshi Sakakibara and Dr. Nori Nakamichi from RIKEN Japan; and Prof. Taku Takahashi and Dr. Jun-ichi Kekahi, Okayama University, Japan.
- The undergraduate students of the Moffatt laboratory, who assisted me technically in conducting many parts of this project: Olga Kazberova, Andy Kong, Lilian Lee, Farah El-zarkout, Ahmed Elzahabi, Danielle Menezes, Shantel Menezes, Marie Leung, Roba Bdeir, Zachary, T. Hull, Natasha Peer, Kameisha Parkins.
- Sarah Schoor, former graduate student of Moffatt laboratory, who initiated the work presented in this thesis, and, Tzann-Wei Wang and Qifa Zheng, research associates of Thompson laboratory, who provided assistance with the two dimentional gel electrophoresis.
- The providers of greatly appreciated expert knowledge throughout this project: Prof. Jaideep Mathur, University of Guelph for microscopic analysis of the mutant; Prof. Sheila Macfee, University of Western Ontario, Canada, for ionomic analysis; and Dr. Alexander N. Plotnikov for MTA inhibition modelling.

- Yong Li, technician of Moffatt laboratory, who taught me technical skills, guided me in designing the cloning and RT-PCR experiments, and gave his fullest support during critical experiments for the project.
- The kind gifts of the seeds of the auxin reporter line DR5*rev*::GFP, the NA overproducing Arabidopsis K1 line, and *tkv* from J. Friml (Ghent University, Belgium), Pierre Czernic (Université Montpellier, France), and Timothy Nelson (Yale University, USA), respectively. Prof. W.D. Kruger, Fox Chase Cancer Center, Philadelphia who donated the hMTAP cDNA; and Prof. M. Niitsu of the Faculty of Pharmaceutical Sciences, Josai University, who provided Tspm.

I would like to thank all the sources that provided funding during my PhD program: Ontario Graduate Student scholarships (OGS), the NSERC discovery grant, the NSERC summer Japan scholarship, travel and other bursaries from the Graduate Student Office, University of Waterloo; graduate student scholarships and research and teaching assistantships from the Department of Biology, University of Waterloo.

My profound thanks to Prof. Carol Peterson and Dr. Arunika Gunewardana: Carol for giving me the opportunity to come to Canada, igniting the scientist in me and guiding me in the building of a firm foundation in plant knowledge, and Arunika for connecting me with Carol and making my dream of graduate studies in Canada a reality.

To all my colleagues at the University of Waterloo, including Katja Engle, Sarah Schoor, Dr. Sanghyun Lee, Tony Facciuolo, Makoto Yanagisawa, and Terry (Shiu Cheung) Lung, and to those at RIKEN, Japan, I thank you for sharing your knowledge and expertise whenever I needed it and also for making the lab a fun place to work.

I am extremely grateful for the faculty, staff, and students of the Department of Biology. Very special thanks go to Linda Zepf, for always lending me a shoulder to lean on when things were not going well at my end. And to Dr. Mungo Marsden and Dr. Simon Chuong, thank you for letting me use your microscopes. Lynn Hoyles was there to guide and advise me every time I encountered problems with my plants on chambers and even with totally unrelated other matters. Thank you Lynn, for always taking care of my problems right away. Dale Weber deserves special thanks for teaching me the fundamentals of confocal microscopy and helping me out in every possible way, whether related to microscopy or not. I also owe Jeannie Redpath-Erb and administrative staff, Gracia Murase, Karen Miinch, Daryl Enstone, and, Ron Socha, thanks for their assistance in a variety of ways during the last four years. I am grateful to Dragana Miskovic and Cheryl Duxbury for trusting in me during TA assignments.

I would like to thank Barbara Trotter for editing this thesis and Erin Harvey for her assistance with the statistical analysis.

I have greatly appreciated all my friends who have been so supportive during this period especially Suramya Mihindukulasekara and Chithral Angammana for assistance and initial support with respect to statistical analysis and for providing technical support for setting up the hydroponic system, respectively. I thank Rasanie Padmathilake for her assistance in tying up the ends of this thesis.

To my parents and my brother's family, I am so grateful for all your love and the confidence you have placed in me. Thaththi (Dad), I lost you when I was four-years-old, but I wish you were here to witness this happy moment. Amma (Mom), thank you for all that you have done for me, including sacrificing your happiness to raise me, provide me with a good education, and taking over the household work so I could concentrate writing the thesis. Ayya (brother) I thank you

for taking over the role of father and for taking care of my mother when she was severely ill so that I could continue my Ph.D. studies. I thank Krishmali Alles (sister-in-law) for taking care of the family during these difficult times. Uncle Marinus (Van prattenburg) and aunty Marie (Van prattenburg), thank you for all your help and encouragement from the moment you heard about our decision to come to Canada up until now.

Anthony (Adikari) uncle, you taught me the importance of education. Here I am at the highest education level one can achieve, and for that I owe you a debt of gratitude. A very special thanks goes to my father-in-law, Karunarathna Jayabahu, who is working on a PhD in his late 60s. Thaththa, you were my motivation to keep going when times were difficult and I wanted to step away. Fr. Roy Mariarathnam, you deserve a huge thank you for exposing me to advanced technology during the early stages of my education.

Nandana, I know I have not been the best wife or best mom for Dylan for most of my graduate career especially during the last few months of writing my thesis. Thankfully, you both have been very understanding and have stood beside me very patiently. What I desire from the bottom of my heart is to be a better wife and mother with the completion of this Ph.D.

Above all, I give thanks to the GOD almighty, for the wonderful blessing he has bestowed on me by surrounding me with all of the people who have helped me in various ways and at various times during my journey towards the successful completion of this thesis. God Bless You all!

Dedication

To the two most wonderful men in my life

One of you is just two months older than the initiation of the work presented in this thesis whereas the other one receives all the credit for inspiring me to continue my studies to earn a PhD and for being the pillar that has held me together so that I could successfully complete this thesis.

To my husband Nandana Jayabahu

and

my son Dylan Jayabahu.

Both of you have made enormous sacrifices just to keep up with me during the past four years of my journey.

Dylan, you are the best son a mother could ever wish for, and

Nandana I am nothing without you and your guidance.

I am enormously blessed to have you both in my life.

I love you both, and I dedicate this most precious document of my life to both of you with gratitude.

x

Table of Contents

List of Figures

List of Supplemental Figures

List of Tables

List of Supplemental Tables

List of Abbreviations

ABA	Abscisic acid
ACC	1-aminocyclopropane-1-carboxylic acid
ACL5	ACAULIS5/ Tspm synthase
ACO	1-aminocyclopropane-1-carboxylic acid oxidase
ACS	1-aminocyclopropane-1-carboxylic acid synthase
ADC	Arginine dearboxylase
Ade	Adenine
Ado	Adenosine
AIH	Agmatineiminohydrolase
ami	artificial microRNA
AMP	Adenosine monophosphate
ARD	Acidoreductone oxygenase
ARF	Adenosine diphosphate Ribosylation Factor-
AT	3-amino-1, 2, 4-triazole
ATHB	Arabidopsis thaliana homeobox
axr6	AUXIN RESISTANT 6
bdl	BODENLOS
bHLH	Type basic-helix-loop-helix
BR	Brassinosteroid
CBL	Calcineurin B-like
CDS	Coding sequences
CK	Cytokinin
Co	Cobolt
Cu	Copper
CuAO	Copper amine oxidase
DAB	3-3’ diaminobenzine
DAG	Days After Germination
DCFA-DA	Dichloro Fluorescin Di Acetate
dcSAM	Decarboxylated S-adenosyl methionine
DEP1	Dehydratase-enolase -phosphatase -complex 1
DHKMP	1, 2-dihydro-3-Keto-5-Methylthiopentene
DHS	Deoxyhypusine synthase
DIC	Differential Interference Contrast

DNA	Deoxyribonucleic acid
eIF5A	eukaryotic initiation factor 5A.
EtOH	Ethanol
Fe	Iron
GA	Gibberellic acid
GAP	Guanine triphosphatase Activating Protein
GCOS	GeneChip Operating Software
GEF	Guanine nucleotide Exchange Factor
GFP	Green Fluorescent Protein
GO	Gene Ontology
GUS	β-Glucuronidase
h	Hour
H_2O_2	Hydrogen peroxide
Hcy	Homocysteine
HD-ZIP III	Homeodomain transcription factor family
IAA	Auxin / Indoleacetic acid
ICP-AES	Inductively Coupled Plasma Atomic Emission Spectroscopy
JA	Jasmonic acid
KMTB	2-keto-4-methylthiobutyrate
lop1	LOPPEDED
LRR	Leucine-Rich-Repeat
MAT1	methionine adenosyltransferases
Met	Methionine
Mn	Manganese
Min	minute
MP	MONOPTEROS
MS	Murashige and Skoog
MTA	5'-Methylthioadenosine
MTAP	5’-Methylthioadenosine phosphorylase
MTI1	5'-Methylthioribose 1-phosphate isomerase 1
MTK	5’-Methylthioribose kinase
MTN	5’-Methylthioadenosine nucleosidase
MTR	5’-Methylthioribose

MTR-1P	5'-Methylthioribose 1-phosphate
MTRu-1-P	5’-Methylthioribulose-1-phosphate
NA	Nicotianamine
NAAT	Nicotianamine aminotransferase
NAS	NA synthase
nas	NAS deficient
Ni	Nickel
NO	Nitric oxide
NPA	1-N-naphthylphthalamic acid
ODC	Ornithine decarboxylase
OsMTN	*Oriza sativa* MTN
PA	Polyamine
PAR	Photosynthetically Active Radiation
PAO	Polyamine oxidase
PAT	Polar Auxin Transport
PDB	Protein Data Base
ph	phloem
PP2A	Protein phoshatase 2A
Put	Putrescine
RLK	Receptor-Like Kinases
RMA	Robust Multi-chip Average
RNA	Ribonucleic acid
RT	Room Temperature
SA	Salicylic acid
SAC51	suppressor of the ACAULIS5
SAH	S-adenosylhomocysteine/AdoHcy
SAM	*S*-adenosyl-*L*-methionine /AdoMet
SAMDC	S-adenosylmethionine decarboxylase
SDS	Sodium Dodecyl Sulfate
Spd	Spermidine
SPDS	Spd synthase
Spm	Spermine
SPMS	Spm synthase
SPSS	Statistical Package for the Social Sciences

SRH	S-ribosylhomocysteine
TAIR	The Arabidopsis Information Resource
TBO	Toluidine Blue O
T-DNA	Transfer DNA
tkv	thick vein
trn	TORNADO
Tspm	Thermospermine
WT	Wild Type
xy	xylem
YSL1	Yellow Strip-Like
Zn	Zinc

Chapter 1: General Introduction

1.1 The model plant Arabidopsis

Arabidopsis thaliana was discovered by Johannes Thal in Germany in the 1500s (Somerville and Koornneef, 2004). This small dicotyledonous species belongs to the Brassicaceae (mustard) family. Unlike some members of this family, which are well known for their agricultural importance (turnip, cabbage, broccoli, and canola being the commonly consumed members), Arabidopsis is not economically important. However, it has been studied in laboratories for more than 40 years for its importance in the generation of fundamental information in the fields of genetics, development, biochemistry, and the physiology of plants [The Arabidopsis Genome Initiative, 2000; The Arabidopsis Information Resource (TAIR), 2011].

This plant has many desirable traits that make it suitable for molecular genetic studies, including its short life cycle (~8 weeks from seed germination to seed set); its generation of selfed progeny with a production of ~10,000 seeds/plant; its ability to grow in a limited space; and a fully sequenced small genome (125 Mb) with low amount of repetitive sequences, small introns, and few gene families (The Arabidopsis Genome Initiative, 2000; Wortman et al., 2003). The complete genome sequence is available publically on many online databases. The Arabidopsis Information Resource (TAIR; http://www.arabidopsis.org/index.jsp) maintains such a database, which contains the complete genome sequence along with many other data relevant to this model plant: information about gene structure, expression, and metabolites; the availability of DNA and seed stocks; genome maps; physical and genetic markers; and information about the Arabidopsis research community. The latest release of the Arabidopsis genome annotation (TAIR10) reports that, out of a total of 33,518 genes, only 27,379 code for proteins (TAIR, 2011). In addition to these online databases, several stock centres with collections of cloned genes and characterized mutants are also available for researchers who are studying Arabidopsis. Many tools have also been developed by the Arabidopsis research community. For example, the floral dip method (Clough and Bent, 1998) for producing transgenic

plants and a large number of well-characterized mutant collections including T-DNA insertion mutants (TAIR, 2011) are used extensively to address a variety of research questions by many Arabidopsis scientists around the world, including our lab group. All of these characteristics have made Arabidopsis an ideal model organism for basic biological research.

The work presented in this thesis uses this model plant and its tools to determine the contribution of methylthioadenosine nucleosidase (MTN; EC 3.2.2.16) activity to plant growth and development.

1.2 Network of essential pathways linked by 5'-Methylthioadenosine nucleosidase activity

5'-Methylthioadenosine nucleosidase (MTN) is located centrally between two essential interconnected pathways: the methionine (Met) recycling pathway and the activated Met cycle (Figure 1.1). The importance of these pathways and their links to others are discussed in this section, with special emphasis on the Met recycling pathway and the polyamine (PA) and nicotianamine (NA) biosynthesis pathways, all of which rely on MTN activity for their continued activity.

1.2.1 Yang cycle/Met recycling pathway

The Met recycling pathway is present in all organisms, from unicellular bacteria to plants and animals, and is thus considered a universal (housekeeping) pathway, the role of which is primarily to recycle sulfur-containing metabolites. 5'-methylthioadenosine (MTA), a key sulfur-containing by-product of several reactions, is an intermediate in this pathway, which is also called the MTA cycle. In plants, this pathway is specifically called the Yang cycle because it was first discovered by Shang Fa Yang in the 1980s (Yang and Hoffman, 1984). The Yang cycle

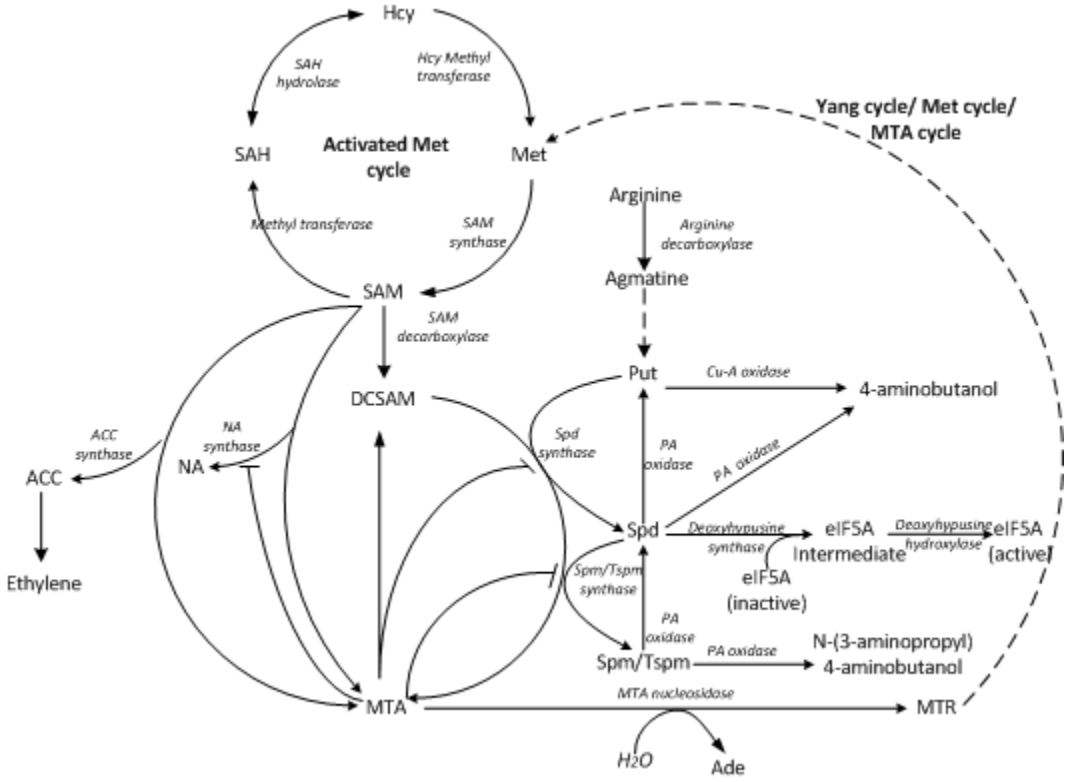

Figure 1.1: Yang cycle and activated Met cycle in Arabidopsis.

MTA, produced as a by-product during PA biosynthesis, NA biosynthesis, and ethylene biosynthesis, is subsequently recycled to Met. SAM regenerated from Met acts as the substrate for SAM decarboxylase, NA synthase, ACC synthase, and Methyl transferase to produce DCSAM, NA, ACC, and SAH, respectively. DCSAM provides the aminopropyl moieties to Spd synthase and Spm/Tspm synthase in order to convert Put to Spm/Tspm via Spd. ACC oxidase generates ethylene from ACC while SAH becomes cleaved into Hcy by SAH hydrolase. Hcy is recycled back to Met. Ade, adenine; ACC, 1-aminocyclopropane-1-carboxylate synthase; Hcy, homocysteine; Met, methionine; MTA, methylthioadenosine; MTR, methylthioribose; NA, nicotianamine; PA, polyamine; Put, Putrescine; Spd, spermidine; Spm, spermine; Tspm, thermospermine; SAH, S-adenosylhomocysteine; SAM, S-adenosylmethionine; DCSAM, decarboxylated SAM; CuA oxidase, Cupper amine oxidase; and eIF5A, eukaryotic initiation factor 5A. PAoxidase, polyamine oxidase.

recycles the MTA that is generated via three biosynthetic pathways: PA (Takahashi and Kakehi, 2011), NA (Negishi et al., 2002) and ethylene (Yang and Hoffman**,** 1984).

1.2.1.1 Biosynthesis of PAs and their functions

PAs are organic cations that are involved generally in many cellular processes, modulating the functions of deoxyribonucleic acid (DNA), ribonucleic acid (RNA), nucleotide triphosphates, and proteins (Igarashi and Kashiwagi, 2010). The diamine putrescine (Put), triamine spermidine (Spd), and tetraamines spermine (Spm) and thermospermine (Tspm) are the PAs most commonly found in living organisms. Although in animals, fungi and young plants Put is derived from either ornithine or arginine (Figure 1.2) mature plants commonly use arginine as the precursor. Unlike most plant species, *Arabidopsis thaliana* lacks ornithine decarboxylase activity (ODC; EC 4.1.1.17; Hanfrey et al., 2001) and thus relies on arginine decarboxylase (ADC; EC 4.1.1.19; Figure 1.1) to generate Put. Put is converted first to Spd by Spd synthase (SPDS; EC 2.5.1.16) and then to Spm and Tspm by Spm synthase (SPMS; EC 2.5.1.22) and Tspm synthase (ACL5; ACAULIS5; EC 2.5.1.79), respectively. Decarboxylated *S*-adenosyl methionine (dcSAM) serves as the aminopropyl donor for all of these reactions. dcSAM is generated from *S*-adenosyl-L-methionine (SAM) by *S*-adenosylmethionine decarboxylase (SAMDC; EC 4.1.1.50). Although it has been known for decades that PAs play a role in cell division, embryogenesis, root formation, fruit development, and responses to abiotic stresses in plants (Kumar et al., 1997), an understanding of their modes of action at the molecular level has just begun to emerge.

Put is involved primarily in abiotic stress responses (Table 1.1; Takahashi and Kakehi, 2010) while both Put and Spd are preferentially essential for embryogenesis (Table 1.1; Imai et al.,

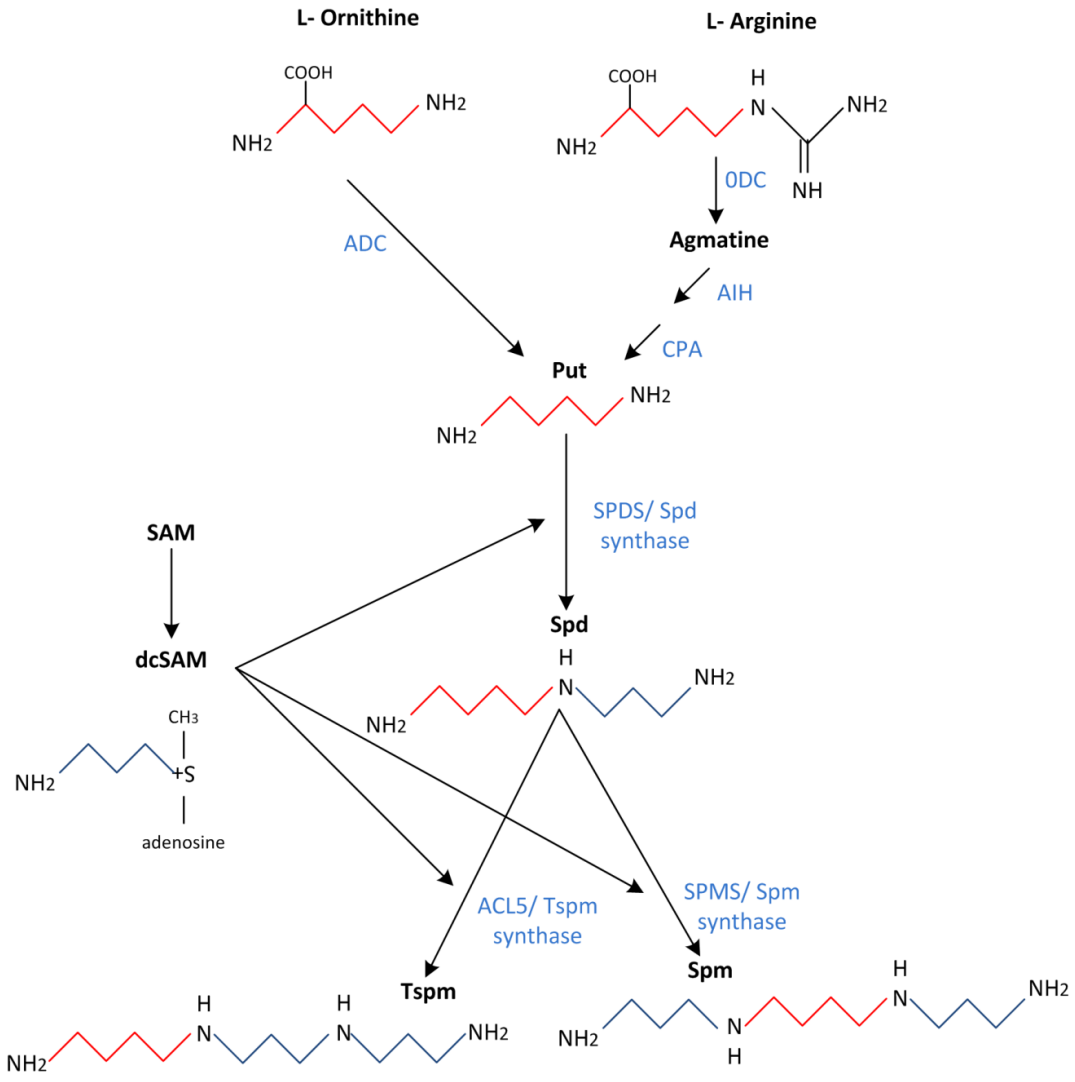

Figure 1.2: Biosynthetic pathway of polyamines in plants.

Put, Putrescine Spd, spermidine; Spm, spermine; Tspm, thermospermine; ADC, arginine decarboxylase; AIH, agmatineimino hydrolase; CPA, N-carbamoyl putrescineamido hydrolase; ODC, ornithine decarboxylase; SAM, S-adenosyl-L-methionine; SAMDC, S-adenosyl-L-methionine decarboxylase; SPDS, Spd synthase; SPMS, Spm synthase; ACL5, Acaulis5; Tspm synthase. Modified from Takahashi and Kakehi (2011).

2004a). One reason for the requirement for Spd could be that it is the source of the butylamine moiety needed for the activation of the eukaryotic translation initiation factor 5A (eIF5A; Figure 1.1). The activation of this factor is essential for cell growth and proliferation (Park, 2006) and possibly also for plant embryo development. Based on this rationale, the mutation in the deoxyhypusine synthase (DHS) gene that is involved in the rate-limiting first step in hypusination of eIF5A results in the arrest of embryo-sac development in Arabidopsis (Pagnussat et al., 2005).

In addition to the roles played by free PA, the contribution of conjugated Spd on the other hand is related to protection against pathogens, the detoxification of phenolic compounds; Spd also functions as a PA reserve in seeds (Takahashi and Kakehi, 2010).

Spm is non-essential for the survival of Arabidopsis (Table 1.1) but participates in signaling pathways by regulating control of ion channels and receptor activities, protecting DNA from being mutated by free radicals (Ha et al., 1998), and mediating signals to protect against plant pathogens (Yamakawa et al., 1998; Takahashi et al., 2003). During this signaling, Spm accumulates in the apoplast and produces H_2O_2 via apoplastic polyamine oxidation, resulting in the up regulation of a subset of defense-related genes (Cona et al., 2006; Moschou et al., 2008).

A structural isomer of Spm, Tspm, plays a critical role in vascular cell differentiation. The gene that encodes Tspm synthase is expressed specifically in early-developing vessel elements and has an upstream promoter element that is auxin sensitive. When this gene is disrupted, the resulting plants are dwarf, with increased xylem proliferation in their stems (*acl5*; Table 1.1; Hanzawa et al., 2000), and have highly vascularized leaves with thicker mid-veins (*tkv*, allelic to *acl5*; Clay and Nelson, 2005). The *acl5* phenotype is restored by a suppresser mutation of *acl5* known as *SAC51* (suppressor of the ACAULIS5; *sac51-d*; Imai et

Table 1.1 : PA biosynthetic mutants.

Mutant /mutagen	Gene/AGI number	Phenotype	Reference
adc1	ADC / AT2G16500/ Arginine decarboxylase	No obvious phenotype under normal growth conditions.	Soyka and Heyer, 1999
adc2		Sensitive to salt stress.	Urano et al., 2004
adc1adc2		Embryo lethal.	Urano et al., 2005
tkv (Diepoxybutane)	ACL5 (TKV)/ AT5g19530/ Tspm synthase	Increased thickness in adult rosette leaves, more veins per square area, short internodes.	Clay and Nelson, 2005
acl5-1, acl 5-3/ (Ethyl methane sulfonate)		Dwarfed phenotype with over-proliferation of xylem tissues.	Hanzawa et al., 1997 Hanzawa et al., 2000.
spms-1 (T-DNA insertion)	SPMS/AT5g53120/ Spm synthase	No obvious phenotype.	Imai et al., 2004
spds1spds2 (T-DNA insertion)	*SPDS1/*AT1g23820 *SPDS2/*AT1g70310 Spd synthase	Embryo development of the double mutant is arrested at the heart stage: each mutant allele shows normal growth.	Imai et al., 2004

al., 2006). Vera-Sirera et al. (2010) proposed a model for the role of Tspm based on the work conducted with respect to *acl5*: Tspm activates *SAC51* translationally to ensure an adequate level of basic helix-loop-helix (bHLH) transcription factors that negatively regulate the genes related to cell death, thereby maintaining differentiating vessel elements alive until maturation by preventing premature cell death (Muñiz et al., 2008).

1.2.1.2 PA catabolism

In contrast to the amount of knowledge available with respect to plant PA biosynthesis, understanding of PA catabolic pathways is just beginning. Two enzyme groups are known to be involved in PA catabolism. A copper-containing amine oxidase (CuAO; EC 1.5.3.3; Figure 1.1) utilizes Put, and a flavin adenine dinucleotide-dependent polyamine oxidase (PAO; EC 1.4.3.6) utilizes Tspm/Spm and Spd as substrates. Arabidopsis contains 12 CuAO isoforms and five PAO isoforms (Takahashi et al., 2010; Wimalasekera et al., 2011). PAO back-converts Tspm/Spm to Put via Spd in order to maintain PA homeostasis within plants (Takahashi et al., 2010). A detailed characterization of PAO activities indicates that PAO1 prefers Tspm and nor-Spm over Spm as its predominant substrate while PAO4 uses Spm. PAO2 and PAO3 back-convert Spd to Put (Takahashi et al., 2010). All of these oxidation reactions produce H_2O_2. H_2O_2 generated during exogenous supplementation of Spd or the overexpression of PAO acts as signals for premature xylem differentiation (Tisi et al., 2011) or for reduced pollen tube growth (Wu et al., 2010). A recent report by Wimalasekera et al. (2011) suggests that these Spd-mediated responses occur via nitric oxide (NO) signaling. NO signaling is known to affect an array of plant functions, including pollen-pistil interactions (Prado et al., 2008). PA biosynthesis, catabolism, and conjugation thus act together to maintain the PA homeostasis that is involved in many aspects of plant growth and development. Since *MTN* - deficient single mutants, *mtn1-1* and *mtn1-2*, have altered PA profiles (Bürstenbinder et al., 2010), factors that affect PA homeostasis may be relevant to understanding their phenotype.

1.2.1.3 NA biosynthesis and its functions

NA, another product of an MTA-generating reaction, is a non-proteinogenic amino acid and a strong metal chelator that is involved in long-distance metal translocation in plants. NA synthase (NAS; EC 2.5.1.43, Figure 1.3A) condenses three amino-carboxylpropyl groups, each arising from S-adenosyl-L-methionine (SAM) molecules, in order to produce one molecule of NA. The structural features of NA are ideal for chelating metals: NA coordinates the centrally bound metal ion via its three amino and three carboxyl groups to form an octahedral complex (Curie et al., 2009; Figure1.3B). NA thus forms stable complexes with manganese (Mn), iron (Fe), cobalt (Co), zinc (Zn), nickel (Ni) and copper (Cu), in increasing order of affinity (Anderegg and Ripperger, 1989). As a result, NA deficiency leads to phenotypes that resemble mutants with altered metal profiles, including interveinal chlorosis and fertility defects (Table 1.2).

Plants are classified as belonging to one of two groups based on their strategies for iron acquisition: strategy I plants (non-graminaceous plants: e.g., Arabidopsis) and strategy II plants (graminaceous plants: e.g., rice). In strategy I plants, ions are acquired by the reduction of Ferric (Fe^{+3}) ions into the more soluble Ferrous (Fe^{+2}) ions. In these plants, NA functions as a chelator of iron in symplastic and phloem transport, as a chelator of Cu in xylem transport, and as a cell protector against oxidative stress. In addition to the roles it plays in strategy I plants, in strategy II plants, NA serves as the precursor for the biosynthesis of the phytosiderophores of the mugineic acid family (Figure 1.3A). These plants excrete these phytosiderophores to form complexes with Fe^{+3}. NA synthesis is thus extremely important for the regulation of iron metabolism in both strategy I and strategy II plants (Curie et al., 2009).

Although *NAS* gene family has been thought to be plant specific, NAS-like genes have been revealed in many organisms, including fungi, and archaea (Herbik et al., 1999; Trampczynska et al., 2006). Arabidopsis contains four *NAS* isoforms. Klatte et al. (2009) reports the phenotype of

two quadruple *nas* mutants (Table 1.2). On one hand the *nas4x-2* mutant that has lost full *nas* function develops chlorotic leaves and is sterile. On the other hand, *nas4x-1*, with an intermediate *nas* function, due to leaky expression of *NAS 2*, is fertile and develops leaf chlorosis that becomes severe upon the transition to the reproductive phase or during Fe deficiency. Moreover, the tomato *nas* mutant *chloronerva* and the transgenic tobacco line that overexpresses NA aminotransferase (NAAT) activity also show leaf chlorosis and sterility as a result of reduced NA (Scholz et al., 1992; Ling et al., 1999; Takahashi et al., 2003). Thus in plants, NA produced by NA synthase plays an important role in ion homeostasis, including Fe content. Since an MTN-deficient double mutant (Bürstenbinder et al., 2010) is sterile, the effects of NA have also been studied in detail in the research for this thesis.

1.2.1.4 Ethylene biosynthesis and its roles in plant development

The gaseous phytohormone ethylene is involved in a number of growth and development processes in plants, including floral development, fruit ripening, response to stresses, and senescence (Bleecker and Kende, 2000). Ethylene is formed from SAM via two steps. First, 1-aminocyclopropane-1-carboxylic acid (ACC) synthase (ACS; EC 4.4.4.14; Yang and Hoffman, 1984) catalyzes the transfer of the aminobutyrate group from SAM to ACC. This is the rate-limiting step (Bleecker and Kende 2000) that produces MTA as a by-product. Subsequently, in the second step, ACC oxidizes to ethylene by means of ACC oxidase (ACO; EC 1.14.17.4: Yang and Hoffman, 1984).

Although the Arabidopsis contains 12 *ACS (ACS 1-12)* annotated genes, only nine genes *(ACS1, ACS2, ACS4–9, and ACS11)* comprise its active multigene family because *ACS3* is a pseudogene, and *ACS10* and *ACS12* are aminotransferases (Yamagami et al., 2003). Of the nine, ACS1 forms a non-functional homodimer while the remainder forms functional

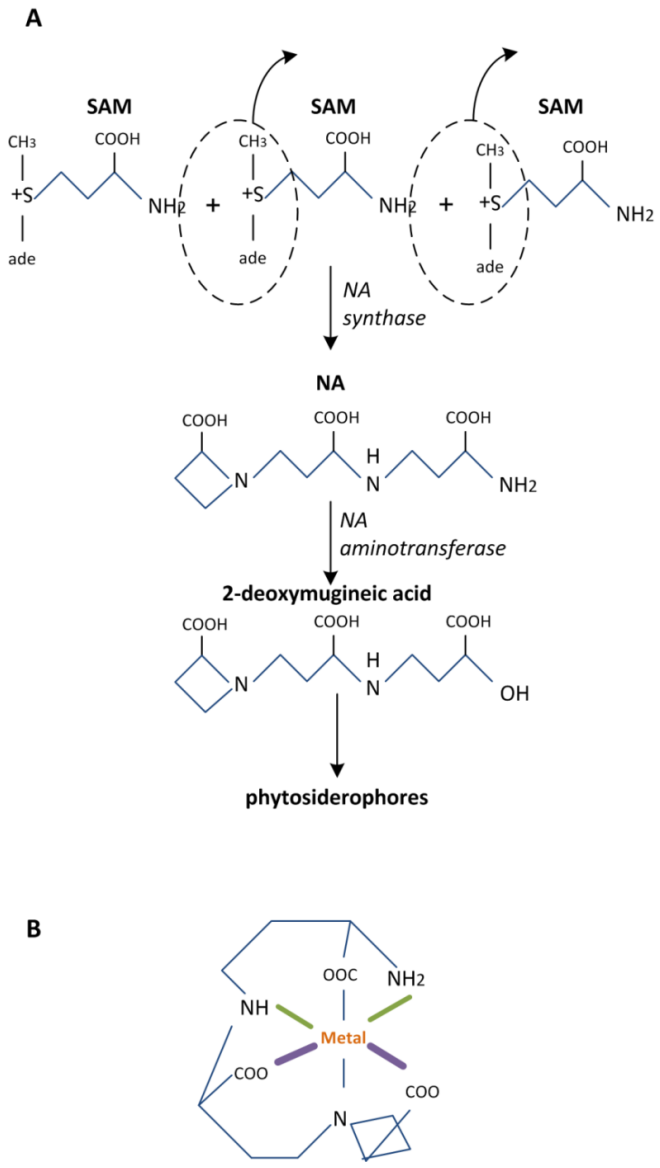

Figure 1.3: Biochemical pathway and chemical structure of nicotianamine (NA).

(A) The position of NA synthase and the way in which it leads to the phytosiderophores of the mugenic acid family. Modified from Takahashi et al. (2003).

(B) Biochemical properties of NA: the proposed chemical structure of the metal complex. Modified from Curie et al. (2009).

Table 1.2: NA biosynthesis mutants.

Mutant /mutagen	Gene Function	Phenotype	Reference
nas4x-1, Arabidopsis (T-DNA insertions in all four isoforms with a partially functional *nas2-1* allele	NA synthase	Mild chlorosis that occurs at the time of first flowering, and is fertile with seeds that have reduced Fe.	Klatte et al. (2008)
nas4x-2 ,Arabidopsis (T-DNA insertions in all four isoforms with a null allele of *nas2*)	NA synthase	Severe chlorosis throughout the life cycle and is sterile.	Klatte et al. (2008)
*Naat,*Tobacco (Constitutively expressing a barley *naat-A* gene)	NA aminotransferase (NAAT) catalyzes the amino group transfer of NA	Interveinal chlorosis phenotype in young leaves, morphological abnormalities in flowers, pollen maturation defects, and late anther dehiscence, long narrow leaves	Takahashi et al. (2003)
Chloronerva,Tomato mutant (Single base mutation in the single *NAS*)	NA synthase	Interveinal chlorosis phenotype in young leaves.	Scholz et al. (1992)

homodimers (Tsuchisaka and Theologis, 2004a). Tsuchisaka et al. (2009) recently showed that knocking down the entire ACS gene family results in embryo lethality. Their detailed characterization of single and multiple mutants revealed the overlapping functions of a variety of ACS members in plant growth and development, including flowering time, response to gravity, and ethylene production. These results show that the ACS gene family that generates MTA as a by-product is a key component in plant growth and development.

The MTA generated in all three of these biosynthetic pathways (PA, NA, and ethylene synthesis) is recycled to Met via a series of reactions collectively called the Yang cycle or Met recycling pathway (Figure 1.1). In this pathway MTA is hydrolyzed to adenine and methylthioribose (MTR, Figure 1.4). In plants MTR is converted back to Met through the production of four successive intermediate products; 5' methylthioribose-1-phosphate (MTR-1-P), 5-methylthioribulose-1-phosphate (MTRu-1-P), 1,2-dihydroxy-3-keto-5-methylpentene (DHKMP) and 2-keto-4-methylthiobutyrate (KMTB). The 5'-methylthioribose kinase (MTK; EC 2.7.1.100) transfers a phosphate group in the process of generating MTR-1-P from MTR (Sauter et al., 2004) whereas acidoreductone oxygenase (ARD; EC 1.13.11.54) converts DHKMP to KMTB (Sauter et al., 2005). The enzymes catalyzing the other two steps have been identified only recently by BLAST searches (http://www.ncbi.nlm.nih.gov/ blast/Blast.cgi); Pommerrenig et al., 2011). 5'-methylthioribose-1-phosphate isomerase1 (MTI1; EC 5.3.1.23) that converts MTRu-1-P to DHKMP and dehydratase-enolase-phosphatase-complex1 (DEP1) that converts DHKMP to KMTB were identified and characterized (Pommerrenig et al., 2011). Although it has been commonly thought that the Yang cycle genes are expressed in almost all plant cells (Pommerrenig et al., 2011), based on the actively translated transcriptome profiling of distinct cell populations (Mustroph et al., 2009), concluded that these enzymes are expressed predominantly in phloem tissues. B-glucuronidase (GUS) reporter gene fusions to all genes of

the Yang cycle reveal that MTN, MTK, ARD (except ARD3), MTI1, and DEP1 are localized primarily in the phloem of Arabidopsis and Plantago (Pommerrenig et al., 2011).

1.2.2 Met/transmethylation cycle

All three biosynthetic pathways that generate MTA as a by product utilize SAM (also abbreviated as AdoMet) as their precursor (for review see Albers, 2009). SAM is also the donor of methyl groups for almost all cellular methylation reactions that mediate important aspects of plant metabolism, such as the synthesis of pectin, lignin, and chlorophyll. *S*-adenosylhomocysteine (SAH or AdoHcy), produced as a by-product in these methylation reactions, is recycled back to Met via homocysteine (Hcy). This cycle is referred to either as the transmethylation cycle or as the SAM cycle. These methylation reactions are critical for the regulation of diverse biological processes, including the methylation of phospholipids and the "modification of DNA, RNA, histones and other proteins, dictating replication, transcriptional and translational fidelity, mismatch repair, chromatin remodeling, epigenetic modifications and imprinting" (Loenen 2006). In addition to methylation, SAM plays many other critical roles: it acts as a co-factor for nucleases and controls transcription or translation by binding to specific RNA molecules called riboswitches (Loenen, 2006). MTN has been studied intensely not only because of its ability to link critical pathways but also because its activity has been shown to be essential for viability.

1.3 Methylthioadenosine nucleosidase

MTA generated via several pathways is converted in either one or two steps to 5'-methylthioribose 1-phosphate (MTR-1-P). In animals, yeasts, cyanobacteria, and archaeae, MTA is cleaved and phosphorylated directly to MTR-1-P by methylthioadenosine phosphorylase (MTAP; EC 2.4.2.28) (Albers, 2009). In plants and most bacteria, MTA is hydrolyzed at the N-glycosyl bond between the ribose and adenine moieties by MTN, releasing MTR and Ade (Figure

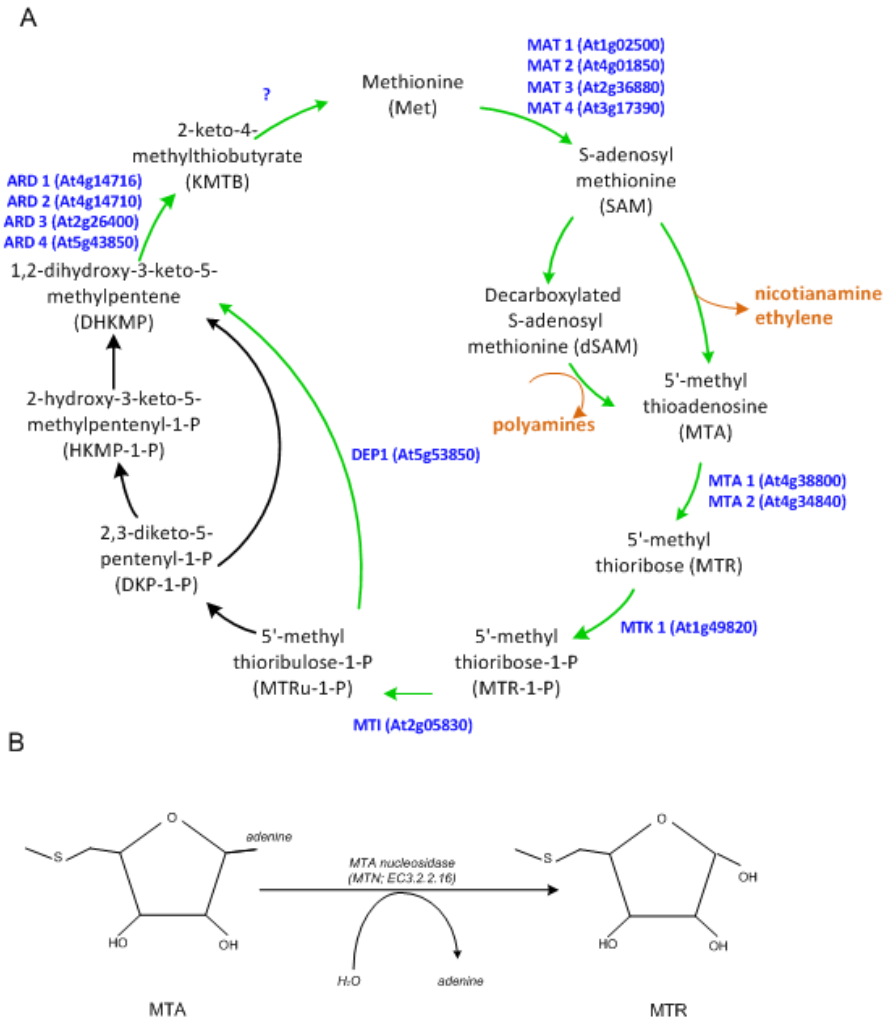

Figure 1.4: Yang cycle reactions and MTA hydrolysis reaction

(A) Yang cycle reactions in plants are indicated in green arrows whereas reactions found in bacteria but not in plants are indicated in black arrows. MAT1 to MAT4, methionine adenosyltransferases (*S*-adenosyl-*L*-methionine synthases); MTN; Methylthioadenosine nucleosidase; MTK, methylthioribose kinase; MT1, methylthioribose-1-phosphate isomerase1; DEP1, dehydratase-enolase-phosphatase-complex1; ADR1 to ADR4, acidoreductone oxygenase. Question marks have been added if direct proof for this function is still missing. Modified from Pommerrenig et al. (2011).

(B) Conversion of MTA to MTR via MTN reaction

1.4B, Guranowski et al., 1981; Cornell et al., 1996). In bacteria, this enzyme, designated as MTAN, also hydrolyses SAH to *S*-ribosylhomocysteine (SRH) and adenine (Lee et al., 2005).

1.3.1 Plant MTNs

Plant MTNs were initially investigated in lupin (*Lupinus luteus* L.) and tomato extracts (Guranowski et al., 1981; Kushad et al., 1985). Kushad et al. (1985) found that MTN activity is required for wound-induced ethylene biosynthesis in tomatoes and cucumbers. The single *MTN* gene of rice (*Oryza sativa* L.), *OsMTN*, was later identified and characterized (Rzewuski et al., 2007). Recombinant *OsMTN* has a kinetic constant (K_m) of 2.1 ± 0.2 μM for MTA but will accept substrates with 5' substitutions on the thiol group (e.g., ethylthioadenosine and butylthioadenosine; Rzewuski et al., 2007). Studies of *OsMTN* revealed that both *MTN* transcript levels and MTN enzyme activity increased with increases in ethylene biosynthesis. MTN activity is also sufficient for the maintenance of the Met and SAM pools during the prolonged periods of ethylene biosynthesis associated with rice submergence (Rzewuski et al., 2007). The work presented in this thesis has examined Arabidopsis MTNs with the goal of understanding the fundamental role of the activity of this enzyme in growth and development.

1.3.1.1 Arabidopsis MTNs

The *Arabidopsis thaliana* genome has two sequences annotated as MTNs along with three other related sequences: At4g24340, At4g24350, At4g28940 (Figure 1.5). The annotated MTN isoforms are *At*MTN1 (At4g38800) and *At*MTN2 (At4g34840) while the MTN-related genes have yet to be analyzed. The coding regions of these two genes share a 73 % nucleotide identity and a 64 % amino acid identity. Based on the phylogenetic tree (Figure 1.5) the MTN-related genes do not belong to the same clade as the *MTN1* and *MTN2* genes. Siu et al. (2008) discovered that both plant isoforms hydrolyze MTA with comparable apparent enzyme kinetics (Table 1.3), substrate preference, and pH values; the optimum pH for MTN1 is 8 while for MTN2, it is 6. However, MTN2 shows activity (14 %) toward SAH,

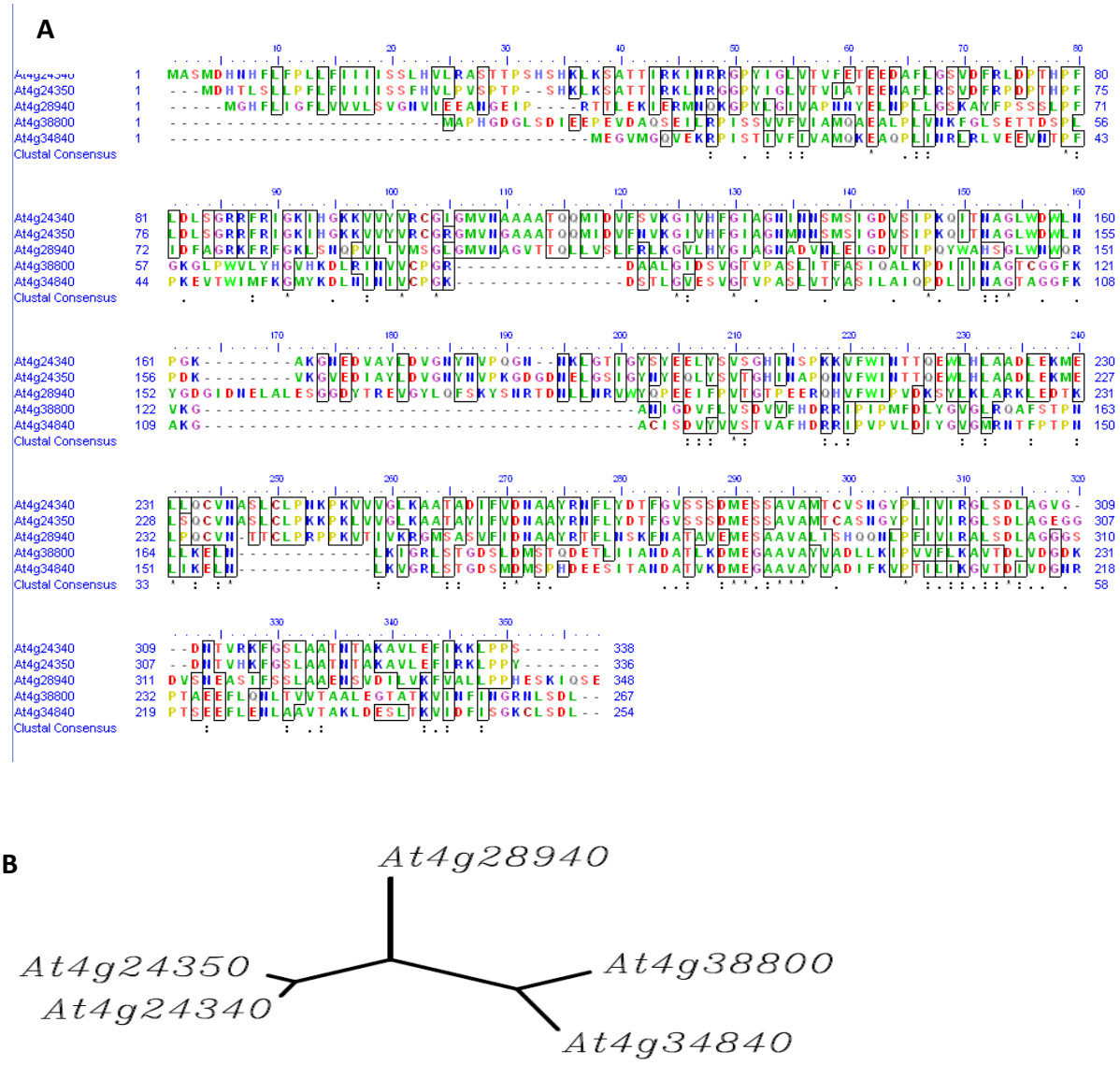

Figure 1.5: Sequence alignment and phylogenetic tree of MT.

(A) Sequence alignment of MTN1, MTN2, and other MTN genes. Strictly conserved residues are boxed.

(B) Phylogenetic tree of MTN genes.

which led the authors to suggest that MTA metabolism is mediated primarily by MTN1 (Siu et al., 2008). A comparison of the crystal structure of MTN1 and a homology model generated for MTN2 revealed changes in the active sites that were thought to be critical for the observed substrate specificity. Recently, Siu et al. (2011) reported that MTN1 binds SAH but is incapable of hydrolyzing it because binding SAH changes the catalytic water molecule, thus rendering hydrolysis impossible.

Table 1.3: Catalytic activities of MTN1 and MTN2 with substrate MTA:

	MTN1	**MTN2**
K_m (μM)	7.1±0.5	3.4±0.2
V_{max} (nmol/min)	3.7±0.1	2.0±0.08
K_{cat} (s^{-1})	18.7	2.0
K_{cat}/K_m (s^{-1} μM^{-1})	2.6	0.6

Data source: Siu et al. (2008).

1.3.1.2 Expression Profiles of Arabidopsis MTNs

MTN is known to be expressed in all organs, primarily in the phloem of vascular tissues. Public microarray data indicate that *MTN*1 transcripts are about 10 times more abundant than *MTN*2 transcripts across different organs (Zimmermann et al., 2004). However *MTN1* and *MTN2* were uniquely expressed in different tissues (Figure 1.6A; Winter et al., 2007) when used tissue specific expression in EFPbrowser (http://efp.ucr.edu/cgi-bin/relative). Using RNA gel-blot analysis Oh et al. (2008) confirmed that *MTN*1 is expressed in roots, stems, flowers and both cauline and rosette leaves. Based on the MTN1::GUS gene expression, MTN1 appears first at the tips of the cotyledons of 3-day-old seedlings and in the shoot apex and leaves of young seedlings particularly in vascular tissues (Oh et al., 2008). In flowers, MTN1 is found specifically in sepals and anthers but not in pistils or petals. Since GUS expression was seen only in the mature anthers and not in immature ones, the authors suggested that MTN1 plays a role in

pollen development. The results of translatome profiling by FLAG tagging of ribosomal protein L18 (Mustroph et al., 2009) provide additional insight. In these experiments, an epitope-tagged ribosomal protein was expressed from a variety of tissue-specific promoters, allowing the recovery of actively translated transcripts. When the results are visualized with translatome eFPbrowser, it is evident that MTN1 is synthesized primarily in phloem tissues and guard cells whereas MTN2 is in phloem tissues and epidermal cells, including guard cells (Figure 1.6B, C). The expression pattern for MTN1 was validated by *pMTN1:: MTN1: GUS* analysis which showed that MTN1 is specifically in phloem but not in xylem (Pommerrenig et al., 2011)

1.3.1.3 Interacting partners of Arabidopsis MTN

In a study designed to determine the interacting partners of Calcineurin B-like (CBL) protein family, Oh and colleagues (2008) found a physical interaction of MTN1 and MTN2 with CBL3 *in vitro* using yeast two-hybrid assays. The interaction between MTN1 and CBL3 inhibits MTN1 activity. Based on this MTN inhibition, ethylene, PA, and NA syntheses are most likely regulated via the Met cycle (Oh et al., 2008). At the cellular level, MTN1 was shown to be localized at the plasma membrane, in the cytoplasm, and in the nucleus. However, the interaction with CBL3 was shown to occur mainly outside of the nucleus.

1.3.2 *MTN*-deficient plants

Four transfer DNA (T-DNA) insertion single *mtn* mutants have recently been described: *mtn1-1* (T-DNA insertion in the third intron of the *MTN1* gene), *mtn1-2* (T-DNA insertion in the sixth exon of the *MTN1* gene), *mtn2-1* (T-DNA insertion in the fourth exon of the *AtMTN2*), *mtn2-2* (T-DNA insertion in the fourth exon of the *MTN2)* (Bürstenbinder et al., 2010). These single mutants, when grown on soil or germinated on sulfur-sufficient media containing 500µM $MgSO_4$, are phenotypically indistinguishable from the wild type (WT). However, when the sulfur source is 500µM MTA, *mtn 1-1* and *mtn1-2* are retarded with respect to both seedling and root

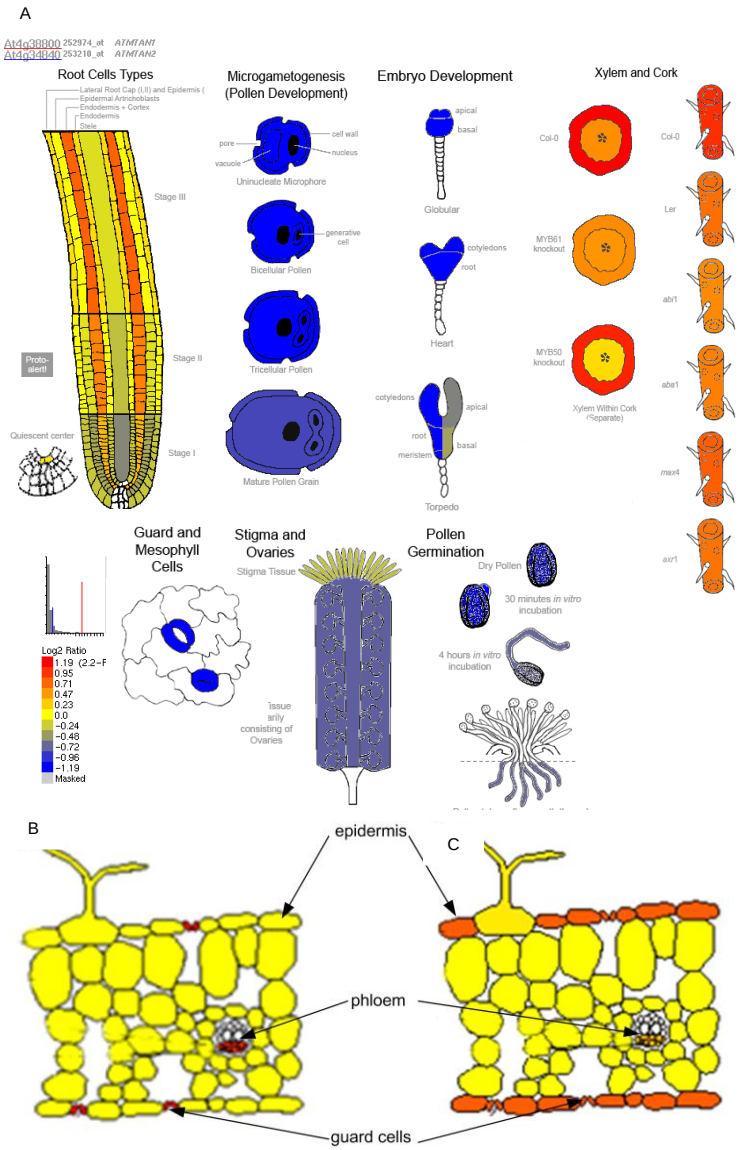

Figure 1.6: Expression pattern of the Arabidopsis MTNs in leaf tissues.

(A) Comparison of transcripts of MTN1 and MTN2 using the publicly available eFP Browser tool Based on the scale presented the abundance of MTN1 is indicated in shapdes of red colour while the MTN2s in shades of blue colour.

(B) MTN1 is preferentially expressed in phloem and guard cells based on the translatome expression patterns

(C) MTN2 is expressed in epidermal cells in addition to the phloem cells

growth (Bürstenbinder et al., 2010). The primary defect of *mtn* single mutants grown on MTA is altered PA metabolism while the NA levels and ethylene levels measured in four-day-old seedlings were not significantly different from those of the WT (Bürstenbinder et al., 2010). The *MTN*-deficient double mutant *mtn1-1mtn2-1* has a pleiotropic phenotype and developmental abnormalities when grown either on ½ Murashige and Skooog (MS) media or on soil. The most obvious defects include delayed bolting and sterility with underdeveloped siliques (Bürstenbinder et al., 2010). Part of the research outlined in this thesis documents in detail the developmental defects of *MTN*-deficient mutants in order to determine the role of MTN in plants.

1.4 Plant development and the role of hormones

A general description of WT Arabidopsis development, including reproductive and vascular milestones, is provided in the next two sections. The key hormone contributions to each of these development stages are also included where appropriate.

1.4.1 General growth and development

Since the work presented in this thesis involved the determination of the function of an enzyme for plant growth and development, it was critical to use well-defined developmental milestones. The Arabidopsis growth and development stages outlined by Boyes et al. (2001) have been used. These metrics provide a structure for identifying phenotypic differences that are a result of genotypic or environmental variations. As listed in Table 1.4, plant development from seed imbibition to plant senescence was categorized as different growth stages, which were adapted by Boyes et al. (2001) from a scale originally presented for crops and weeds (Lancashire et al., 1991). The time required for WT Columbia (Col-0) to reach each of these stages when grown under conditions that included a 16 h day was used as a reference. Figure 1.7 shows the phenotypes that correspond to the principal growth stages listed in Table 1.4.

1.4.2 Reproductive development

Plant reproduction depends on the formation of reproductive organs along with the male and female gametes that are produced within specialized structures in flowers. Because plant reproduction is strongly influenced by *MTN* deficiency and is thus a major focus of this research, the detailed developmental stages of flowers as described by Smyth et al. (1990) were followed (Table 1.5). These stages were used as a basis for determining when to harvest tissues for hormone, metabolite, and microscopic analyses.

1.4.2.1 Flower development

The mature Arabidopsis flower exhibits the simple structure of a typical Brassicaceae (Figure 1.8). It has a calyx and a corolla with four sepals and four petals, respectively. The six stamens vary in arrangement and length: the four medially arranged stamens are longer than the two relatively shorter laterally arranged ones. The gynoecia are superior with two carpels that enclose ovules.

1.4.2.2 Stamen and pollen development

Floral identity genes specify the stamen primordia at flower development stage 5 (Figure 1.9A). These primordial cells then differentiate to form a basal filament and an anther. An anther containing the male sporogenous tissue develops in two phases: microsporogenesis and microgametogenesis. During the microsporogenesis, morphogenesis and meiosis take place (Figure 1.10; Alvarez-Buylla et al., 2010; Sanders et al., 1999), and when the tetrads release microspores, microgametogenesis is initiated, which involves the maturation of microspores into pollen. During this process, the tapetum, which provided nutrients and structural components to the pollen mother cells, also nurtures the developing pollen. Elongation of the filament and enlargement of the anthers also occur simultaneously. Finally, the anther enters

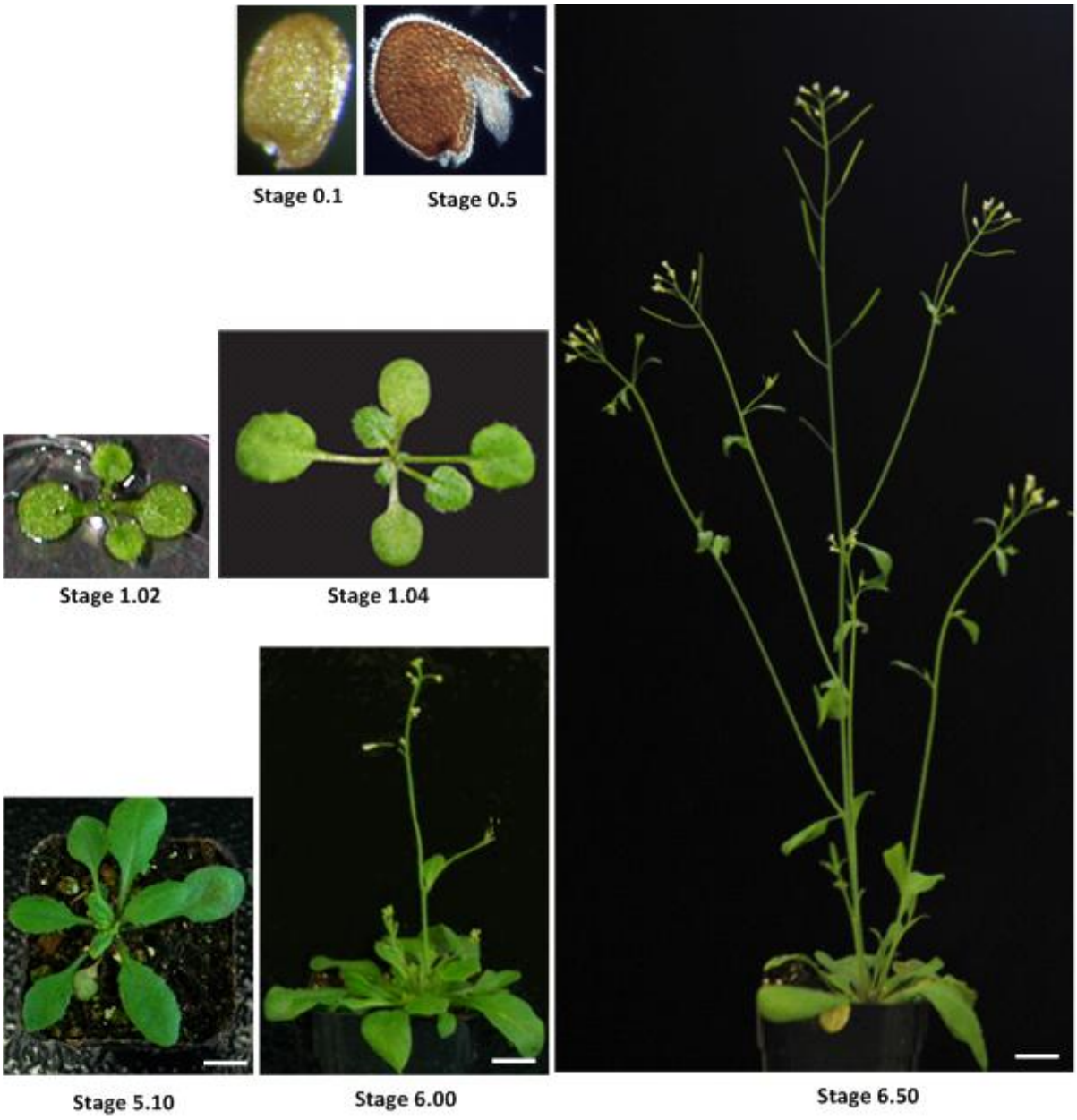

Figure 1.7: Representative growth stages of Arabidopsis

The growths staged are as described in Table 1.4. Scale bars = 12mm. Modified from Boyes et al, (2001).

Table 1.4: Arabidopsis growth stages on plates

*Average days from sowing, including three-day stratification at 4°C to synchronize germination. Plants were grown under standard long day conditions.

Stage	Description	Days (Col-0)*
Principal growth stage 0	Seed germination	
0.10	Seed imbibition	3.0
0.50	Radicle emergence	4.3
0.7	Hypocotyl and cotyledon emergence	5.5
Principal growth stage 1	Leaf development	
1.0	Cotyledons fully opened	6.0
1.02	2 rosette leaves > 1mm	10.3
1.04	4 rosette leaves > 1mm	14.4
Principal growth stage 5	Inflorescence emergence	
5.10	First flower buds visible	26
Principal growth stage 6	Flower production	
6.0	First flower open	31.5
6.5	50% of flowers are open	43.5
6.9	Flowering complete	49.4
Principal growth stage 9	Senescence	
9.7	Senescence completed with seeds ready to collect	ND

Data source: Boyes et al. (2001)

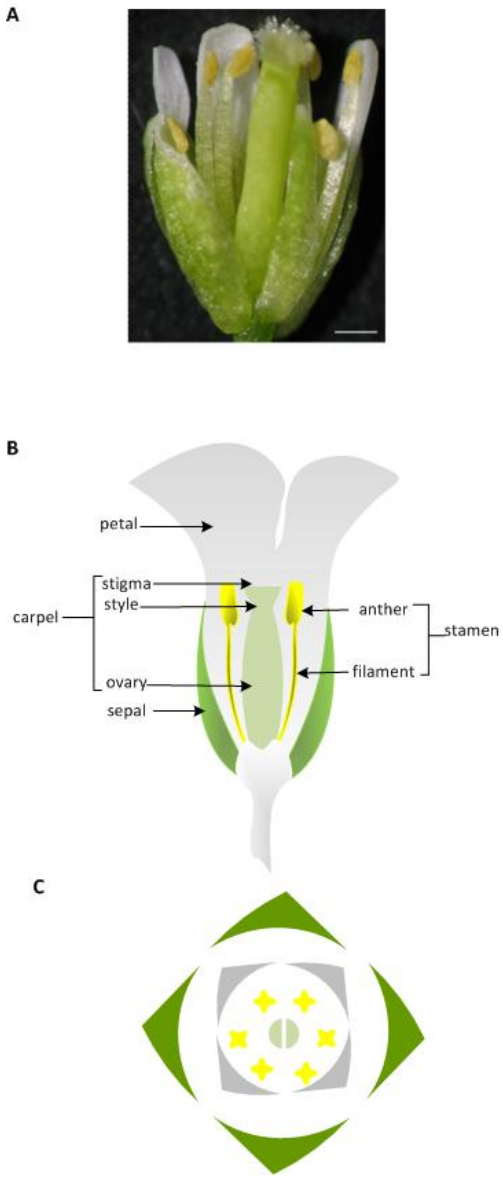

Figure 1.8: The Arabidopsis flower

(A) Mature flower at anthesis. Scale bar = 0.3mm.

(B) Cartoon of a lateral section through a mature flower, with organ types indicated

(C) Floral diagram showing the relative placement of floral organs. Organ types are colored as in (B). Modified from Irish et al. (2010)

Table 1.5: Summary of the stages of flower development

Flowers are collected from plants that are grown on standard long day conditions.

Stage	Landmark Event at Beginning of Stage	Duration (h)	Age of Flower at End of stage (days)
1	Flower buttress arises	24	1
2	Flower primordium forms	30	2.25
3	Sepal primordia arise	18	3
4	Sepals overlie flower meristem	18	3.75
5	Petal and stamen primordia arise	6	4
6	Sepals enclosed bud	30	5.25
7	Long stamen primordia stalked at base	24	6.25
8	Locules appear in long stamens	24	7.25
9	Petal primordia stalked at base	60	9.75
10	Petals level with short stamens	12	10.25
11	Stigmatic papillae appear	30	11.5
12	Petals level with long stamens	42	13.25
13	Bud opens, petals visible, anthesis	6	0.5
14	Long anthers extend above stigma	18	1
15	Stigma extends above long anthers	24	2
16	Petal and sepals withering	12	2.5
17	All organs fall from green siliques	192	10.5
18	Siliques turn yellow	36	12
19	Valves separate from dry siliques	Up to 24	13
20	Seed fall		

Data source: Smyth et al. (1990)

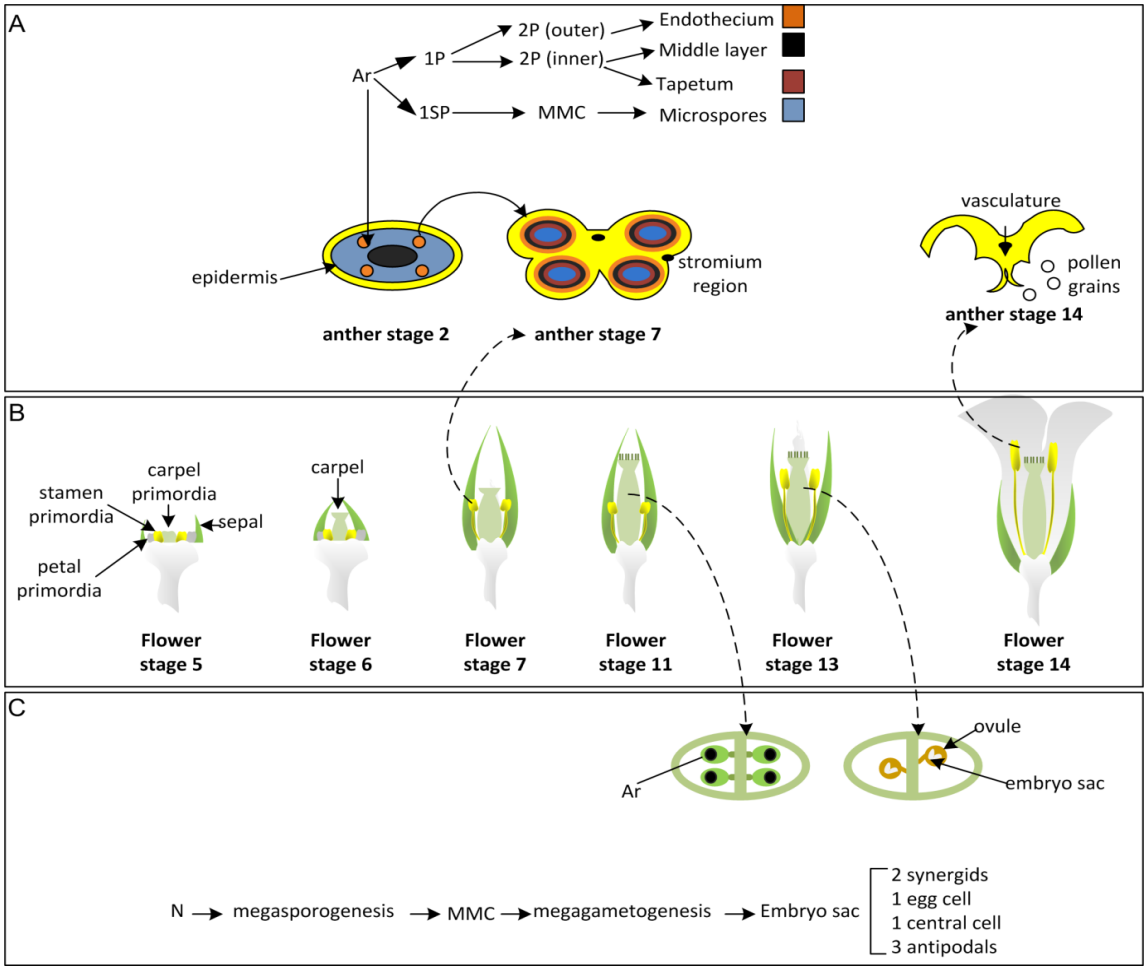

Figure 1.9: Development of Arabidopsis reproductive organs.

(A) Stamen development. When the anther is at stage 2 During stage 2, the four archesporial cells (Ar)arise in the L2 layer. Before meiosis these Ar cells divide and procuce the primary parietal layer (1P) and the primary sporogenous layer (1Sp). The 1P then divides into two secondary parietal layers (outer and inner, 2P) while the 1Sp generates the microspore mother cell (MMC).

(B) Flower stages according to Smyth et al. (1990)

(C) Carpel development modified from Alvarez-Buylla et al. (2010)

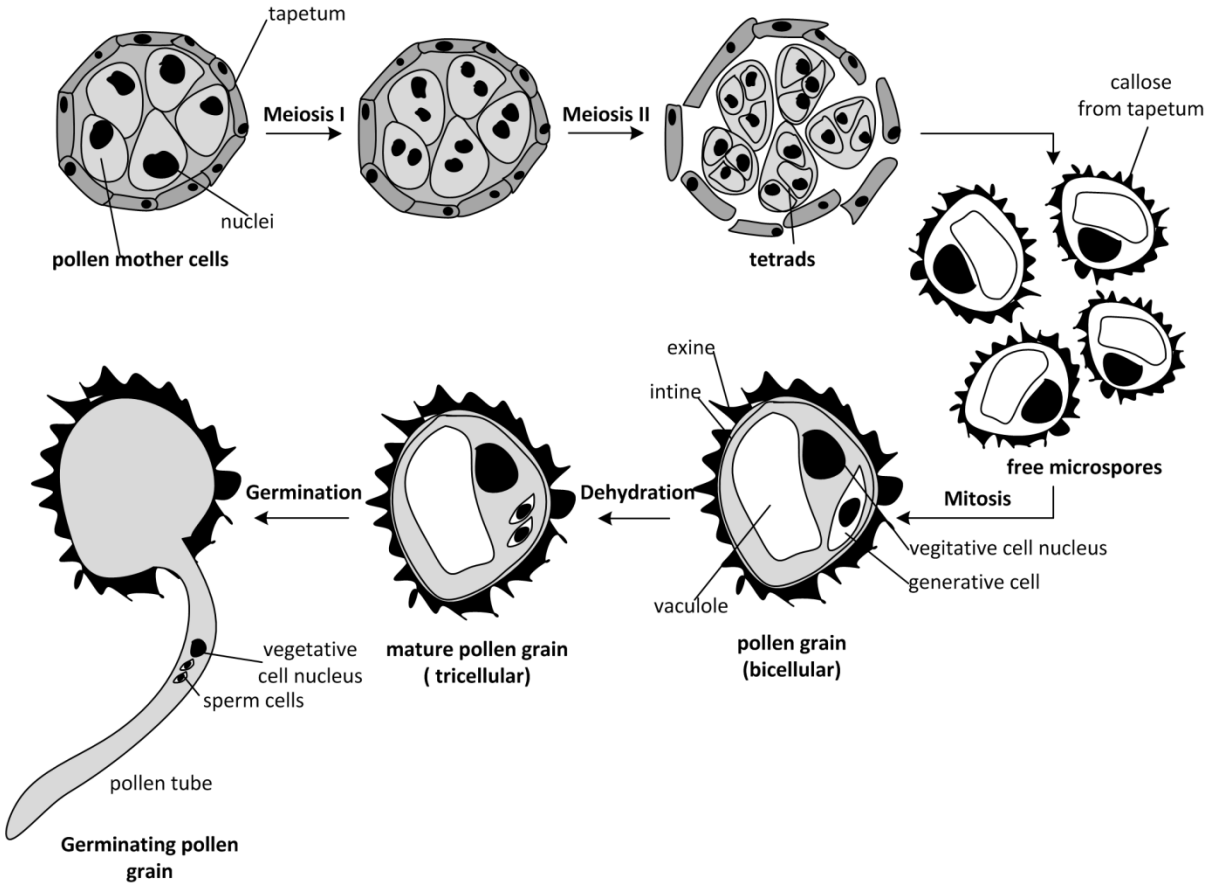

Figure 1.10: Pollen development

Modified from McCormick et al. (2004)

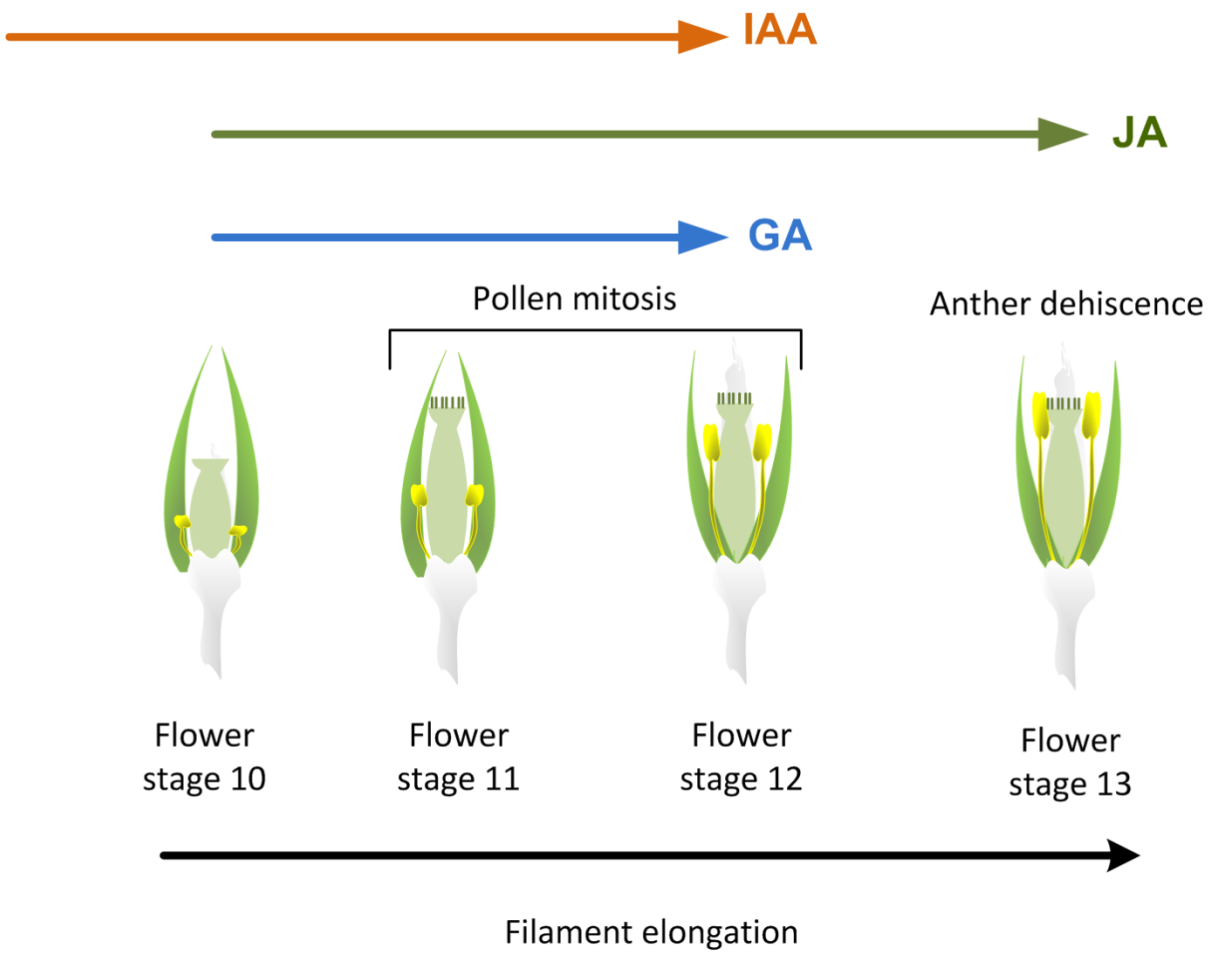

Figure 1.11: Hormones at a later stage of flower development

Modified from Alvarez-Buylla et al. (2010)

the dehiscence stage, releasing mature pollen (Goldberg et al., 1993). The later stages of stamen development are known to be under the control of hormones such as auxin (IAA), gibberellic acid (GA), and jasmonic acid (JA) (Figure 1.11; Alvarez-Buylla et al., 2010).

1.4.2.3 Carpel and embryo sac development

Carpel primordia, which are specified by the floral identity genes, develop into gynoecia with a central ovary, distal stigma with papillae, and a style that connects the stigma to the ovary (Alvarez-Buylla et al., 2010). The two carpels of the ovary are separated by a septum, and the ovules are attached to this septum by a placenta (Figure1.9C). At flowering stage 11, the inner and outer integuments of the ovules are formed, and these cover the nucellus completely by flowering stage 12, at which time megagametogenesis occurs (Figure 1.12; Bowman, 1994). The megasporocyte undergoes meiosis and produces four haploid megaspores. Three of these cells degrade while the remaining megaspore divides mitotically to generate the embryo sac (Figure 1.12). The embryo sac of the Arabidopsis contains seven cells representing four cell types: an egg cell, a central cell, two accessory synergid cells, and three antipodal cells. The development of these cells depends on the asymmetric distribution of auxin (Figure 1.12, Pagnussat et al., 2005). This auxin gradient depends on the auxin synthesis that takes place at specific locations, in contrast to the auxin efflux that produces auxin gradients in the remainder of the plant (Pagnussat et al., 2005).

1.4.2.4 Fertilization

During fertilization, two sperm cells from each pollen grain are delivered through a pollen tube into the embryo sac. One of these sperm cells fertilizes the egg whereas the other fertilizes the central cell (Costa et al., 2004; Berger et al., 2006). This double fertilization forms a diploid zygote, which gives rise to the future embryo, and a triploid endosperm, which forms nutritional tissue for the embryo.

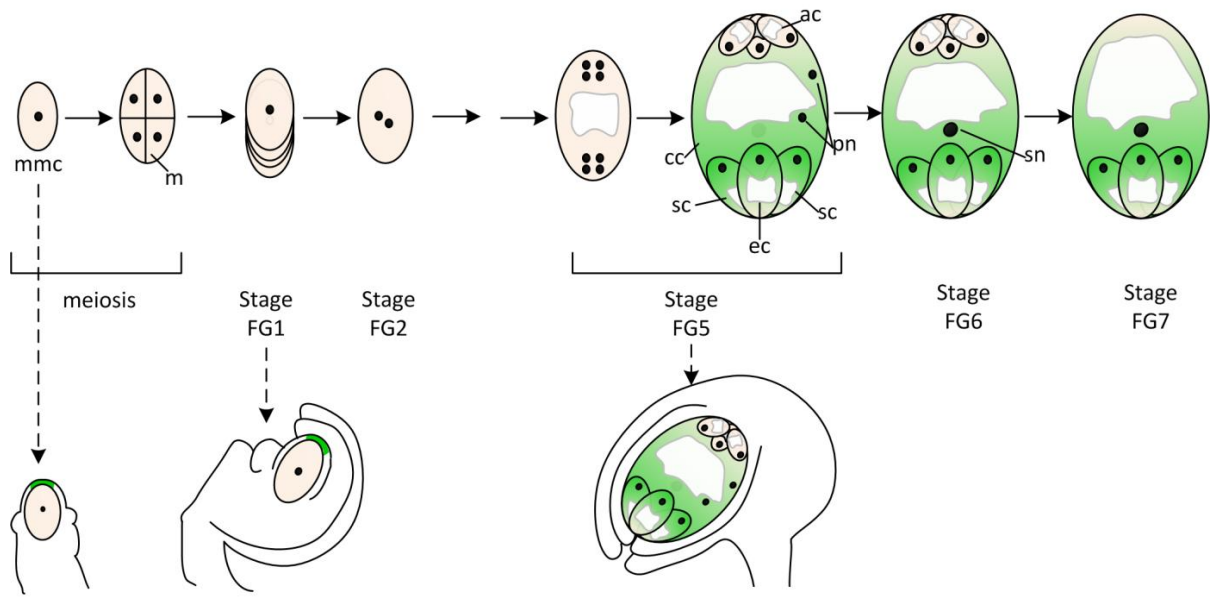

Figure 1.12: Embryo sac development

FG indicates female gametophyte; mmc, microspore mother cell; m, microspore; ac, antipodal cells; cc, central cell; ec, egg cell; pn, polar nuclei; and sc, synergid cells; sn, synergid nucleus. Modified from Pagnussat et al. (2009)

After fertilization, the ovary is called a silique, and the ovules are called seeds. These seeds are connected to the replum (septum) through a funiculus (placenta). The funiculus that provided the route for the pollen tube growth during fertilization now provides the route for nutrients from the maternal plant to reach the developing embryo.

1.4.2.5 Embryo development

The diploid zygote transforms into a mature embryo during the process of embryogenesis. During embryogenesis, many stages of embryos can be identified: pro embryo (8 cells), pre-globular (16 cells), globular (32 cells), transition, heart, linear, early curled, curled and mature (Figure 1.13). Three tiers can be identified at the proembryo stage: an apical tier, a basal tier, and suspensor cells (Figure 1.13). The apical tier gives rise to the shoot meristem and the adaxial side of the cotyledons while the basal tier forms the abaxial part of the cotyledons, hypocotyl, and the root and its meristem. The suspensor connects the embryo to maternal tissue. The periclinal divisions of the proembryo give rise to the protoderm and ground tissues of the pre-globular embryo. At the globular stage, the hypophysis which is the uppermost suspensor cell divides asymmetrically. In the transition stage, the radial symmetry of the proembryo changes to bilateral symmetry (Figure 1.13). Mature embryos consist of two cotyledons, plus an embryonic stem and root.

1.4.2.6 Auxin and PIN protein localization

The plant hormone auxin is responsible for many aspects of plant development and the ability of plants to adapt to ever-changing environments (Grunewald and Friml, 2011). The spatial distribution of this hormone is governed by polar auxin transport (PAT) which is central to the establishment of auxin gradients (maxima and minima). PAT occurs via the membrane localized auxin efflux carriers of PIN-FORMED (PIN) family proteins that direct auxin fluxes. A large number of internal and external signals is required for the determination of the polar

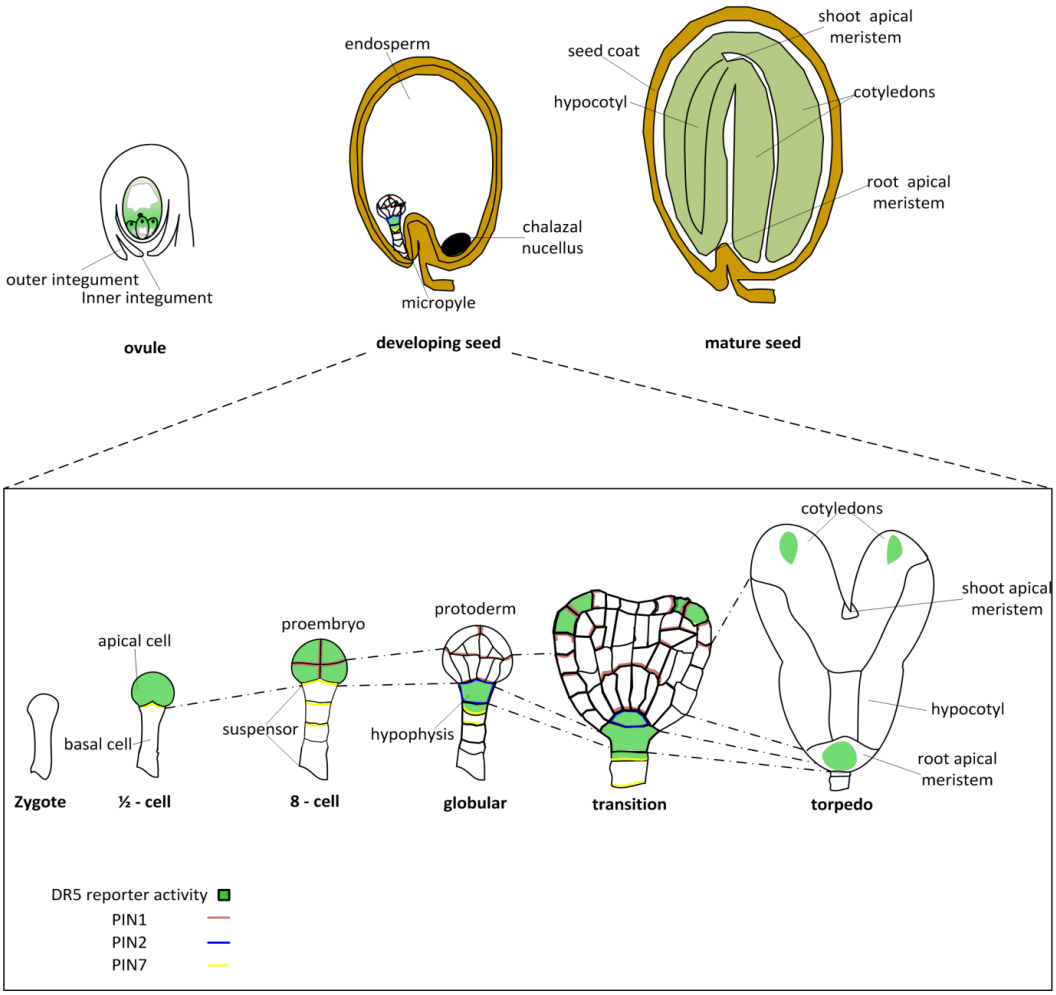

Figure 1.13: Arabidopsis embryogenesis.

Cartoon diagrams of ovule containing embryo sac, the developing seeds and mature seed. The embryo stages within the developing seeds were detailed along with localization of PIN proteins and DR5 activities. Adapted from Pagnussat et al. (2005).

localization of the PINs. The Adenosine diphosphate Ribosylation Factor- Guanine triphosphatase Activating Protein/ Guanine nucleotide Exchange Factor (ARF-GAP/GEF) family of proteins that mediate vesicle transport are essential for PAT and plasma membrane PIN localization. PIN proteins are not localized statically on plasma membranes but are recycled by endo-exocytosis between membranes and endosomes (Dhonukshe et al., 2007, 2008). GNOM/VAN7, an ARF-GEF associated with auxin signaling, determines the recycling of PINs from endosomes to either apical or basal membranes (Geldner et al., 2003; Kleine-Vehn et al., 2008). The serine-threonine kinase PINOID (PID) and Protein phosphatase2A (PP2A) determine the phosphorylation status of PIN proteins (Bennett et al., 1995; Benjamins et al., 2001; Friml et al., 2004; Michniewicz et al., 2007). Phosphorylated PIN proteins are targeted to the apical plasma membrane, whereas dephosphorylated PIN proteins are targeted to the basal plasma membrane.

During embryogenesis, PIN7 is the first PIN protein to be expressed upon zygote division, directing the auxin flow first into the apical cell and subsequently, by re-locating to reverse the auxin efflux, to the suspensor cells (Figure 1.13). PIN1 is expressed in the early stages, becoming basally localized in the pro-vascular cells next to the hypophysis by the globular stage. In the transition stage, PIN1 and PIN7are repositioned toward the flanks of the apical domain. At this same stage, PIN4 is expressed in the hypophysis and later PIN3 in the columella precursor cells. The directions of the auxin flow predicted by these PINs correspond with the expression of green fluorescent protein (GFP) directed by the synthetic auxin-responsive promoter DR5 in DR5*rev*::GFP transgenes (Figure 1.13). DR5 is a minimal promoter having multiple copies of the TGTCTC auxin response element whereas DR5*rev* consists of nine repeats of the DR5 element in reverse orientation directing expression of a modified GFP that is targeted to the endoplasmic reticulum (Friml et al., 2003). Improper auxin distribution disrupts the apical-basal axis of the embryos (Friml et al., 2003). Auxin continues to maintain its gradient even after germination

and organ initiation including the initiation of roots, leaf primordia, leaves, and inflorescences (Benkova et al. 2003). Auxin distribution is also critical for vascular formation (Scarpella et al., 2006), ovule development (Benkova et al., 2003), gamete specification (Pagnussat et al., 2005), fruit formation, and seed dispersal (Sorefan et al., 2009).

1.4.3 Vascular development

The vascular system is a network of cells that interconnects all major plant organs and provides a route for the transport of water, nutrients, and signaling molecules; it also contributes physical support to plants helping them remain upright and avoid the effects of pathogens (Figure 1.14; Berleth and Mattsson, 2000; Dengler and Kang, 2001; Fukada, 2004). The vasculature of an adult plant is pre-established in the embryo and differentiates at predictable positions and times during development. However, these arrangements can change in response to local signals (Fukada, 2004).

1.4.3.1 Establishment and maintenance of vascular stem cells

In plants, the establishment of vascular stem cells in the embryo is relatively less complex than the vascular arrangement that appears in mature plants (Goldberg et al., 1994). The genetic programs that establish these stem cells need to be active and continue post-embryonically. These genetic programs, including the regulatory networks of vascular stem cell initiation and establishment, have been studied extensively in recent years. The phytohormones auxin, cytokinin (CK), and brassinosteroids (BR), along with signaling components such as Leucine-Rich-Repeat (LRR), Receptor-Like Kinases (RLK), and the Clavata 3/ Endosperm surrounding region (CLE) peptide have been identified as key regulators of vascular development (Zhou et al., 2011).

1.4.3.2 Xylem and phloem tissue differentiation

All vascular tissues are derived from vascular stem cells (meristematic cells): pro-cambium and vascular cambium. Procambial cells give rise to the precursor cells of phloem or xylem depending on their position, with cell-to-cell communication playing a role in the determination of this position. For example, in most higher plant stems the phloem is positioned toward the periphery while xylem is isolated toward the centre. On the other hand, long-distance signaling plays a role in the formation of continuous vascular strands in the apical-basal direction. The xylem and phloem precursor cells become differentiated into distinct types of cells (Figure 1.15). Phloem precursor cells differentiate into the sieve tube elements, companion cells, phloem parenchyma and phloem fibres; all cells comprise the phloem tissue. Xylem precursor cells differentiate into xylem cells, which consists of tracheary elements (vessels and tracheids), xylem parenchyma, and xylem fibres. At maturity, the tracheary elements differentiate further through the deposition of secondary cell wall material and then undergo programmed cell death to form the hollow tubes that allow fluid movement. The cell wall thickenings of the tracheary elements, which may be annular, spiral, reticulate, or pitted, provide strength and keep these hollow tubes from collapsing (Demura and Fukuda, 2007).

1.4.3.3 Factors affecting vascular differentiation

Vascular cell differentiation depends on many factors, including auxin, transcription factors and Cks (Figure 1.16; Demura and Fukuda [2007]). Auxin triggers the vascular development program whereas the activity of the homeodomain transcription factor (HD-ZIP III) family directs the gene expression underlying the spatial information necessary for regulating cambial cell specification and proliferation. CK on the other hand initiates and maintains the procambial cells.

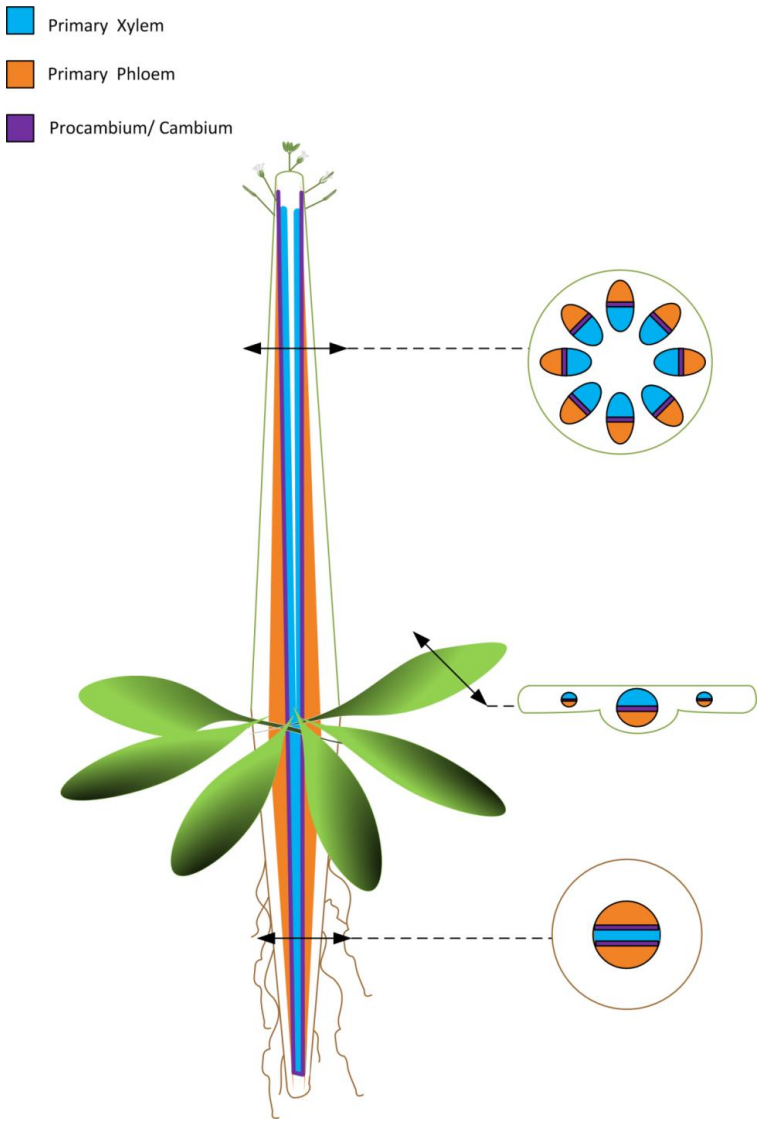

Figure 1.14: Schematic representation of the organization of the primary vascular tissues in Arabidopsis

Vascular tissue arrangement of the whole plant in longitudinal view together with cross-section of shoot, cross-section of leaf, and cross-section of root tip. Adapted from Nieminen et al. (2004).

1.4.3.3.1 Auxin

It is commonly thought that auxin ensures the continuation of vascular formation throughout plant life. MONOPTEROS (*mp*) is a mutant whose defects in auxin signaling and lower rate of auxin transport cause it to fail to establish vascular stem cells (Hardtke and Berleth, 1998); other mutants that fail to transport auxin, such as *pin1*/(PIN-FORMED1)*, trn1*/(TORNADO1), and *lop1*/(LOPPEDED), are also severely defective in vein formation (Galweiler et al., 1998; Carland and McHale, 1996; Cnops et al., 2006). Similar vein
phenotypes are evident in plants in which auxin transport is inhibited by 1-N-naphthylphthalamic acid (NPA, Mattsson et al., 1999). Moreover, mutants that cannot perceive auxin, such as *axr6/(*AUXIN RESISTANT-6), and *bdl/* (BODENLOS), are also incapable of proper vein formation (Hamann et al., 2002; Hamann et al., 1999; Hobbie et al., 2000). Thus, defects in auxin signaling, transport, and/ or perception have a significant effect on the formation of vasculature.

The common element that links these auxin phenotypes can be traced back to problems in PIN protein localization to the plasma membrane via vesicle transport (Figure 1.17; PIN trafficking; Grunewald and Friml, 2011). The PIN auxin efflux carriers are located on specific points on the plasma membrane that contact the basal end wall in both procambial cells and xylem parenchyma cells. Interestingly, PINOID is also expressed primarily in xylem precursor cells and xylem parenchyma cells. Thus, GNOM, which directs PINs to their proper apical basal membranes, and PINOID, which phosphorylates PINs, together determine the localization of PIN and ultimately establish the auxin gradients necessary for proper vascular differentiation, as detailed in section 1.4.2.6.

Dengler (2006) presented an auxin-based model that explains the relationship between the internal vascular arrangement and the external arrangement of lateral organs (phyllotaxis). For

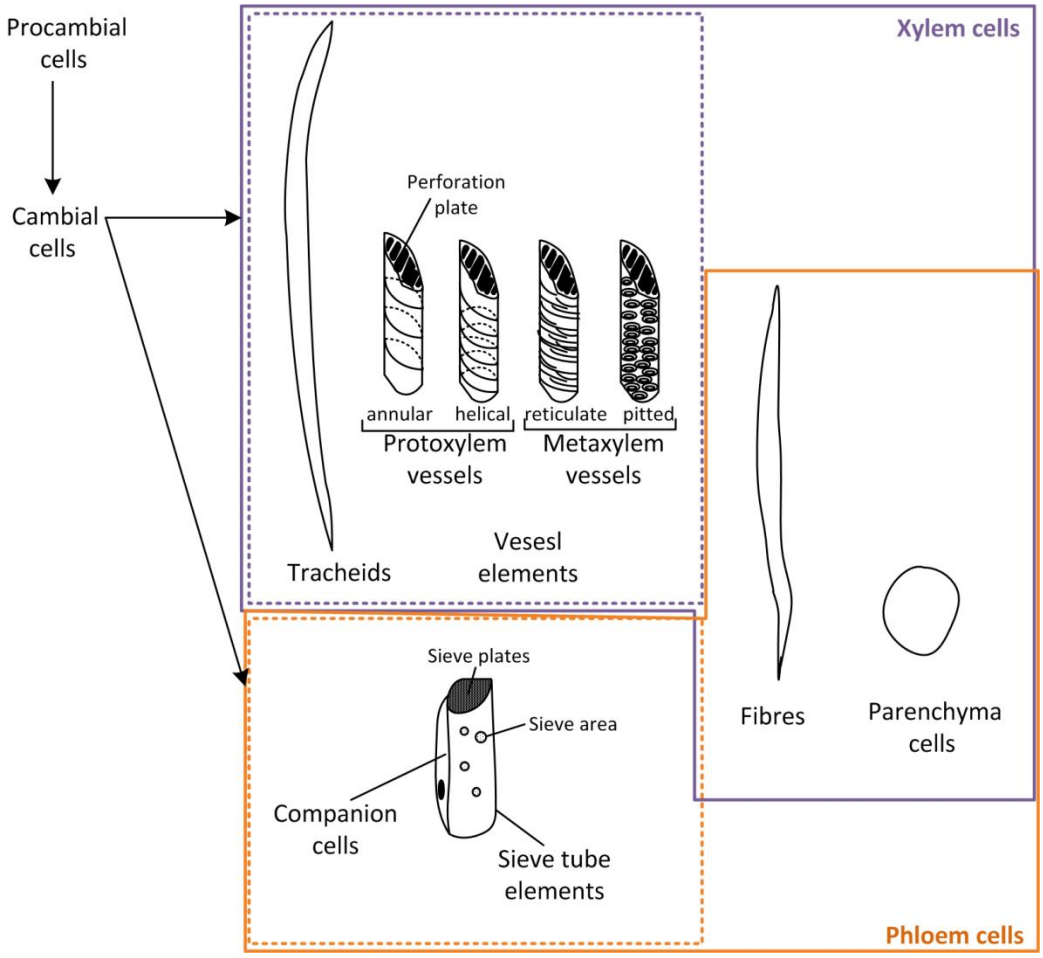

Figure 1.15: Schematic model of xylem formation.

Procambial cells produced cambial cells that differentiate into phloem cells and xylem cells. Xylem cells include tracheary elements (tracheids and vessel elements) and phloem cells include sieve tube elements and companion cells. Both fibres and parenchyma cells are part of xylem and phloem tissue. Based on the pattern of cell wall deposition two types of vessels are observed: protoxylem vessels commonly have annular and spiral wall thickenings and metaxylem vessels have reticulate and pitted thickenings. Modified from Demura and Fukuda, (2007).

example, a vascular bundle that is seen in the stem cross-section represents either an individual leaf trace or a parent strand that gives rise to a leaf trace. Based on the Dengler model auxin first moves uniformly towards the shoot apical meristem from regions outside of it, and then through the polar localization of PIN proteins, auxin is concentrated at points that identify the positions of forthcoming leaf primordia. Following the outgrowth of the primordia, the PIN proteins are redistributed toward the interior of the meristem along a narrow cell file to form the procambial strand of the future midvein (Figure 1.18).

1.4.3.3.2 HD-ZIP III family

Arabidopsis thaliana homeobox (ATHB) genes, ATHB8 and ATHB15, of the HD-ZIP III family are expressed strictly in the procambial or xylem precursor regions (Baima et al., 1995; Ohashi-lto and Fukuda 2004). In regulating cambial

activity, these transcription factors act antagonistically: overexpression of ATHB8 or down regulation of ATHB15 increases proliferation of xylem cells. Thus, members of the HD-ZIP III family together regulate the specification and proliferation of xylem.

1.4.3.3.3 Cytokinin

CK also plays a critical role in the formation and maintenance of procambial cells. The genes involved in CK biosynthesis are expressed in the tips of root vascular bundles (Mähönen et al., 2000). The CK receptor histidine kinase encoded by the *WOL/CRE1/AtHK4* (Mähönen et al., 2000) genes are expressed preferentially in the procambium whereas two other CK receptor genes (*AtHK2* and *AtHK3*) are expressed in vascular cells. CK also induces response regulators that negatively or positively control CK signaling responses in vascular tissues: ARR15 in procambial cells but not in xylem and phloem cells, and ARR16 in the pericycle. Taken together, these factors indicate that CK is a contributing regulator for the maintenance of procambial activity. In addition, CK also plays a role in the specification of phloem (Mähönen et al., 2000) and in the inhibition of protoxylem differentiation (Mähönen et al., 2006).

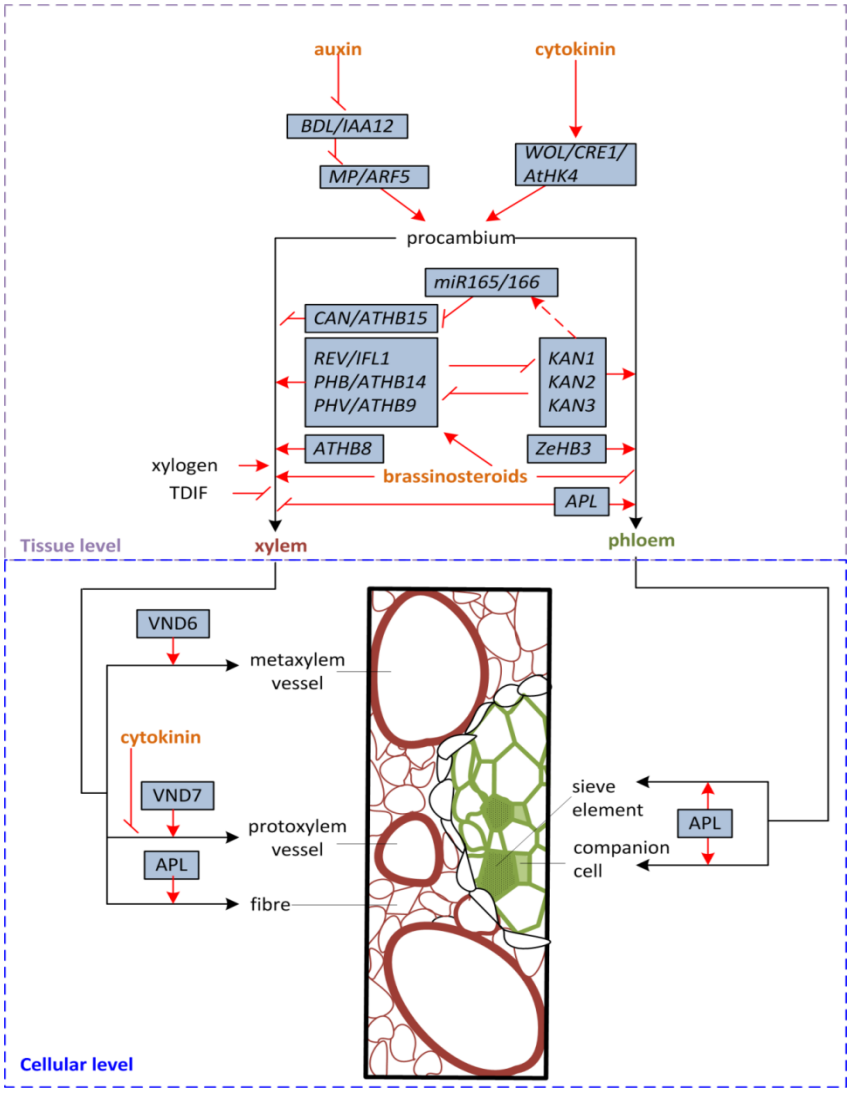

Figure 1.16: Factors effecting vascular development

Genes (blue boxes) and phytohormones (orange) interactions in xylem and phloem development both at cellular and tissue level are presented. Modified from Demura and Fukuda, (2007).

1.4.3.3.4 Brassinosteroids

The phenotype of BR biosynthetic and signaling mutants reveals that this steroid hormone is involved in promoting xylem differentiation (Caño-Delgado et al., 2004). BR biosynthesis-deficient mutants, *constitutive photomorphogenic dwarf* (*cpd*; Szekeres et al., 1996) and *dwarf7* (Choe et al., 1999), have decreased xylem formation. Yamamoto et al. (1997, 2007) report that BRs are involved in tracheary development such as secondary cell wall formation and programmed cell death. As well, the inhibition of BR signaling with brassinazole or the phenotype of BR receptor mutants (*bri*) has led to the suggestion that BRs specify xylem precursor cells in order to maintain a proper ratio between the phloem and the xylem (Asami et al., 2000; Caño-Delgado et al., 2004).

Ibañes et al. (2009) used mathematical modeling to show that the pattern of vascular bundle arrangement in Arabidopsis stem sections is coordinated by auxin and BR. Their model predicts that BRs affect vascular patterning by controlling the proliferation of pre-vascular cells. BR signaling mutants, *bri1* and *cpd,* have fewer pro-cambial cells, leading to the generation of fewer vascular bundles than in the WT.

In addition to the effects of auxin, HDZIP III, CK, and BR that are described above, many other factors including non-classical types of arabinogalactan proteins, xylogens, transcription factors (eg., NAC), and microRNAs have been implicated in vascular development (Figure 1.16). The contribution of the PA, Tspm, to vascular development is also of emerging importance (Zhou et al., 2011).

1.4.3.3.5 Thermospermine and plant development

Tspm that is generated from Spd is present in very low quantities in plants (Kakehi et al., 2008). Although PA genes have been reported to be preferentially expressed in phloem (Pommerrenig

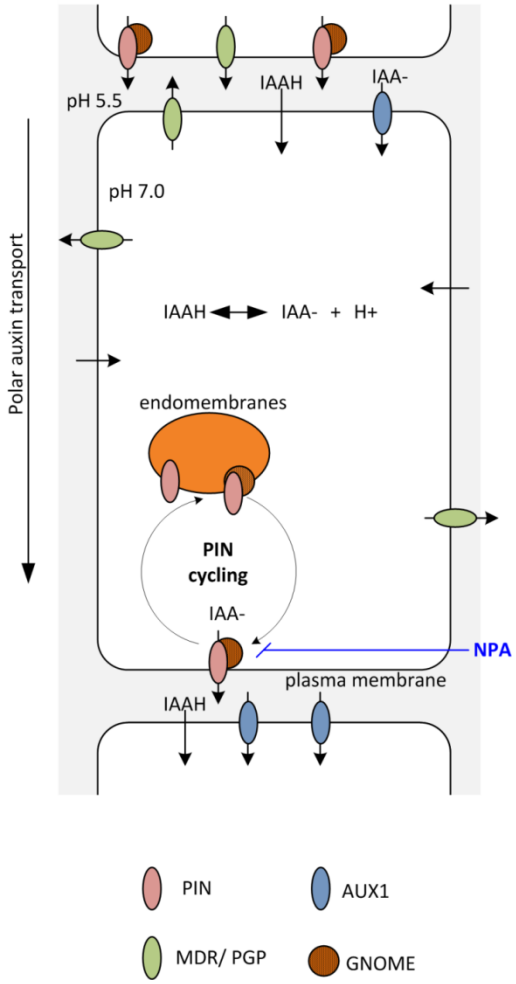

Figure 1.17: The molecular mechanism of auxin transport

Auxin can move from one cell to another either by diffusion (arrows) or via transmembrane proteins. Auxin influx carriers (AUX proteins) are localized to the apical membrane whereas auxin efflux carriers (PIN proteins) are localized to the basal membrane. This asymmetrical PIN localization causes a polarized flow of auxin. PIN proteins are recycled in cells: transported from endomembranes to the plasma membrane by endosomes. Modified from Fukuda (2004) and Berleth etal. (2000).

et al. 2011), studies with RNA *in situ* hybridization and GUS reporter gene analysis shows that *ACL5* is expressed specifically in the pro-cambium during embryogenesis, starting in early globular embryos and persisting into the bent cotyledon-staged embryo phase (Clay and Nelson, 2005). Its expression has also been detected during primary root development and early leaf development and in axillary buds and vascular bundles in stems. The recent high-resolution observation of ACL5 expression with *in situ* hybridization and GUS analysis of resin-embedded sections has revealed that the expression is specifically in the xylem vessel elements of the stems, hypocotyls, and in the transition zone between the silique and the pedicels (Muñiz et al., 2008). The ACL5 expression was visualized soon after the expansion of the vessel elements but before the initiation of the secondary wall deposition. Cross-sections of leaf midveins and of the inflorescence stems of *acl5* mutants show an increased number of xylem, phloem, and cambial cells (Hanzawa et al., 1997; Clay and Nelson, 2005). Interestingly, these mutants have reduced capability with respect to polar auxin transport (66.2 % compared to the WT) and an unregulated transcript level of five HDZIP III genes, including ATHB8 (~ 7 fold; Imai et al., 2006). In addition, Muñiz et al. (2008) provide evidence that Tspm prevents the premature maturation of the xylem vessels, thus supporting the premise that Tspm is involved in vascular development.

Based on the literature presented here, the MTN activity that links many critical pathways could potentially affect plant growth and development, specifically in the areas of reproduction and vascular development. However, the specific effects or modes of action in plants remain unclear.

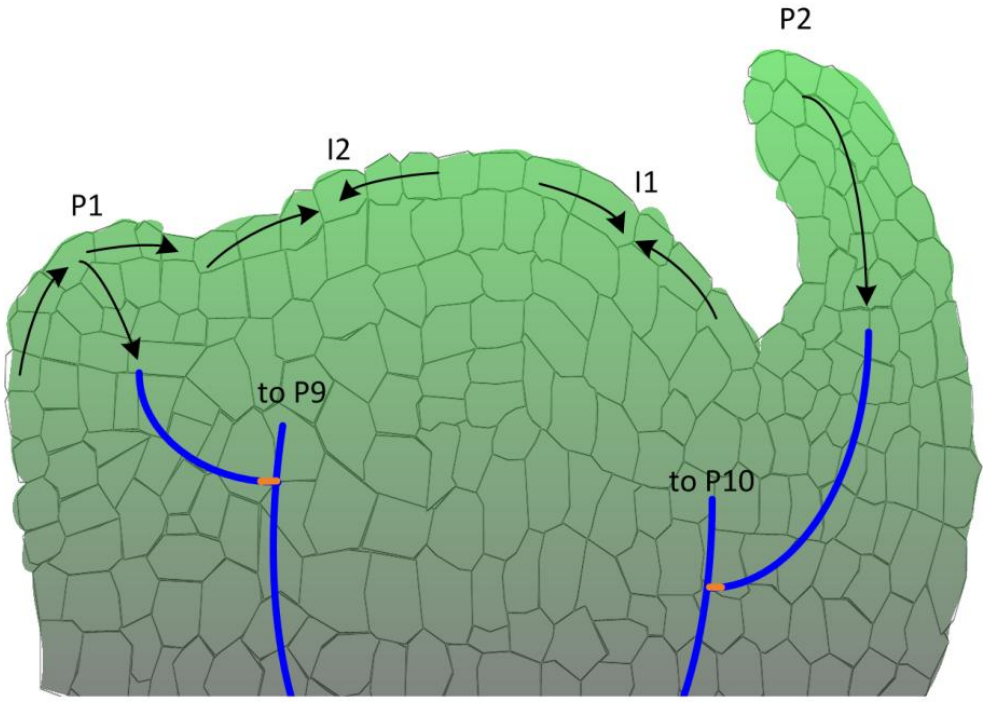

Figure 1.18: Model showing the direction of auxin movement, leaf primordia initiation, and vascular strand formation

Arrows show the auxin flow that is directed by the PIN1 proteins toward the centre of the incipient primordia (I1, I2) and toward internal tissues during primordia growth (P1, P2). The long blue lines indicate the parent vasculature; the short blue lines, the primordial vasculature; and the orange lines, the connecting procambium. Modified from Dengler (2006).

1.5 Objectives of the research

Most of the research work presented in this thesis was obtained by designing experiments with the aim of determining the functional significance of MTN in plant growth and development. The first two chapters contain the findings that address the following objectives:

1. To characterize the *MTN*-deficient *mtn1-1mtn2-1* mutant in detail.
2. To dissect the primary defect of *MTN*-deficiency in plant growth and development.

During this study I discovered that the application of exogenous Spd changed the sterile phenotype of *mtn1-1mtn2-1* to be fertile. Chapter 3 contains research findings to examine this Spd-dependent fertility recovery with the following objective.

3. To establish the basis behind Spd-dependent fertility recovery of *mtn1-1mtn2-*

Chapter 2: Recycling of methylthioadenosine is essential for normal vascular development and reproduction in *Arabidopsis thaliana*

2.1 Overview

5'-methylthioadenosine (MTA) is the common by-product of polyamine (PA), nicotianamine (NA) and ethylene biosynthesis. The methylthiol moiety of MTA is salvaged by 5'-methylthioadenosine nucleosidase (MTN) in a reaction producing methylthioribose (MTR) and adenine.. The MTN double mutant, *mtn1-1mtn2-1,* retains ~14% of the MTN enzyme activity present in the wild type, and displays a pleiotropic phenotype that includes altered vasculature and impaired fertility. These abnormal traits were associated with increased MTA levels, altered PA profiles and reduced NA contents. Exogenous feeding of PAs partially recovered fertility whereas NA supplementation improved fertility and also as reversed interveinal chlorosis. The analysis of PA synthase crystal structures containing bound MTA suggests that the corresponding enzyme activities are sensitive to MTA content. Mutant plants that expressed either MTN or human methylthioadenosine phosphorylase (which metabolizes MTA without producing MTR) appeared wild type, proving that the abnormal traits of the mutant are due to MTA accumulation rather than reduced MTR. Based on our results, we propose that the possible key targets affected by this increase in MTA content are thermospermine synthase and eukaryotic initiation factor 5A modification.

2.2 Introduction

The Met recycling pathway (or Yang cycle) is present in all types of organisms where its primary role is to recycle sulfur-containing metabolites (Albers, 2009). In most plants, bacteria and protozoa, 5'-methylthioadenosine (MTA) nucleosidase (MTN; EC 3.2.2.16) irreversibly hydrolyses MTA to methylthioribose (MTR) and adenine (Figure 2.1); the resulting MTR is phosphorylated to 5'-methylthioribose 1-phosphate (MTR-1P) by MTR kinase (MTK; EC 2.7.1.100). Recently, two novel enzymes that act as intermediate steps in generating Met from MTR-1P were identified and characterized: 5'-methylthioribose-1-phosphate isomerase and dehydratase-enolase-phosphate-complex1 (Pommerrenig et al., 2011). The activities of both enzymes, along with the others of the Yang cycle, are expressed primarily in phloem tissue but some are also weakly expressed in shoot bundle sheaths (e.g. MTRK) and leaf epidermis (e.g. MTN2).

In some eukaryotes, such as humans, MTA is converted to MTR-1P by methylthioadenosine phosphorylase (MTAP; EC 2.4.2.28). Continuous MTA metabolism is extremely important in mammals as loss of MTAP activity is associated with cancer (Bertino et al., 2011), while accumulation of MTA has been linked to tumor progression (Stevens et al., 2009).

MTA metabolism may be equally important to plants, as it is the by-product of polyamine (PA), nicotianamine (NA) and ethylene biosynthesis (Figure 2.1). PAs such as putrescine (Put), spermidine (Spd), spermine (Spm) and thermospermine (Tspm) are cationic organic molecules that are essential for plant development and stress responses. Some of the documented roles of PAs include vascular differentiation, embryogenesis, cell division and responses to abiotic stresses such as salt, osmotic, drought and wounding (Vera-Sirera et al., 2010; Takahashi and Kakehi, 2010). For example, recent evidence suggests roles for both Tspm and H_2O_2 produced from PA catabolism in the control of xylem differentiation (Muñiz et al., 2009; Tisi et al., 2011).

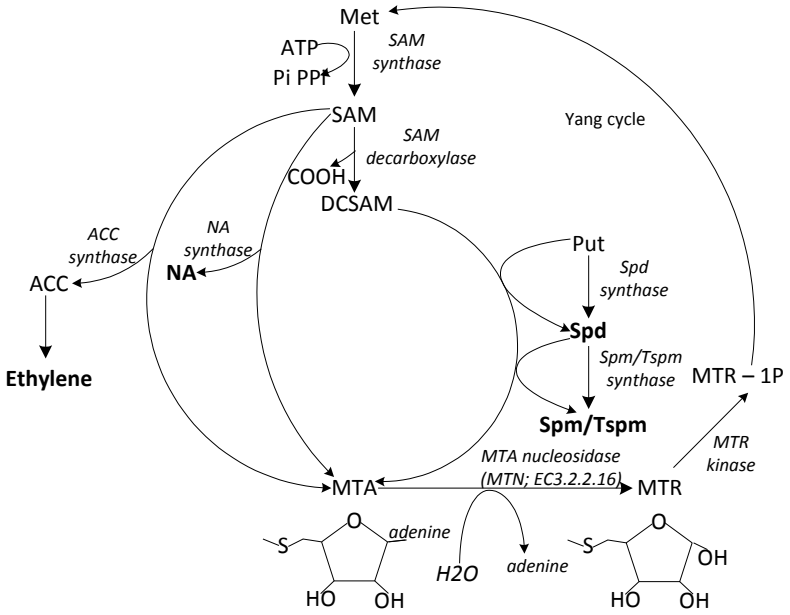

Figure 2.1: Overview of enzymatic reactions that generate 5'-methylthioadenosine (MTA)

MTA is generated as a by-product of polyamine (PA), nicotianamine (NA) and ethylene biosynthesis. 5'-methylthioadenosine nucleosidase (MTN, EC 3.2.2.16) hydrolyses MTA to 5'-methylthioribose (MTR) and adenine. The MTR is converted to Met through several steps, the first of which, MTR kinase (EC 2.7.1.100), catalyzes the production of MTR-1P. Methionineadenosyltransferase (EC 2.5.1.6) condenses Met and ATP to form S-adenosylmethionine (SAM). SAM decarboxylase (SAMDC, EC 4.1.1.50) removes carboxyl group from SAM to generate decarboxylated SAM (DCSAM). An aminopropyl group is transferred from DCSAM when putrescine (Put) is converted to spermidine (Spd) via Spd synthase (SPDS, EC 2.5.1.16). Similarly, another aminopropyl group is transferred from DCSAM when Spd is converted to spermine (Spm) or its isomer thermospermine (Tspm) via Spm synthase (SPMS, EC 2.5.1.22) or Tspm synthase (ACL5, EC 2.5.1.79) respectively. NA is produced from the condensation of three SAM molecules by NA synthase (NAS, EC 2.5.1.43). 1 amincyclopropane-1-carboxylic acid (ACC) is also derived from SAM by ACC synthase (ACS, EC 4.4.1.14) in the rate-limiting step in the biosynthesis of ethylene. The dotted line indicates that there are many steps involved in converting MTR into Met. The compounds that are in bold letters are the key compounds of interest in the present study.

PAs have also been implicated in RNA processing, chromatin remodeling, membrane fluidity and protein activation (Baron and Stasolla, 2008, Takahashi and Kakehi, 2010). NA, a product of another MTA generating reaction, is a metal chelator involved in long distance transport of ions. NA ion complexes ultimately support gametogenesis and embryo development (Curie et al., 2009 and Lan et al., 2011). Finally, ethylene is a phytohormone that impacts numerous processes, including seed germination, seedling growth, fruit ripening, flower development and abscission (Yang and Hoffman, 1984).

The Arabidopsis genome has two MTN-encoding genes (At4g38800 and At4g34840) that are annotated as *AtMTN1* (*MTN1*) and *AtMTN2* (*MTN2*), respectively (Rzewuski et al., 2007). Public microarray data indicate that *MTN1* transcripts are about 10 times more abundant than *MTN2* transcripts across different organs (Zimmermann et al., 2004). Using a northern blot of *MTN1* Oh et al. (2008) confirmed that *MTN1* is expressed in roots, stems, flowers and both cauline and rosette leaves. However, when the microarray data expression abundance of the MTN genes was compared in the tissues, *MTN1 and MTN2* were uniquely expressed in different tissues (Winter et al., 2007). *MTN1* is expressed in cortex of roots and xylem of stems. On the other hand, *MTN2* is expressed in apical basal tissues of embryos, developing pollen stages, stigma and ovules, and leaf guard cells (Winter et al., 2007). Recently it has also been shown that both *MTNs* are abundant in the phloem tissue (Pommerrenig et al., (2011). Although MTN1 and MTN2 polypeptide sequences share 64% amino acid sequence identity they have distinct substrate specificities and pH optima (Siu et al., 2008). Thus, it was initially inferred that these two enzymes may have distinct roles in plant metabolism: *in vitro* MTN1 accepts only MTA as a substrate while MTN2 can also accept *S*-adenosylhomocysteine to a limited extent (Siu et al., 2008). More recent crystallography and protein dynamic analyses revealed that MTN1 binds to *S*-adenosylhomocysteine but is incapable of hydrolysing it (Siu et al., 2011).

Recently we described the physiology of several single T-DNA insertion mutants in *MTN1* and *MTN2*: *mtn1-1* (T-DNA insertion in the third intron), *mtn1-2* (T-DNA insertion in the sixth exon),

mtn2-1 (T-DNA insertion in the fourth exon) and*mtn2-2* (T-DNA insertion in the fourth exon) (Bürstenbinder et al., 2010). Based on biochemical analyses, we established that MTN1 is responsible for 80% of the MTN activity in crude extracts of four-day-old seedlings and rosette leaves of three-week-old plants grown on media (Bürstenbinder et al., 2010). When grown on soil or germinated on sulfur sufficient-media containing 500µM $MgSO_4$, seedlings of single mutants were phenotypically indistinguishable from the wild type (WT). However, when the sulfur source is 500µM MTA, both *mtn1-1* and *mtn1-2* mutants have impaired seedling and root growth (Bürstenbinder et al., 2010). These MTN-deficient seedlings also have altered PA profiles with increased Put and Spm compared to seedlings grown on media containing 500µM $MgSO_4$. Interestingly, no significant changes in either NA content or ethylene production were detected in either *mtn1-1* or *mtn2-1*. In an attempt to lower MTN levels further, the two homozygous mutant lines were crossed and isolate a double mutant was isolated The resulting *mtn1-1mtn2-1* plants exhibited a pleiotropic phenotype with developmental abnormalities (Bürstenbinder et al., 2010). The details and physiological basis for these pleiotropic traits, in terms of MTN's enzyme activity and MTA regulation in general was unclear.

Here, we investigate the effect of MTN deficiency by a comprehensive examination of the development and physiology of the homozygous *mtn1-1mtn2-1* double mutant. In addition to measuring its residual MTN enzyme activity and profiling relevant metabolites, we analyzed the effect of MTA accumulation based on the estimated structures of Spd and Tsp synthases co-crystallized with this ligand. The effect of exogenous supplementation of relevant compounds on the mutant phenotype was tested to reveal abnormalities in the cellular metabolism of the MTN-deficient plants. The results of these analyses reveal the critical importance of MTA recycling maintaining the biosynthesis of NA and PAs that are essential for normal plant vascular development and reproduction.

2.3 Methods

2.3.1 Plant material and growth conditions

2.3.2 Microscopy

Seeds for *mtn1-1* (SALK_085385)and *mtn2-1* (SALK_071127)single *T*-DNA insertion lines used to generate *mtn1-1mtn2-1* were obtained from the Arabidopsis Biological Resource Center. The male sterile mutant, *apt1-3* (Moffatt and Somerville, 1998), was used for reciprocal crosses. All *A*rabidopsis seeds were surface sterilized with chlorine gas before sowing on plates with half strength MS medium solidified with 0.8% (w/v) agarose (Murashige and Skoog, 1962); these plates were incubated in the dark at 4°C for 48 h for seed stratification. On the third day after sowing, plates were transferred to a tissue culture chamber (TC7, Conviron, Winnipeg, Canada) under continuous light: 24h at 21^0C with 80µmol $m^{-2}s^{-1}$ photosynthetically active radiation for 10 days. Seedlings were then transplanted to individual pots (25 cm^2) containing a 1:1 soil mixture of Sunshine LC1 mix and Sunshine LG3 germination mix (SunGro Horticultural Inc, Washington, USA) and maintained in a growth chamber (Conviron, Winnipeg, Canada)under long day conditions: 16h at 22^0C with 150 µmol $m^{-2}s^{-1}$ photosynthetically active radiation. The plants were watered every two days and fertilized with 20:20:20 (N: P: K) fertilizer mix (Plant products Co Ltd, Brampton, Canada) once a week until maturity. Hydroponic experiments were set up as described in Pierre et al. (2003) and maintained in the same growth chambers.

To document the first obvious developmental defect of *mtn1-1mtn2-1* compared to WT, plate-based-growth and soil-based-growth assays were conducted as detailed in Boyes et al. (2001). In the plate-based assay the time taken to develop the first true leaves >1mm along with daily lengths of roots were measured over duration of 11 days. The reproductive defects were evaluated in the stage 14 flowers as described by Smyth et al. (1990).

Buds and rosette leaf samples were obtained from WT and *mtn1-1mtn2-1* plants two weeks after bolting unless otherwise stated. When sampled, WT plants were five-weeks-old whereas *mtn1-1mtn2-1* plants were approximately seven-weeks-old in order to similar developmental stages to be evaluated. Samples were collected before noon for all the experiments.

2.3.2.1 Bright- light microscopy

Developmentally similar (i.e., having the same number of first order veins arising from the mid vein) WT and *mtn1-1mtn2-1* rosette leaves and stage 14 pistils (Smyth et al., 1990) were first incubated in clearing solution (3:1, glacial acetic acid:ethanol [EtOH]) for 2 h. Upon clearing, the tissue was rehydrated by moving it from 70% EtOH to water in a gradient series of 15 min intervals each, and softened by incubating overnight in 8 M NaOH. For visualization, leaf samples were then stained with 0.1% (w/v) Toluidine Blue O (TBO; pH 6.8) for 15s and observed with a Zeiss Axiovert 200M microscope (Carl Zeiss Inc, Toronto, Canada). The ovules of the cleared pistils were observed with Differential Interference Contrast (DIC) optics of a Zeiss Axiovert 200M microscope.

The same stage leaves of both genotypes were fixed in solution (50 mM sodium cacodylate, 2% paraformaldehyde [w/v, pH 7], 0.1% glutaraldehyde) for 1 h under vacuum at room temperature (RT). The samples were then transferred to fresh fixative and incubated overnight at 4°C. After the appropriate amount of fixation, the samples were dehydrated in a series of EtOH under vacuum at RT, going from 10 to 70% EtOH in 15% intervals for 1 h each. The samples were left in 70% EtOH and 0.2% eosin overnight at 4°C. Once fully dehydrated, the tissue was slowly infiltrated with LR White plastic resin (hard grade, Canemco, Mississauga, Canada), in a series of EtOH to resin volumes: 3:1, 1:1, 1:3 for 2 h each, then 100% LR white for 1 h, then in fresh LR overnight. Once the samples were fully infiltrated with resin, the LR white was refreshed and the samples were polymerized in a 60-65°C oven for 2-24 h. Once the resin

had hardened, tissue was sectioned at 1 µm thickness using an ultramicrotome (UltracutE, Reichert, New York, USA) and stained with TBO for observation with Zeiss Axiovert 200M microscope.

2.3.2.2 Scanning Electron Microscopy

Anthers of stage 14 flowers from WT and*mtn1-1mtn2-1*were placed in fixative (4% [w/v] paraformaldehyde [pH 7], 2% [w/v] glutaraldehyde, 1x potassium bisulphite) for 1 h under vacuum at Room Temperature (RT). Upon replacing the fixative solution, the samples were left to incubate overnight at 4°C. The tissue was then dehydrated in a 10% ethanol gradient (50% - 95%) at 30 min intervals under vacuum. Upon reaching 95% EtOH concentration, samples were left overnight at 4°C.The samples were then moved to HPLC-grade acetone for 2 h at RT. The samples were dried using a mass critical point dryer, mounted on 2″ stubs and sputter coated with gold particles. The tissue was visualized using a Hitachi S570 scanning electron microscope.

2.3.2.3 Laser Scanning Confocal Microscopy

The expression patterns of *DR5rev::GFP*stem sections of both WT and *mtn1-1mtn2-1* backgrounds were observed using a Carl Zeiss LSM 510 confocal microscope (Carl Zeiss Inc. Jena, Germany). The GFP signals were excited with an argon ion laser at 488 nm, and emissions were captured with a 505/530 nm band pass filter. Chlorophyll autofluorescence was also excited at 488 nm and was a captured with 650 nm long pass filter.

2.3.3 Chemical complementation experiments

Seeds were placed on ½ MS media supplemented with one of the following chemicals: 20 µM of NA (crude KI extract, see below), 20 µM of WT extract, 100 µM Spd, 100 µM Spm, and 50 µM Tspm. After two days of cold incubation these plates were transferred tocontinuous light for 21 days. The seedlings were then transplanted to soil or hydroponic media and grown under long

day conditions. In the case of soil-grown plants, chemicals were supplied daily as drops (~20µl) in ½ MS to each vegetative and reproductive meristems over a period of 3-4 weeks. However, Tspm was not applied as daily drops due to its limited availability.

2.3.4 Extraction of NA from K1 plants

NA-overproducing Arabidopsis transgenic lines (K1, Pianelli et al., 2005) were grown until the full rosette stage. NA was extracted from the rosette leaves ground in 80^{o}C; corresponding extracts from WT leaves were used as controls. The K1 extract were quantified and had 50 pmol mgFW^{-1} NA compared to WT and neither KI nor WT extracts contained detectable PAs, indicating that the K1 is a unique source of NA.

2.3.5 Complementation of *mtn1-1mtn2-1*

For complementation, pMTN1::MTN1, UBQ10::MTN1 coding sequences (CDS) and UBQ10::hMTAP CDS were introduced to *mtn1-1mtn2-1* mutants. The UBQ10(AT4G05320) promoter (693bp) was amplified using UBQ10pF and UBQp blunt R primers (Table S1) and cloned in to pSAT5.nosP.RNAi.nosT (EUO49865) with *Age*I and *Hinc*II to generate pSAT5.UB10p.nosT.This vector was then used to introduce the UBQ10 promoter for MTN1 and hMTAP CDSs. Binary vectors pGreenII 0229 (www.pgreen.ac.uk) and pPZP-RCS2-BAR (CD3-1057, Arabidopsis Biological Resource Centre) were used for *Agrobacterium*–mediated transformation.

Genomic MTN1 was amplified using the following primers: gMTN1-F and gMTN1-R (Table S1). The 1.9 kb genomic MTN1 fragment with162 bp of promoter was then digested with *Spe*1 and *Bam*HI and cloned directly into binary vector pGreenII 0229. The MTN1 cDNA was amplified with the following primers: MTN1CDS-F and MTN1CDS-R (Table S1). The resulting 0.8kb fragment was digested with *Xma*I and *Bam*HI and cloned first into pSAT5.UB10p.nosT.

After (Table S1), cloned into the *Sma*I site of pSAT5-UBQ10p-nosT and the resulting UBQ10::hMTAP cassette inserted into pPZP-RCS2-BAR.

sequencing, the UB10p::CDS cassette was transferred top PZP-RCS2-BAR. Similarly, the 0.8 kb hMTAP cDNA fragment was amplified from hMTAP cDNA with hMTAP-F and hMTAP-R primers MTN1 constructs were introduced into *Agrobacterium* strain GV3101Soup, while UBQ10::MTN1CDS and UBQ10::hMTAP were placed in *Agrobacterium* strain GV3101. Homozygous *mtn1-1* plants were transformed with their respective *Agrobacterium* strains using the floral dipping method (Bechtold et al, 1993). Transgenic T1 individuals were selected for by spraying 10 day-old soil grown seedlings with 40 mg/ L Basta (Glufosinate Ammonium, Wilson laboratories inc. Dundas, Canada). The expression of MTN1 and hMTAP in the surviving T1 plants was confirmed by immunoblot, and successful transformants were crossed with *mtn1-1/mtn1-1MTN2-1/mtn2-1*plants. The resulting F1 progeny was germinated on media containing Basta and genotyped by PCR to identify *mtn1-1mtn2-1* F2 individuals. F2 seeds of three lines were selected and screened on Basta supplemented MS media and genotyped to identify *mtn1-1mtn2-1*seedlings.

2.3.6 RT-PCR

Total RNA was extracted from leaves and buds of WT and *mtn1-1mtn2-1* plants using Tri Pure Isolation Reagent (Roche). Two micrograms of total RNA was used for first strand synthesis with SuperScript^{TM} reverse transcriptase (Invitrogen) according to the manufacturer's instructions. PCR reactions were performed as described in Bürstenbinder et al., 2007 using AtMTN1-F3, AtMTN1-R3, AtMTN2-F1, AtMTN2-R1 and Actin 8F and Actin 8R primers (Table S1) to determine the transcript abundance of *MTN1* (851bp), *MTN2* (306bp) and actin (700bp).

2.3.7 MTN enzyme assay

Bud protein extracts were prepared from developmentally matched flowering plants in 50mM potassium phosphate buffer [pH 7, Bürstenbinder et al., 2010]. Twenty micrograms of soluble a DU530 spectrophotometer (Beckman Coulter, Krefeld, Germany) at 470 nm modified from the protocol outlined in Bürstenbinder et al. (2010).

protein from buds was used to determine MTN specific activity using a xanthine oxidase-coupled enzyme assay (Lee et al., 2005). Absorbance was measured every 10 min over 1 h with

2.3.8 Polar auxin transport assay.

Polar auxin transport in primary inflorescence stem segments of WT, *mtn1-1mtn2-1,* and *tkv* was measured using a modification of procedure provided by Okada et al. (1991) method as described in Clay and Nelson (2005). The inflorescence stem segments were immersed in ^{14}C labeled IAA (Sigma) in either an acropetal or basipetal orientation. After 19h of incubation, the uppermost 5mm of the stem segments were removed and incubated overnight in liquid scintillation cocktail (Cytoscint, MP Biomedicals, and Toronto, Canada). Released radioactivity was counted using a scintillation counter (Model LS 1701, Beckman, Munich, Germany).

2.3.9 Immunoblot analysis

Ten micrograms of total soluble protein was extracted as described above, separated on a 12.5% SDS polyacrylamide gel (Laemmli, 1970) and transferred onto a polyvinylidenedifluoride membrane using a semi-dry electro-blotting system (Bio-Rad laboratories, Mississauga, Canada). The membrane blot was cut near the 34 kDa marker so the bottom portion could be incubated for 2 h with anti-MTN1 (1: 2500) antibody, while the top portion was incubated for the same time with monoclonal antibody for actin (MP Biomedicals, Toronto, Canada; 1: 3000). Bound antibodies were detected following incubation with horseradish peroxidase-conjugated

secondary antibodies, using the ECL Plus Western Blotting Detection System (GE Healthcare, Mississauga, Canada) and Amersham Hyperfilm^{TM} ECL.

2.3.10 Two- dimensional electrophoresis

Protein was extracted using phenol followed by ammonium acetate-methanol precipitation as described by Zheng et al., (2007). focusing on a Multiphore II system (GE Healthcare, Mississauga, Canada) using immobiline dry strip gels with non-linear pH gradients (pH 4-7NL). Protein was quantified using RC/DC protein assay kit (Bio-Rad laboratories, Mississauga, Canada). These proteins were then separated based on isoelectric These strips were placed on SDS polyacrylamide (12.5%) gels as detailed in Zheng et al., (2007). The separated proteins were then blotted as described for immunoblot analysis above. The membrane blot was then incubated overnight at 4^0C, with eIF5A specific primary antibody (1: 3000).The blots were detected as described above. Digital images of these films were analysed using Image Quant TL analysis software (GE Healthcare, Mississauga, Canada).

2.3.11 Determination of PA content

Rosette leaves and inflorescences of WT and *mtn1-1mtn2-1* were mixed with 5% (v/v) perchloric acid at a ratio of 1:4 (w/v) and frozen at -20^o C. Samples were further processed and Put, Spd and Spm were quantified by high performance liquid chromatography as described by Minocha et al. (1990, 1994).

2.3.12 Determination of NA content

Nicotianamine was extracted from leaves and inflorescences of the WT and *mtn1-1mtn2-1* plants and quantified after labeling with 9-fluorenyl methyl chloroformate as described in Supplementary material S1 of Klatte et al. (2009).

2.3.13 Determination of MTA content

Leaves and inflorescences of the WT and *mtn1-1mtn2-1* plants (0.1 g) were ground in liquid nitrogen to a fine powder, which was extracted with 1 ml of 0.1 M HCl for 15 min at 4°C. Cell debris were removed by centrifugating twice at 28,000 g for 15 min at 4°C. MTA was determined as described in Rzewuski et al. (2007) using the same HPLC system.

2.3.14 Detection of metal contents

Samples were dried for constant weight at 60^{o}C, and subjected to acid digestion with Omni-Trace1 nitric acid (EMI Scientific), and then heated to 85 – 90^{o}C. Nitric acid blanks were processed to ensure that metals were not added during sample preparation. The standardsTomato (NIST Standard #1573a) and Corn (NIST Standard # 1573a) leaves were also processed without sample to quantify the recovery of Zn, Cu, Mn and Fe during the extraction procedure. Filtered samples were prepared and analyzed for metals as described by Gadapati and Macfie (2005) by inductively coupled plasma atomic emission spectroscopy (ICP-AES).

2.3.15 Modeling of MTA inhibition for Tspm synthase and Spd synthase 1

A 3-D model of ACL5 was built by Swiss-Model suite (Arnold et al., 2006) using the crystal structure of PA aminopropyl transferase from *Thermus thermophilus* (PDB ID 1UIR; Ohnuma et al., 2011) as a template (39% identity). The crystal structure of *Arabidopsis* Spd synthase1 is available in PDB (PDB ID 1XJ5). To obtain Tspm synthase-MTA and Spd synthase1-MTA complexes, MTA was docked using DOCK 4.0 (Ewinget al., 2001). Programs COOT (Emsley and Cowtan,2004) and PyMOL(DeLano Scientific, San Carlos, Canada) were used for structure visualization and figure preparation.

2.4 Results

2.4.1 MTN activity in *mtn1-1mtn2-1* mutants reflects decreased transcript and protein abundance

RT-PCR was performed on cDNA isolated from the buds and rosette leaves of WT and *mtn1-1mtn2-1* plants. In both organs, *MTN1* transcript levels were higher than *MTN2* in the WT background (Figure 2.2A). A comparison of transcript abundance in *mtn1-1mtn2-1* revealed substantially decreased *MTN1* and undetectable levels of *MTN2* in both leaves and buds. Immunoblot analysis (Figure 2.2B) showed a similar abundance of MTN1 protein in WT leaves and buds but reduced levels in *mtn1-1mtn2-1*. Interestingly, MTN-deficient buds had higher amounts of MTN1 than leaves. As documented previously by Bürstenbinder et al. (2010), MTN2 protein cannot not be detected in either WT or *mtn1-1mtn2-1* tissues by immunoblotting with the appropriate antibody.

WT and mutant bud extracts were assayed for MTN enzyme activity to determine whether or not this correlated with MTN protein abundance and phenotype. Floral buds were chosen for the assay based on preliminary studies indicating that this organ had the highest MTN specific activity (Figure S1). Compared to the 7 - 8% retained MTN activity observed in *mtn1-1* seedlings grown on MTA (Bürstenbinder et al., 2010), *mtn1-1mtn2-1* buds had 14% residual MTN activity (1.21 ± 0.27 nmol mg^{-1} protein min^{-1} in WT; Figure 2.2C). Thus our results show that *mtn1-1mtn2-1* is a knock-down mutant, with MTN1 contributing to the residual MTN activity. Attempts to create a mutant completely lacking MTN activity by crossing homozygous knock-out lines, *mtn1-2* and *mtn2-2,* failed due to embryo lethality.

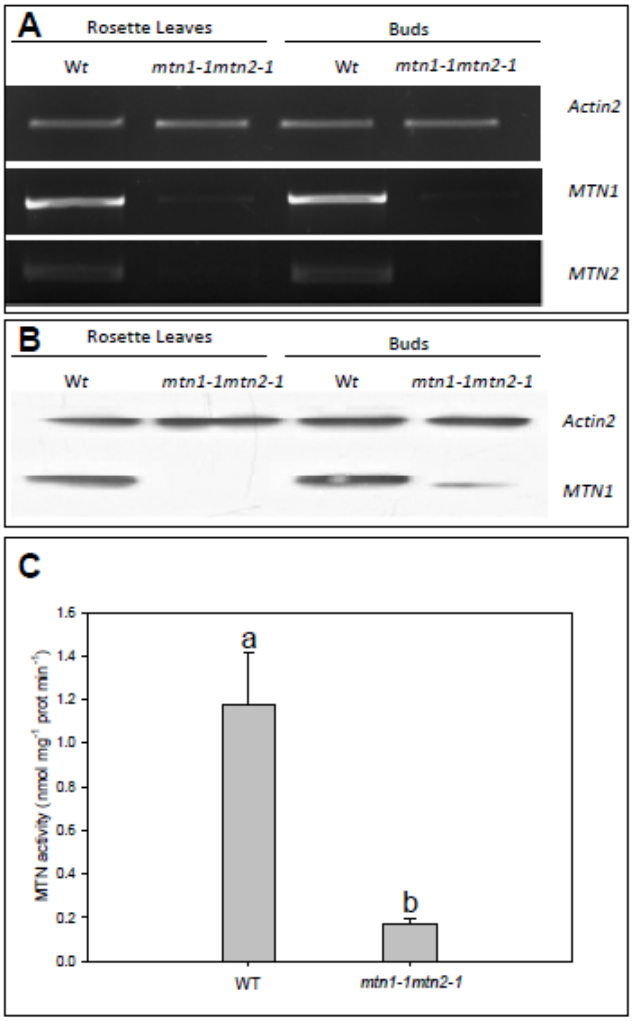

Figure 2.2: MTN transcript and protein abundance with corresponding enzyme activity

Results are averages (± SD) of 3-10 independent biological replicates.

(A) RT-PCR showed that *MTN1* and *MTN2* transcript abundance was reduced in *mtn1-1mtn2-1*. Actin was used as the reference gene to ensure equal loading of the cDNA. N=3.

(B) Immunoblot analysis indicated that MTN1 was present in buds and leaves of WT. In *mtn1-1mtn2-1* MTN1 was considerably lower in buds and undetectable in the leaves. Detection of actin protein confirmed equal protein loading. N=3.

(C) Specific enzyme activity of MTN1 was measured in buds harvested from plants two-weeks after bolting. Statistically significant variables are indicated by different letters ($P < 0.05$; $N = 10$).

2.4.2 MTN deficiency affects both vegetative and reproductive development

The *mtn1-1mtn2-1* mutants developed no obvious defects until the formation of the first true leaves. Subsequently an array of abnormalities developed upon activation of the floral meristem. Here we focus on the changes in vascular development and reproduction.

2.4.2.1 Vegetative phase phenotypes

Ten days after germination (DAG), the first true leaf of WT seedlings is greater than 1 mm in length (stage 1.02 described in Boyes et al., 2001; Figure 2.3A). In comparison to WT, *mtn1-1mtn2-1* seedlings did not reach this stage until 12 days after sowing. In addition to their delayed development, the first true leaves of *mtn1-1mtn2-1* exhibited interveinal chlorosis (Figure 2.3B): a condition where the veins of the leaf remain green while the area between the veins becomes yellow in color. This chlorosis was most notable in emerging young leaves when seedlings were grown on ½ strength Murashige and Skoog (MS; Murashige and Skoog, 1962) medium (as opposed to soil). Upon maturation of the leaves or transfer of the plants to soil, the interveinal chlorosis gradually disappeared.

As the *mtn1-1mtn2-1* mutants matured, abnormalities of the rosette leaves became apparent. Clearing and observation of the 6th leaf revealed an increase in venation, particularly adjacent to the leaf margins (Figure S2.2A, B). Leaves of *mtn1-1mtn2-1* leaves also had thicker mid-veins (Figure 2.3C, D). Further examination of embedded leaf sections showed that the thicker veins in *mtn1-1mtn2-1* resulted from increased numbers cells in the xylem, phloem and cambial cells (Figure 2.3E, F). Irrespective of the larger leaves, the leaf vasculature of *mtn1-1mtn2-1* was similar to that of the Tspm synthase mutant, thick vein (*tkv*, Clay and Nelson 2005), which is allelic to acaulis5 (*acl5*; Hanazawa et al., 1997; Kakehi et al., 2008). ACL5 is specifically expressed in xylem vessel elements and both *acl5* and *tkv* have an over-proliferation of xylem vessels in their stems. This increased xylem is proposed to result from reduced polar auxin

transport (PAT; Clay and Nelson 2005). Thus based on similarities to *tkv* and *acl5*, we assayed auxin transport and followed vascular patterning in the stems of *mtn1-1mtn2-1*.

Auxin transport was measured in WT and mutant inflorescence stem segments using ^{14}C-indole acetic acid (IAA). The basipetal transport of ^{14}C-IAA in the *mtn1-1mtn2-1* mutant was 46% of that detected in WT stems while the acropetal transport in the stem segments was normal. IAA transport in *tkv*, measured as a control, was 64% that of WT (Figure 2.4A) which is consistent with the initial description of this mutant by Clay and Nelson (2005).

We next examined stem cross-sections of the MTN double mutant in more detail. These WT stems contain 6-8 symmetrically arranged vascular bundles ~2-3 cm above the base of primary inflorescence (Figure 2.4B) whereas corresponding sections of *mtn1-1mtn2-1* stems usually had ten or more vascular bundles. These mutants also have increased number of small cells in all stem tissues (Figure 2.4C). Furthermore, the symmetrical arrangement of the vascular bundles in the WT was disrupted in the *mtn1-1mtn2-1* mutant, leading it to have an irregular stem circumference.

Auxin maxima developed from differences in auxin distribution in the shoot apical meristem determine the position of leaf primordial initiation and formation of leaf traces (Dengler 2006). These leaf traces are evident as vascular bundles in stem sections. Since the *mtn1-1mtn2-1* mutants have an increased number of vascular bundles compared to WT. We examined GFP production from a synthetic auxin-responsive promoter D*R5rev::GFP* (Friml et al., 2003) in this mutant back ground. The resulting images showed that *mtn1-1mtn2-1* stem cross sections always had a greater number of auxin maxima than WT, corresponding to the mutant's increased number of vascular bundles (Figure 2.4D-G).

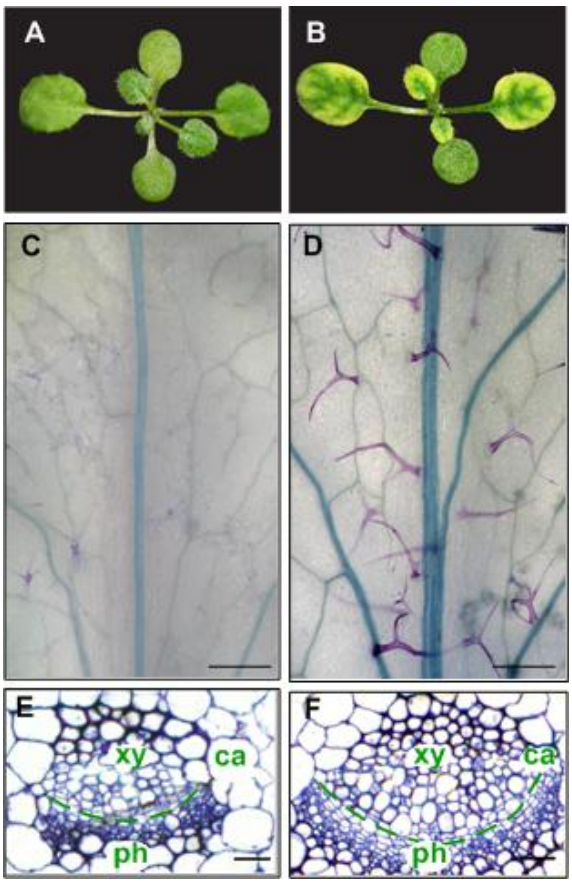

Figure 2.3 : Vegetative phenotypes of *mtn1-1mtn2-1* compared to WT.

(A, B) WT and *mtn1-1mtn2-1* seedlings at the 1.02 development stage, when first true leaves are > 1mm. WT seedlings had green true leaves (A) compared to mutant seedlings that exhibited interveinal chlorosis (B).

(C, D) Developmentally matched adult leaves (equal number of secondary veins arising from the mid veins) of WT (C) and *mtn1-1mtn2-1* (D), were cleared and stained with Toluidine Blue O to reveal the increased vein thickness in *mtn1-1mtn2-1.* Trichomes of the mutant were larger and the leaves tended to acquire more stain compared to the WT. Scale bars = 1.5 mm.

(E, F) Transverse sections through the mid veins of developmentally matched adult leaves of WT (E) and *mtn1-1mtn2-1* (F) plants. The *mtn1-1mtn2-1* exhibited an increase number of xylem (xy), phloem (ph) and cambial (ca) cells. Scale bars = 15 µm.

2.4.2.2 Reproductive phase phenotypes

The *mtn1-1mtn2-1* siliques arrested when they were 2-3 mm (stage 16 of the developmental milestones described by Smyth et al., [1990]) and very few siliques produced viable seeds. To determine the basis for this observed sterility, reciprocal crosses were performed: WT pollen was applied to *mtn1-1mtn2-1* pistils and *mtn1-1mtn2-1* pollen grains were transferred to stigma of the male sterile mutant *apt*1-3. The resulting fertilization was documented by recording the number of crosses producing viable seeds (Table 1). Both *mtn1-1mtn2-1*and *apt1-3* pistils were receptive to WT pollen, and *mtn1-1mtn2-1* pollen was able to germinate on WT and *apt1-3* pistils resulting in successful seed production in all cases. Thus, both *mtn1-1mtn2-1* male and female gametes were capable of producing viable heterozygous progeny but with reduced efficiency relative to WT.

Table 2.1: Viable seeds obtained from reciprocal crosses between WT and mutants (*apt1-3* and *mtn1-1mtn2-1*).

Crosses were collected from 10 plants.

	Percentage of crosses with viable seeds	Number of crosses
apt1-3(ϕ) x WT (σ)	84%	N = 25
mtn1-1mtn2-1(ϕ) x WT (σ)	14%	N = 50
apt1-3(ϕ) x *mtn1-1mtn2-1*(σ)	28%	N = 50

Data source: Sarah Schoor

Further examination revealed several factors that contribute to decreased fertility in *mtn1-1mtn2-1*. Anthers of stage 14 *mtn1-1mtn2-1* flowers were indehiscent (Figure 2.5A). In order to observe pollen, anthers of *mtn1-1mtn2-1* needed to be opened manually (Figure 2.5D). These anthers contained abnormally formed pollen grains (Figure 2.5E, F). Specifically, most of the *mtn1-1mtn2-1* grains were round in shape and lacked the groove presentin WT pollen (Figure 2.5B, C). To assess the viability of the abnormal pollen grains, anthers of stage 14 flowers were

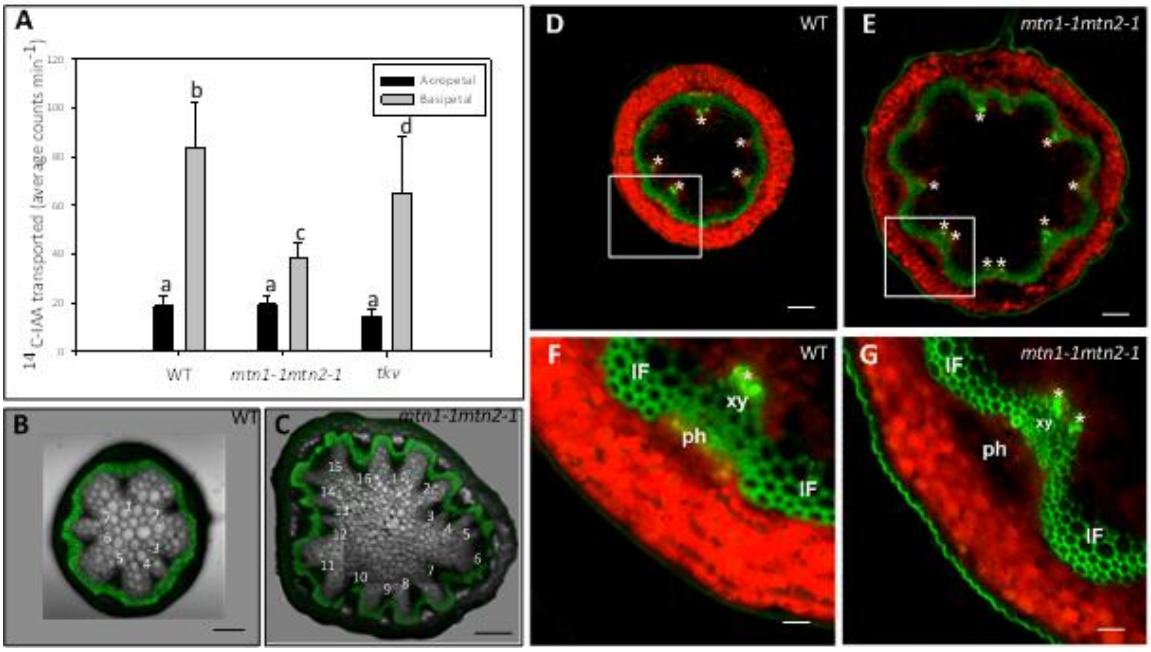

Figure 2.4: Polar auxin transport and stem vascular arrangement

(A) Reduced polar auxin transport of ^{14}C-IAA in excised inflorescence stem segments of *mtn1-1mtn2-1* mutants placed basipetally (inverted orientation) in ^{14}C-IAA. Three independent experiments were conducted using segments of 32 plants for each genotype. Error bars indicate SE. Statistically significant values ($P < 0.05$) are indicated in different letters.

(B-C) Free hand cross sections of *mtn1-1mtn2-1* and WT taken at the basal end of the primary inflorescence stem. Composite images of confocal laser scanning image and pseudo DIC image. Psedo DIC image shows the increased number of vascular bundles of the *mtn1-1mtn2-1* (C) compared to WT (B). Confocal laser image shows the lignified inter and intra fascicular fibers stained with berberine. Scale bars: B, C= 50 µm.

(D-G) Auxin maxima (*) visualized using DR5*rev*::GFP mostly corresponded to number of vascular bundles in cross-sections taken from the basal end of the primary inflorescence stem (D, E) of WT (D, F)and *mtn1-1mtn2-1* backgrounds (E, G). Higher magnification images reveal auxin maxima primarily localized to the xylem (xy) tissue of the vascular bundles (F, G). Note that the green fluorescence observed on lignified xylem of the inter-fascicular and intra-fascicular (IF) was autoflorescence. Scale bars: D, E = 50 µm: F, G = 150 µm.

stained with fluorescein diacetate, a stain that is taken up into viable cells. Almost all of the WT pollen studied was able to take up the fluorescein diacetate (N = 45), whereas *mtn1-1mtn2-1* had more unstained than stained pollen: 37% of MTN-deficient anthers had no viable pollen, 20% had less than five viable pollen grains, almost half (40%) had five to ten and only 3% had an excess of ten viable pollen grains (N= 65).

Next, *in vivo* pollen tube formation was assessed; pistils were fixed 24 h after pollination and visualized with aniline blue (Figure S2.2C to H). Reciprocal crosses performed between *mtn1-1mtn2-1* and WT pollen proved the mutant stigma to be receptive to pollen, with 90% of the successfully pollinated pistils containing pollen tubes. Attempts to manually pollinate *apt1-3* or *mtn1-1mtn2-1* with *mtn1-1mtn2-1* pollen were not successful as no pollen tubes were observed for either cross 24 h later. Collection of stage 14 *mtn1-1mtn2-1* flowers and staining them with aniline blue showed that 22% had self-pollinated and of those pollinated, 48% had pollen tubes. Thus, *mtn1-1mtn2-1* pollen is capable of forming pollen tubes *in vivo* but apparently need longer than 24 h to extend.

Carpel and ovule development was also aberrant in stage 14 *mtn1-1mtn2-1* flowers; carpels had wide or duplicated stigmas, while ovules of the pistils had un-extended integuments when compared to WT (Figure 2.5G, H). About 10% of *mtn1-1mtn2-1*flowers examined contained one-three fully developed ovules that appeared to WT.

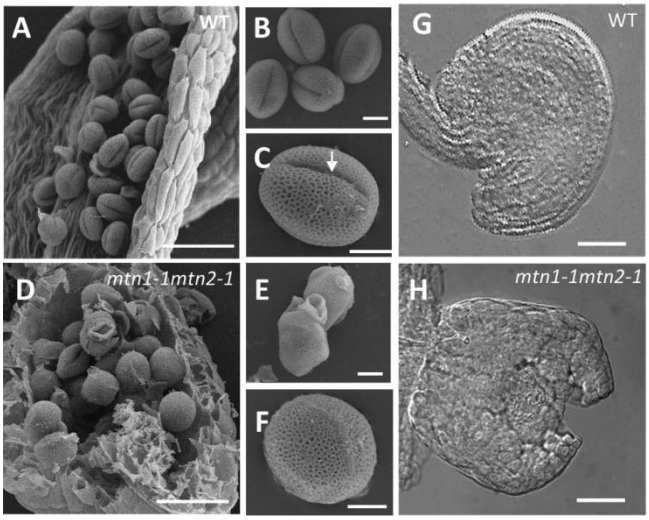

Figure 2.5: Reproductive abnormalities of *mtn1-1mtn2-1*

(A-F) Scanning electron micrographs of WT (A) and manually opened (D) anthers sacs showed abnormal pollen development in the mutant. The *mtn1-1mtn2-1* pollen grains were irregularly shaped (F), and lacked the characteristic furrow (indicated by the arrow) seen in the WT (B, C). At times the mutant pollen appeared clumped with each other (E) compared to WT (B). Scale bars = A, B = 45 µm; B, C E, F= 5 µm.

(G-H) Differential interference contrast (DIC) images of stage 14 flower pistils. WT had mature ovules post-fertilization stage (G) while the *mtn1-1mtn2-1* ovules (H) corresponded to those normally observed in stage 12 WT flowers: outer integuments were not fully extended over the nucellus. Scale bars = 25 µm.

2.4.3 The *mtn1-1mtn2-1* phenotype complemented by MTN1 over-expression

In the Yang cycle MTA is converted to MTR-1P via two steps: first, MTA is hydrolysed by MTN to form MTR and adenine, and the resulting MTR is subsequently metabolized by MTK. Unlike *mtn1-1mtn2-1* seedlings, MTK-deficient seedlings are not impaired in their growth and development when provided with sulfur-sufficient conditions (Sauter et al., 2004) suggesting MTN is the more crucial of the two enzyme activities. In order to verify that the complex phenotype of *mtn1-1mtn2-1* was solely due to MTN deficiency, the MTN1 gene was re-introduced to the double mutant. The pleiotropic phenotype of *mtn1-1mtn2-1* was fully complemented by a 2.4 Kb genomic fragment that contained the full length coding sequence of *MTN1* along with 356bp of the upstream region (Figure 2.6A). These results were further confirmed by the ectopic expression of *MTN1*cDNA under a polyubiquitin 10 (UBQ10) constitutive promoter in the *mtn1-1mtn2-1* background. We therefore concluded that the pleiotropic phenotype of *mtn1-1mtn2-1*was the result of MTN-deficiency, and that replenishing MTN1 alone was sufficient to compensate for the lack of MTN2.

2.4.4 The basis of *mtn1-1mtn2-1* phenotype is accumulation of MTA, not loss of MTR

Although the observed vascular and reproductive defects of *mtn1-1mtn2-1* were restored by MTN transgene expression, we reasoned that these abnormal traits could be due to either a lack of MTA metabolism or a decreased MTR. Targeted profiling of Met metabolites in inflorescences and rosette leaves, revealed statistically significant increases of MTA in *mtn1-1mtn2-1* ($p < 0.05$). MTA was elevated two-fold in rosette leaves (Figure 2.6B) and five-fold in the mutant inflorescences, leading us to conclude that MTN deficiency leads to increased MTA content. However, based on these data, it could not be excluded that the lack of MTR might also contribute to the complex phenotype of the mutant. To test this, we

Figure2.6: Complementation of *mtn1-1mtn2-1* phenotype by MTN1, MTA concentration and complementation of *mtn1-1mtn2-1* phenotype by hMTAP.

(A) Complementation of *mtn1-1mtn2-1* with MTN1::*MTN1* 3 weeks after bolting.

(B) Steady state levels MTA of inflorescences and rosette leaves. Mean values of five replicates were plotted with error bars indicating the SD. Statistically significant values ($P < 0.05$) are indicated in different letters.

(C) Complementation of *mtn1-1mtn2-1* with UBQ10::*hMTAP* shown at bolting.

introduced a cDNA encoding human *MTAP* activity (UBQ10::hMTAP) into the mutant. This enzyme phosphorylates MTA directly into MTR-1P without producing MTR. The phenotype of the double mutant was fully complemented by constitutive expression of hMTAP (Figure 2.6C).

2.4.5 Modeling of Spd synthase and Tspm synthase complexed with MTA

MTA is a potent inhibitor of both human Spm synthase (approximate K_i =0.3 μM) and Spd synthase (K_i= 2-10 μM, Wu et al., 2007). Analysis of crystal structures containing bound ligands of these enzymes with MTA explains the difference in affinity: the hydrophobic binding site of Spm synthase is larger allowing it to have more extensive interactions with the adenine residue of MTA than does Spd synthase. The conserved structural folds of the human and plant PA enzymes allowed us to model MTA binding to these targets. 3-D models were developed for Arabidopsis Spd synthase1and Tspm synthase and then their MTA complexes were visualized as for human Spd synthase1 and Spm synthase (Wu et al., 2008). Analysis of these 3-D models revealed that the MTA-binding pockets of Spd synthase1 and Tspm synthase are very similar (Figure 2.7A,B): the CH_3S moiety of MTA makes van der Waals contact with L90, L92 and V156 of Spd synthase1, or L76, I78 and V142 of Tspm synthase. The ribose ring of MTA is predicted to establish hydrogen bonds with the side chains of Q76 and E151 of Spd synthase 1 or the side chains of Q62 and E137 of Tspm synthase. N-6 of MTA adenine forms hydrogen bonds with the side chain of D182 of Spd synthase1 or D168 of Tspm synthase. The adenine ring of MTA is placed between I137 on one side and L187 and L199 on the other side in the Tspm synthase-MTA complex. In Spd synthase1-MTA complex, the adenine ring of MTA is sandwiched between I151 and L212. The residues I151 and L212 of Spd synthase1 and the residues I137 and L199 of Tspm synthase are structurally conserved, while the L187 residue of Tspm synthase is substituted by Serine (S202) in Spd synthase1 (Hanazawa et al., 2000). Therefore, the hydrophobic surfaces involved in interaction with the adenine ring of MTA are predicted to be very

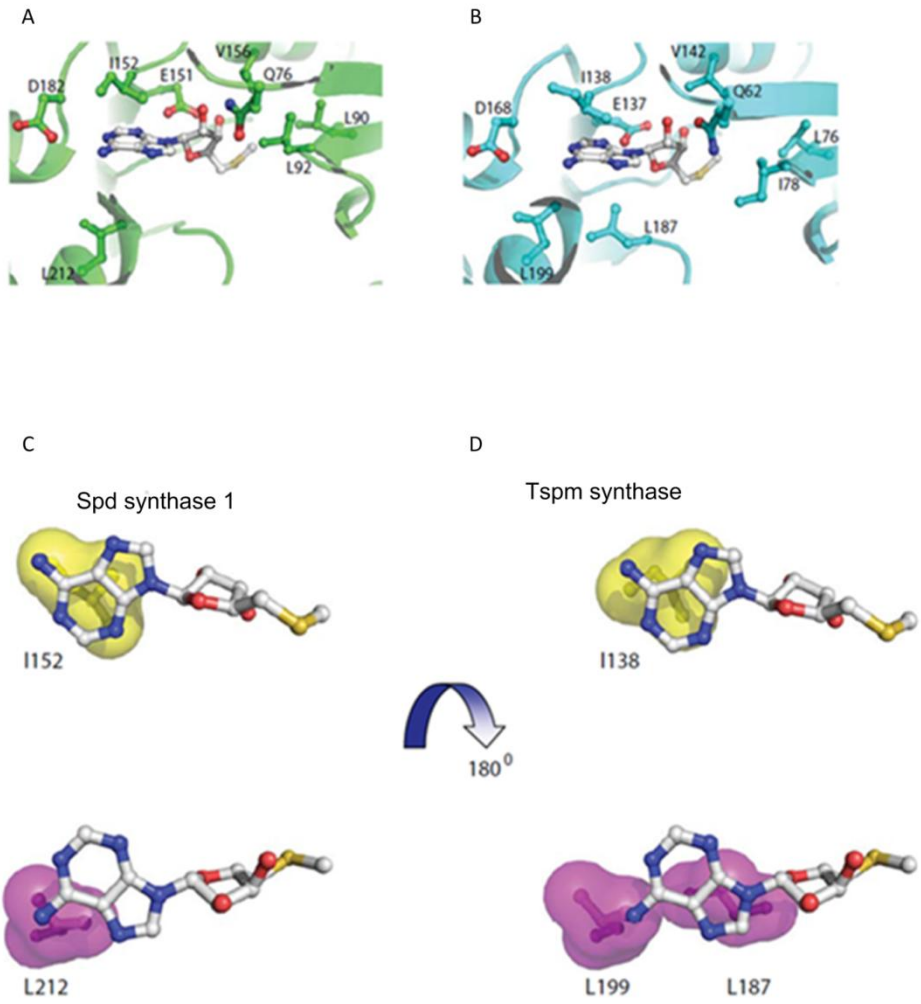

Figure 2.7: Structural basis for inhibition of Spd synthase 1 and Tspm synthase enzymes by MTA

(A, B) Close-up views of the MTA-binding pocket for Spd synthase 1 and Tspm synthase, respectively. MTA and the residues interacting with MTA in both structures are shown in stick-and-ball representation, while carbon atoms for residues are in the same color as the corresponding structure, whereas carbon atoms of MTA are in gray.

(C, D) The hydrophobic surfaces interacting with the adenine ring in MTA. The two surfaces stacking with the adenine ring are in magenta and yellow.

different. The hydrophobic surface (in *yellow*) made by I152 in Spd synthase1 is similar to the corresponding one in Tspm synthase (I138) (Figure 2.7C, D). On the other side of the adenine ring of MTA, the hydrophobic surface (in *magenta*) of Spd synthase1 made by L212 is shifted and partially covers the adenine ring of MTA, whereas in the Tspm synthase, the hydrophobic surfaces made by L187 and L199 are large and positioned to cover the adenine ring completely. Although MTA binds to all three PA synthases, these modeling experiments predict that similar to human Spm synthase, Tspm synthase may be more sensitive to inhibition by MTA than Spd synthase1 due to extensive hydrophobic interactions between Tspm synthase and the adenine moiety of MTA.

2.4.6 *mtn1-1mtn2-1* plants exhibit altered PA profiles.

We next investigated whether increased MTA abundance in the mutant was associated with changes in free PA content. To do this, we monitored both leaves and inflorescences for Put, Spd, and Spm using HPLC analysis. Unfortunately Tspm abundance was so low that it was not readily detected in WT samples (Naka et al., 2010) and as a result, could not be measured. For those PAs that could be measured, differences were observed in both *mtn1-1mtn2-1* leaves and inflorescences: Put levels increased in *mtn1-1mtn2-1* whereas Spd and Spm levels decreased (Figure 2.8A, B). Of these, a statistically significant difference was only observed in the Put content of inflorescences.

We reasoned that if these changes were physiologically relevant, reactions dependent on PAs would be affected. Spd is a cofactor for the post-translational activation of the translation initiation factor eIF5A. The butylamine moiety that is provided solely by Spd is transferred to eIF5A in a two-step reaction causing it to become hypusinated on a specific lysine residue (Pegg and Casero, 2011). Thus we tested the degree of hypusination of eIF5A in *mtn1-1mtn2-1* leaf

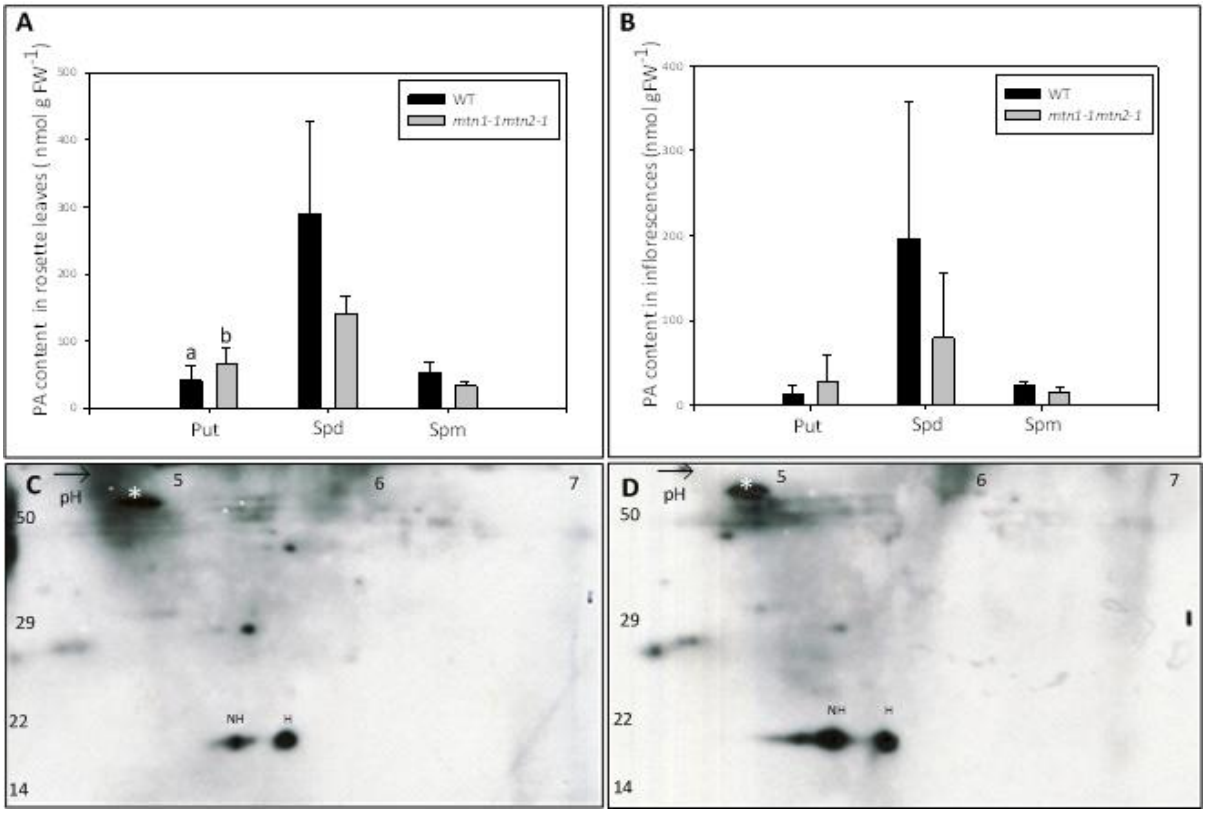

Figure 2.8: PA profiles and two dimensional gels showing eukaryotic initiation factor 5A (eIF5A)

(A, B) Altered PA profiles of inflorescences (A) and rosette leaves (B) of *mtn1-1mtn2-1* and WT (N = 4). Error bars represent SD. Statistically significant values ($P < 0.05$) are indicated in different letters.

(C, D) The hypusinated (H) and non-hypusinated (NH) eIF5A in rosette leaves of *mtn1-1mtn2-1* (D) compared to WT (C). Images are representations of three replicates. The Rubisco large sub unit polypeptide dot was used as the reference for quantification (*). N=3. Molecular mass standards (in KDa) are indicated to the left in C, D.

extracts by 2-D gel electrophoresis followed by immunoblotting with eIF5A-specific antibodies as an indicator of intracellular Spd availability. The amount of hypusinated eIF5A was two-fold lower in *mtn1-1mtn2-1* indicating a clear reduction in hypusination of elF5Ain comparison to WT leaf extracts (Figure 2.8C, D).

2.4.7 *MTN*-deficiency results in altered NA levels

Upon recognizing that the free PA profiles changed in response to increased MTA abundance, we next analyzed NA levels of *mtn1-1mtn2-1*.We determined that NA was significantly reduced in inflorescences and mature rosette leaves of *mtn1-1mtn2-1* compared to WT ($p < 0.05$; Figure 2.9A). In WT plants, the highest NA content (268 ± 58 pmol mg FW^{-1}) was detected in inflorescences with leaves having 60% less NA (106 ± 50 pmol mg FW^{-1}) whereas the NA content of *mtn1-1mtn2-1* inflorescences was 34% lower than WT and undetectable in rosette leaves.

Since NA is known to play a key role in ion homeostasis and long distance transport, we investigated whether the ion content (Cu, Fe, Zn, and Mn) of *mtn1-1mtn2-1* was different from WT, using inductively coupled plasma atomic emission spectroscopy (Gadapati and Macfie, 2006). In the mutant inflorescences, contents of Cu, Fe and Zn were significantly lower, with Fe and Zn showing the greatest reduction compared to WT ($p< 0.05$; Figure 2.9B). The ion profiles of mutant and WT rosette leaves were similar with reduced Zn and Cu abundance, except the Mn content in the mutant was significantly higher than in the WT ($p< 0.05$; Figure 2.9C). Interestingly, *mtn1-1mtn2-1* had significantly decreased Fe levels in the inflorescences compared to WT while these levels were not significantly different in rosette leaves ($p< 0.05$). Confirming these results, interveinal chlorosis was absent in the reproductive leaves of mature *mtn1-1mtn2-1* mutants.

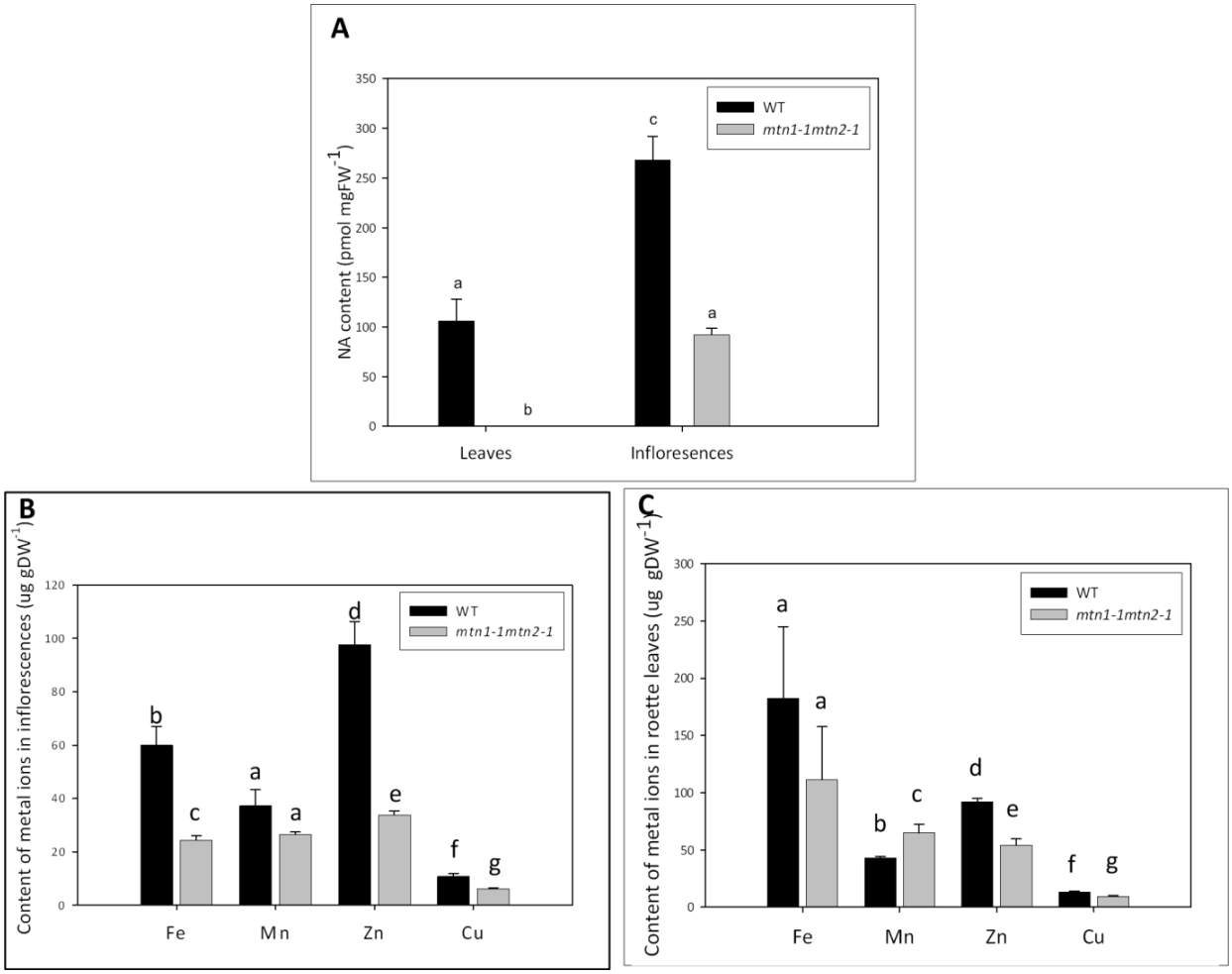

Figure 2.9: Nicotianamine content and metal profiles of leaves and buds.

Nicotianamine could not be detected in the rosette leaves (A; N = 5) compared to WT and was lower in mtn1-1mtn2-1 inflorescences (N = 3). In addition to Nicotianamine, Fe, Mn, Zn and Cu levels were also reduced in mtn1-1mtn2-1 inflorescences (B) and leaves (C; N = 5) compared to WT. Each n is a pool of three biological replicates. Error bars indicate the standard error of the mean; FW, fresh weight; DW, dry weight. Statistically significant values ($P < 0.05$) are indicated in different letters while insignificant values indicated in same letters.

2.4.8 Exogenous feeding of PA and NA partially restored fertility of *mtn1-1mtn2-1*

2.4.8.1 Chemical rescue of fertility

Since both free PA and NA levels were affected in the *mtn1-1mtn2-1* mutant, we postulated that MTA -producing reactions were being product inhibited. We then hypothesized that the exogenous application of target compounds would reverse abnormal phenotypes. To test this, we chemically complemented*mtn1-1mtn2-1* mutants with exogenous application of Spd, Spm, Tspm or NA (NA was extracted from NA over-producing transgenic Arabidopsis plants).

To treat MTN-deficient plants, F2 seeds of *MTN1-1/mtn1-1mtn2-1/mtn2-1* plants were grown on media supplemented with Spm, Spd, Tspm or NA. After 2-3 weeks on media, seedlings were transplanted to soil and genotyped via PCR. With the exception of Tspm, drops of the corresponding compound were then applied daily to shoot apices of *mtn1-1mtn2-1* plants until the plants were eight-weeks-old. Examination of the treated plants showed that *mtn1-1mtn2-1* fertility was partially recovered using any of three compounds (Spm, Spd or NA): partial recovery of fertility was indicated by the presence of extended siliques (Figure 2.10A) with fertile seed (Figure 2.10B to E) on individual branches. Surprisingly partial fertility was also recovered in a similar manner when the seeds were germinated on the indicated compounds for 14 or more days and transferred to soil without being provided with further supplement (Figure 2.10F).

Generally, siliques with unfertilized ovules fail to extend beyond 3.5mm, while siliques containing 60 seeds reach a maximal length of 15 mm (Meinke, 1994). Thus the fertility of the plants without further supplement was scored by categorizing the siliques length in to three groups: (1) 5-7 mm, (2) 8-10 mm and (3) more than 10 mm (Figure 2.10A). Most of the

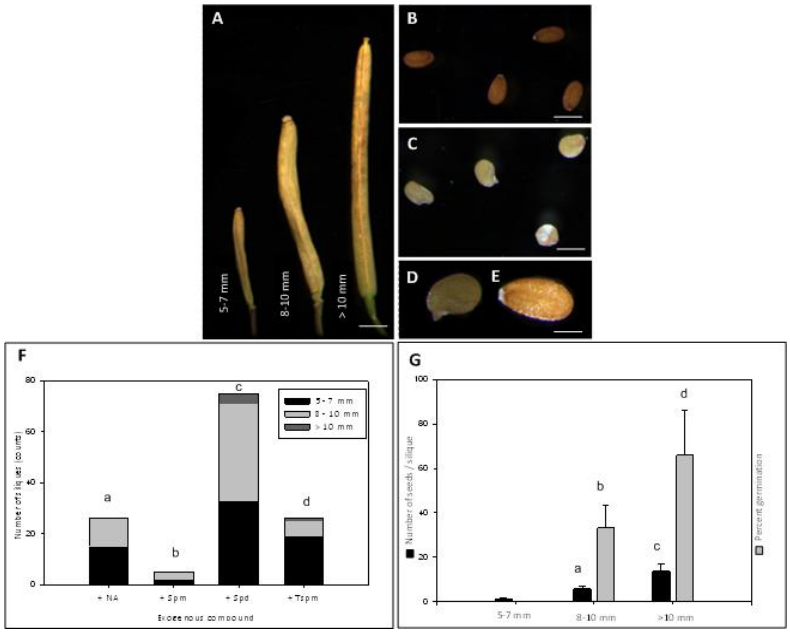

Figure 2.10: Exogenous NA and PA restored the fertility phenotype of *mtn1-1mtn2-1*

(A-E) Silique and seed morphology of restored plants. The restored seeds of *mtn1-1mtn2-1* were categorized in groups based on their lengths; most of the seeds of > 10 mm siliques has normal WT-looking seeds (B) while the former two categories had seeds with abnormal color and shape (C). Closer observation of these abnormal seeds showed (D) that they had developed seed coats similar to WT (E). Scale bars: A = 1.5 mm, B, C= 300 µm, D, E 100 µm.

(F) Number of siliques that developed when *mtn1-1mtn2-1* was grown in ½ MS media supplemented with 20 µM NA, 100 µM spermine (Spm), spermidine (Spd) or 50 µM thermospermine (Tspm). The restored siliques were of various lengths they were categorized into three groups based on their lengths (N = > 20 siliques per treatment). Statistically significant values (P< 0.05) are indicated in different letters.

(G) Number of seeds/ silique and percent seed germinated from *mtn1-1mtn2-1* plants grown on ½ MS supplemented with 100 µM Spd. Seed counts were average of 60 siliques from 6 plants for 5–7 mm and 8-10 mm categories while 36 siliques from 6 plants for > 10mm category. Percent germination was assessed only on seeds collected for latter 2 categories (N = 6 siliques). Bars represent the standard deviation (SD). Statistically significant values (P< 0.05) are indicated in different letters while insignificant values indicated in same letters.

siliques produced were in the first two categories while only Spd and Tspm gave rise to siliques that were >10 mm long. Of the four treatments, the most effective was 100 µM Spd (78 ± 5 siliques / plant) and the least effective was100 µM Spm (Figure 2.10F). Both NA and Tspm treatments produced 25-35 siliques/ plant.

The number of seeds and or silique in each group of the Spd experiment was further determined: 5-7cm group had 1 ± 0.4 seeds per silique, while the 8-10 mm and >10 mm group had 6 ± 1, and 14 ± 4 seeds per silique, respectively. Some seeds in the 5-7 mm and 8-10 mm category showed abnormal shape and color (Figure 2.10B) when compared to WT (Figure 2.10C). To determine the viability of these abnormal seeds approximately 100 seeds from 6 siliques were germinated on media and scored: 8-10 mm and >10 mm siliques had 33 ± 10 % and 66 ± 20% germination, respectively (Figure 2.10G).

2.4.8.2 Chemical rescue of interveinal chlorosis by NA

In addition to testing for recovered fertility, rescue of interveinal chlorosis with the application of exogenous PAs (Put, Spd, Spm or Tspm)or NA was also investigated. Of the compounds tested, onlymedia supplemented with NA completely eliminated the interveinal chlorosis normally observed at 10DAG in *mtn1-1mtn2-1* seedlings. Similarly, mutant seedlings that already exhibited interveinal chlorosis on ½ MS developed green leaves two days after transplanting to ½ MS supplemented with NA. Moreover, hydroponically grown *mtn1-1mtn2-1* supplemented with 20µM NA lacked interveinal chlorosis (N= 8, Figure S2.3).

2.5 Discussion

Our detailed characterization of the *mtn1-1mtn2*-mutant has established a correlation between MTN deficiency, abnormal vasculature and low reproductive efficiency. The first distinct phenotype of *mtn1-1mtn2-1* coincides with the development of true leaves. As recently reported, the Yang cycle (i.e. MTA recycling) in Arabidopsis and *Plantago major* mainly occurs in leaf veins (Pommerrenig et al., 2011). Thus, it is likely that the flux of MTA synthesis first increases substantially in leaves as vein development proceeds.

Molecular characterization of the *mtn1-1mtn2-1* mutant showed a reduction in MTN transcript levels consistent with the presence of a T-DNA insertion within the transcribed region of each gene. Protein abundance and enzyme activity reflected transcript levels, with the *mtn1-1mtn2-1* mutant having ~14 % residual MTN activity, indicating its substantially reduced capacity for MTA hydrolysis. The MTN assay results were consistent with *mtn1-1* and *mtn1-2* single mutant seedlings grown on sulfur-deficient medium supplemented with MTA. These seedlings have less than 20% of the MTN activity of WT, and displayed severe growth retardation. Interestingly, they also had increased MTN activity when grown in the presence of MTA. Since MTN transcript levels did not change under these conditions, the activation of MTN must occur at the protein level (Bürstenbinder et al., 2010). While the molecular basis of this activation remains unknown, we assume that the increased MTA content in the double mutant activates the residual MTN enzyme, leading to cellular variations in enzyme activity.

2.5.1 MTA accumulation is the basis for *mtn1-1mtn2-1* phenotype

While our data pointed to the lack of MTA hydrolysis as being the cause of the abnormalities in *mtn1-1mtn2-1* plants the contribution of reduced MTR content could not be excluded. The latter consideration arose from comparing the completely normal phenotype of MTR kinase mutants (Sauter et al., 2004) with the complex phenotype of MTN-deficient plants. Both

mutants are unable to salvage Met, yet MTR kinase mutants have MTR and are normal whereas the MTN-deficient plants lack MTR and are abnormal. We tested the involvement of MTR deficiency in the phenotype of *mtn1-1mtn2-1* by introducing constitutive expression of *MTN1* and h*MTAP* transgenes into *mtn1-1mtn2-1* plants. MTAP metabolizes MTA to MTR-1P without producing MTR. Complementation of the mutant phenotype by either transgene confirms that the abnormal development of MTN-deficient plants is due to their increased MTA content rather than a lack of MTR or Met salvage itself.

MTA accumulates in cells of *mtn1-1mtn2-1* that are actively synthesizing PA or NA; this MTA accumulation is obviously both tissue-specific and developmentally dependent. When *mtn1-1* seedlings are grown on sulfur-deficient media supplemented with MTA, presumably all their cells are exposed to MTA resulting in retarded shoot and root growth (Bürstenbinder et al., 2010). We propose that these phenotypes are also due to MTA inhibition of NA and PA synthases based on the similarity of their metabolite profiles with those of *mtn1-1mtn2-1*plants.

The MTA abundance in the leaves of *mtn1-1mtn2-1* plants was two-fold higher than in WT: 1.7 ± 0.2 pmol mgFW^{-1} as compared to 0.8 ± 0.1 pmol mgFW^{-}1in WT. This change was in the same range as thatof*mtn1-1* grown on MTA: a two-fold increase in four-day-old seedlings and 1.5-fold increase in three-week-old plants (Bürstenbinder et al., 2010). Interestingly, the MTA accumulation in the double mutant was greater in flowers than in leaves. The MTN level of the *mtn1-1mtn2-1* inflorescences was 24 ± 2 pmol mg FW^{-1} compared to 4.6 ± 0.2 pmol mg FW^{-1} in WT. Thus, in *mtn1-1mtn2-1* plants, MTA accumulation is tissue specific. In accordance with our MTA abundance values, Tassoni et al. (2000) and Naka et al. (2010) found that all PAs(Put, Spd, Spm and Tspm) are higher in WT flowers compared to mature leaves. Thus flowers must have an increased requirement for MTN activity.

2.5.2 MTA binds NA synthase, SPD synthase, SPM synthase and TSPM synthase

MTA is known to inhibit PA synthetic enzyme activities, while increasing SAMDC activity (Albers, 2009). For example, mammalian Spm synthase and Spd synthase activities are MTA sensitive (Pegg, 1981; Wu et al., 2008). *Insilico* modelling leads us to propose that MTA inhibits Arabidopsis Spd synthase and Tspm synthase with the latter being the most sensitive. This inhibition is likely quite dynamic since the stimulation of SAMDC by MTA theoretically increases flux to PA synthesis and further enhances MTA production.

Barley NA synthase is product inhibited by MTA (K_i = 5 µM; Herbiket al, 1997).We suspect that the Arabidopsis enzyme is similarly affected given its amino acid sequence identity (46%) and similar domains (Herbik et al., 1999). Moreover, the mutant plants have chlorotic leaves that are reversed by NA supplementation. Thus, MTA inhibits PA and NA synthases in a spatially and temporally dependent manner reflecting the flux through the Yang cycle and the cellular abundance of the target enzyme activities.

2.5.3 Molecular basis of the altered vascular development of *mtn1-1mtn2-1*

The increased venation of *mtn1-1mtn2-1* rosette leaves likely contributes to the variation in their free PA content as PA biosynthesis predominantly occurs in leaf vasculature (Pommerrenig et al., 2011).Increased vein thickness of the MTN mutant rosette leaves is similar to that reported for *tkv* (Clay and Nelson 2005). Since our modeling predicted that Tspm synthase activity is inhibited by MTA, and Tspm is required for normal xylem differentiation (Muñiz et al., 2008), it was of interest to examine Tspm content. Unfortunately, Tspm quantification is a challenge due to its low abundance; Tspm was not detected in our system. Despite this observation, our results lead us to believe that *mtn1-1mtn2-1* plants have reduced Tspm.

Aside from Tspm effects, PA catabolism may also contribute to the changes in vascular development in *mtn1-1mtn2-1.*The altered PA content of the mutant(e.g. increased Put) may

lead to increased PA oxidase activity and H_2O_2, a documented signal for increased vascular tissue differentiation (Tisi et al., 2011). However, we did not detect increased H_2O_2 in 14d-old *mtn1-1mtn2-1* seedlings using a histochemical stain (Figure S4). Similarly, semi-quantitative RT-PCR of mature leaves of *mtn1-1mtn2-1* did not show significant changes in the transcript levels of three representative PA oxidases (PAO1, PAO2, PAO5) compared to WT (Figure S4). However, further analysis is necessary to determine if PAO activities change in the mature mutant plants, or as a result of Spd treatments.

The vascular abnormalities of *mtn1-1mtn2-1* appear to be a direct effect of changes in PAT. We base this conclusion on the similarities between the *mtn1-1mtn2-1* vasculature and the effects of reducing PAT by naphthylphthalamic acid treatment (Mattsson et al., 1999); both sets of plants have thick veins in their rosette leaves, and an increased number of vascular bundles in stem sections. Ibañes et al. (2009) created a computational model for vascular bundle development based on DR5::GUS expression of naphthylphthalamic acid-treated plants and anatomical analysis of brassinosteroid (BR) signalling mutants. Their model predicts PAT-related auxin maxima determine the spacing between vascular bundles while BR controls bundle number. If this is the case, then our results suggest that BR signalling changes may also contribute to the vascular phenotype of *mtn1-1mtn2-1*.

The question arises then, why do *acl5* and *tkv* that also have reduced PAT (Clay and Nelson, 2005; Vera-Sirera et al., 2010) lack the increase in vascular bundles characteristic of *mtn1-1mtn2-1* plants? We propose that the differing phenotypes of these Tspm-deficient plants reflect the degree to which PAT is inhibited. *mtn1-1mtn2-1* plants have less residual auxin transport as compared with *tkv* (46% versus 64%, respectively). Their more severe reduction in PAT may lead to an increase in their BR content or sensitivity causing them to have an increased number of bundles. The modest PAT changes in *tkv* (and *acl5*) may not be sufficient to trigger

the crosstalk with BR. This reasoning is consistent with the proposal that the PAT changes in *acl5* are secondary to their vascular defects (Vera-Sirera et al., 2010). Direct investigation of BR content and signaling in Tspm-deficient mutants is needed to clarify its involvement in these phenotypes.

2.5.4 NA deficiency of *mtn1-1mtn2-1* causes altered ion homeostasis leading to interveinal chlorosis and reproductive abnormalities

In addition to free PAs, NA levels were significantly affected in *mtn1-1mtn2-1* tissues: NA was undetectable in double mutant rosette leaves, while inflorescences exhibited a 3.7-fold reduction relative to WT. This NA deficiency is similar to that of the *chloronerva* tomato mutant (Bohme and Scholz, 1960), quadruple NA synthase Arabidopsis mutants (*nas4x-2 and nas4x-1;* Klatte et al., 2009), and transgenic *naat* tobacco lines over-expressing NA aminotransferase (Takahashi et al., 2003). All these plants have interveinal chlorosis and reduced fertility along with reduced NA content. In all cases, this deficiency is associated with altered profiles of Fe, Zn, Mn and Cu. Similar to the previously published reports describing mutants with decreased NA, *mtn1-1mtn2-1* plants had lower levels of all these ions in both inflorescences and rosette leaves, with the exception of Mn which increased in leaves.

2.5.5 Restoration of seed set in *mtn1-1mtn2-1*

The reduced presence of double mutants in the segregating progeny of *MTN1/mtn1-1mtn2-1mtn2-1* plants is also indicative of a reproduction problem. The double mutant was commonly recovered from these segregating populations at a frequency of 1/7thto 1/10th, in contrast to the expected 1/4. Whereas Spm synthase mutants are normal, *spds1-1spds2-1* double mutants that lack Spd (but have increased Put content) arrest as embryos (Imai et al., 2004). *mtn1-1mtn2-1* mutants have a similar change in their PA profile suggesting that the distortion in the segregation ratio of *mtn1-1mtn2-1*may be due to altered PA homeostasis during

embryogenesis. The suggestion that conjugated forms of Spd serve as PA reserves in seeds to release Spd in developing tissues (Luo et al., 2009) supports this conclusion. If so, a decrease in the amount of Spd conjugate from maternal tissues may underlie the reduced recovery of homozygous double mutants and account for the variation in the segregation ratios of different F2 seed populations. Alternatively changes in polyamine metabolism may affect fertilization since mutants with reduced PAO3 activity have abnormal pollen tube growth (Wu et al., 2010). *mtn1-1mtn2-1* mutants experience both male and female gamete abnormalities together with mis-timing of reproductive developmental events leading to poor fertilization.

Exogenous supply of 20 µM NA, 100 µM Spd, 100 µM Spm or 50 µM Tspm improved the fertility of *mtn1-1mtn2-1* to a limited extent. When each of these chemicals was supplied exogenously, the plant need not attempt to generate these chemicals via biosynthesis. As a result the amount of MTA generated *invivo* by these biosynthetic pathways is presumably reduced and thus alleviates the product inhibition of PA or NA synthases to improve fertility. Among the compounds tested, 100 µM Spd was the most effective; Spm was the least and Tspm and NA had intermediate effects. Application of 100 µM Put, 10 or 100 µM of IAA, or 5 µM of ACC did not produce observable differences. The simplest explanation of Spd recovery is that exogenous Spd provides an increased precursor pool for Tspm synthesis. The Tspm may induce more normal xylem differentiation and restore sufficient transport of compounds essential for seed development including phytohormones and metal cofactors. Interestingly, a recent report by Tisi et al. (2011) shows that increased xylem differentiation and secondary wall deposition is induced in maize roots by exogenous Spd feeding. This is apparently induced by H_2O_2 arising from PA catabolism. Similar H_2O_2 signaling may contribute to the Spd effect on *mtn1-1mtn2-1* plants reported here. It is also possible that the Spd acts by another route aside from simply being the precursor for Tspm or affecting PA catabolism, such as via eIF5A modification. A recent study based on pumpkin has shown that the eIF5A modification occurs in companion

cells (Ma et al., 2010) of phloem tissues where both MTN enzymes occur predominantly (Pommerrenig et al., 2011). A comprehensive developmental and metabolite analysis of Spd-treated *mtn1-1mtn2-1* plants will be required to elucidate the molecular mechanism underlying the effects of both MTN deficiency and Spd feeding. A deeper understanding of this process will provide important insight of the long recognized link between PA and plant development.

2.6 Conclusion

Although MTN-deficient plants have a complex phenotype, each abnormal trait can be traced back to an effect of MTA accumulation. Given the different enzyme activities inhibited by MTA and their wide ranging contributions to plant metabolism, increases in MTA content have a broad impact on both a cellular and developmental scale.

2.7 Data contributed by others.

The work presented in this chapter was a team effort of many personnel. Ishari Waduwara-Jayabahu (IW-J) navigated the project, designed and conducted most of the experiments. Sarah Schoor, a former student of Moffatt lab, who first started on this project analysed most of the reproductive defects of this mutant including the data presented in Table 1.1, Figure 2.5. and Figure S2.2C-H. Zachary T. Hull, an undergraduate student of Moffatt lab, took the lead in MTN assays (Figure 2.2C) with the assistance of IW-J. IW-J sent the tissues harvested from plants grown at University of Waterloo to Yasmin Oppermann, Universität Kiel, Germany who determined the PA content presented in Figures 2.8A, B. Yasmin also conducted initial MTN assays on different tissues (Figure S2.1). Tissues were also send to Dr. Markus Wirtz, University of Heidelberg, Germany who determine the NA content (Figure 2.6B) and Met-related metabolites (Figure 2.9A). MTA inhibition for Tspm synthase and Spd synthase 1 was modeled by Dr. Alexander N. Plotnikov, Mount Sinai School of Medicine, USA who is responsible for the Figure 2.7.

2.8 Supplemental material

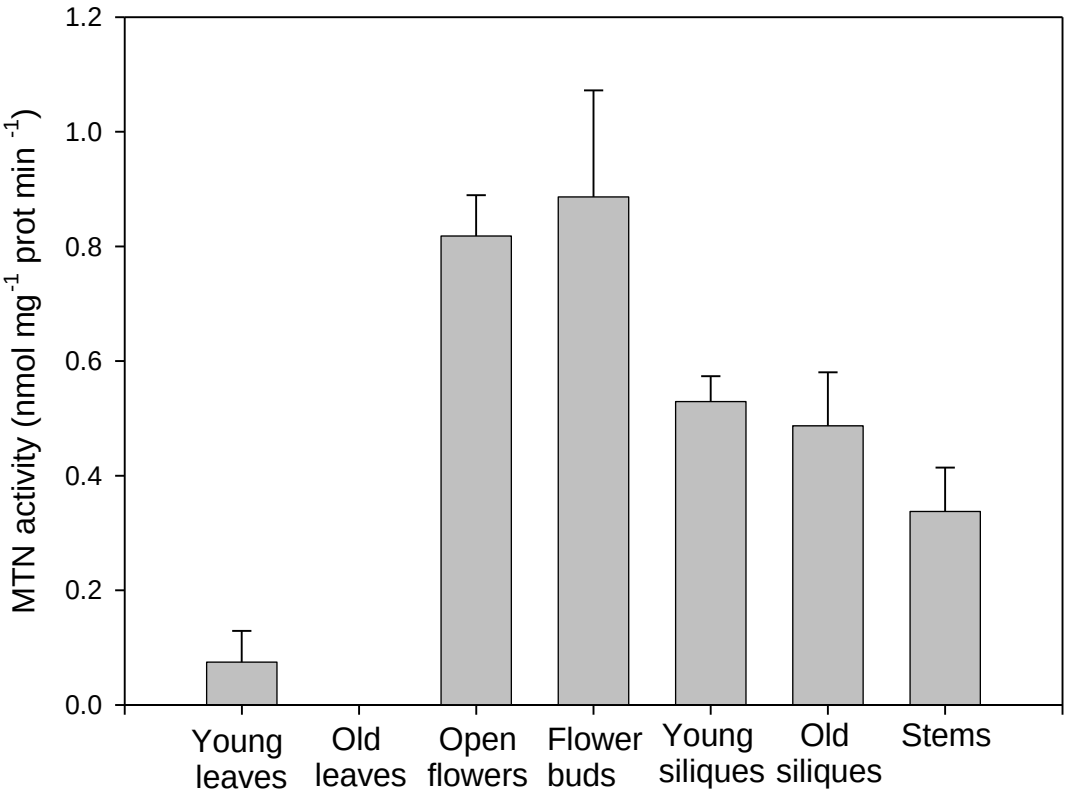

Figure S2.1: MAN activity of various organs harvested from 6-week-old WT plant.

(Data source: Yasmin Oppermann)

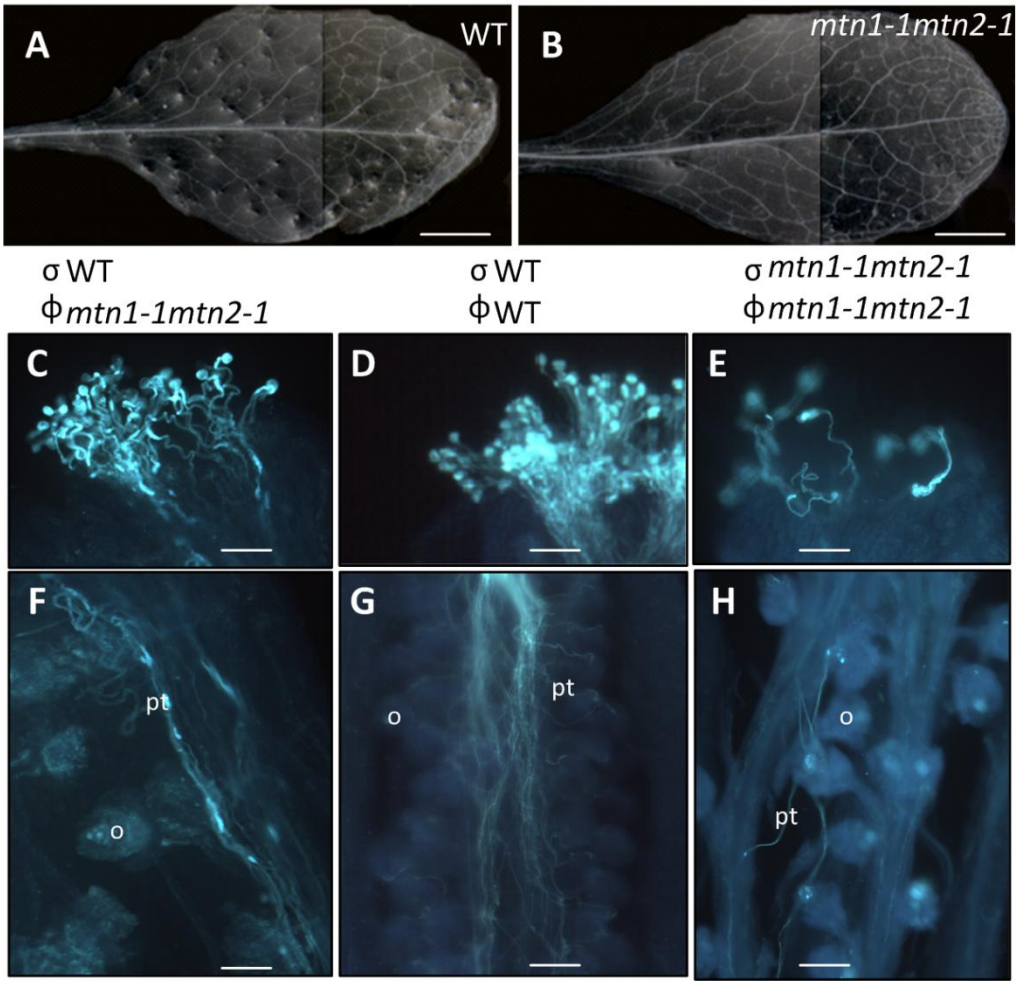

Figure S2.2: Leaf vein pattern and pollen tube growth of mtn1-1mtn2-1 compared to WT.

(A, B) Cleared 6th rosette leaf of *mtn1-1mtn2-1* mutant and WT. (B) The *mtn1-1mtn2-1* shows increased vascularisation of the leaf compared to (A) WT.

(C-H) Aniline blue stained images of (C-E) stigma and (F-H) ovaries of (C, E, F, H) *mtn1-1mtn2-1* and (D, G) WT. o = ovule, pt = pollen tube. WT pollen tube growth on stigma and style of *mtn1-1mtn2-1* (C, F), WT pollen tube growth on WT stigma and style (D, G) and *mtn1-1mtn2-1* pollen tube growth on *mtn1-1mtn2-1* style and stigma (E, H) are shown. (Source: C-H, Sarah Schoor)

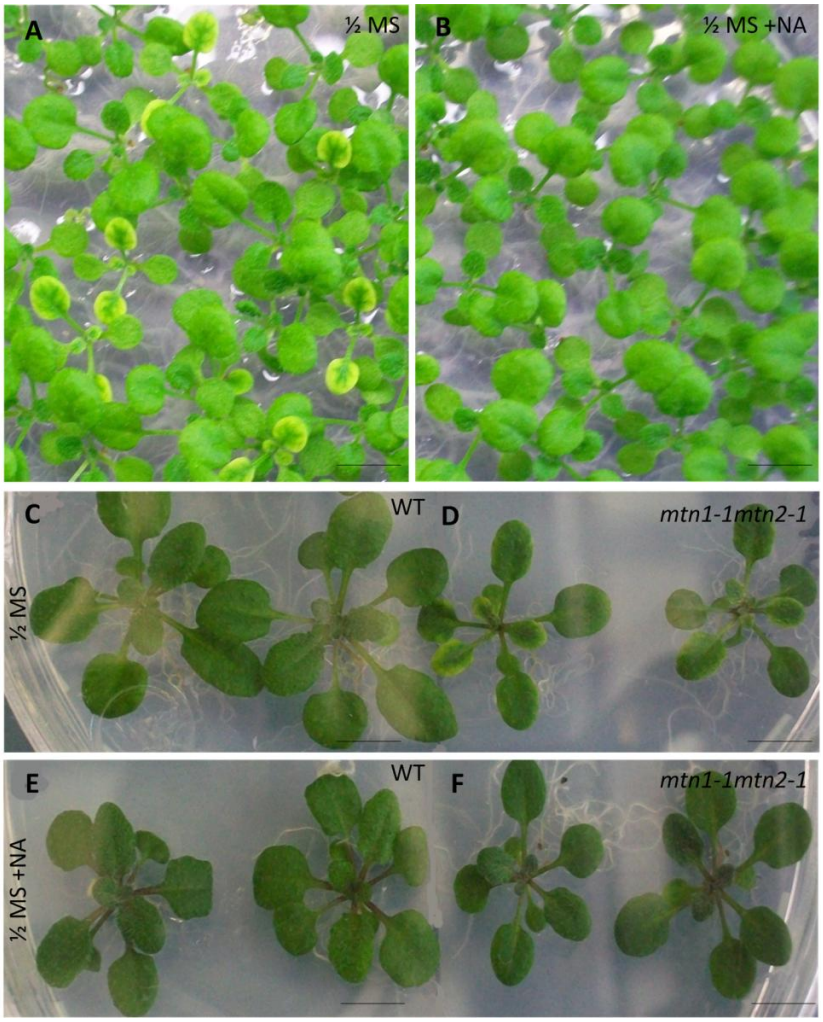

Figure S2.3: Interveinal chlorosis by Nicotianamine (NA)

(A, B) Seedlings of *MTN1/mtn1-1.mtn2-1/mtn2-1* segregating seeds placed on ½ MS and ½ MS supplemented with 20 µM NA. The (A) *mtn1-1mtn2-1* seedlings on ½ MS could be readily identified based on interveinal chlorosis whereas this phenotype was not observed, if these seedlings were (B)supplemented with NA.

(C, D) WT and mutant seedlings identified from (A) were transplanted to fresh ½ MS medium.

(E, F) WT and mutant seedlings identified from (A) were transplanted to fresh ½ MS medium supplemented with NA. The NA eliminated interveinal chlorosis in the mutant.

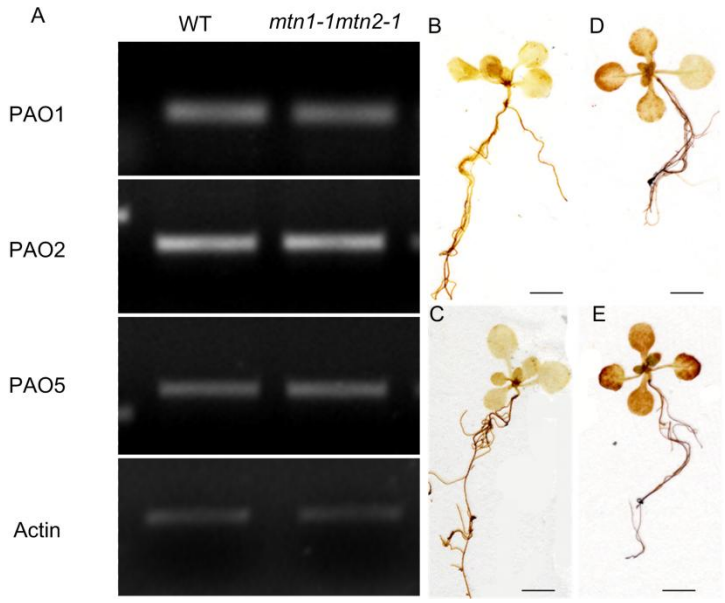

Figure S2.4: Relative transcript abundance of polyamine oxidises and H2O2 production.

(A) RT-PCR of *PAO1, PAO2* and *PAO5* conducted on the leaves of WT and *mtn1-1mtn2-1* harvested two weeks after bolting. Among the five Arabisopsis PAO genes three representative genes were selected. *PAO2-4* is distinct from *PAO1* and *PAO5* based on amino acid sequence identity (Fincato et al., 2011). The *PAO1* is particularly interested as it is suggested to use Tspm as a substrate *in vivo*. The *PAO2* that is expressed primarily in leaf veins (Takahashi et al., 2010) was selected to represent *PAO2-4* subfamily. PAO5 was used as it is expressed in all tissues (Takahashi et al., 2010).

(B-E) Detection of H_2O_2 produced by (B, D) WT and developmentally similar (C, E) 14-day-old *mtn1-1mtn2-1* seedlings using DAB staining. Scale bars, 4mm. No differences were visible between WT and *mtn1-1mtn2-1* staining intensities in the leaves of the seedlings grown on (B, C)½ MS. Seedlings that were grown (E,F) ½ MS supplemented with 3-amino-1,2,4-triazole (AT), catalase inhibitor that induce oxidative stress, served as controls and stained both WT and *mtn1-1mtn2-1* leaves.

Table S2.1: Primer sequences

Primer name	Description	Primer Sequence
mtn1-1F	Forward primer for mtn1-1(At4g38800); SALK_085385	TGACGGAGACCAACTCCATAC
mtn1-1R	Reverse primer for mtn1-1 (At4g38800); SALK_085385	GAGGCTCTTCCTTTGGTCAAC
mtn2-1F	Forward primer for mtn2-1 (SALK_071127)	CCTTGCTTACGTGGCATAAAC
mtn2-1R	Reverse primer for mtn2-1 (SALK_071127)	GGAAAGGGCAAAAATATATGG
LBb1.3	Left-border for SALK lines	ATTTTGCCGATTTCGGAAC
UBQ10 p F	Forward primer for UBQ 10 promoter with 3' Age I	TAACCGGTAACGATCGTTAAATCTCAAC
UBQ10p blunt R	Reverse primer for UBQ10 promoter with 5'-blunt end	CTGTTAATCAGAAAAACTCAGAT
AtMTN1-F3	Forward primer to MTN1 RTPCR	GAATCGGAAGAGAGGGATAAG
AtMTN1-R3	Reverse primer to MTN1 RTPCR	ATAAAAAAGGAAGAGAACAGAAG
AtMTN2-F1	Forward primer to MTN2 RTPCR	CAACAGATTACGCCTCGTTG
AtMTN2-R1	Reverse primer to MTN2 RTPCR	ACAGGTATTCTTCTGTCATGG
Actin 2F	Forward Primer for Actin (At5G09810)	CCG ATG GTG AGG ATA TTC AGC C
Actin 2R	Reverse Primer for Actin (At5G09810)	TGT CAC GGA CAA TTT CCC GTT CTG C
gMTN1-F	Forward Primer for genomic MTN1	AACCCGGGATGGCTCCTCATGGAGATGG
gMTN1-R	Reverse Primer for genomic	ATGGATCCGTTTAAAGGTCCGAAAGGTTTCT

	MTN1	
MTN1CDS-F	Forward Primer for MTN1 coding sequence	AACCCGGGATGGCTCCTCATGGAGATGG
MTN1CDS-R	Reverse Primer for MTN1 coding sequene	ATGGATCCGTTTAAAGGTCCGAAAGGTTTCT
hMTAP-F	hMTAP CDS cloning ATG blunt 5' end	ATGGCCTCTGGCACCAC
hMTAP-R	hMTAP CDS cloning TAA blunt 3' end	TTAATGTCTTGGTAATAAAACAG
PAO1 RT-F	Forward Primer For PAO1	TTATTGGCCTTCACCGAGTC
PAO1 RT-R	Reverse Primer For PAO1	GGAGACGCGTTAGCTATTTCA
PAO2 RT-F	Forward Primer For PAO2	CAGCTTGCCAAAGACATTGA
PAO2 RT-R	Reverse Primer For PAO2	AAACGATCCGACACGAGAAT
PAO5 RT-F	Forward Primer For PAO5	GGGAGGATTCCGAGTTTAGG
PAO5 RT-R	Reverse Primer For PAO5	TTCTCTAAACACATTACCCCAAAA

Chapter 3: Dissecting the complex phenotypes associated with 5'-methylthioadenosine nucleosidase deficiency

3.1 Overview

5'-methylthioadenosine is a by-product of polyamine, nicotianamine, and ethylene biosynthesis, which is recycled into Met by 5'-methylthioadenosine nucleosidase (MTN). In Arabidopsis, MTN is encoded by two genes: *AtMTN1* and *AtMTN2*. Mutants that have disruptions in both of these genes have pleiotropic developmental defects, including abnormal vasculature and reproductive problems. The goal of this research was to define the fundamental abnormal trait associated with reduced MTN activity. To this end, a series of *MTN*-deficient lines with differing residual MTN activity were developed using two approaches: crossing different *MTN* knock-down single alleles and creating transgenic lines that express an artificial microRNA (ami) against *MTN2* in an *mtn1-1* background. The single T-DNA insertion *mtn* mutants used for the crosses were *mtn1-1* (SALK_085385), *mtn1-2* (GK_568C06.18), *mtn1-4* (SALK_088214C), *mtn2-1* (SALK_ 071127), *mtn2-2* (GK_845B05), and *mtn2-5* (SALK_022510). The following lines were generated (1) *mtn1-4mtn2-1,* (2) *mtn1-1mtn2-1*, (3) *mtn1-1mtn2-5*, (4) ami5.3, and (5) ami2.8. The complete loss-of-function MTN mutant, *mtn1-2mtn2-1,* was embryo lethal. Based on an analysis of the anatomy and development of these lines, three with distinct phenotypes were selected for detailed study: *mtn1-1mtn2-5*, *mtn1-1mtn2-1,* and ami5.3. They were further assessed and compared to the WT with respect to their MTN activity and Met-related metabolite content. Their residual MTN activity correlated with the severity of their phenotype. The *mtn1-1mtn2-1* has only 14 % of the MTN activity and have a complex pleiotropic phenotype, while *mtn1-1mtn2-5* with 28 % of the MTN activity of the WT, has a delayed transition to flowering (bolting) along with the xylem proliferation defects associated with *mtn1-1mtn2-1*. The ami5.3 line, with 16 % MTN activity, is phenotypically similar to *mtn1-1mtn2-1* and shares delayed bolting, xylem proliferation defects, and delayed

senescence. Based on these analyses we conclude that the delayed bolting is the fundamental trait associated MTN deficiency.

3.2 Introduction

5'-methylthioadenosine nucleosidase (MTN, EC 3.2.2.16) activity is essential for the hydrolysis of methylthioadenosine (MTA), which is generated in plants by means of three essential biochemical pathways: polyamine (PA), nicotianamine (NA), and ethylene biosynthesis (Figure 3.1). Phenotypic analysis of mutants with disruptions in the genes that encode the enzymes involved in these three pathways has revealed the critical roles of PA [putrescine (Put), spermidine (Spd), spermine (Spm), and thermospermine (Tspm)], NA, and ethylene in plant growth and development.

Analysis of Arabidopsis PA biosynthesis mutants has shown that Put and Spd are essential for plant survival and growth because knocking down many of the PA biosynthesis pathway components leads to embryo lethality. In this pathway, arginine decarboxylase (ADC; EC 4.1.1.19) converts arginine to Put and subsequently to Spd by means of Spd synthase (SPDS; EC 2.5.1.16; Figure 3.1). Spd is catalyzed to either Spm or Tspm via Spm synthase (SPMS; EC 2.5.1.22) and Tspm synthase (ACL5; EC 2.5.1.79), respectively. *S*-adenosyl-*L*-methionine (SAM) decarboxylase (SAMDC; EC 4.1.1.50) provides the aminopropyl group necessary for the conversion of Put to Spd, of Spd to Spm, and of Spd to Tspm. Double mutants of ADC (*adc1adc2*; Urano et al., 2005), Spd synthases (*spds1spds2*; Imai et al., 2004b), and SAM-decarboxylase (*samdc1samdc4*; Ge et al., 2006) show lethality at the embryo stage. The involvement of Tspm in vascular development has been revealed through the study of ACAULIS5 (*acl5*) mutants (Hanazawa et al., 1997; Vera-Sirera et al., 2010). *ACL5* encodes Tspm synthase, which is expressed in vascular tissues (Clay and Nelson, 2005), specifically in the

xylem vessel elements during xylem differentiation (Muñiz et al., 2008). A point mutation in *ACL5* leads to dwarf plants with short internodes (*acl5*,

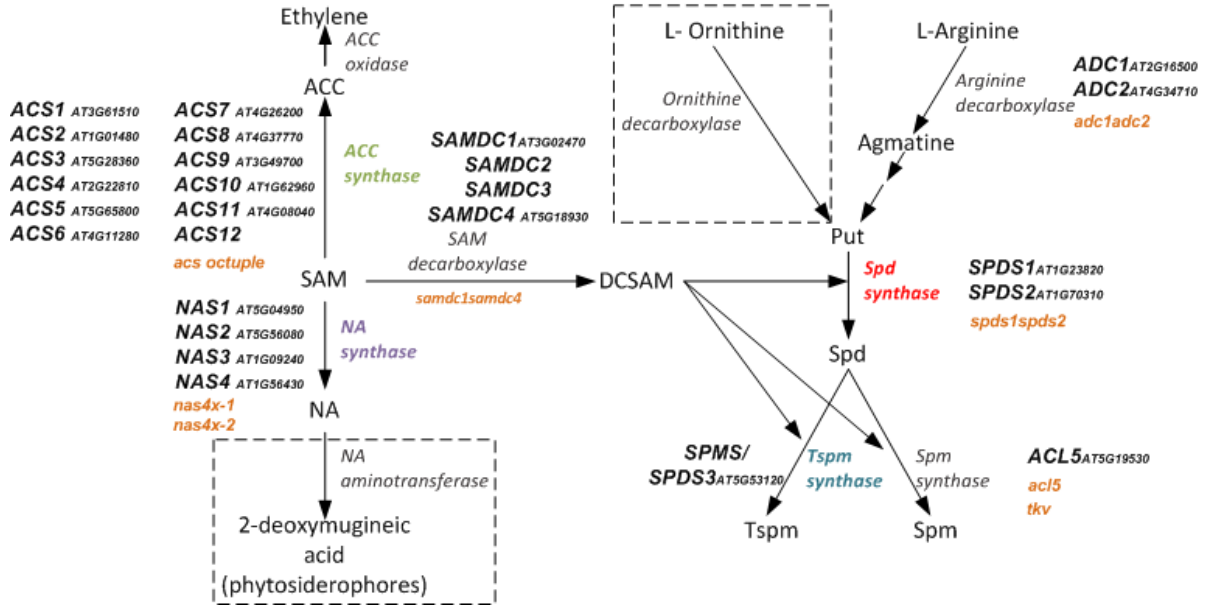

Figure 3.1: Pathways affected by MTA accumulation

The PA (Put, Spd, Spm, and Tspm), NA, and ethylene biosynthesis pathways share SAM as a common precursor and produce MTA as a by-product. The different gene isoforms of MTA-generating and Put-generating enzymes, their gene ID numbers, and the Arabidopsis mutants (orange) that exhibit these disrupted genes are shown. The boxed reaction does not occur in Arabidopsis.

Hanazawa et al., 1997) along with altered secondary vascular development that completely lacks pitted xylem vessel elements and xylem fibres (Muñiz et al., 2008). Based on these observations, it has been proposed that Tspm prevents the premature death of the developing xylem vessels (Muñiz et al., 2008). It has also been shown that Tspm translationally activates *SAC51,* which encodes a basic-helix-loop-helix (bHLH-type) transcription factor (Imai et al., 2006) generally involved in the regulatory transcriptional programs (Toledo-Ortiz et al., 2003). *Thick-vein* (*tkv),* another mutant of *ACL5,* has small leaves with thicker leaf mid veins due to an increased number of xylem (xy), phloem (ph), and cambial cells. The *bud2* mutant, which has a mutation in SAM decarboxylase 4 also displays enlarged vascular systems in inflorescences, roots, and petioles (Ge et al., 2006). On the other hand, the *spms* mutant, which is defective in its synthesis of Spm, shows WT morphology under normal growth conditions (Imai et al., 2004a). Taken as a whole, the evidence indicates that Put and Spd are essential for embryogenesis and that Tspm is essential for proper vascular development.

Plant lines deficient in NA content have been created either by mutagenizing NA synthase (NAS; EC 2.5.1.43) genes or by introducing a transgene that metabolizes endogenous NA. Takahashi and his colleagues (2003) created a tobacco line that constitutively expresses a barley gene for encoding nicotianamine aminotransferase (NAAT; EC 2.6.1.80), which converts endogenous NA into a non-functional product, resulting in undetectable NA content. The NA-deficient *chloronerva* tomato mutant has a point mutation in its single NA synthase gene (Bohme and Scholz, 1960) whereas the *nas4x-2* mutant of Arabidopsis has mutations in all four NA synthase isoforms (Klatte et al., 2009). All of these lines have the altered metal profiles that are associated with interveinal chlorosis and reproductive abnormalities.

Tsuchisaka et al. (2009) describe a series of ethylene-deficient Arabidopsis mutants created by multiple genetic crosses between point mutants in each of the nine genes (*ACS1*, *ACS2*, *ACS4-9*,

and *ACS11*). In these mutants ethylene is synthesized from SAM in two steps in which the catalysts are aminocyclopropane-1-carboxylic acid (ACC) synthase (ACS; EC 4.4.1.14) and ACC oxidase (ACO; EC 1.14.17.4), respectively. Each single ACS mutant has a WT phenotype while the higher order mutants (pentuple, hexuple, heptuple, or octuple) have an array of abnormalities. The knock-out of all nine ACS activities resulted in embryo lethality. The octuple ACS mutant has a lower ethylene production than the pentuple, hexuple, or heptuple mutants and shows delayed senescence.

PA-, NA- and ethylene-deficient mutant analysis led to the discovery of the connection of these metabolites to a specific phenotype: Put or Spd with embryo development and Tspm with vascular development. NA, on the other hand, is responsible for ion transport and seed production, and ethylene affects many aspects of growth and development, including senescence.

The *MTN*-deficient double mutant, *mtn1-1mtn2-1,* with disruptions in both its genes [*MTN1* (At4g38800) and *MTN2* (At4g34840)] has only ~ 14 % of the MTN activity present in WT (buds) and two-fold to five-fold higher MTA content (Chapter 2). MTA is known to product inhibit the enzymes that catalyze the biosynthesis of PA, NA, and ethylene in plants (Albers, 2009; Hyodo and Tanaka, 1986; Herbik et al., 1997; Chapter 1). Changes in MTA metabolism thus have the potential of impacting a vast number of processes, including PA, NA, and ethylene biosynthesis and the developmental programs they coordinate. In agreement with this assessment is the fact that *mtn1-1mtn2-1* is deficient in NA content with altered PA profiles: increased Put with decreased Spd and Spm (Chapter 2). This mutant, which also has reduced auxin transport and altered auxin maxima shows a pleiotropic developmental defects, including delay in the emergence of the inflorescence stem (bolting) along with defects in reproduction and vascular development (Bürstenbinder et al., 2010; Chapter 2). The *mtn1-1mtn2-1* is sterile, with defects

in both male and female reproductive structures. The male defects include abnormal and non-viable pollen production with indehiscent anthers, and the female reproductive defects include improper ovule maturation. The vascular defects in the leaves are evident as thicker mid-veins each with increased xylem and phloem production. The stems have an increased number of asymmetrically arranged vascular bundles that track to the altered auxin maxima. Thus, an understanding of the role of *MTN* in plant development requires the dissection of the complex phenotypes observed in the *mtn1-1mtn2-1.*

In this study, an allelic series of *MTN*-deficient lines with variable phenotypes and MTN activities were comprehensively examined in order to identify and investigate the primary traits in order of manifestation that result from MTN deficiency.

3.3 Methods

3.3.1 Plant materials and growth conditions

All of the *MTN*-deficient lines were first germinated on ½ MS media after the surface sterilization of the seeds and incubation at 4^{o}C for 48 h. After 14 d, 10 seedlings from all eight lines including the wild type (WT, ecotype Columbia), were transplanted to soil and grown under standard long day conditions: 8 h dark (21^{o}C) and 16 h light (23^{o}C).

3.3.2 Plate and soil-based growth assays

Sterilized seeds were placed on ½ MS and the growth and developmental stages of all *MTN*-deficient lines were compared to those of the WT using plate-based growth assays and soil-based-growth assays conducted as detailed in Boyes et al. (2001). For the plate-based assays, the time taken for the radicle to emerge (stage 0.5), the cotyledons to open (stage 1), and the first set of true leaves > 1mm to be produced (stage 1.02) was recorded (usually a period of 14 days). These seedlings were then transplanted to soil for the soil-based assay. For this assay, the number of leaves, the percentage of plants the inflorescence stems of which had emerged, and the time taken for the first rosette leaf that turns yellow was recorded. Mature plants were used to determine the final height, the number of cauline nodes, the number of cauline branches, the number of first order rosette branches, and the number of second order rosette branches.

3.3.3 Generation and identification of the amiRNA *MTN*-deficient mutants

With the use of MicroRNA Designer (http://wmd.weigelworld.org), a specific amiRNA was designed to target only *MTN*2. The amiRNA was generated by using four primers amiMTN2-I-IV (Table S3.2) and a pRS300-based vector as a template (Schwab et al., 2006). The amplified amiRNA fragment was cloned into the *Eco*RI/*Bam*HI site of pSAT4. These constructs were then transferred into the I-*Sce*I site of the pPZP-RCS2 binary vector to enable plant transformation, as

detailed in Chapter 2. The T1 seeds were screened by spraying with 0.067 % (v/v) (40 mg/mL) herbicide glufosinate ammonium (Basta; Wipeout from Wilson Laboratories Inc.; Dundas, Canada) daily after true leaf emergence; the presence of the amiRNA was confirmed in the resistant plants by PCR with pSAT-F with amiMTN2-IV primers.

3.3.4 Development of double-mutant lines

The *mtn1* (*mtn1-1, mtn1-2, mtn1-4*) and *mtn2* (*mtn2-1, mtn* 2-2 *and mtn2-5*) homozygous single mutants were crossed, and the resultant F2 progeny were screened for double mutants by PCR, using left border and gene-specific reverse primers and a second reaction with two flanking primers. Homozygous *mtn1-4mtn2-1*, *mtn1-1mtn2-5,* and *mtn1-1mtn2-1* lines were identified by means of PCR amplification using primers listed in Table S3.2. The T-DNA insertion genomic location was confirmed by sequencing the resultant PCR products with left border primers (data not shown).

3.3.5 Screening for MTN-deficient double mutants

For some allele combinations, *mtn* double mutants were not obtained after screening > 100 F2 plants (e.g. *mtn1-2mtn2-2*) and in some cases, the recovery rate of the double mutant was much lower than the expected based on simple Mendelian segregation (e.g., *mtn1-1mtn2-1*). To analyze the genotypes of the progeny in these cases, a plant that was segregating progeny for only one mutant allele was identified from F2 populations and used for further analysis. Using light microscopy, the seeds in three self-fertilized F2 stage 17b siliques from these plants were compared visually with those from developmentally matched WT siliques in order to determine the percentages of aborted ovules. All of the seeds from the three siliques from each of these mutants were then germinated and the F3 seedlings genotyped through PCR in order to determine the segregation ratio. All of the seeds from a replicated set of three siliques were also cleared in Hoyer's solution (30 g gum arabic, 200 g chloral hydrate, 20 g glycerol, and 50 mL

water; Truernit et al., 2008) to enable the detection of whole-mount embryos using light microscopy.

3.3.6 Microscopic analysis

Free-hand stem cross-sections of all of the *MTN*-deficient lines were stained with 0.1 % Toluidine Blue O (TBO) and observed using light microscopy. The stage 17b siliques were placed individually onto the surface of double-sided tape which had been attached to slides. After the valves were gently removed with fine-point tweezers, the seeds were observed with a dissecting microscope and their contents scored according to the number of normal seeds, abnormal seeds and unfertilized ovules. The developing seeds were placed in Hoyers's solution overnight. The slides were viewed using a Zeiss Axiovert 200M microscope with differential interference contrast optics and Axiovision Rel. 4.63 software.

3.3.7 MTN assay and measurement of MTA and NA

The MTA activity of the crude protein extracts from the unopened floral buds of *mtn1-1mtn2-5*, ami 5.3, *mtn1-1mtn2-1,* and the WT was determined using a spectrophotometric assay, as described in Chapter 2. HPLC methods were used to measure the MTA and NA contents in the rosette leaves and inflorescences of *mtn1-1mtn2-1*, ami5.3, *mtn1-1mtn2-5,* and the WT, as described in Chapter 2.

3.4 Results

3.4.1 Mutant generation

3.4.1.1 *MTN1* and *MTN2* T-DNA double mutants

MTN-deficient single mutants were selected from either the SALK collection (http://signal.salk.edu/cgi-bin/tdnaexpress; Alonso et al., 2003) or the GABI collection (http://www.gabi-kat.de) based on the flanking sequence data provided. Four of the *MTN*-deficient single mutants (*mtn1-1*, SALK_085385, T-DNA insertion in the third intron; *mtn1-2*, GK_568C06, T-DNA insertion in the sixth exon; *mtn2-1*, SALK_ 071127, T-DNA insertion in the fourth exon; *mtn2-2*, GK_845B05, T-DNA insertion in the fourth exon) are phenotypically WT in standard growth conditions (Bürstenbinder et al., 2010). However, the *mtn1-1mtn2-1* double mutant showed pleiotropic phenotypes. To generate MTN-deficient double mutants that have phenotypes less severe from those of the *mtn1-1mtn2-1* mutant, two new MTN-deficient single mutants, *mtn1-4* (SALK_088214C, T-DNA insertion in the 5' UTR) and *mtn2-5* (SALK_022510, T-DNA insertion in the promoter), were crossed with the existing *mtn1-1* and *mtn2-1* single mutants (Figure 3.2, Table S3.1). Two new *MTN*-deficient double mutants were recovered: *mtn1-4mtn2-1* and *mtn1-1mtn2-5*. The genotypes of these mutants were confirmed by PCR using gene-specific and left border primers (Figure S3.1, Tables S3.2, S3.3). Repeated attempts to recover *mtn1-2mtn2-2* failed.

3.4.1.2 MTN-deficient artificial microRNA (amiRNA) lines

Using the oligonucleotide sequences generated by Web MicroRNA Designer (http://wmd.weigelworld.org; Schwab et al., 2006), several unsuccessful attempts were made to engineer *MTN*-deficient amiRNA lines targeted at both MTN genes. Several lines that expressed an amiRNA targeted at *MTN2* in an *mtn1-1* background were ultimately created.

Based on a preliminary analysis of 15 lines, two (ami2.8 and ami5.3) that shared some traits in common with the *mtn1-1mtn2-1* plants were selected for further analysis.

3.4.2 Detailed analysis of the *mtn1-1mtn2-1* mutant phenotype

To establish the phenotypic extremes of *MTN* deficiency, the *mtn1-1mtn2-1* mutants that had the strongest phenotype compared to those of the WT were first analyzed. The *mtn1-1mtn2-1* mutants exhibits a slight delay (less than a day) in radicle emergence (growth stage 0.5 as described in Boyes et al., 2001; Figure S3.2A) and cotyledon opening (growth stage 1.0, as described in Boyes et al*.,* 2001; Figure S3.3). The *mtn1-1mtn2-1* mutants had shorter roots than WT (Figure S3.2B), which may be a consequence of the delayed emergence of their radicles. These mutants also exhibit delayed development of their first true leaves, which have interveinal chlorosis, as described in Chapter 2. Another phenotype that was observed in the same growth stage of *mtn1-1mtn2-1* plants was their defective leaf cuticle. This trait was assayed using the rapid visualization method described by Tanaka et al. (2004). In this simple method, leaves with cuticle defects become purple when stained with TBO which is excluded by the waxy surface of WT leaves (Figure S3.4 A-C). Using this test, the *mtn1-1mtn2-1* mutant adaxial rosette leaf surface stained purple (Figure S3.4B) similarly to that of a mutant with previously documented cuticle defects (*fiddlehead*, *fdh-13*; Fig S3.4C). The *mtn1-1mtn2-1* was classified as having a patchy cuticle defect (class II) based on the scheme developed by Tanaka et al. (2004). As expected, WT did not exhibit an evident staining pattern (Figure S3.4A).

As the plants matured into the vegetative phase, the *mtn1-1mtn2-1* mutants generated an increased number of thick, long, narrow brittle-textured dark green rosette leaves compared to the leaves of the WT plants (Figure 3.3; Figure S3.4D, E). Both the *mtn1-1mtn2-1* and the WT plants developed five juvenile-vegetative phase rosette leaves with round margins and trichomes only on their adaxial surfaces. Next vegetative leaves developed with serrated

margins and trichomes present on both surfaces. The *mtn1-1mtn2-1* plants grew 7 ± 1 adult vegetative phase rosette leaves as compared to the 4 ± 1 vegetative phase rosette leaves produced by the WT.

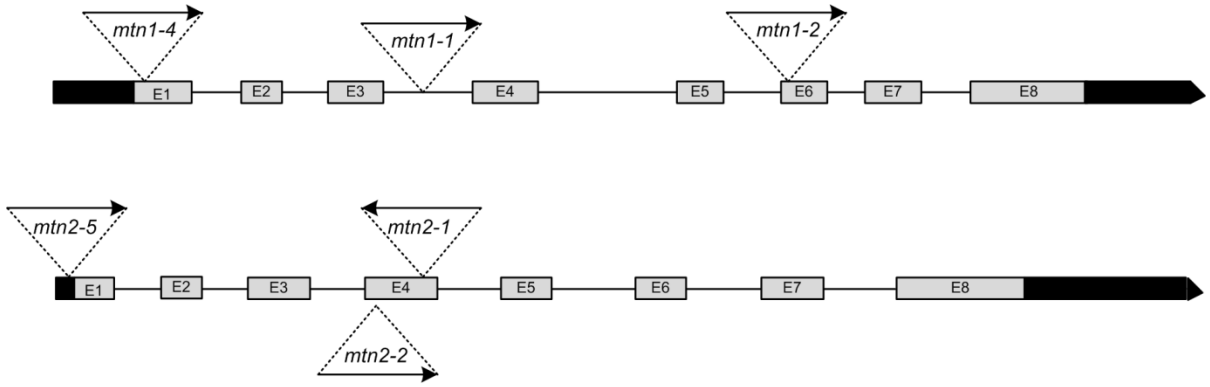

Figure 3.2: Gene structure of MTN genes

Gene structure of MTN1 (top) and MTN2 (bottom) showing the T-DNA insertions for *1-1, 1-2, 1-4, 2-1, 2-2* and *2-5.*

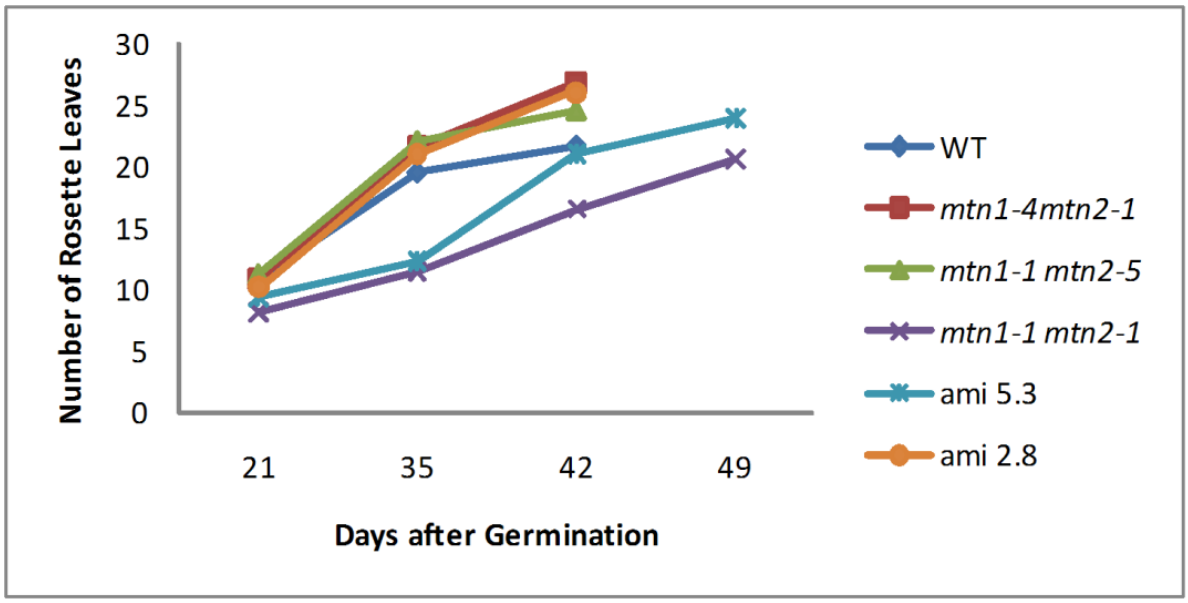

Figure 3.3: Total number of rosette leaves of *MTN*-deficient lines.

The *mtn1-1mtn2-1* plants produced 12 ± 1 adult rosette leaves without petioles compared to the WT production of 2 ± 1 at bolting. Both adult-vegetative phase rosette leaves and adult reproductive-phase rosette leaves contribute to the overall increased number of leaves evident in the *mtn1-1mtn2-1* mutant. As described in Chapter 2, these *mtn1-1mtn2-1* rosette leaves have an increased vasculature, with thicker-mid veins due to the increased xylem proliferation. (N = 5-8).

In the reproductive phase, 17 days after germination, 50 % of the WT population reached growth stage 5.10 (Boyes et al., 2001), which occurs when the first flower buds are visible (bolting). It is notable that formation of the first flower buds was delayed in the *mtn1-1mtn2-1* mutant by six days and that, because of individual variation, six weeks were required for the entire population to transit to the flowering stage (Figure 3.4A, B). Compared to the WT plants, the mature *mtn1-1mtn2-1* plants were shorter and bushier with enhanced shoot branching (Figure 3.5A, F). The mutant plants remained shorter than the WT ones at each developmental time point up to 40 days after sowing, as indicated by the height of the primary inflorescence (Figure 3.4A). However, since the mutant plants continued to increase in height and show delayed senescence, they reached a final height of 26 ± 3 cm versus the 24 cm height of the WT plants at maturity (Figure 3.5A, B).

Arabidopsis has two types of nodes that produce first-order branches: cauline nodes, located on the primary inflorescence stem, and rosette nodes, located on the hypocotyl. The number of cauline nodes was 3 ± 1 for both *mtn1-1mtn2-1* and the WT plants, with a similar number of first-order branches arising from the primary inflorescence stem. On the other hand, the number of first-order branches produced from the rosette nodes was greater in the *mtn1-1mtn2-1* plants than in the WT plants (Figure 3.6B). Moreover, in the *mtn1-1mtn2-1* plants an increased number of second-order branches were also produced from the first-order rosette

branches. The overall increase in number of branches produced a bushy shoot architecture in the *mtn1-1mtn2-1* mutant (Figure 3.5D). At times, two or more cauline leaves arose from the same cauline node and two or more first-order branches grew out from the same cauline node, which are indications of abnormal phyllotaxy. The first-order cauline branches or the second-order rosette branches of the *mtn1-1mtn2-1* mutant were most commonly fascinated with the axillary cauline leaves (Figure 3.6G). Occasionally, the branches of these *mtn1-1mtn2-1* mutants became extremely thick and flattened (Figure 3.6H). When compared to WT inflorescences the *mtn1-1mtn2-1* inflorescences also had altered phyllotaxy with deformed flowers. These mutants were also sterile due to poor ovule development and irregular microsporogenesis, resulting in reduced fertilization efficiency (Chapter 2).

In keeping with the delay in many of the developmental stages, the time to senescence (stage 9.0 in Boyes et al. (2001) was also delayed. On average, 50 % of the WT plants reached this stage 43 days after germination whereas the *mtn1-1mtn2-1 plants* took 48.5 days to senesce.

One phenotype exhibited in both the vegetative and reproductive stages was organ twisting. This was observed in almost all organs of *mtn1-1mtn2-1* plants which were twisted to some extent (Figure S3.5): the hypocotyl, rosette leaves, stems, flower parts (pedicels, stigmas, anther filaments), siliques (stage 16), and roots. The twisting observed was very subtle in the vegetative phase but became more pronounced upon the transition to the reproductive phase. In each organ, the twisting occurred at random locations with an unfixed handedness. For example, along the length of the anther filament shown in Figure S3.5M, the epidermal cell files are arranged in both right- and left-handed directions: towards the anther, the cell files were twisted in a right-handed direction while towards the filament base the files were arranged in a left-handed direction.

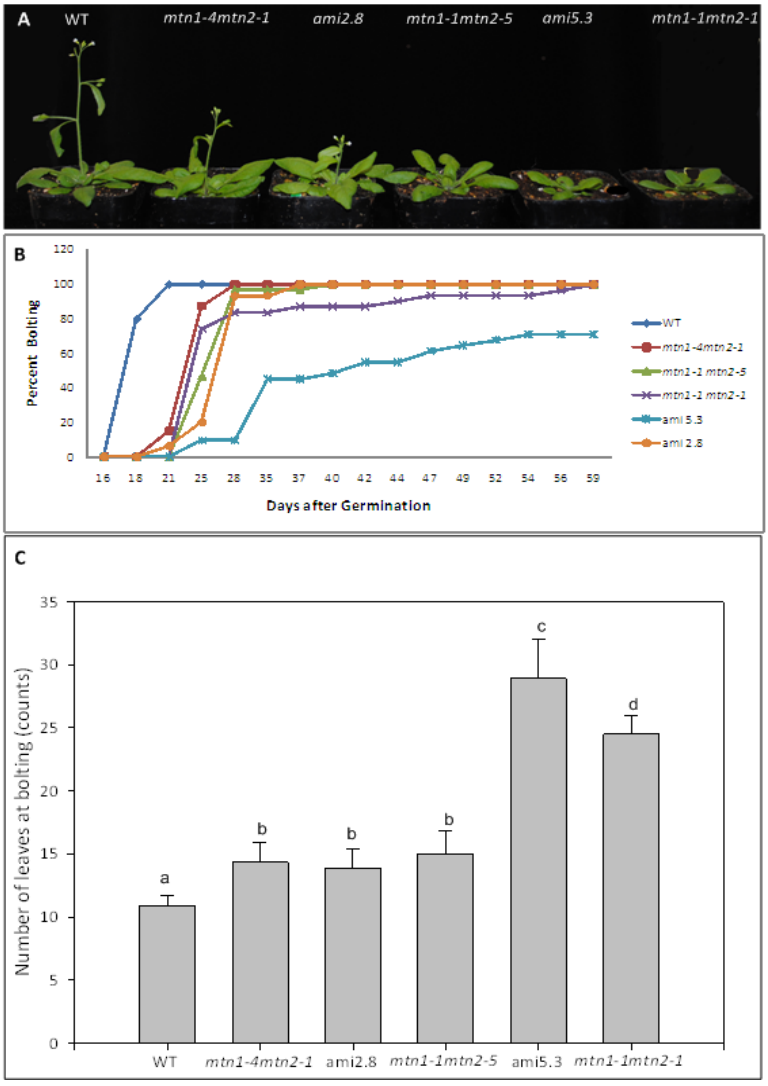

Figure 3.4: Delayed bolting phenotype of *MTN*-deficient plants.

(A) Primary inflorescence stems at 20 days after germination

(B) Percentage bolted over a period of six weeks (N = 15 for WT and ami2.8; N = 30 for all other genotypes).

(C) Number of leaves at the time of bolting. Different letters indicate the statistically significant variations. Means were compared using an independent sample t-test. Average ± SD. (N = 5-8).

The pleiotropic developmental defects in the *mtn1-1mtn2-1* mutant are believed to be due to the binding of accumulated MTA to Spd synthase, Tspm synthase as shown in the present work (Chapter 2). Similarly, MTA binding is also repoted for NA synthase (Herbik et al., 1997) and possibly ACC synthase (Hyodo and Tanaka, 1986). Thus, MTA binding of these enzymes inhibit their activities. Some of the traits observed in this mutant are clearly secondary effects. To determine the fundamental primary target affected by MTA deficiency, phenotypes that could be traced back to a specific enzyme activity that is affected by MTA were examined in less severe *MTN*-deficient mutants. The following representative phenotypes were investigated: embryo lethality and bolting time, which were interpreted as Spd-deficient phenotypes; stem vasculature defects, which were attributed to Tspm-deficient phenotypes; interveinal chlorosis and limited seed production, which were considered to be NA-deficient phenotypes; and delayed senescence, an ethylene-deficient-phenotype.

3.4.3 Variations in the PA-related phenotypes and the degree of *MTN*-deficiency

3.4.3.1 Embryo development

Spd is essential for embryo development (Imai et al., 2004b), so the progenies of three different F2 populations that segregated for one *mtn* allele (i.e., heterozygous for *mtn1* and homozygous for *mtn2,* or vice versa) were genotyped by PCR. All the seeds of the individual siliques were germinated on ½ MS, and the F2 progeny were genotyped. The *mtn1-4mtn2-1* and *mtn1-1mtn2-5* double mutants were recovered from the corresponding F2 population with an expected frequency of $1/4^{th}$ (Table 3.1). However, *mtn1-1mtn2-1* double mutants were recovered at a lower than expected frequency of $1/7^{th}$ (Table 3.1). In the F2 progeny of *mtn1-1mtn1-1/MTN2mtn2-1,* 25 % of the seedlings were expected to be double mutants, but only 14 % of these seedlings were confirmed to be *mtn1-1mtn1-1* and 6 % did not germinate (N = 3 siliques from 3 plants). The frequency of this *mtn1-1mtn2-1* double

Figure 3.5: The mature phenotype of *MTN*-deficient lines.

(A)The WT, (B) *mtn1-4mtn2-1*, and (C) ami2.8 senesced earlier than the (D) *mtn1-1mtn2-5*, (E)ami5.3, and (F)*mtn1-1mtn2-1*. The fully matured green siliques were observed in all lines except *mtn1-1mtn2-1*. The close up images of primary inflorescences show the relative abundance and lengths of the siliques of *mtn1-1mtn2-5* and ami5.3 compared to those of the WT and *mtn1-1mtn2-1*.

mutant recovery was significantly different from the 1/4th that was expected based on chi square analysis (χ^2 = 5.9; df = 2**;** P = 0.05). The *mtn1-2mtn2-2* mutant with T-DNA insertions in exons of both *MTN* genes was not identified even after > 100 F2 seedlings were genotyped. Thus, we concluded that in the lines tested, embryo development is reduced in *mtn1-1mtn2-1,* whereas *mtn1-2mtn2-2* is embryo lethal.

The morphology of the seeds produced from the self-pollinated *MTN1mtn1/mtn2mtn2* plants was analyzed using microscopic observation of dissected stage 17b (Smyth et al., 1990) siliques. In agreement with the expected double mutant recovery from the segregation analysis, the *MTN1mtn1-4/mtn2-1mtn2-1* and *MTN1mtn1-1/mtn2-5mtn2-5* siliques contained large green seeds similar to those in the WT siliques (Figure 3.7A). The *MTN1mtn1-1/mtn2-1mtn2-1* siliques contained 8 % (N = 8-10 siliques from each of 4 plants) aborted ovules along with WT-like seeds (Figure 3.7A).

Table 3.1: Segregation analysis of the *MTN1mtn1/mtn2mtn2* T-DNA alleles

Chi-squared values were calculated for the expected segregation ratio. Statistically significant deviation (P > 0.05) from this ratio is indicated by an asterisk (*).

	Total	**Homo (-/-)**	**Het (+/-)**	**Homo (+/+)**	**Non – germinated seeds**	**χ^2 [hypothesis)**
MTN1mtn1-4/ mtn2-1mtn2-1	420	115	199	106	0	1.54 (1:2:1); N=9
MTN1mtn1-1/ mtn2-5mtn2-5	252	65	129	58	0	0.53 (1:2:1); N=6
MTN1mtn1-1/ mtn2-1mtn2-1	69	10	33	26	8	7.55* (1:2:1); N=3

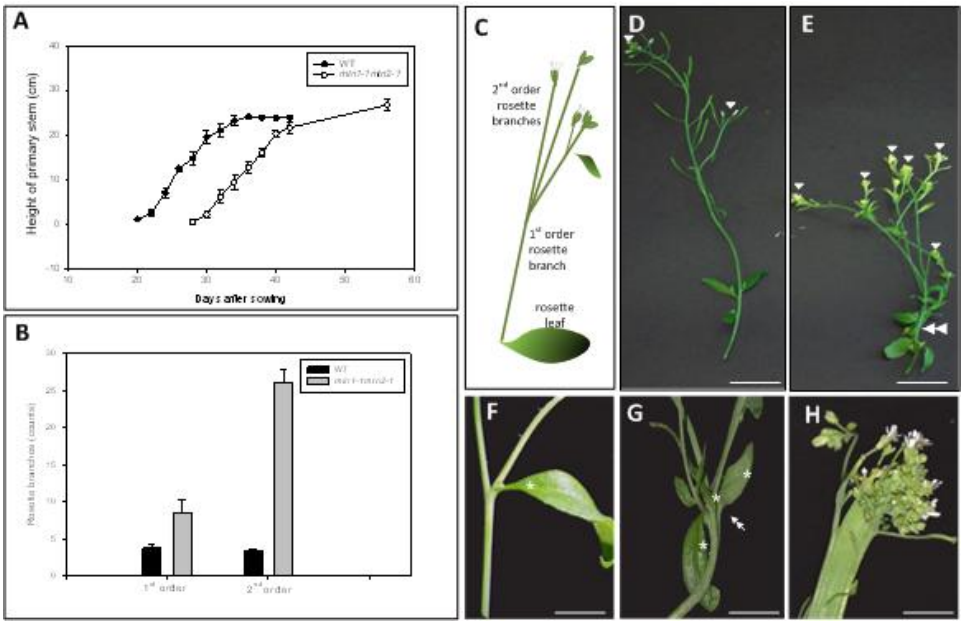

Figure 3.6: Shoot architecture of the mature plant or architecture of the mature plant shoots

(A) Height of the primary inflorescence over a period of eight weeks

(B) Number of first- and second order lateral branches arising from rosette nodes at the cessation of flower production: after 45-46 days after germination for WT and after 84 days after germination for *mtn1-1mtn2-1* (N = 30; Error bars represent Standard deviation).

(C) Diagram of primary and secondary rosette branches.

(D-E) Rosette branches of the (D) WT compared to those of the (E) *mtn1-1mtn2-1*. The first-order rosette branches (double arrowheads) that arise from the rosette nodes subsequently give rise to many second-order rosette branches (single arrowheads) in the *mtn1-1mtn2-1* mutant.

(F-H) Representative branches of WT and *mtn1-1mtn2-1* shoots. In the (F) WT plants, the first-order rosette branch axil with a single cauline leaf gives rise to a single lateral branch whereas in the (G) *mtn1-1mtn2-1* mutant an axil may have many cauline leaves (asterisks) and gives rise to many lateral branches which are indicative of altered phyllotaxy. The cauline leaves of the *mtn1-1mtn2-1* are often fasciated to the rosette branches (double arrowhead); occasionally, (H) stems are fasciated and generate flat structures.

To determine whether the embryos in the WT-like seeds in the *MTN1mtn1-1/MTN2-1mtn2-1* siliques had developmental defects, all of the seeds from 10 stage 16 and 17b siliques were cleared and observed. In the WT plants, seeds develop synchronously within each silique, resulting in similar stage embryos within an individual silique (i.e., stage 17b siliques contain 100 % mature embryos (Figure 3.7B, D).

However, in the *MTN1mtn1-1/MTN2mtn2-1* plants, embryos at different stages (i.e., stage 17 b siliques contained topedo-stage embryos among the majority of mature embryos [Figure 3.7C] or developmentally delayed same-stage embryos [Figure 3.7E]) were observed. The proportion of defective embryos was in agreement with the expected double mutant frequency *(*1/16th) of the total seeds in each silique. However, based on the segregation analysis, the 6 % (Table 3.1) of seeds that did not germinate suggest that some of these embryos were arrested and unable to develop into a seedling.

In summary, the F2 populations of *MTN1mtn1-4/mtn2-1mtn2-1* and *MTN1mtn1-1/ mtn2-5mtn2-5* (or *mtn1-1mtn1-1/MTN2mtn2-5*) segregate in the expected Mendelian ratios whereas F2 populations of *mtn1-1mtn1-1/MTN2mtn2-1* segregate fewer homozygous double mutants than expected. Detailed analysis of the seeds and embryos of *MTN1-1mtn1-1/mtn2-1mtn2-1* suggest that most likely these heterozygous plants have fertilization defects similar to those described for *mtn1-1mtn2-1* (Chapter 2), but to a lesser degree. In contrast to the general observation that 100 % of the ovules in *mtn1-1mtn2-1* are unfertilized, only ~8 %, (Table S3.4) of the ovules in these plants are unfertilized. In a group of fertilized ovules that gave rise to developmentally delayed embryos, ~ 6 % did not germinate into *mtn1-1mtn2-1* seedlings. Of the *MTN*-deficient lines tested, only F2 populations of the *MTN1mtn1/mtn2mtn2* lines have developmental defects in the embryo.

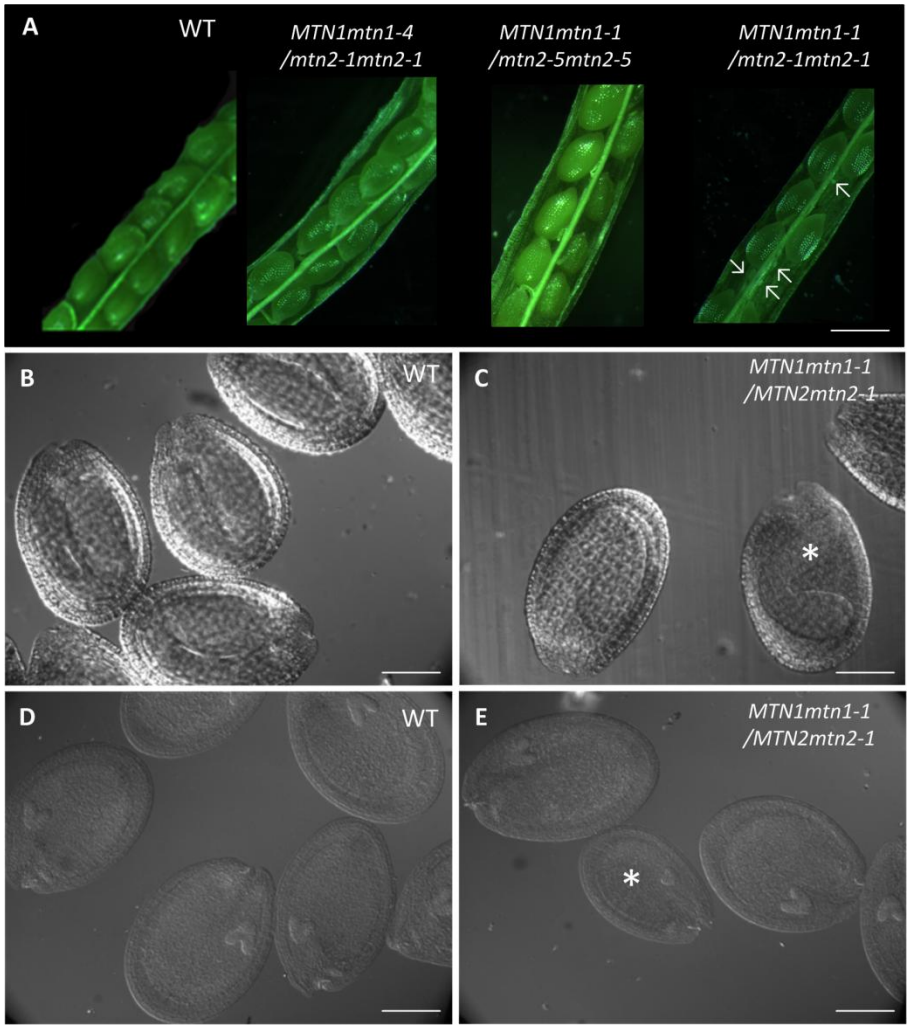

Figure 3.7: Leaf vein pattern and pollen tube growth of mtn1-1mtn2-1 compared to WT.

(A) Images showing normal seeds of the WT, *MTN1mtn1-4/mtn2-1mtn2-1*, and *MTN1mtn1-1/mtn2-5mtn2-5* plants and aborted ovules (↑) of *MTN1mtn1-1/mtn2-1mtn2-1*.

(B-E) Embryos within cleared seeds. (B, C) stage 17b siliques and (D, E) stage 16 siliques of (B, D) the WT and (C, E) the *MTN1mtn1-1/MTN2mtn2-1* plants. In WT siliques only one stage of embryos were pbserved: mature embryos at silique stage 17b and heart stage embryos at silique stage 16. On the other hand the some of the embryos of *MTN1mtn1-1/MTN2mtn2-1* were delayed as indicated by asterisks (*). Scale bars = 25 µm.

3.4.3.2 Delayed bolting

The next step was to determine the effect on bolting of the MTN-deficient mutants. The first floral buds were visible at the rosette apex 16 days after germination (DAG) in the WT, 18 DAG in both *mtn1-4mtn2-1* and ami2.8, and 21 DAG in *mtn1-1mtn2-5*, *mtn1-1mtn2-1*, and ami5.3. Inflorescence stems emerged in 100 % of the WT plants at 21 DAG, while the ami2.8, *mtn1-4mtn2-1*, and *mtn1-1mtn2-5* reached 100% seven days later (28 DAG), and the *mtn1-1mtn2-1* population reached 100 % at 59 DAG. At that time, only 70 % of the ami5.3 had bolted. All MTN-deficient lines thus showed delayed emergence of inflorescence stems compared to the WT. In general a tight correlation exists between the time to flower and the total number of leaves (Koornneef et al., 1991), and therefore it was important to determine whether a correlation could be observed between the number of leaves produced and the onset of flowering in the MTN-deficient plants. At the point of transition to flowering the WT plants had 11 ± 1 rosette leaves while all the other MTN-deficient mutants had a variable number of leaves (Figure 3.4C). The number of the leaves of *mtn1-4mtn2-1*, ami2.8, and *mtn1-1mtn2-5* did not differ significantly among each other but were significantly different from those of the *mtn1-1mtn2-1* (24 ± 2) and ami5.3 (29 ± 3). The time for the inflorescence stem to emerge, a common trait across all the MTN-deficient lines, was correlated directly with the number of rosette leaves as expected, with a correlation coefficient of 0.97.

3.4.3.3 Vascular defects

Tspm-deficient mutants (*tkv/acl5*) have very thin stems with severely increased xylem proliferation (Hanazawa et al., 2000; Clay and Nelson, 2005). Increased xylem proliferation has also been documented in the stems of the *mtn1-1mtn2-1* mutant (Chapter 2) compared to the WT, but less severely than in the *tkv*. The stem vasculature of the *MTN*-deficient lines was therefore analyzed in order to determine how the vascular defects varied (Figure 3.8A-C). A closer comparison of the vascular bundles showed that *mtn1-1mtn2-5* and ami5.3 had

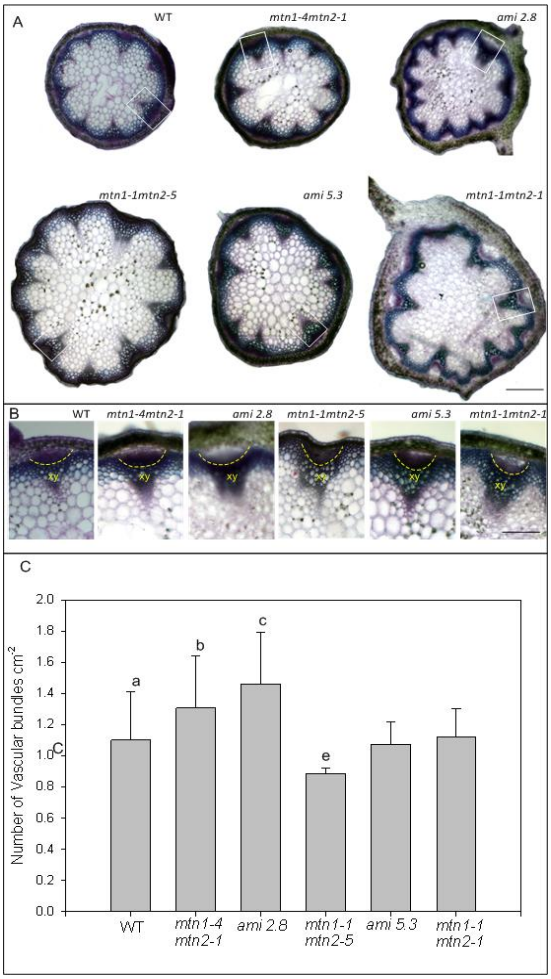

Figure 3.8 Vascular phenotype of *MTN*-deficient mutants/lines.

(A) Representative stem cross-sections of inflorescence stems taken ~2-3cm above the base from all six lines two weeks after bolting. Scale bars = 50 µm

(B) The most proliferated vascular bundle of each stem section (white boxes in A) was enlarged to enable comparison of the vascular tissues between the lines. The yellow dotted line indicates the location of the cambium, which generates phloem (ph) toward the stem epidermis and xylem (xy) toward the stele. Scale bars = 150 µm

(C) The number of vascular bundles per unit area was calculated from cross-sectional images that were magnified 15 fold. The same letters indicate the significant differences ($P < 0.05$). Values are mean ± SD. (N = 3-4).

higher levels of xylem proliferation than the WT (Figure 3.8B) but lower levels than *mtn1-1mtn2-1.* In contrast, the extent of xylem proliferation in *mtn1-4mtn2-1* and ami2.8 remained comparable to that of the WT (Figure 3.8B).

In addition to their increased xylem, the stems of the MTN-deficient lines also differed in thickness, and the number and the asymmetrical arrangement of vascular bundles (Figure 3.8A). With respect to stem thickness, the *mtn1-4mtn2-1* and ami2.8 were comparable to the WT whereas the *mtn1-1mtn2-5*, ami5.3, and *mtn1-1mtn2-1* had ~ 1.5-fold thicker stems (Table S3.5). Compared to the 7 ± 1 vascular bundles of the WT and the *mtn1-1mtn1-4*, all other lines had an increased number of vascular bundles (Table S3.5). To determine whether the increased number of vascular bundles in the mutant is the result of an increase in the size of the shoot apical meristem, the number of vascular bundles per unit area was calculated. This ratio was expected to be unchanged if the increase in the vascular bundle number was the result of a proportional increase in the size of the shoot apical meristem size. On the other hand, if the increased number of vascular bundles was independent of the size of the meristem, an altered ratio would be expected. A significant difference was observed when the *mtn1-4mtn2-1* and ami2.8 were compared to the WT ($P<0.05$; Figure 3.8C). These discrepancies indicate that the number of vascular bundles did not change proportionally with the increase in stem thickness in these lines. Moreover, this ratio was the same in *mtn1-1mtn2-5*, ami5.3, and *mtn1-1mtn2-1,* when compared to the WT. In these cases, the number of vascular bundles increased proportionally to stem thickness. Both the increased number of vascular bundles per unit area and the xylem proliferation defects were together confined to the severely *MTN*-deficient lines: *mtn1-1mtn2-5*, ami5.3, and *mtn1-1mtn2-1*.

The xylem proliferation related to Tspm deficiency in *acl5* is suppressed by several mutations, all of which affect the expression of *SAC51* that encodes a bHLH transcription factor thought to

affect the timing of xylem differentiation. The strongest suppressor is a dominant mutation designated *sac51d* (Imai et al., 2006). To test the hypothesis that the xylem defects of *mtn1-1mtn2-1* relate to Tspm deficiency, the triple mutant *mtn1-1mtn2-1sac51d* was generated. This plant is indistinguishable from *mtn1-1mtn2-1* with respect to the seed set and the number of leaves and branches (Figure S3.7). Thus, the introduction of the *sac51d* mutation into the *MTN*-deficient mutant did not restore any of its phenotypes, including the stem vasculature of the *mtn1-1mtn2-1,* as was observed in the *acl5* mutant.

3.4.4 Alteration of NA-related phenotypes of *MTN*-deficient mutants

3.4.4.1 Interveinal chlorosis

As described in Chapter 2, the *mtn1-1mtn2-1* mutant displays prominent interveinal chlorosis in its first true leaves. However, none of the other *MTN* lines display this trait. The ami5.3 had an occasional slight chlorosis in its first true leaves. The chlorosis persisted less than 24 h, less time than with the typical chlorosis observed between the first true leaf veins of the *mtn1-1mtn2-1* mutants.

3.4.4.2 Seed development

Apart from *mtn1-1mtn2-1*, all the MTN-deficient mutants examined were fertile (Figure 3.5). The *mtn1-4mtn2-1* and ami2.8 lines were fertile, with WT-like silique and seed development (Figure 3.5A-C). Unlike the *mtn1-1mtn2-1* siliques which did not develop seeds throughout their life cycle (Figure 3.5F, J), *mtn1-1mtn2-5* and ami5.3 developed siliques with seeds (Figure 3.5 D - J) at a later stage of their life cycles. At maturity, the fertility of the *mtn1-1mtn2-5* is indistinguishable from that of the WT whereas ami5.3 had relatively low seed production. Interestingly, both the interveinal chlorosis and seed production, which can possibly be interpreted as NA-related phenotypes, were restricted to the *mtn1-1mtn2-1* mutants.

3.4.5 Ethylene-related alterations of the phenotype of *MTN*-deficient mutants

The *MTN*-deficient mutant lines were examined for the time to senescence. The initiation of senescence was recorded as the time at which the leaf blade of any leaf of the rosette first began to turn yellow (Figure 3.9). Since the plants in all of the populations did not reach senescence synchronously, the initiation of senescence was recorded over two weeks. The number of days taken for 25 % of the population (N = 8) to initiate senescence was 42 DAG (WT), 44 DAG (*mtn1-4mtn2-1*), 45 DAG (ami2.8), 46 DAG (ami5.3), 47 DAG (*mtn1-1mtn2-5*), and 48 DAG (*mtn1-1mtn2-1*). On the other hand, the number of days for all eight plants in each population to show signs of senescence were 49 DAG (ami2.8), 52 DAG (WT), 52 DAG (*mtn1-4mtn2-1*), 52 DAG (*mtn1-1mtn2-5*), and 54 DAG (*mtn1-1mtn2-1*) and 56 DAG (ami5.3). Taken together, these results show that ami2.8, *mtn1-4mtn2-1*, and *mtn1-1mtn2-5* initiate senescence at the same time as the WT, whereas the *mtn1-1mtn2-1* plants reach this stage two days later and the ami5.3 plant four days after the WT, respectively.

In summary, the *MTN*-deficient lines exhibited variable behavior in terms of embryo development, the appearance of first buds, stem xylem proliferation and number of vascular bundles, and senescence. Since the *mtn1-4mtn2-1* mutants and the ami2.8 plants showed phenotypes similar to those of the WT, these lines were excluded from further analysis.

3.4.6 Variable MTN activity in different allelic combinations and amiRNA lines

Using a colorimetric assay (Lee et al., 2005) for MTN activity, *mtn1-1mtn2-5*, ami5.3, and *mtn1-1mtn2-1* MTN activity was determined in order to correlate phenotypes with MTN activity. Based on this assay, the *mtn1-1mtn2-5* mutant was found to have only 28 % of WT MTN activity whereas the ami5.3 and *mtn1-1mtn2-1* mutants have 16 % and 14.9 % residual

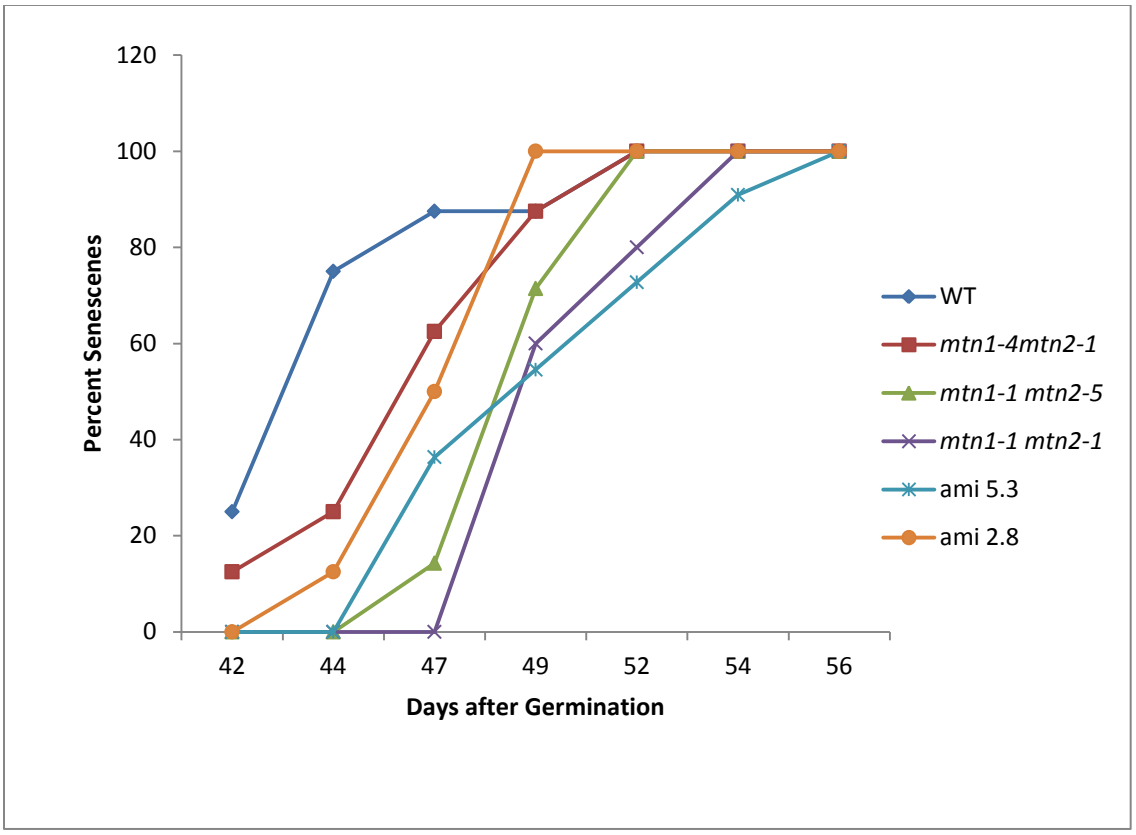

Figure 3.9: Time taken for the leaf edges to become yellow (senescence).

activities, respectively (Figure 3.10; N = 5). The MTN activity in each line was significantly reduced compared to that evident in the WT ($P < 0.05$), but no significant difference was observed between the activity in the ami5.3 and the *mtn1-1mtn2-1*. Next we examined whether the phenotypes observed correlated with the content of Met-related metabolites.

3.4.7 Variable MTA content in the leaves of *MTN*-deficient mutants

It was expected that the MTA content of the mutants would correlate inversely with the amount of residual MTN activity determined in crude bud extracts (Figure 3.10). However, this expected trend was found only in the case of the MTA content of rosette leaves: all lines were significantly different from one another ($P< 0.05$, Figure 3.11A). The MTA content of the *mtn1-1mtn2-1* (2.2 ± 0.1 pmol mg FW^{-1}), which had 14.9 % MTN activity of WT, was 2.4-fold greater than that in the WT (0.9± 0.2 pmol mg FW^{-1}), and the ami5.3, with 16 % of the MTN activity an MTA content only 1.7 fold greater, resulting from increased MTA content (1.5 ± 0.2 pmol mg FW^{-1}). In contrast, the MTA content of the *mtn1-1mtn2-5* was 0.6 ± 0.1 pmol mg FW^{-1} (0.7 fold change compared to WT) with 28 % of the MTN activity. In the inflorescences, a statistically significant increase in MTA was observed only in the *mtn1-1mtn2-1* compared to the level in the WT, ($P< 0.05$, Figure 3.11B). The MTA content of the other two lines was indistinguishable both from the level of the other line and from that of the WT.

3.4.8 NA content in *MTN*-deficient lines

The NA content of both the rosette leaves and the inflorescences was decreased in *MTN*-deficient lines compared to the levels in the WT, except in the ami5.3 leaves (Figure 3.12A, B). The NA content of the *mtn1-1mtn2-1* rosette leaves was significantly reduced compared to that in the WT leaves ($P<0.05$; Figure 3.11A). Significant differences were also observed between the *mtn1-1mtn2-5* and the *mtn1-1mtn2-1* rosette leaves ($P<0.05$; Figure 3.11A). However, as with the MTA content, only the *mtn1-1mtn2-1* inflorescences showed a

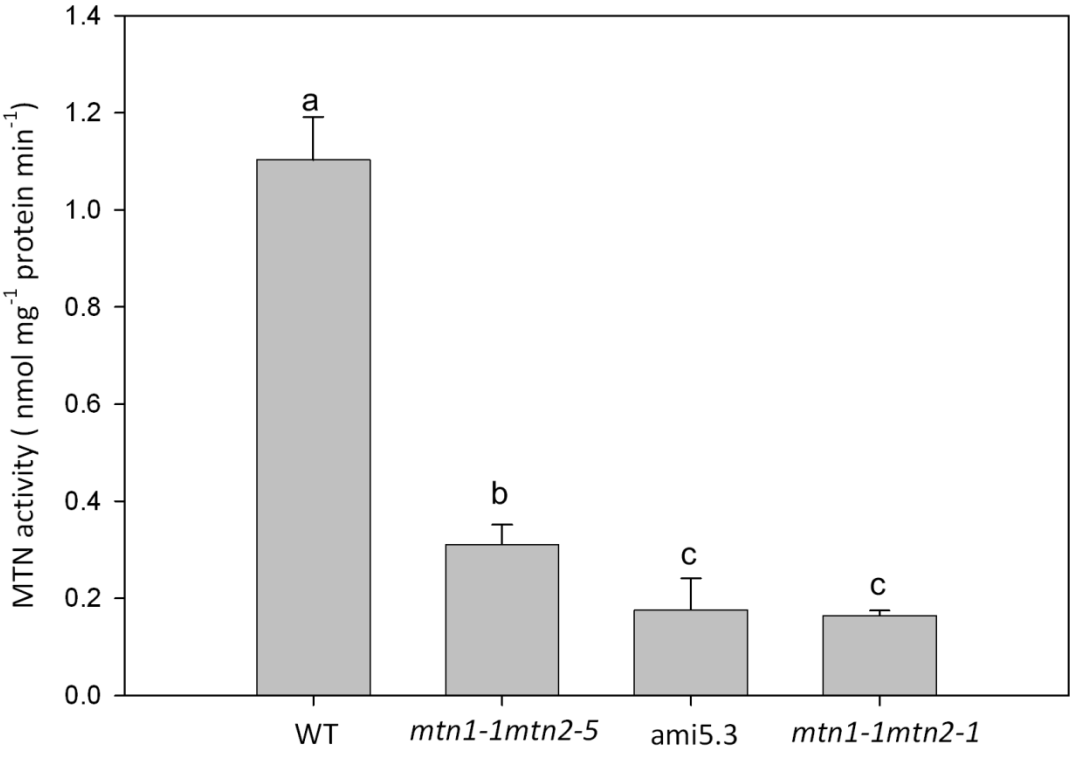

Figure 3.10: MTN activity of MTN-deficient plants.

The different letters indicate the significant differences ($P < 0.05$). Values are mean ± SD. ($N = 5$).

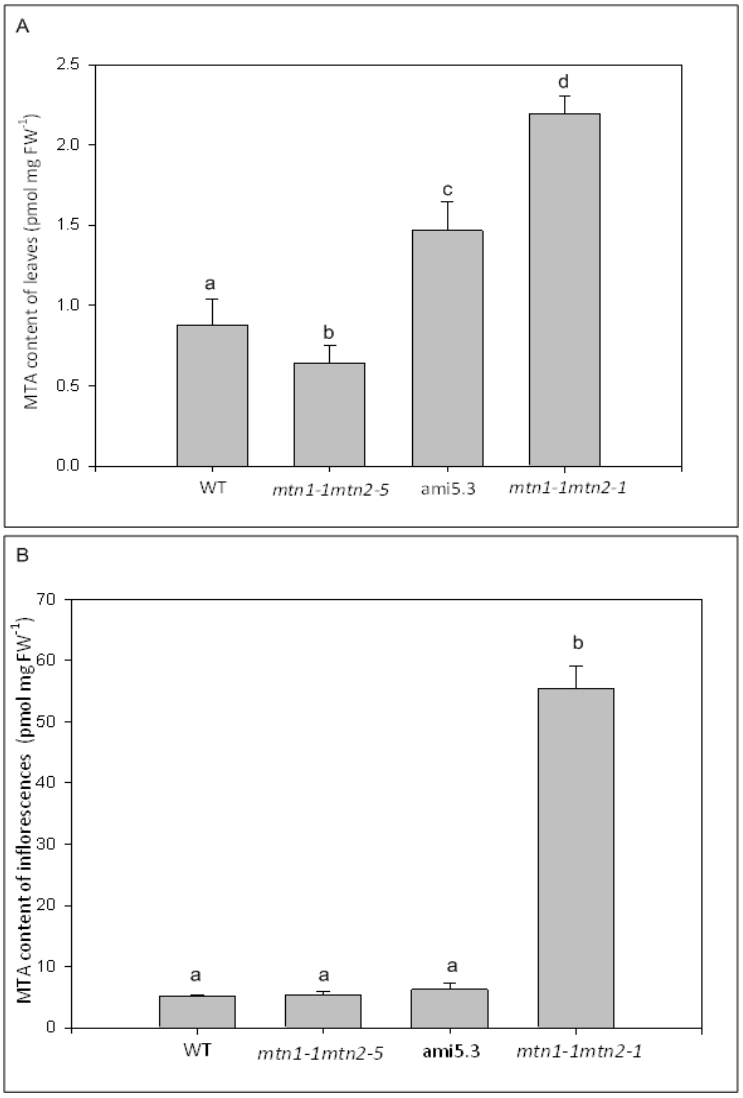

Figure 3.11: MTA concentration of MTN-deficient lines.

Different letters indicate the statistically significant differences between genotypes ($P < 0.05$). ($N = 4$).

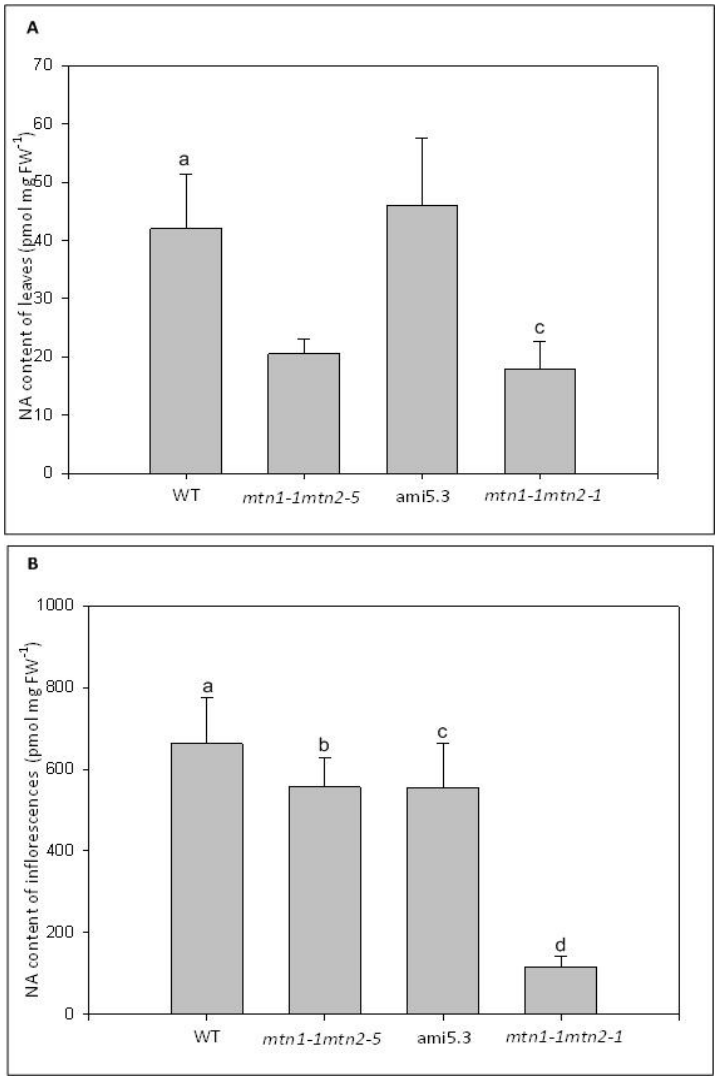

Figure 3.12: NA content of *MTN*-deficient lines.

Different letters indicate the statistically significant differences between genotypes ($P < 0.05$). ($N = 4$).

significant reduction in NA when compared to the WT inflorescences ($P<0.05$) (Figure 3.12B). The anomalous NA content of the ami5.3 leaves most likely reflects inefficient or variable silencing in the leaves.

3.5 Discussion

3.5.1 MTN activity and phenotypes of the *MTN*-deficient lines

This study has compared the phenotypes and Met-related metabolites of two groups of plants relative to WT: three double mutants with reduced MTN activity due to T-DNA insertions and a line created by artificial microRNA expression. The *mtn1-4mtn2-1* and *mtn1-1mtn2-5* exhibited phenotypes that were less complex than those of *mtn1-1mtn2-1*. *mtn1-1mtn2-1* contains two insertion mutations, one in the third intron of *MTN1* (*mtn1-1*) and another in the fourth exon of *MTN2* (*mtn2-1*), and has a severe pleiotropic phenotype (Bürstenbinder et al., 2010; Chapter 2). The *mtn1-1* and *mtn2-1* alleles were combined with weaker alleles [i.e., *mtn1-4*, which has a T-DNA insertion in the 5' untranslated region (UTR) of *MTN1,* and *mtn2-5,* which has a T-DNA insertion in the promoter of *MTN2*] to generate plants with moderate MTN deficiencies. The observations of their phenotypes are in agreement with the findings from a survey of 136 T-DNA insertion mutants (Wang et al., 2008), which revealed that insertions in either the promoter or 5' UTR are less effective in generating knockout mutants than insertions in either exons or introns. When the T-DNA is inserted before the start codon, the translation of the gene is often weakly reduced, resulting in a leaky phenotype (Wang et al., 2008). Since *MTN1* contributes 80 % of the total MTN activity in the leaves (Bürstenbinder et al., 2010), combining a weak allele for *MTN1* with the knock-out *mtn2-1* resulted in a plant (*mtn1-4mtn2-1*) with a 98 % MTN level of activity. Surprisingly, this modest MTN deficiency resulted in a two-day delay in the formation of the first flower buds. On the other hand, plants containing the weak allele for *MTN2* along with the somewhat leaky *mtn1-1* mutation (*mtn1-1mtn2-5*) showed only 28 % of the MTN activity of the WT and exhibited a phenotype closer to that of the *mtn1-1mtn2-1,*

including delayed formation of the first flower buds and increased xylem proliferation. The final observation is that *mtn1-2mtn2-2* plants containing knock-out insertions in the sixth exon of *MTN1* (*mtn1-2*) and the fourth exon of *MTN2* (*mtn2-2*) were apparently lethal; this double mutant was not recovered from repeated screenings of F2 populations (N = 3; > than 100 F2 seedlings). The combination of mutant alleles that affect cis elements with those located within exons or introns thus enabled the generation of mutants with moderate MTN activity and variable phenotypes compared to those of *mtn1-1mtn2-1*.

Artificial microRNA silencing of *MTN* proved to be difficult. Attempts to simultaneously reduce both *MTN1* and *MTN2* by one amiRNA (two different designs) or two individual amiRNAs failed: the T1 plants resulting from these transformations appeared identical to the WT, with no evidence of MTN silencing. It was concluded that the silenced plants were lethal and that only plants that did not express the amiRNA effectively had been recovered. Taking the approach of reducing *MTN2* expression (the less active *MTN* gene) in an *mtn1-1* background led to the generation of multiple ami*MTN* lines, although substantial variation was observed among the progeny of the more silenced lines. The ami5.3 line was the most strongly affected and had three distinct progeny phenotypes: WT-like, *mtn1-1mtn2-1*-like and *tkv*-like (Figure S3.8). Since the degree of silencing in an amiRNA line corresponds to the levels of expression of the amiRNA (Schwab et al., 2006), we assume that the phenotypic and metabolic variation of ami5.3 plants reflects fluctuations in silencing that contribute to variations in the biochemical inhibition caused by MTA.

3.5.2 Effect of MTN-deficiency on the embryo and seed development of MTN-deficient mutants

A correlation was discovered between MTN activity and seed production in the plant lines studied. The *mtn1-1mtn2-1,* with 14.9 % MTN activity, did not produce seed, and ami5.3 with

16 % activity, developed seeds only sparsely. The *mtn1-1mtn2-5* with 28 % MTN activity showed normal seed production. It is highly unlikely that the 1 % difference of MTN activity between *mtn1-1mtn2-1* and ami5.3 could have an effect on seed production. However, the variable silencing of ami5.3 in the later development stages could be a possible explanation for this difference.

Many processes occur during seed development, which begins with double fertilization and ends with the production of dormant seeds that become the next generation (Raghavan, 2006). These processes include embryo differentiation (Gehring et al., 2004; Huh et al., 2008), endosperm formation (Braybrook, 2008), and seed coat development (Haughn and Chaudhury, 2005).

Analysis of the seeds within the siliques of *MTN1mtn1-1/mtn2-1mtn2-1* plants resulted in ~8 % (N = 8-10 siliques each of four plants) of the ovules being identified as unfertilized, a result consistent with the reduced fertilization efficiency previously noted in this line (Chapter 2). In addition, 14 % (N = 3 siliques from 3 plants) of the progeny of *MTN1mtn1-1/mtn2-1mtn2-1* plants were *mtn1-1mtn2-1* homozygotes that had completed embryo differentiation, endosperm formation, and seed coat development. On the other hand, 6 % (N = 3 siliques from 3 plants) of the seeds with a developed seed coat did not germinate to produce seedlings; these embryos most likely arrested at some point during embryo development.

Several factors might cause the MTN-deficient embryos to become lethal: (1) Spd is required for embryogenesis (Imai et al., 2004b), and given that *mtn1-1mtn2-1* plants have reduced Spd content, their embryos may be affected similar to spd-deficient mutants, either because of MTA inhibition of PA synthesis or because of lower production of Spd conjugates (Luo et al., 2009); (2) the nutrient supply to the embryo from the maternal tissues may be disrupted either

due to the reduced NA-mediated transport of essential metals, or as a result of vascular development defects that hinder the nutrient transfer between the maternal tissue and the embryo. At this point, there are no data to distinguish between these possibilities.

3.5.3 Correlation of the variable level of MTN activity with altered xylem proliferation

The *MTN*-deficient mutants exhibited an array of vascular stem defects including an increased number of asymmetrically arranged vascular bundles and an over proliferation of xylem within the vascular bundles. Of these traits, xylem proliferation and the symmetry of the bundle arrangement were inversely correlated with residual MTN activity: *mtn1-1mtn2-5*, ami5.3, and *mtn1-1mtn2-1* with a 28 %, 16 %, and 14.9 % MTN activity, respectively, exhibited an increased degree of xylem proliferation (Figure 3.8B). In contrast, the number of vascular bundles per unit area was not significantly different among *mtn1-1mtn2-5*, ami5.3, and *mtn1-1mtn2-1* (Figure 3.8C). The vascular phenotype that most strongly correlates with MTN activity is an increase in xylem proliferation. The Tspm-deficient mutants *acl5* and *tkv* (Hanazawa et al., 1997; Clay and Nelson, 2005) have similar xylem proliferation abnormalities. In the case of *acl5,* this phenotype was suppressed by a mutation in an upstream of a bHLH gene (*sac51d* mutation; Imai et al., 2006). Based on the model proposed by Imai et al. (2006), *sac51d* suppression of the *acl5* phenotype is the result of the Tspm-mediated activation of *SAC51* translation. In WT plants, one of the short upstream open reading frames (uORFs) of *SAC51* encodes a 53 amino acid polypeptide. This peptide represses the translation of the main open reading frame (mORF) of *SAC51*. ACL5 (Tspm synthase) expression leads to Tspm synthesis, which inhibits repression by the uORF peptide, thereby allowing the synthesis of SAC51. The *acl5* mutant, which is thought to produce essentially no Tspm, has low or no SAC51 production. The *sac51d* point mutation in the fourth uORF of *SAC51* leads to the premature termination of the uORF peptide, resulting in the synthesis of a 3-amino-acid polypeptide rather than the 53-amino-acid polypeptide. This 3-

amino-acid polypeptide is incapable of repressing mORF expression and thus allows SAC51 production in the absence of Tspm (Imai et al., 2006).

The *sac51d* mutation did not suppress any of the abnormal traits of the *mtn1-1mtn2-1* plants. Again, several factors may have contributed to this outcome. The *sac51d* mutation is in the *Landsberg erecta* background while the MTN mutants are the Columbia ecotype. It is possible that the differences in their genotypes affect the efficiency of *sac51d* suppression. A possible factor is that Tspm is not the only basis of the *mtn1-1mtn2-1* mutant phenotypes, which means that even if the *sac51d* suppressed the Tspm defects, the plant would not restore the WT phenotypes. The effect of the constitutive over-expression of *SAC51* on the restoration of *mtn1-1mtn2-1* morphology to the WT is currently under investigation.

3.5.4 Possible reduction in ethylene biosynthesis resulting from MTN deficiency

Both *mtn1-1mtn2-1* and ami5.3 plants have low MTN activity (< 16 %) and delayed leaf senescence. These observations suggest that this phenotype may correlate with MTN deficiency. These mutants/silenced lines may possess low ethylene levels similar to those in octuple ACS mutants (Tsuchisaka et al., 2009). However, many other factors, including other phytohormones, interact in a complex manner to determine the onset of senescence (He et al., 2001; van der Graaff et al., 2006). This could also be a result of delay on seed production. At this point, the exact nature of the cause of senescence in the *mtn1-1mtn2-1* is not known.

3.5.5 Delayed emergence of inflorescence stems in *MTN*-deficient plants

The degree of delay in the emergence of inflorescence stems in the *MTN*-deficient lines correlates with their increased number of leaves. In addition, an increased number of primary/secondary branches, flowers, and buds (data not shown) were evident in *mtn1-1mtn2-1* mutants. These changes in lateral organ arrangement are known to correspond closely to the internal architecture of the vascular system (Dengler, 2006). The main vascular bundles and

their divergence to leaf traces therefore determine the number of vascular bundles in a stem. Based on this logic, the increased number of vascular bundles in the stems of the *MTN*-deficient mutants develops as a result of the increased number of leaves.

The plant hormones auxin and brassinosteroids (BR) are essential for the initiation of vascular tissues and for their differentiation (Fukuda, 1997; Berleth et al., 2001). Mutation in the auxin transport efflux carrier PIN1 or the chemical inhibition of the auxin transport with naphthylphthalamic acid (NPA; Mattsson et al., 1999) leads to increased xylem differentiation. Interestingly, as with *mtn1-1mtn2-1,* plants treated with NPA also have an increased number of vascular bundles. According to Ibañasa et al*.* (2009) the directed auxin maxima of the polar auxin transport determines the space between the vascular bundles whereas BR promotes early procambial division in order to control the number of vascular bundles. An increased number of vascular bundles in the stems is therefore a combined effect of altered auxin maxima and increased BR signalling. It has already been reported that *mtn1-1mtn2-1* mutant stems show altered auxin maxima (Chapter 2), but changes in responses to BR have yet to be examined in this mutant.

From another perspective, the enlarged meristem of the *mtn1-1mtn2-1* mutant may have given rise to its larger number of vascular bundles and thicker stems as compared to the WT. Since a balance between cell division and cell differentiation is essential for determining the size of the meristem, any change in the auxin- and cytokinin-mediated communication between CLAVATA3 and WUS would contribute to changes in the MTN-deficient mutants (Sui et al., 2011). Ultimately the PIN protein-directed increase in the number of auxin maxima may initiate increased number of leaf primordia giving rise to an increased number of leaves (Dengler 2006). This increased production of leaves may delay the transition of the shoot apical meristem to the inflorescence apical meristem, thus causing a delay in the emergence of the inflorescence stem.

3.5.6 Correlation of the MTN activity and the metabolite levels of the *MTN*-deficient lines with their phenotypes

Detailed analysis of the phenotypes selected that could be traced back to pathways affected by MTA content enabled the determination of the primary developmental defects caused by MTN deficiency. MTN activity and the severity of the traits correlated well across the *MTN*-deficient mutants.

The MTA content correlated inversely with residual MTN activity. The levels of accumulated MTA were lowest in the leaves of *mtn1-1mtn2-5* which had a 28 % level of MTN activity, whereas the highest were in *mtn1-1mtn2-1,* which had a with 14.9 % level of MTN activity (Figure 3.11A). In ami5.3 the MTA levels were intermediate, as was the MTN activity. In the leaves, increased MTA levels were associated with decreased MTN activity. The vegetative trait interveinal chlorosis was evident only in the *mtn1-1mtn2-1* mutant whereas increased xylem proliferation and an increased number of vascular bundles per unit area were evident in *mtn1-1mtn2-5*, ami5.3 and *mtn1-1mtn2-1.* Surprisingly, the delayed emergence of the inflorescence stem was exhibited by all of the MTN-deficient lines, including *mtn1-4mtn2-1*. This delayed emergence corresponds to the level of MTN activity.

Since interveinal chlorosis is a result of NA deficiency (Takahashi et al., 2003), it was expected that NA levels would be low only in the *mtn1-1mtn2-1*, which displays this phenotype. However, low NA levels were observed in both *mtn1-1mtn2-5* and ami5.3 in addition to the expected *mtn1-1mtn2-1. mtn1-1mtn2-5* had slight but significantly higher

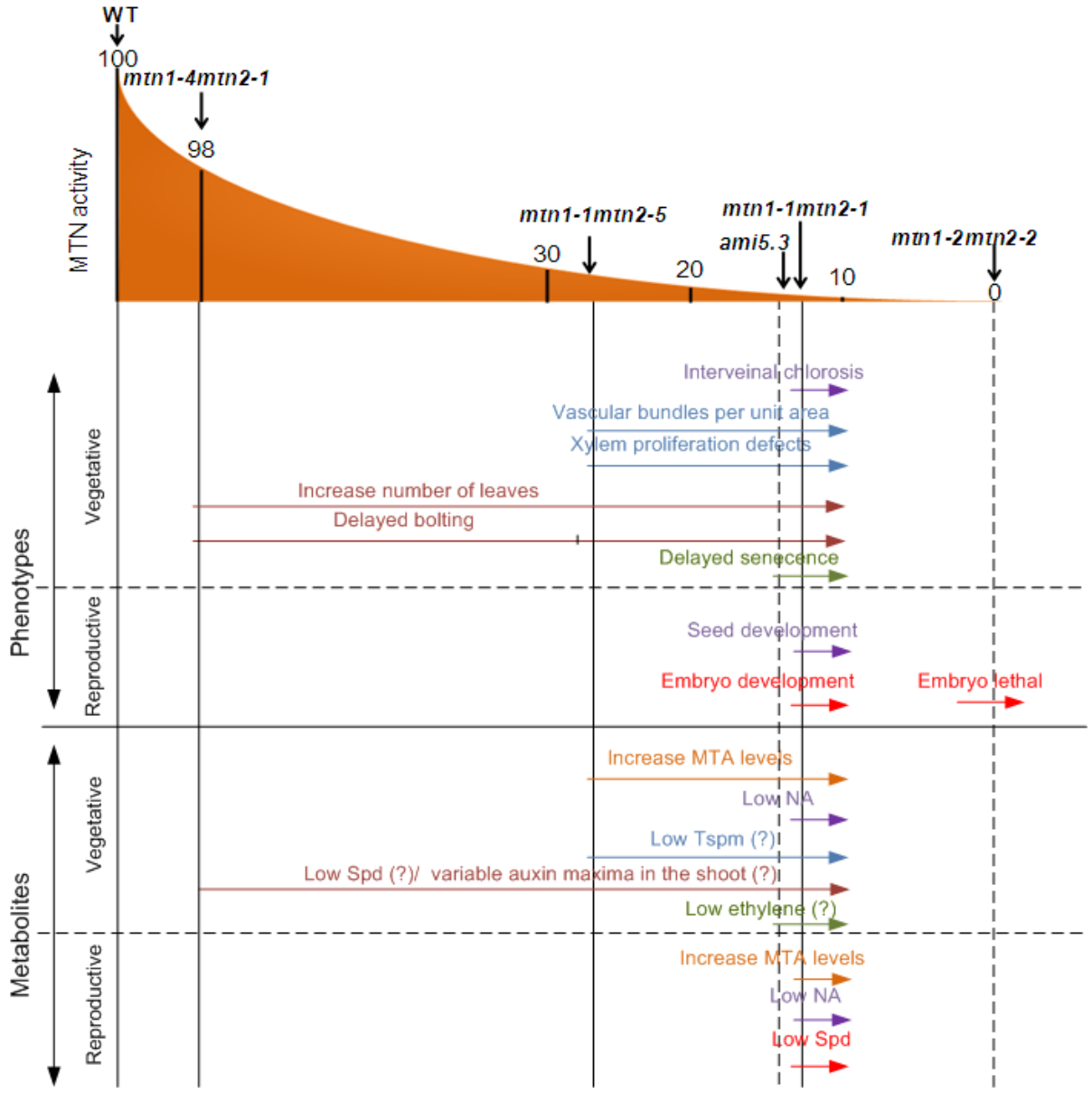

Figure 3.13: Schematic summary that illustrates the primary developmental defects of the *MTN*-deficient mutant

NA levels, which could be adequate for these mutants not to show the interveinal chlorosis phenotype. However the increased NA levels in the ami5.3 could only be due to insufficient or variable production of amiMTN2s to silence the MTN2 gene product in the leaves at two weeks after bolting. Increased MTA content was detected only in the *mtn1-1mtn2-1* inflorescences, whereas the MTA levels in *mtn1-1mtn2-5* and ami5.3 were not significantly different from those in the WT (Figure 3.11B). Consistent with this accumulation pattern, the altered reproductive abnormalities, in embryo development and in seed development were observed only in *mtn1-1mtn2-1.* Moreover, NA levels in the inflorescences were also significantly decreased only in the *mtn1-1mtn2-1,* which is sterile with no seed development: an NA-related phenotype (Takahashi et al., 2003; Klatte et al., 2009).

Taken together, these findings lead to the conclusion that NA synthase activity is sufficiently inhibited when the MTN activity is ~14% of that in the WT. The following summary is proposed as a means of incorporating these observations and those reported in the literature (Figure 3.12): when plants have ~ 28 % of the WT MTN activity, they have increased xylem proliferation defects related to Tspm deficiency as well as delayed emergence of the inflorescence stem related to possible auxin defects. When the MTN activity is reduced further to ~16 %, delayed senescence related to ethylene inhibition becomes apparent in these plants. At ~14 % of MTN activity, these plants have interveinal chlorosis and the inability to produce seeds, which are NA-deficient phenotypes. When the MTN levels are very low probably closer to 0 % embryo lethality resulting from low Spd occurs. Experiments are currently underway to measure Spd and Tspm levels of these MTN-deficient lines in order to confirm this proposed model. Although MTA and NA data were consistent among the five replicates, another independent metabolite analysis will also be conducted in order to confirm these results.

3.6 Conclusion

Xylem proliferation defects and delayed bolting are the primary key defects (symptoms) caused by of MTN deficiency. However, it is possible that the auxin defects that cause a delay in bolting in all *MTN*-deficient lines, including *mtn1-4mtn2-1,* underlie all of these traits.

3.7 Technical assistance by others

Ishari Waduwara-Jayabahu designed and conducted the pilot experiments and executed all of the experiments described in this chapter, with the technical assistance of Natasha Peer, Zachary T. Hull, Andy Kong, Yong Li, Olga Kazberova, and Roba Bdeir. Natasha Peer helped monitor the growth metrics in the mutant lines and performed some of the PCR segregation analysis; Zachary T. Hull conducted the MTN assays. Andy Kong created ami MTN transformants in the *mtn1-1* background with Yong Li's technical guidance, and Roba Bdeir analyzed T2 MTN lines to identify ami2.8 and ami5.3. Olga Kazberova carried out the earlier attempts to create amiMTN lines. Sarah Schoor conducted some of the SEM analysis. Markus Wirtz (University of Heidelberg, Germany) measured the MTA and NA content of plants grown at the University of Waterloo.

3.8 Supplemental material

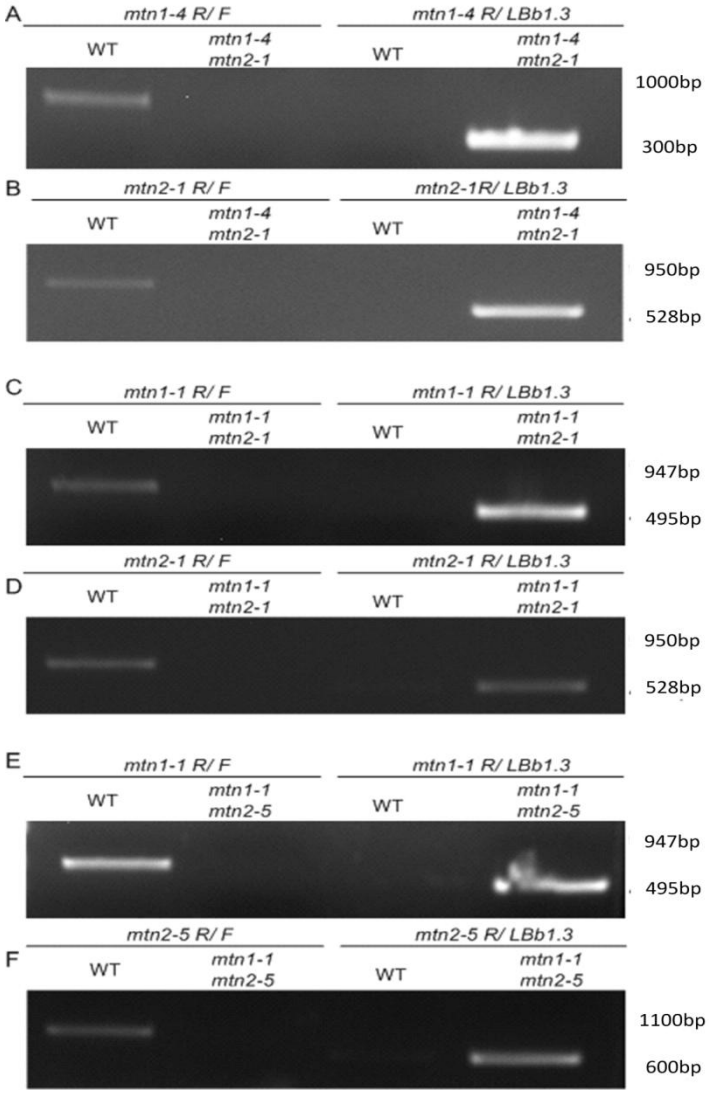

Figure S3.1: Gel images confirming the genotypes of the *MTN*-deficient mutants

Flanking and left border reactions for *mtn1-4 mtn2-1, mtn1-1mtn2-1,* and *mtn1-1mtn2-5*. Homozygous plants were identified when the left border reaction (gene-specific reverse and T-DNA border primer) gave bands along with no bands with flanking reactions (gene-specific reverse and forward).

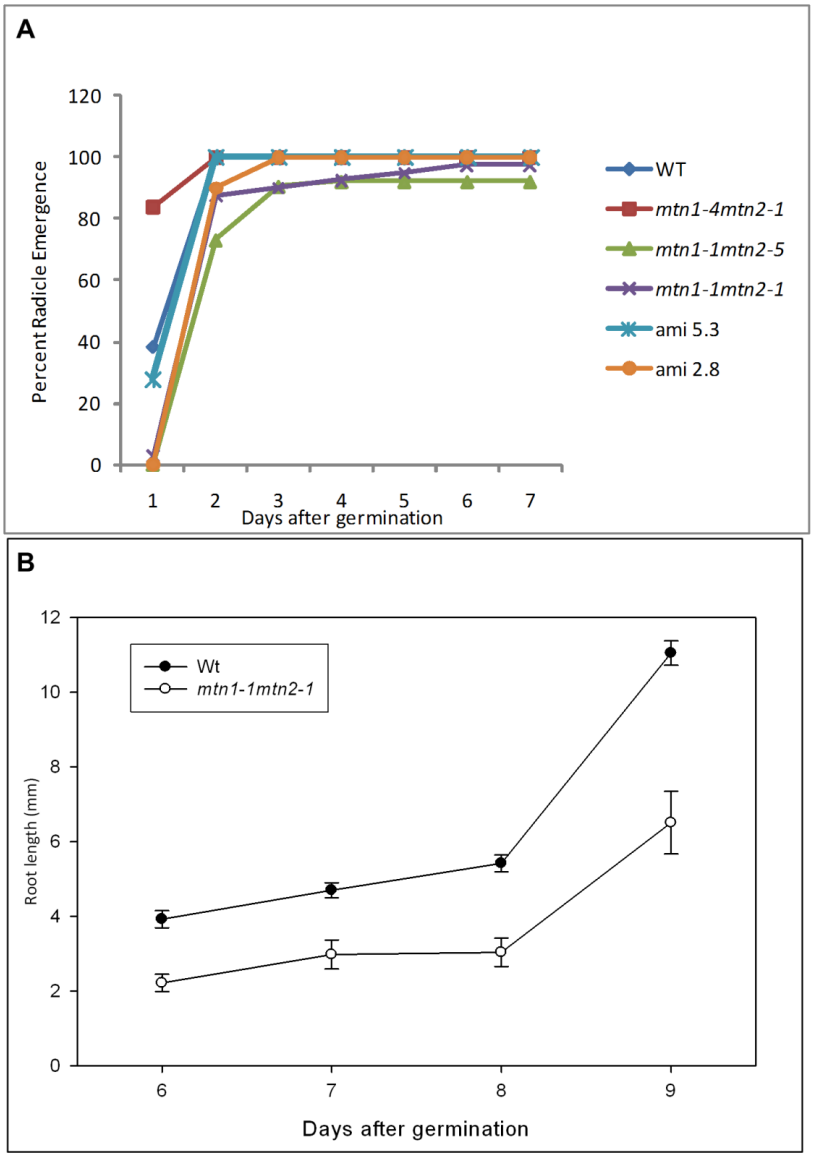

Figure S3.2 Root characteristics of *MTN*-deficient mutants.

(A) Time taken for radicle emergence in *MTN*-deficient lines (N = 9).

(B) Root lengths of *mtn1-1mtn2-1* compared to those of the WT. (N = 10; Error bars indicate ±SD)

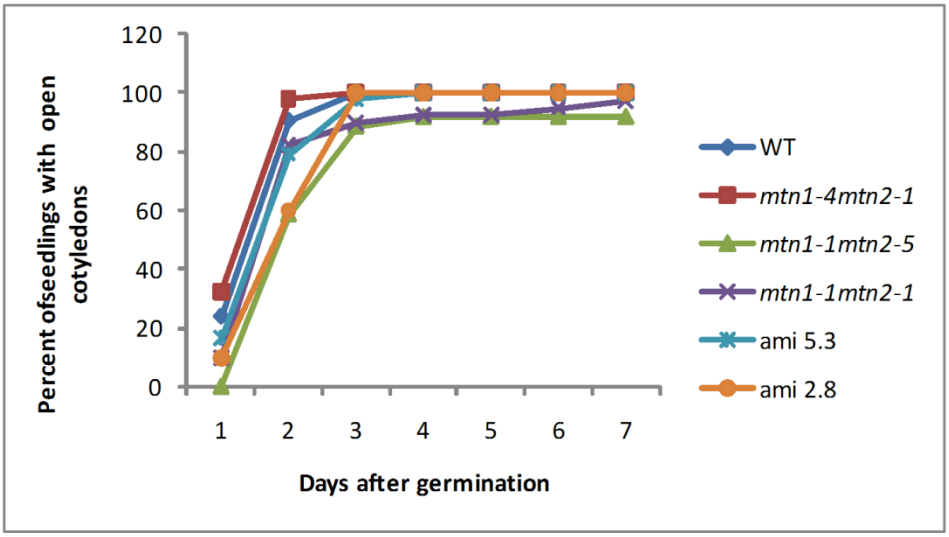

Figure S3.3: Number of days after germination for *MTN*-deficient seedlings to open their cotyledons. (N = 8).

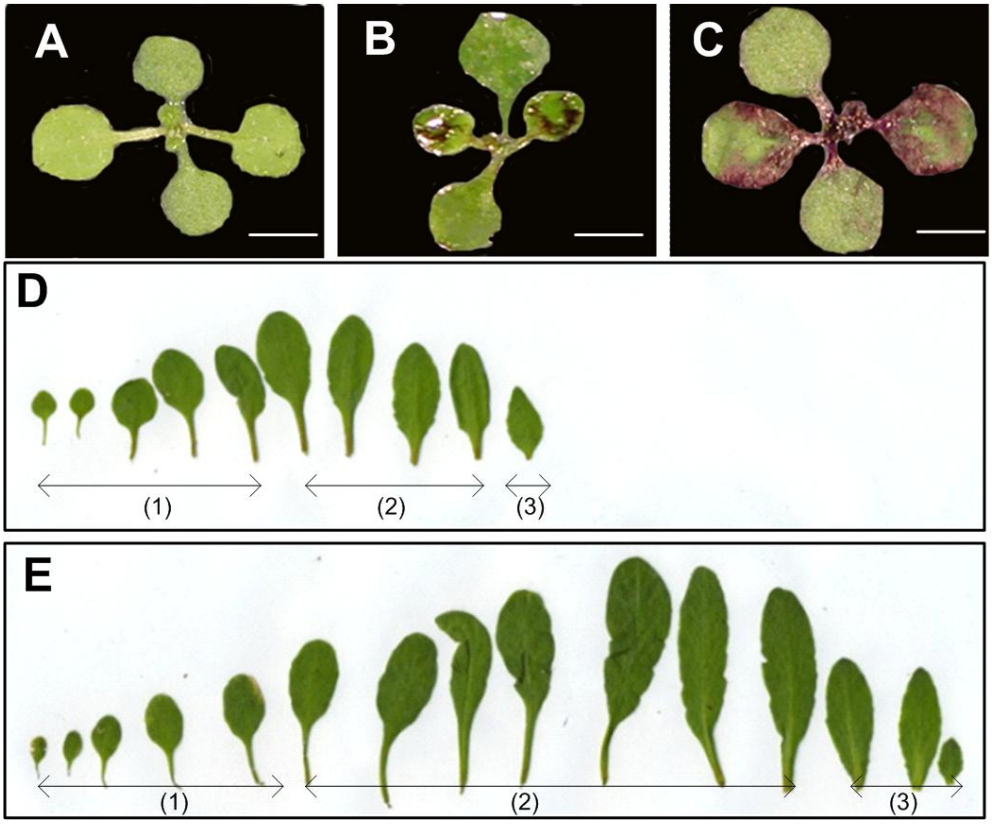

Figure S3.4: Cuticle defects and number of leaves in *mtn1-1mtn2-1* compared to those in the WT.

(A-C) Cuticle defects of seedlings observed based on staining with TBO. (A) WT appeared unstained while (B) *mtn1-1mtn2-1* and (C) *fiddlehead* appeared patchy-stained in the first true leaves. Scale bars = 2.5mm.

(D-E) Number of leaves in (D) WT compared to those in (E) *mtn1-1mtn2-1* the 28 days after sowing. The leaves were separated into three categories based on the appearance of the margins and presence of trichomes: (1) juvenile vegetative-phase rosette leaves, (2) adult vegetative-phase rosette leaves, and (3) adult reproductive-phase rosette leaves.

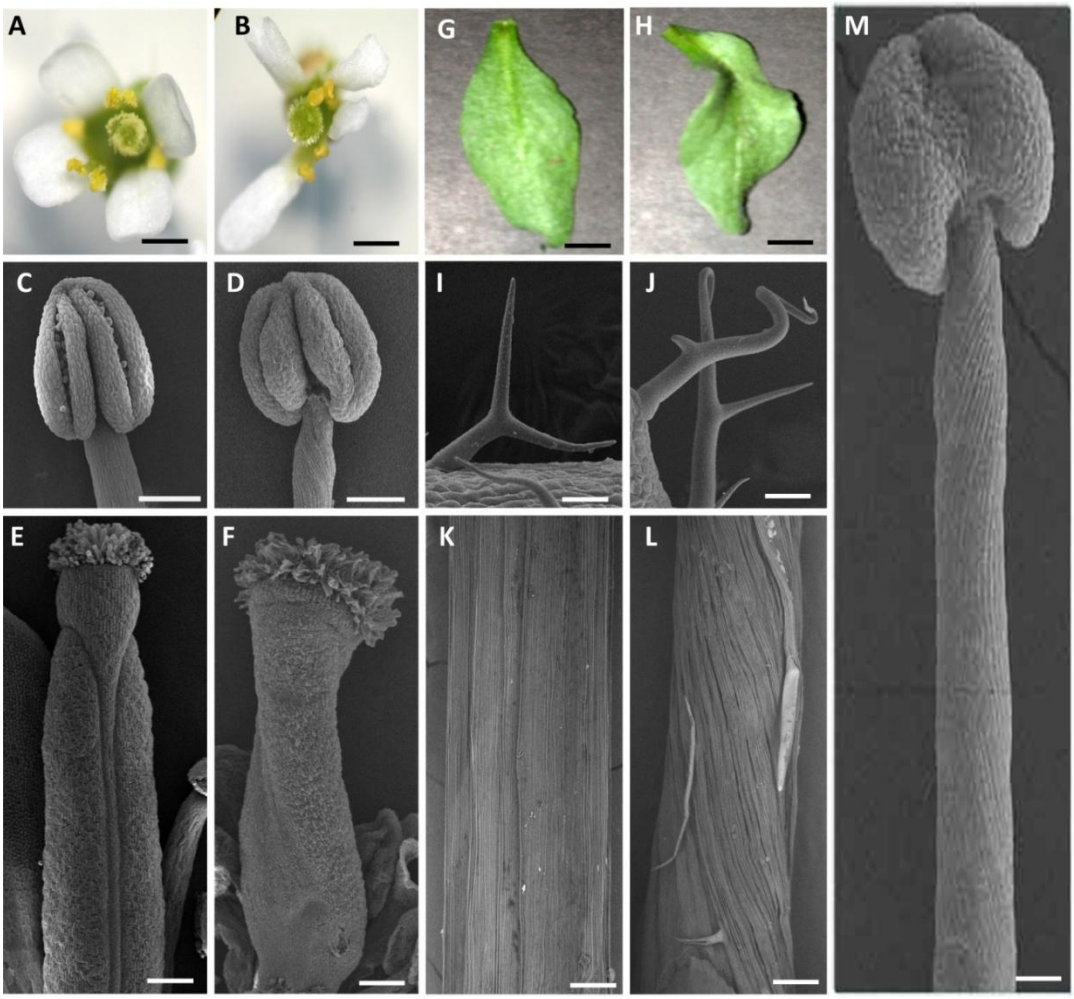

Figure S3.5: Organs of *mtn1-1mtn2-1* mutants that were twisted.

(B, D, F, H, J, L) The twisted organs of *mtn1-1mtn2-1* mutants compared to regular organs of the (A, C, E, G, I, K) WT: (A, B) twisted petals; (C, D) anther filaments; (E, F) carpels; (G, H) leaves; (I, J) trichomes; and (K, L) stems. Most of these *mtn1-1mtn2-1* organs are twisted in left- and right- handed directions, as shown in the young (M) anther filament. Scale bars: A, B = 0.3mm; C, D = 0.12mm; E, F = 0.19mm; G, H= 1mm; I, J= 60µm; K, L= 100µm; M=60µm. DIJM image courtesy of Sarah Schoor.

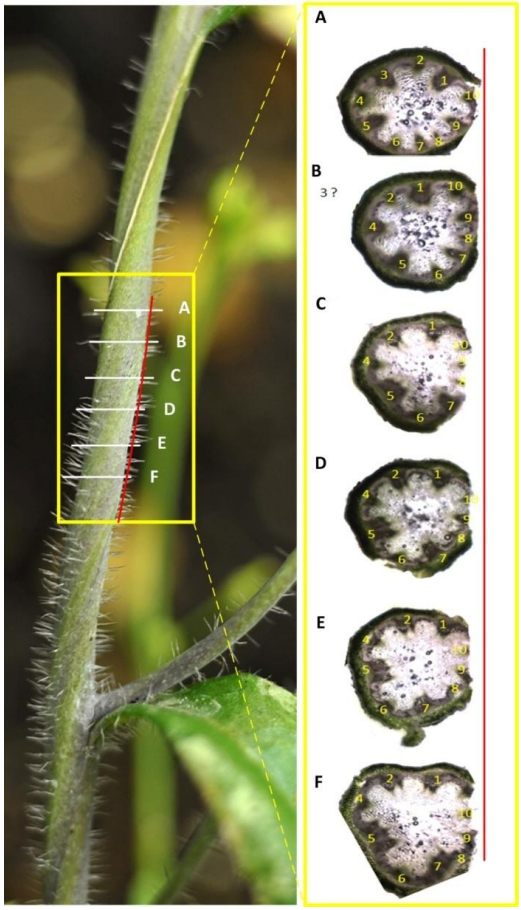

Figure S3.6: Twisted stem and cross-sections along the stem showing the altered vascular arrangement.

Consecutive free-hand sections (A-F) obtained at 0.5 cm intervals along a prominently twisted *mtn1-1mtn2-1* stem segment. The orientation of the stem sections was maintained by marking a nick along one side of the segment (red line). Inset shows the aligned sections with altered vascular bundle arrangement along the twisted area.

Figure S3.7: Phenotype of *mtn1-1mtn2-1sac51d* triple mutant compared to that of *mtn1-1mtn2-1* four weeks after bolting.

The triple mutant exhibited traits similar to those of *mtn1-1mtn2-1*, with sterile flowers and bushy shoot architecture.

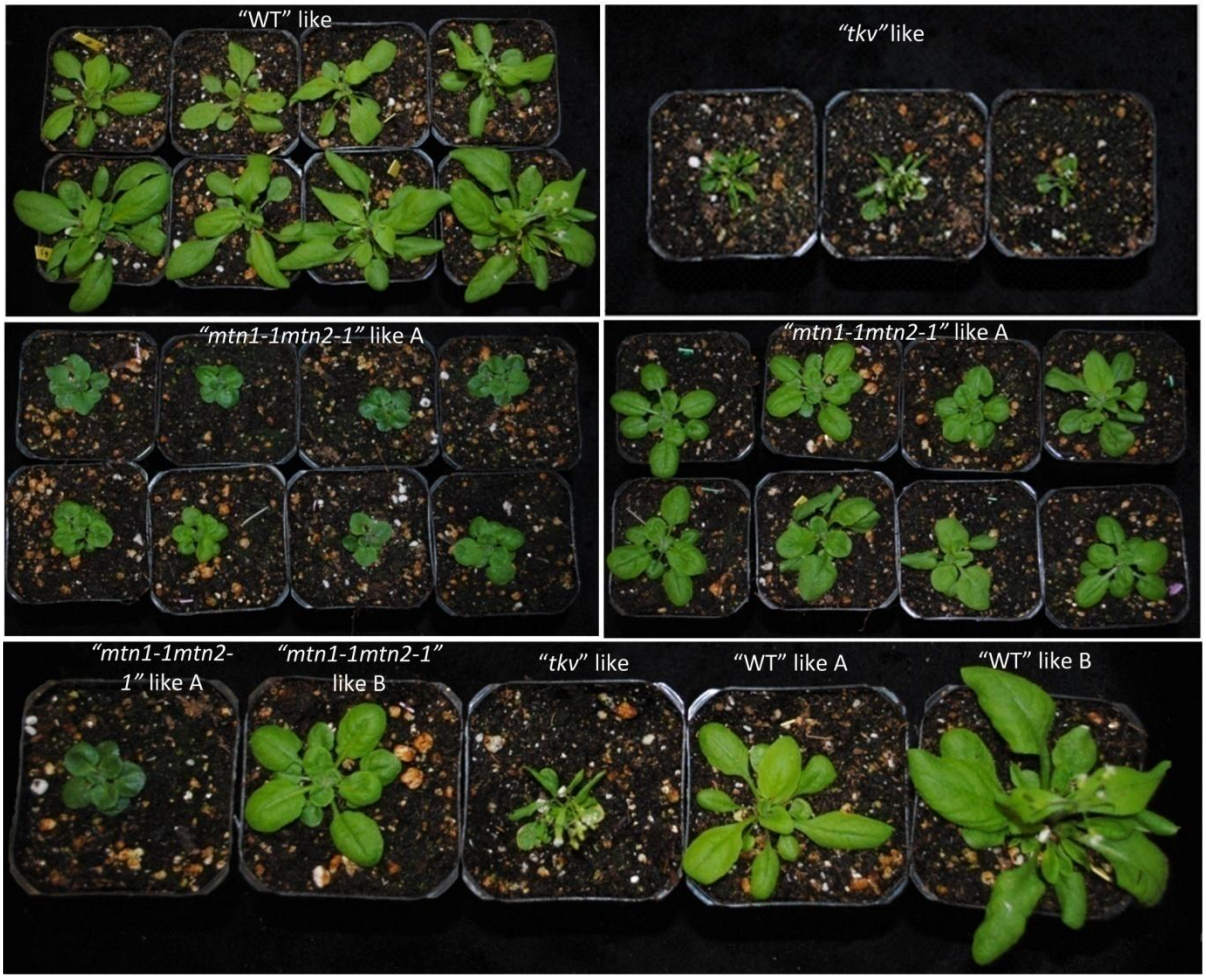

Figure S3.8: Segregating phenotypes of the amiMTN 5.3 line.

The ami5.3 line of MTN segregates, due to the variable degree of silencing of the native MTN gene. Based on the strength of the phenotype, the progeny could be categorized into three groups 21 days after germination: (1). "WT"-like, (2). "*mtn1-1mtn2-1*"-like, and (3). *"tkv"*-like. Both WT-like and *mtn1-1mtn2-1*-like could be further grouped, based on bolting: (A) non-bolted and (B) bolted.

Table S3.1: Description of *MTN*-deficient single mutants.

Gene	Gene ID	Alleles	Description
MTN1	At4g38800	*mtn1-1*	T-DNA insert in an third intron; SALK_085385
		mtn1-2	T –DNA insert in an sixth exon; GK_568C06.18
		mtn1-4	T-DNA insert in an exon; SALK_088214C
MTN2	At4g34840	*mtn2-1*	T-DNA insert in an fourth exon; SALK_ 071127
		mtn2-2	T-DNA insert in an fourth exon; GK_845B05
		mtn2-5	T-DNA insert in the promoter; SALK_022510

Table S3.2: Primer sequences.

Primer name	Sequence	Description
mtn1-1-F	Forward primer for *mtn1-1*; SALK_085385	TGACGGAGACCAACTCCATAC
mtn1-1-R	Reverse primer for *mtn1-1*; SALK_085385	GAGGCTCTTCCTTTGGTCAAC
mtn1-2-F	Forward primer for *mtn1-2*	GAATCGGAAGAGAGGGATAAG
mtn1-2-R	Reverse primer for *mtn1-2*	CTTCTGTTCTCTTCCTTTTTTAT
mtn1-4-F	Forward Primer for *mtn1-4* ;SALK_088214C	TGG GGA GTA TAA TGT TGC AGC
mtn1-4-R	Reverse Primer for *mtn1-4* ;SALK_088214C	GCA TTG AGT GCA AAG CTT ACC
mtn2-1-F	Forward primer for *mtn2-1*; SALK_071127	CCTTGCTTACGTGGCATAAAC
mtn2-1-R	Reverse primer for *mtn2-1*; SALK_071127	GGAAAGGGCAAAAATATATGG
mtn2-2-F	Forward primer for *mtn2-2*	CAACAGATTACGCCTCGTTG
mtn2-2-R	Reverse primer for *mtn2-2*	CCATGACAGAAGAATACCTGT
mtn2-5-F	Forward Primer for *mtn2-5;* SALK_022510	ACT GTG CCA ACA CTC TCA ACC
mtn2-5-R	Reverse Primer for *mtn2-5;* SALK_022510	AAG ATT TCC GCT TCC TGA AAG
LbB1.3	Left-border for SALK lines	ATTTTGCCGATTTCGGAAC
GABI LB	GABI Left Boarder	ATTGACCATCATACTCATTGC
miMTN2-I	amiRNA targeting MTN2	GATTTTATTAGAATCGTAGGCGCTCTCTCTTTTGTATTCC
miMTN2-II	amiRNA targeting MTN2	GAGCGCCTACGATTCTAATAAAATCAAAGAGAATCAATGA
miMTN2-III	amiRNA targeting MTN2	GAGCACCTACGATTCAAATAAATTCACAGGTCGTGATATG
miMTN2-IV	amiRNA targeting MTN2	GAATTTATTTGAATCGTAGGTGCTCTACATATATATTCCT

Table S3.3: Primer combinations used to identify MTN-deficient alleles.

Gene	Genotype	Primer combination	Band size
MTN1	MTN1-1	*mtn1-1*F/R	947bp
	mtn1-1	*mtn1-1*R/ LbB1.3	495bp
	MTN1-2	mtn1-2F/R	1630bp
	mtn1-2	*mtn1-2*F/ GABI LB	1300bp
	MTN1-4	mtn1-4F/R	1000bp
	mtn1-4	*mtn1-4*R/ LbB1.3	300bp
MTN2	MTN2-1	mtn2-1F/R	950bp
	mtn2-1	*mtn2-1*R/ LbB1.3	528bp
	MTN2-2	mtn2-2F/R	1459bp
	mtn2-2	*mtn2-2*F/ GABI LB	593bp
	MTN2-5	mtn2-5F/R	1100bp
	Mtn2-5	*mtn2-5R*/ LbB1.3	600bp

Table S3.4: Number of aborted seeds and unfertilized ovules in stage 17b siliques.

(N = 8-12 siliques of three different plants were observed).

	Normal seeds	Aborted seeds	Unfertilized ovules	N
MTN1-4mtn1-4/mtn2-1mtn2-1	1436	0	0	26
MTN1-1mtn1-1/mtn2-5mtn2-5	1231	0	0	25
MTN1-1mtn1-1/mtn2-1mtn2-1	1639	1	138	34

Table S3.5: Variation in the number of vascular bundles and the cross-sectional area of the stem sections in *MTN*-deficient lines.

	WT	***mtn1-4 mtn2-1***	**ami2.8**	***mtn1-1 mtn2-5***	**ami5.3**	***mtn1-1 mtn2-1***
Number of vascular bundles in a sem section	7±1	7±1	9±3	8±2	8±0.5	12±2
Total area of the stem section (cm^2)	7±1	5±1	6±1	10±2	8±1	10±1
Number of bundles / area	1.1±0.3	1.3±0.3	1.5±0.3	0.89±.03	1.07±0.2	1.12±0.2
N	4	4	4	4	3	4

Chapter 4: Spermidine-Dependent Fertility Recovery of *mtn1-1mtn2-1*

4.1 Overview

The accumulation of the Yang cycle metabolite MTA in *mtn1-1mtn2-1* mutants leads to pleiotropic phenotypes including no seed production. This reproductive defect was partially restored by supplying the seedlings with Spermidine (Spd) for 14 days. This partial recovery included the formation of a few siliques that contained viable seeds. The measurement of Met-related metabolites and morphological observations of the flower organs, particularly the female gynoecia, the profiling of hormones, and transcripts of 14-day-old seedlings, were used to investigate the possible effects of Spd treatment on *mtn1-1mtn2-1* mutants. Several findings were indicative of the involvement of auxin in Spd treatment: Spd-treated seedlings recovered WT IAA levels, transcript levels of the auxin efflux carrier protein gene and of the endomembrane system-related genes were increased, and DR5*rev*::GFP expression was recovered in the restored siliques. In addition, the arrangement of the vascular bundles in the restored branches was normal. This vascular recovery could also be due to proper auxin distribution, which could ultimately lead to the recovery of fertility. The increased abundance of *S*-adenosyl-*L*-methionine decarboxylase and copper-amine oxidase transcripts indicate additional factors that may contribute to vascular recovery. A model incorporating these observations is presented for the Spd-mediated recovery of seed production in *mtn1-1mtn2-1*. This model proposes that the seed production in *mtn1-1mtn2-1* could be either a direct effect of proper auxin distribution or an indirect effect of proper xylem differentiation.

4.2 Introduction

The Yang cycle regenerates methionine (Met) from 5'-methylthioadenosine (MTA) via series of reactions, the first of which hydrolyzes MTA to methylthioribose (MTR) and adenine (Figure 4.1). The key enzyme involved in this hydrolysis is methylthioadenosine nucleosidase (MTN). Based on the data presented in Chapter 2, MTN-deficiency in plants leads to the accumulation of its substrate MTA, which in turn, inhibits the synthesis of polyamine (PA) and nicotianamine (NA). PA and NA biosynthesis are two of the predominant pathways that utilize *S*-adenosyl-L-methionine (SAM) to generate MTA as a by-product in plants.

Xylem development, and PA and metal homeostasis are among the many critical factors that affect reproduction in plants. Current research related to PAs shows that spermidine (Spd) an essential factor in plant embryogenesis (Urano et al., 2005; Imai et al., 2004b; Ge et al., 2006). Although the basis of this requirement has not been determined, it is known that Spd modifies the eukaryotic translation initiation factor 5A (inactive eIF5A) post-translationally to form the unique amino acid hypusine (active eIF5A; Park, 2006). This activation occurs via two enzymatic steps involving deoxyhypusine synthase (DHS, EC2.5.1.46) and deoxyhypusine hydroxylase (DHH, EC 1.14.99.29; Figure 4.1). Hypusine biosynthesis has been correlated with critical functions during plant development (Feng et al., 2007) and during female gametophyte development (Pagnussat et al., 2005). As a metal chelator, NA is also involved because it facilitates the long-distance transport of ions needed for the proper formation of pollen and seeds (Bohme and Scholz, 1960; Takahashi et al., 2003; Klatte et al., 2009).

Normal vascular development is crucial for plants because it transports essential components, including ions and phytohormones (Krizek et al., 2011). Of the many factors that affect vascular development, the PA thermospermine (Tspm) is particularly crucial because it prevents premature xylem maturation (Hanazawa et al., 1997; Imai et al 2004a,b;

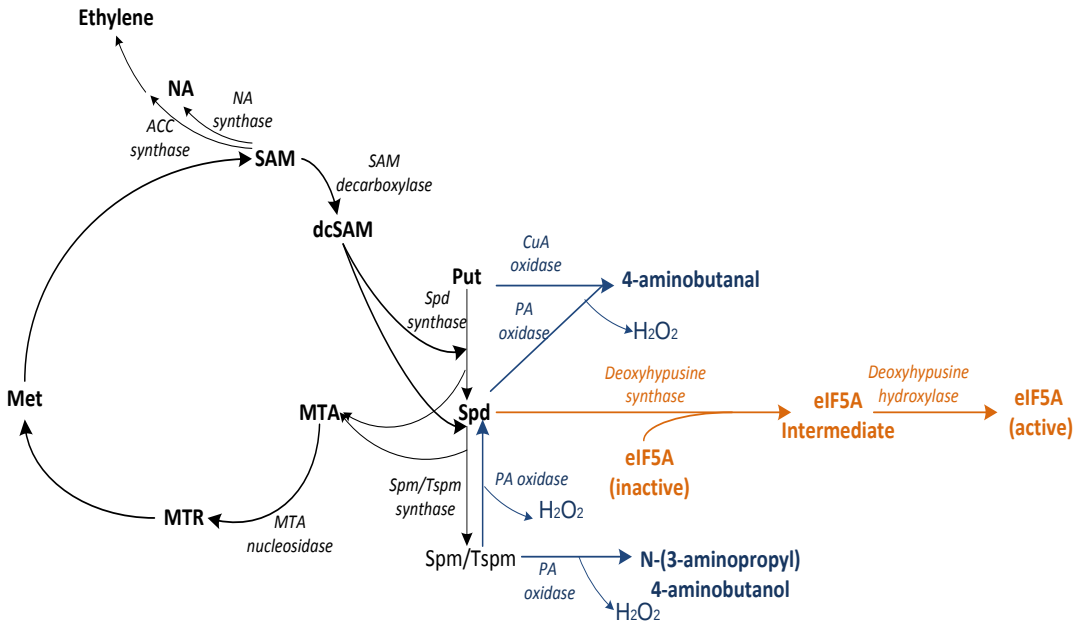

Figure 4.1: Polyamine biosynthesis, catabolism, and links to the Yang cycle and eIF5A

Black lines indicate the Yang cycle and PA biosynthesis, blue lines indicate PA catabolism and back conversion, and orange lines indicate the involvement of Spd in the hypusination of eIF5A.

Kakehi et al., 2008; Muñiz et al., 2008). Reproductive and vascular-related defects are also associated with the catabolism of PAs. PA catabolism includes the oxidation of Spermine (Spm) and/or Tspm to N- (3-aminopropyl) 4-aminobutanol and Putrescine (Put) and/or Spd to 4-aminobutanol (Figure 4.1; Baron and Stasolla, 2008). Polyamine oxidases (PAO; EC 1.5.3.11) are responsible for the catalysis of Spd, Spm, and Tspm and for the back conversion of Spm/Tspm to Spd, while copper-containing amine oxidases (CuAO; EC 1.4.3.6) mediate the catabolism of Put. All of these reactions generate hydrogen peroxide (H_2O_2), which acts as a signaling molecule to enhance xylem differentiation (Tisi et al., 2011). H_2O_2 also induces an influx of Ca^{+2} into the pollen tube cytosol as a means of regulating reproduction by reducing the growth of the pollen tubes (Wu et al., 2010). Phytohormones also play a central role in synchronizing and implementing processes that are essential for successful seed production in plants.

Auxin, which is produced by all cells at all stages of flower development (Aloni et al., 2006), acts as the master regulator of reproductive success by providing positional cues for apical-basal patterning, floral identity and organogenesis, organ vascularization, gamete development, and the timing of fertilization (Mattsson et al., 1999; Krizek et al., 2011). The *mtn1-1mtn2-1* mutants are sterile and do not produce seeds. Inpart this is due to decreased fertilization efficiency associated with developmental defects in both ovules and pollen. Ovules arrest with non-extended integuments; pollen development, on the other hand, is variably delayed. Taken together with this mutant's indehiscent anthers and poor pollen tube growth, it is evident that several factors contribute to its infertility (Chapter 2). Amazingly, seedlings provided with exogenous Spd during their early vegetative phase (first 14 days after germination) produced a small number of seeds during the later stages of reproductive phase (56 days after germination). These seeds arise in randomly on different branches (Chapter 2).

In this chapter, the mechanistic basis of this exogenous Spd-dependent fertility recovery in *mtn1-1mtn2-1* plants is explored. Hormones, transcripts, and metabolites of *mtn1-1mtn2-1* and WT seedlings grown on ½ MS and ½ MS that had been supplemented with Spd were profiled. The combined analyses point to auxin distribution and vascular development as the key mediators of the Spd-mediated recovery of seed production in *mtn1-1mtn2-1*.

4.3 Methods

4.3.1 Plant material and growth conditions

Arabidopsis thaliana WT (Col) and *MTN1mtn1-1/mtn2-1mtn2-1* progeny seeds were placed on ½ MS or ½ MS media that had been supplemented with 100 µM Spd (Sigma). After the plates were incubated for 48 h at 4^{o}C in the dark, they were transferred to continuous light at 22^{o}C for 14 days. A set of these seedlings were then transplanted to peat soil (KUREHA, Tokyo, Japan) for harvesting of aerial organ tissues. Another set of seedlings were transplanted to a hydroponic system (Pierre et al., 2003) for the harvesting of root tissue. Both sets of seedlings, the soil transplants and the hydroponic transplants, were grown under 16 h of light at 22^{o}C with 150 µ mol m $^{-2}$ s $^{-1}$ of photosynthetically active radiation.

Samples were collected simultaneously for hormone, microarray, and metabolite analyses; all samples were collected at the same time of the day. Flower stages were collected in accordance with Smyth et al. (1990). Aerial organs and roots were harvested two weeks after bolting (i.e., five-week-old WT and seven-week-old *mtn1-1mtn2-1*).

4.3.2 Microscopic analysis

4.3.2.1 Light microscopy

Stage 14 flowers, as described by Smyth et al. (1990), were cleared (glacial acetic acid: ethanol) for 2 h, after which the pistils and ovules were observed. Stage 15 siliques of *mtn1-1mtn2-1*, restored siliques of the *mtn1-1mtn2-1* that had been supplied with 100 µM Spd, and WT stage 17 siliques were manually opened, and all the seeds/ovules were scraped into a drop of Hoyer's clearing solution (50 g of chloral hydrate, 2.5 mL of glycerol, 3.75 g of Gum Arabic and 15 mL of water) for embryo observation. The pistils were observed with bright light optics while the ovules and embryos were observed with Differential Interference Contrast (DIC) optics of a Zeiss Axiovert 200M Microscope (Carl Zeiss Inc, Toronto, Canada).

Histochemical staining for H_2O_2 with 3-3' diaminobenzine (DAB) of the Arabidopsis seedlings that were 14 days old, taken from ½ MS, ½ MS supplemented with 100 µM Spd or from ½ MS supplemented with 50 µM 3-amino-1,2,4-triazole (AT; oxidative stress inductive media; May and Leaver, 1993) were vacuum infiltrated for 20 min with a 3,3'-diaminobenzidine (DAB) solution (Sigma, 1mg/ml, pH 3.8) and then incubated at room temperature for 6 h (Nakagami et al., 2006). The seedlings were cleared for 4 h in glacial acetic acid: ethanol (3:1). When DAB polymerizes with H_2O_2, a visible brown stain is produced (Nakagami et al., 2006).

4.3.2.2 Scanning electron microscopy and laser scanning confocal microscopy

Stage 14 flowers from the WT and *mtn1-1mtn2-1* were placed in fixative, critical point dried, mounted, sputter coated and visualized using a Hitachi S570 scanning electron microscope, as described in Chapter 2. The expression patterns of DR5*rev::*GFP in the seeds and ovules of both the WT and *mtn1-1mtn2-1* were observed using a Carl Zeiss LSM 510 confocal microscope, as detailed in Chapter 2.

4.3.3 Microarray analysis

Using an RNeasy Plant Mini Kit (Qiagen, Hilden, Germany), RNA was extracted from 14-day-old WT and *mtn1-1mtn2-1* seedlings grown on ½ MS and ½ MS supplemented with 100 µM Spd. Each replicate contained 10 seedlings. Microarray analysis was performed using an ATH1 Gene Chips Arabidopsis Genome array (Affymetrix, Santa Clare, USA) as detailed in Nakamichi et al. (2009). Relative expression values and detection values (genes were tagged as "present, P"; "marginal, M"; or "absent, A") were generated for each transcript with the use of the MAS5.0 algorithm of the GeneChip Operating Software (GCOS, Affymetrix). The raw image of the chip (.dat) was used to generate an Affymetrix CEL file. The generated CEL data files were used to calculate a robust multi-chip average (RMA) in order to normalize and estimate the intensity of the signal (Irizarry et al., 2003)

To identify genes the expression of which had changed significantly with the treatment, the CEL files were evaluated using the RMA. False discovery rate (FDR)-controlled q-values < 0.01 were defined as in (QVALUE; http//genomine.org/qvalue/). Gene Ontology (GO) analysis was performed using Chip Enrich software (Orlando et al., 2009), available at http://www.arexdb.org/software.jsp. This analysis was performed by Dr. Nori Nakamichi, RIKEN, Japan.

4.3.4 Hormone analysis

For the hormone analysis, 14-day-old seedlings and the aerial organs, and roots of mature plants were collected from the WT and *mtn1-1mtn2-1* that had been germinated either on ½ MS or on ½ MS supplemented with Spd. Seven organs were collected from mature plants: unopened buds, stage 14 flowers, stage 15 siliques, stage 17b siliques, rosette leaves, stems, and roots. A leaf developmentally similar to the WT 6th rosette leaf was harvested from the mutant. With respect to the stems, 2 cm stem segments were harvested between the first and

third nodes of the primary shoot. These tissues were subjected to hormone extraction, detection, and analysis, as described in Kojima et al. (2009). This analysis was performed by Mikiko Kojima, RIKEN, Japan.

4.3.5 Metabolite analysis

Using UPLC-TQD (Waters) as previously described in Sawada et al. (2009), Met-related metabolites were determined. For this metabolite analysis, 50 mg - 100 mg of stage 14 flowers from both the WT and *mtn1-1mtn2-1* plants that were grown on ½ MS and from the plants that were grown on ½ MS supplemented with Spd were collected. This analysis was performed by Yuji Sawada, RIKEN, Japan.

4.4 Results

4.4.1 Defective reproductive development of *MTN*-deficient plants

4.4.1.1 Abnormal floral organogenesis

To determine the initial cause of sterility in *MTN*-deficient plants, reproductive organ initiation and development were observed in detail. An obvious defect in the inflorescences was their altered phyllotaxy (irregular pedicel arrangement, (Figure 4.2A, B). Compared to the WT, the mutant inflorescences showed an increased number of buds that had opened and that had exposed immature reproductive organs (as shown by a comparison Figure 4.2C, D). The flowers were also deformed in *mtn1-1mtn2-1*. In contrast to the WT flowers, which have a symmetrically arranged pattern of four sepals, four petals, and six stamens (Figure 4.2G), the mutant flowers variously had (1) an inconsistent number of petals (Figure 4.2H) and anthers; (2) asymmetrically arranged long narrow petals (Figure 4.2E) and anthers; (3) wide stigmas (Figure 4.2F and H); and (4) fused flowers with fasciated pedicels (Figure 4.2F).

4.4.1.2 Underdeveloped ovules

As reported in Chapter 2, *mtn1-1mtn2-1* plants did not produce seeds as a result of their reduced fertilization efficiency. One of the reasons for this reduced fertility is that ovule development arrests prematurely. To determine the mechanism or timing of this arrest, the pistils of the WT and *mtn1-1mtn2-1* plants were cleared and observed with DIC optics. The developmental stages of these embryos were designated according to Schneitz et al. (1995). During megasporogenesis (stage 2), the mother cell undergoes meiosis, and two distinct layers of integument form to surround the dividing nucellus. When stage 2-III ovules were examined in the WT (Figure 4.3A, C) and *mtn1-1mtn2-1* (Figure 4.3D), the initiation of the inner and outer integument was evident in both genotypes. Stage 2-V ovules also displayed development that was similar in the WT (Figure 4.3B) and *mtn1-1mtn2-1* (Figure 4.3E), with the formation of the

tetrad nuclei and extension of both integuments towards the apex of the nucellus. Upon megagametogenesis (stage 3), however, ovule development in *mtn1-1mtn2-1* was noticeably abnormal. In WT stage 3-II, the tetrad was replaced with a binuclear embryo sac with the outer integument nearly surrounding the nucellus (Figure 4.3C). Despite the double mutant having two nuclei, the outer and inner integuments did not extend past the point where they were at stage 2-V (Figure 4.3F). Thus based on these results, the ovule development of the *mtn1-1mtn2-1* mutants is arrested at stage 2-V (Schneitz et al., 1995).

4.4.1.3 Disrupted gynoecia vasculature

According to Schneitz et al. (1995), the major developmental event preceding the extension of integuments at ovule stage 2-V is the appearance of the lateral vasculature. To determine whether vascular development differed in the *mtn1-1mtn2-1* female gynoecia, cleared stage 14 flower pistils were compared to those of the WT. The WT carpels contained four veins (Figure 4.3G): two medial and two lateral, consistent with the description provided by Nemhauser et al. (2000). Moreover, at the boundary of the style and ovary, lateral veins terminated and the medial veins bifurcated to heavily vascularize the stylar region. In contrast, *mtn1-1mtn2-1* gynoecia were much more vascularized, with at least six thick veins that could not be clearly distinguished as either medial or lateral (Figure 4.3H). However, this distinction was visible only near the base of these gynoecia where the medial veins contained multiple bifurcations. The increased vascularization of the mutant gynoecia suggested that the auxin gradient required for proper gynoecia pattern formation is disrupted in *mtn1-1mtn2-1*. The pistils were therefore observed by SEM to further document morphological variations in the gynoecia pattern. The WT gynoecia contained regional boundaries that clearly demarcated the stigma, style, ovary, replum, and stipe while most of these boundaries were altered in the *mtn1-1mtn2-1* gynoecia. The stigma,

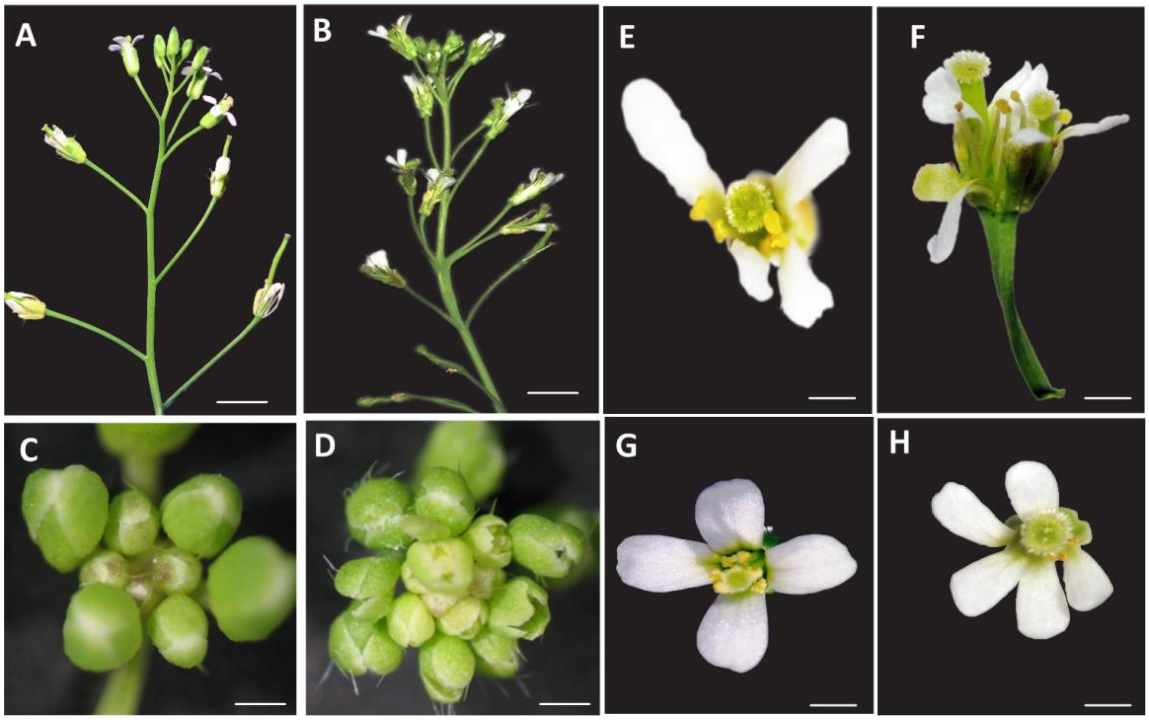

Figure 4.2: Floral organ defects in the *mtn1-1mtn2-1*

(A, B) Altered phyllotaxy and fasciation of the *MTN*-deficient inflorescences. In comparison with (A) the WT spiral inflorescence phyllotaxy, (B) the phyllotaxy of *mtn1-1mtn2-1* mutants is irregular with multiple insertions of floral pedicels (as indicated by the arrow).

(C, D) Sepals of (C) WT buds were closed to protect the immature reproductive organs whereas (D) the *mtn1-1mtn2-1* reproductive organs were exposed with wide-open sepals.

(E-H) Stage 14 flowers: (G) WT flowers displayed four petals and six fully extended stamens in a symmetrical pattern. In (H) *mtn1-1mtn2-1* mutants, a variety of single flower phenotypes were observed, including variable numbers of petals, (E) an asymmetrical organization of long narrow petals, and (F) fused flowers with fasciated pedicels.

replum, and stipe could be identified in the *mtn1-1mtn2-1,* but these tissues were much wider than in the WT. Furthermore, the style and valve of the *mtn1-1mtn2-1* were indistinguishable. Closer observation revealed that this area consisted of square-shaped cells that are usually seen only in WT valves (Nemhauser et al., 2000). Since auxin gradients play a role in patterning and forming regional boundaries in gynoecia (Nemhauser et al., 2000), these results suggest that the auxin distribution within *mtn1-1mtn2-1* may be altered, disrupting the gynoecia pattern, regional boundaries, and vascular supply and possibly causing the early arrest of ovule development. As discussed in Chapter 2, male gametophytic defects also contribute to the reduced fertilization efficiency of *mtn1-1mtn2-1.* However, *mtn1-1mtn2-1* partially recovered seed production when seeds were grown on media supplemented with 100 µM Spd for 14 days (Chapter 2).

4.4.2 Reduced MTA levels in flowers restored by exogenous Spd

To explore the Spd-dependent partial recovery of seed production in the *mtn1-1mtn2-1*, Met-related metabolites were measured in the mutants grown with and without Spd supplementation. When the mutants were grown on either medium, their adenine, adenosine, and Met levels were not significantly different from those of the WT, indicating that the homeostasis of these metabolites was unaffected by MTN deficiency or exogenous Spd treatment. However, as reported in Chapter 2, the MTA content was higher in the mutant than in the WT (Figure 4.4). MTA levels were significantly decreased by Spd treatment both in the WT and in the mutant ($P < 0.05$). These results suggest that exogenous Spd feeding reduced the MTA through an MTN-independent mechanism. Interestingly, the SAM content was also statistically significantly decreased in the Spd-supplemented mutants but not in the WT (Figure 4.4).

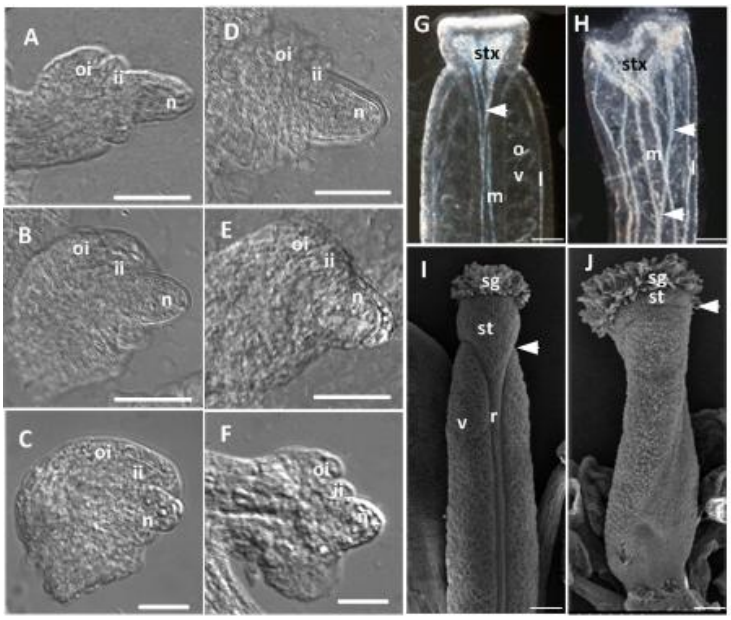

Figure 4.3: *mtn1-1mtn2-1* ovule development and pistil morphology compared to those of the WT.

(A-F) Using DIC optics: (A-C) WT and (D-F) *mtn1-1mtn2-1* ovules have similar development during (A, D) stages 2-III and (B, E) 2-V. However, when (C, F) stage 3-II is reached, it is clear that the outer (oi) and inner integuments (ii) of *mtn1-1mtn2-1* do not extend over the nucellus (n). Scale bars = 25 µm.

(G, H) Bright field images of cleared pistils from stage 14 flowers of (H) *mtn1-1mtn2-1* compared to those from (G) the WT, showing medial veins (m), lateral veins (l), and stylar xylem (stx). The bifurcations of the medial veins are indicated by arrows. Scale bars = 0.9 mm.

(I, J) SEM images showing the gynoecia pattern of (J) *mtn1-1mtn2-1* compared to that of (I) the WT. In the WT, the stigma (sg), style (st), valve (v), and replum (r) are clearly distinguishable in contrast to the indistinguishable st and v of *mtn1-1mtn2-1.* Arrow head indicated base of style. Scale bars = 0.6 mm.

4.4.3 Increased Cytokinin, Auxin, and Gibberellic Acid Content in *mtn1-1mtn2-1* compared to those in the WT

Since hormones regulate both male and female gametophyte development and their efficient fertilization (Cecchetti et al., 2004; Jaillais and Chory, 2010), the first step was to determine the hormone profiles of the *mtn1-1mtn2-1* mutants compared with those of the WT. The auxin (IAA), cytokinin (CK), gibberellic acid (GA), abscisic acid (ABA), jasmonic acid (JA), and salicylic acid (SA) contents were compared for four floral-development stages, as defined by Smyth et al. (1990): unopened buds with stage 13 and smaller buds, stage 14 open flowers with long anthers extending above the stigma, stage 16 with no petals and sepals attached, and stage 17b extended green siliques (Figure 4.5A-D). Total CK, IAA, GA, ABA, and JA were higher in all four *mtn1-1mtn2-1* organs than in those of the WT, except for stage 16, which had lower JA (Figure 4.5C). SA was decreased in all *mtn1-1mtn2-1* organs compared to those of the WT. However, of all of these changes, statistically significant differences were observed only in the total CK, IAA, and GA of the unopened buds ($P< 0.05$;Figure 4.5A) and stage 14 flowers (Figure 4.5B).It was therefore reasoned that the sterility of the *mtn1-1mtn2-1* mutants may be due in part to their altered hormone content.

4.4.4 Spd-reduced IAA and CK levels in the *mtn1-1mtn2-1*

Since *mtn1-1mtn2-1* produced a few seeds after germination on the media supplemented with 100 µM Spd for 14 days (Chapter 2), the next step was to profile the hormones in the 14-day-old seedlings (Figure 4.6A, B). In these *mtn1-1mtn2-1* seedlings, the overall abundance of all six hormone classes was increased compared to the WT levels, but only the CK, ABA, and SA contents were significantly different (Student's t-test; $P< 0.05$; Figure 4.6A). The exogenous feeding of Spd appeared to produce no significant differences

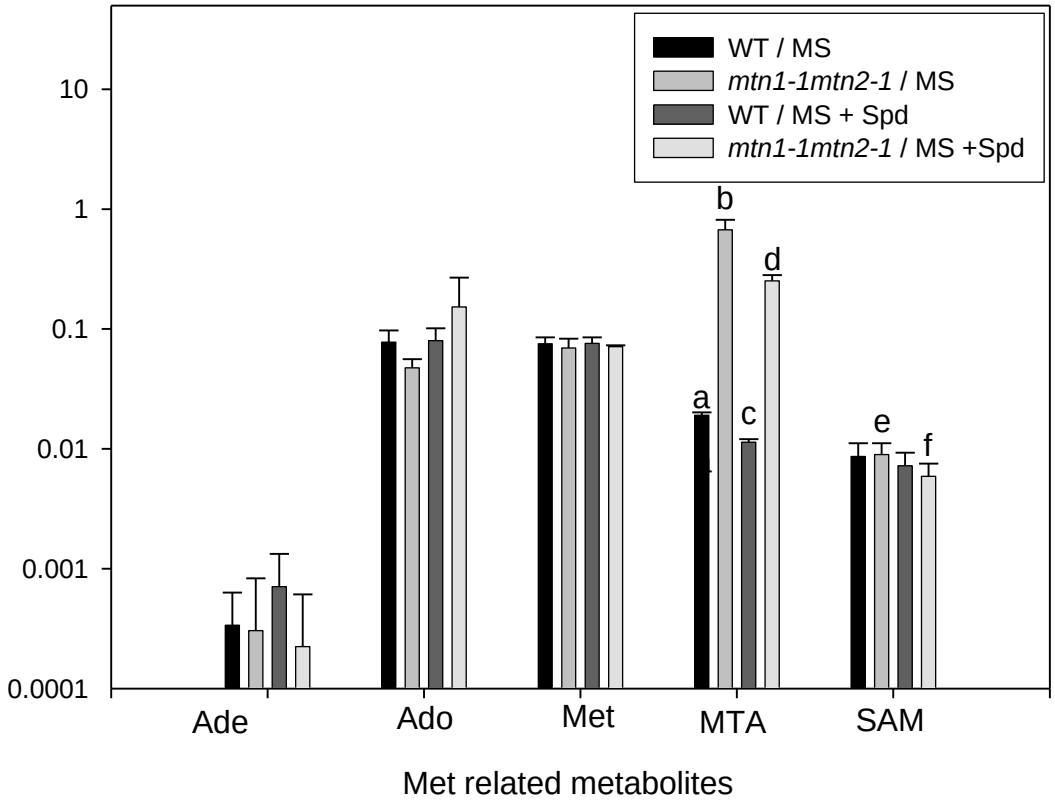

Figure 4.4: Met cycle-related metabolites of stage 14 flowers.

Tissues were harvested from plants grown on ½ MS and ½ MS supplemented with Spd for 14 days. The adenine (Ade), adenosine (Ado), methionine (Met), methylthioadenosine (MTA), and *S*-adenosyl-*L*-methionine (SAM) contents of the *mtn1-1mtn2-1* flowers relative to those of the WT are shown on a logarithmic scale. Different letters indicate statistical significant variations. Values are Mean ± SD. (N=3; P=< 0.05) (Data source: Yuji Sawada)

in the content of any of the hormone classes compared to those of the WT, aside from the total CK (Figure 4.6B). In the presence of Spd, CK levels were significantly decreased in the mutant. These results suggested that the application of exogenous Spd resulted in the recovery of the *mtn1-1mtn2-1* altered hormone content (except total CK) to WT levels.

To determine whether the Spd effects detected in *mtn1-1mtn2-1* after 14 days on Spd persisted into the unopened buds and stage 14 flowers eight weeks later, the hormone content of these organs was evaluated in comparison to that of same-stage tissues collected from *mtn1-1mtn2-1* grown on ½ MS. In the unopened buds and stage 14 flowers of these ½ MS-grown plants, IAA was found to be ~four-fold higher in *mtn1-1mtn2-1* compared to the levels in the WT (Figure 4.7A; Figure S1; Figure S2). The IAA content of both of these organs harvested from exogenous Spd-fed plants was reduced to WT levels. In contrast, WT IAA levels in unopened buds and stage 14 flowers (Figure 4.7A) increased as a response to Spd. In all four stages, total CK levels in *mtn1-1mtn2-1* grown on media supplemented with Spd were reduced to the same level as those in the WT grown on ½ MS (Figure 4.7B). The GA levels followed the same trend irrespective of the genotype or growth medium, indicating that Spd did not affect GA levels (Figure 4.7C). Taken together, these results make it clear that, compared to the WT levels, in the *mtn1-1mtn2-1* mutant, the IAA and CK levels were decreased by Spd.

4.4.5 Restoration of the normal endomembrane system transcript profile with Spd treatment

To gain further insight into the effect of Spd on fertility in *mtn1-1mtn2*-1, a transcript profiling experiment was conducted using the Affymetrix ATH-1 GeneChip. RNA for these arrays was extracted from a subset of the seedlings grown simultaneously in the same growth conditions as those used for hormone profiling: WT seeds grown on ½ MS media without Spd (MS –Spd), WT seeds grown on ½ MS media with Spd (WT + Spd),

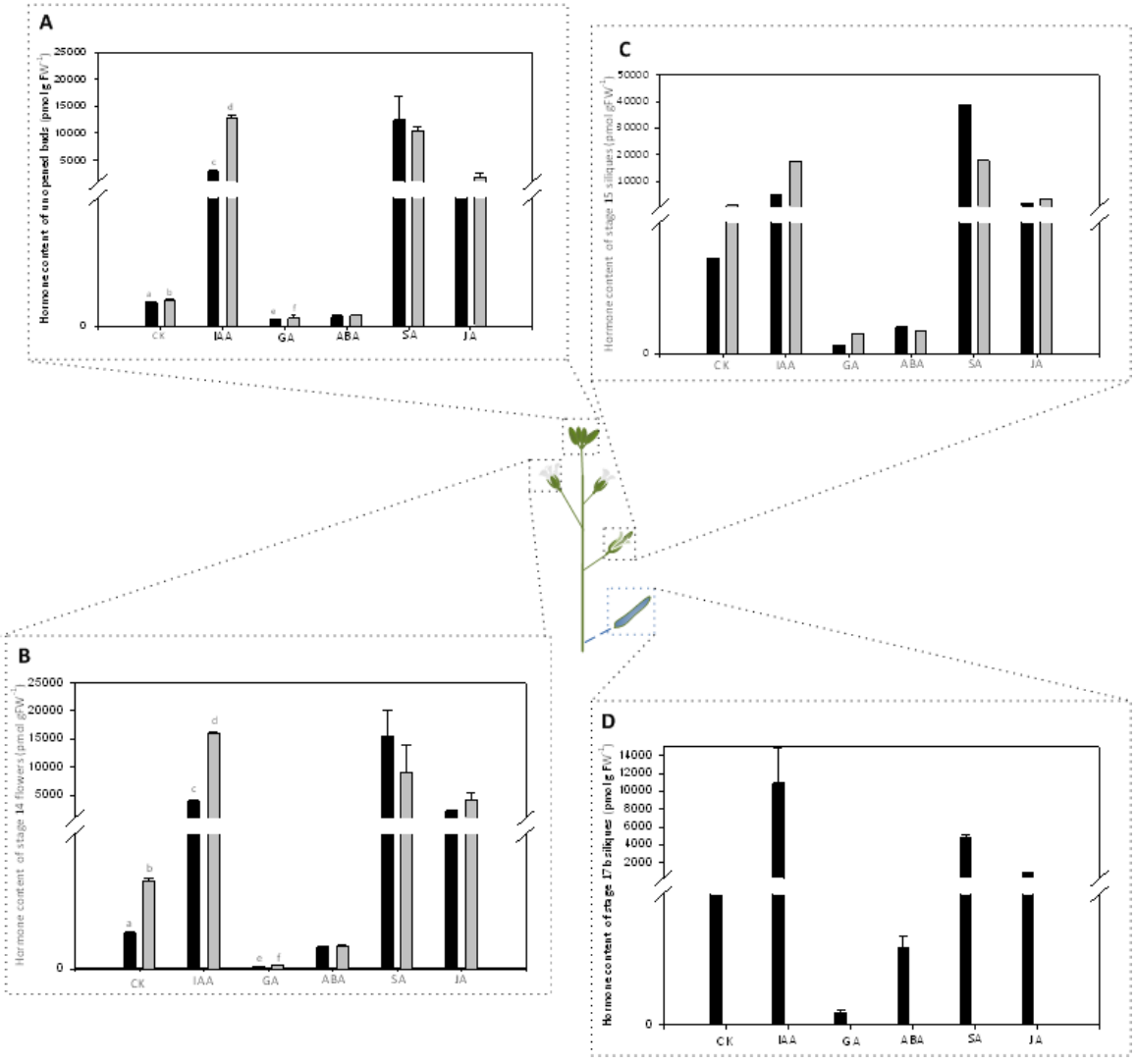

Figure 4.5: Hormone profiles of the floral organs.

Hormones were quantified in four floral organs harvested from both WT (black bars) and *mtn1-1mtn2-1* (gray bars) plants grown on ½ MS: (A) unopened buds, (B) stage 14 flowers, (C) stage 15 siliques, and (D) stage 17b. Different letters indicate the significant changes of hormone levels in *mtn1-1mtn2-1* compared to WT ($P < 0.05$). Note: (1) data for stage 15 siliques were a result of two representative replicates (C; N=2) while for all others representatibe of three replicates (A, B, D; N=3), (2) the *mtn1-1mtn2-1* grown on ½ MS were sterile and do not have stage 17b siliques (D). (Data source: Mikiko Kojima)

mtn1-1mtn2-1 seeds grown on ½ MS media without Spd (Mut-Spd) and *mtn1-1mtn2-1* seeds grown on ½ MS media with Spd (Mut+Spd). Three independent replicates were analyzed for each genotype in order to unravel the possible transcriptional network underlying the Spd-mediated responses in the mutant compared to those in the WT. The average number of detectable "present" genes in the array experiment was between 15,600 and 16,200 out of 22,747 (Appendix 4C).

To identify genes whose expression is up- or down-regulated by an underlying *MTN* deficiency, the array data for (WT-Spd) and for (Mut-Spd) were compared. The *MTN* mutation resulted in the significantly increased expression of 141 genes (Appendix 4D), and the decreased expression of 191 genes (Appendix 4E), based on the FDR criteria ($q<0.01$). To investigate the biological processes of these genes, a significant enriched Gene Ontology (GO) analysis was performed. The GO analysis revealed that categories of "response to cold" and "defense response" were significantly enriched (Fisher's test $P< 10^{-4}$) in up-regulated genes in the *mtn1-1mtn2-1* compared to those in the WT (Table S4.1). On the other hand, the "endomembrane system" "lipid binding" and "lipid metabolism" categories were significantly enriched in the down-regulated genes in the mutant ($P < 10^{-11}$, 10^{-7},10^{-5}, respectively, Table S4.2). The next investigation was conducted to examine whether the expression of representative genes in the three categories were recovered by the Spd in the mutants. As shown in Table 4.1, most of these genes were up-regulated by the Spd treatment, suggesting that the endomembrane system and lipid-related biological processes are key targets of the Spd–dependent recovery of fertility.

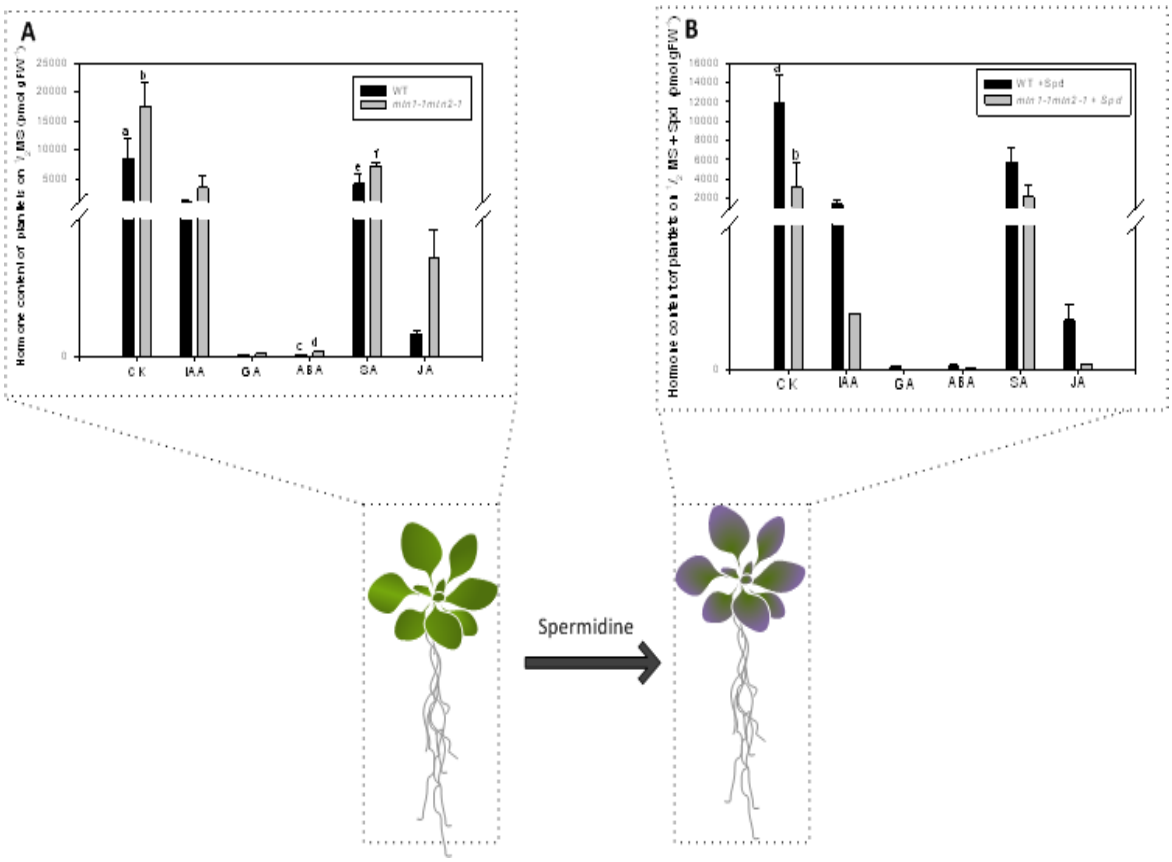

Figure 4.6: Hormone content of 14-day-old *mtn1-1mtn2-1* compared to that of the WT.

Seedlings were grown on (A) ½ MS and (B) ½ MS supplemented with Spd. Different letters indicates the statistical significant hormone changes in the two genotypes (N = 3, P< 0.05). The purple colour indicates that the plants were fed exogenous Spd. (Data source: Mikiko Kojima)

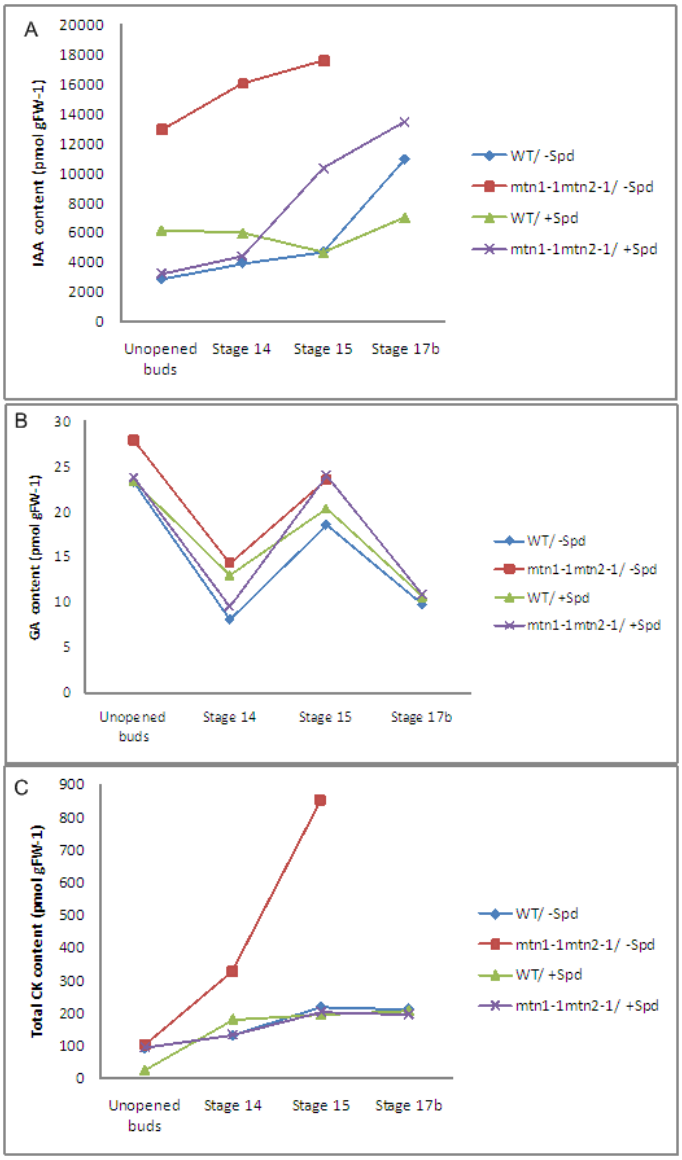

Figure 4.7: Hormone changes during flower development.

Comparison of IAA (A), total CK (B), and GA (C) levels in four different flower development stages of *mtn1-1mtn2-1* and the WT grown on ½ MS and on ½ MS supplemented with Spd.(N = 3). (Data source: Mikiko Kojima)

Table 4.1: Up-regulated genes as a response to Spd in three GO categories

Colours are assigned based on the scale below.

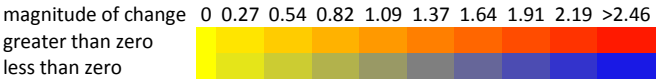

AGI	Description	Fold change	
		Mut-Spd/ WT-Spd	Mut+ Spd/ WT + Spd
GO:0012505	**Endomembrane system**		
At1g06830	Glutaredoxin (thioltransferase)	0.6	1.8
At1g11850	Expressed protein	0.6	1.4
At1g12570	Glucose-methanol-choline (GMC) oxidoreductase	0.6	1.4
At1g13080	Cytochrome P450 monooxygenase	0.6	1.3
At1g18980	Germin-like protein	0.5	1.4
At1g23205	Pectin methylesterase inhibitor	0.5	1.3
At1g25450	Very-long-chain fatty acid condensing enzyme	0.5	1.6
At1g26560	Glycosyl hydrolase family 1 protein	0.5	1.8
At1g29660	GDSL-motif lipase/hydrolase	0.6	1.4
At1g30530	UDP-glucoronosyl/UDP-glucosyl transferase	0.5	1.3
At1g30700	FAD-binding domain-containing protein	0.5	1.5
At1g51840	protein kinase-related proteins	0.6	1.5
At1g63710	cytochrome P450	0.4	1.7
At1g65490	expressed protein	0.6	2
At1g68850	peroxidase	0.6	1.2
At1g75030	pathogenesis-related thaumatin-like protein	0.6	1.3
At2g03200	aspartyl protease	0.6	1.2
At2g16005	MD-2-related lipid recognition protein	0.4	1.9
At2g20870	cell wall protein precursor	0.5	1.5
At2g21100	disease resistance-responsive protein-related	0.6	1.3
At2g22510	hydroxyproline-rich glycoprotein family protein	0.6	1.2
At2g23540	GDSL-motif lipase/hydrolase	0.6	1.3
At2g32270	zinc transporter (ZIP3) identical to zinc transporter	0.6	1.7
At2g35380	peroxidase 20 (PER20)	0.4	1.5
At2g42250	cytochrome P450	0.2	2.7
At2g43590	chitinase,	0.5	1.4
At2g44460	glycosyl hydrolase]	0.6	2
At2g47880	Glutaredoxin (thioltransferase)	0.5	1.7
At3g01420	pathogen-responsive alpha-dioxygenase	0.5	1.2
At3g13650	disease resistance response protein-related	0.6	1.1
At3g22060	receptor protein kinase-related	0.4	2.2
At3g28740	Structure-specific recognition protein 1 homolog (HMG)	0.5	1.3

At3g44970	cytochrome P450	0.4	2.1
At3g50400	GDSL-motif lipase/hydrolase	0.5	1.2
At3g52720	Carbonic anhydrase anhydrase	0.6	1.5
At3g54420	class IV chitinase (CHIV)	0.6	1.3
At3g55710	UDP-glucoronosyl/ glucuronosyl	0.5	1.7
At4g04955	Amidohydrolase	0.5	1.9
At4g11460	Protein kinase domain	0.4	1.5
At4g13410	glycosyl transferase	0.5	1.4
At4g15210	beta-amylase	0.5	1.9
At4g17215	expressed protein	0.6	1.3
At4g24140	hydrolase	0.6	1.3
At4g28780	GDSL-motif lipase	0.6	1.3
At4g28940	Nucleosidase-related contains weak similarity to MTN	0.5	1.3
At4g29030	glycine-rich protein	0.6	1.4
At4g38080	hydroxyproline-rich glycoprotein	0.6	1.3
At5g03350	legume lectin family protein	0.5	1.7
At5g09480	hydroxyproline-rich glycoprotein	0.6	1.3
At5g09520	hydroxyproline-rich glycoprotein	0.5	1
At5g14130	peroxidase, putative identical to peroxidase	0.6	1
At5g18430	GDSL-motif lipase/hydrolase	0.5	1.5
At5g33370	GDSL-motif lipase/hydrolase	0.4	2.1
At5g36910	thionin	0.5	1.1
At5g37690	GDSL-motif lipase	0.6	1.4
At5g44550	integral membrane protein	0.6	1.2
At5g47635	expressed protein	0.6	1.2
At5g50200	expressed protein	0.5	1.7
At5g50260	cysteine proteinase	0.4	1.4
At5g55720	pectate lyase]	0.5	1.5
At5g65730	xyloglucan:xyloglucosyl transferase,	0.4	1.5
GO:0008289	**lipid binding**		
At1g55260	seed storage/lipid transfer protein (LTP)	0.5	1.5
At2g48130	seed storage/lipid transfer protein (LTP)	0.5	1.3
At2g48140	seed storage/lipid transfer protein (LTP)	0.6	1.2
At3g08770	lipid transfer protein 6 (LTP6)	0.5	1.9
At4g12500	seed storage/lipid transfer protein (LTP)	0.5	1.2
At5g13900	seed storage/lipid transfer protein (LTP)	0.6	1.1
At5g48490	seed storage/lipid transfer protein (LTP)	0.5	1.2
At5g55450	seed storage/lipid transfer protein (LTP)	0.3	2.6
At5g59320	lipid transfer protein 3 (LTP3)	0.6	2.1
GO:0006629	**lipid metabolism**		
At1g29660	GDSL-motif lipase/hydrolase	0.6	1.4

At2g23540	GDSL-motif lipase/hydrolase	0.6	1.3
At3g01420	pathogen-responsive alpha-dioxygenase peroxidase	0.5	1.2
At3g50400	GDSL-motif lipase/hydrolase	0.5	1.2
At4g28780	GDSL-motif lipase/hydrolase	0.6	1.3
At4g37070	patatin, putative similar to patatin-like latex allergen	0.6	1.2
At5g18430	GDSL-motif lipase/hydrolase	0.5	1.5
At5g33370	GDSL-motif lipase/hydrolase	0.4	2.1
At5g37690	GDSL-motif lipase/hydrolase	0.6	1.4

4.4.6 Spd responses in Yang cycle-related transcripts

To detect the underlying metabolic network connecting the various genes that exhibit changes in transcript abundance, AraCyc visualization tools (Mueller et al., 2003; http://arabidopsis.org/tools/aracyc/) were employed to map gene expression data (changed >2 fold) to the corresponding metabolic pathways (Mueller et al., 2003). The affected pathways are summarized in Figure S4.3. Since it was assumed that Spd decreased MTA levels in the stage 14 flowers in an MTN mutation-independent manner, the genes related to the Yang cycle pathway were considered in detail.

Consistent with the RT-PCR results reported in Chapter 2, the transcript abundance in both *MTN1* (33-fold) and *MTN2* (4-fold) was down-regulated in *mtn1-1mtn2-1* compared to that of the WT, when grown on ½ MS (Table 4.2). When supplemented with Spd, the transcript abundance in *MTN1* in the *mtn1-1mtn2-1* decreased 14-fold compared to WT (19-fold total reduction). On the other hand, *MTN2* did not change as a response to Spd. In addition, the transcripts associated with MTA cycle-related reactions were also differentially expressed: NA synthase (*NAS)*, ACC synthase (*ACS*), and adenosylmethionine decarboxylase (*DCSAM*) (Table 4.2). Interestingly, *NAS2* was up-regulated in *mtn1-1mtn2-1* compared to the WT regardless of whether the plants were grown in the presence or absence of Spd. The *NAS2* mRNA abundance increased 1.7-fold as a response to Spd in *mtn1-1mtn2-1* plants. Although *DCSAM, ACS 6,* and

ACS 11 were not included in the transcripts that increased two fold in *mtn1-1mtn2-1* plants grown on ½ MS, they were detected in that category of expression in both the WT and *mtn1-1mtn2-1* plants fed with Spd. The levels of both DCSAM and ACS6 in *mtn1-1mtn2-1* were approximately 2.6 times those of the WT, whereas the level of ACS11 was four times less. These results suggest that the genes related to the Yang cycle are regulated at the transcript level in the presence of exogenous Spd.

4.4.7 Increased H_2O_2 production in Spd-fed seedlings

Since the H_2O_2 produced during PA catabolism either by PAO and CuAO acts as a signal in xylem differentiation, DAB staining was used to qualitatively monitor the level of H_2O_2 production in seedlings grown on ½ MS and on ½ MS supplemented with Spd (Figure 4.8). The control group for this test were seedlings grown on oxidative-stress-inductive AT media that leads to H_2O_2 production due to stress.

Table 4.2: Yang cycle related genes that are changed in the *mtn1-1mtn2-1* mutant compared to WT on both MS media supplemented with Spd

The values are averages of 3 independent replicates. Colours are assigned based on the scale below.

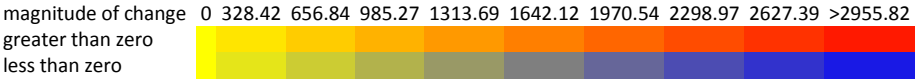

AGI	Description	WT -Spd	Mut -Spd	WT + Spd	Mut + Spd
GO:0009116	**nucleoside metabolism**				
At4g38800	Methylthioadenosine nucleosidase (MTN1)	3284.2	97.3	3236.8	227.7
At4g34840	Methylthioadenosine nucleosidase (MTN2)	105.8	26.2	102.9	29.4
GO:0030418	**Nicotianamine biosynthesis**	166.7	635.8	108.5	603.3
At5g56080	Nicotianamine synthase (NAS 2)	65.6	172.2	60.1	181.2
At1g 09240	Nicotianamine synthase (NAS 3)				
GO:0030419	**Polyamine biosynthesis**				
At5g15950	Adenosylmethionine decarboxylase (DCSAM)	0	0	220	606.6
GO:0009693	**Ethylene biosynthesis**				
At4g11280	ACC Synthase (ACS 6)	0	0	524.9	1390.7
At4g08040	ACC Synthase (ACS 11)	0	0	297.7	71.3

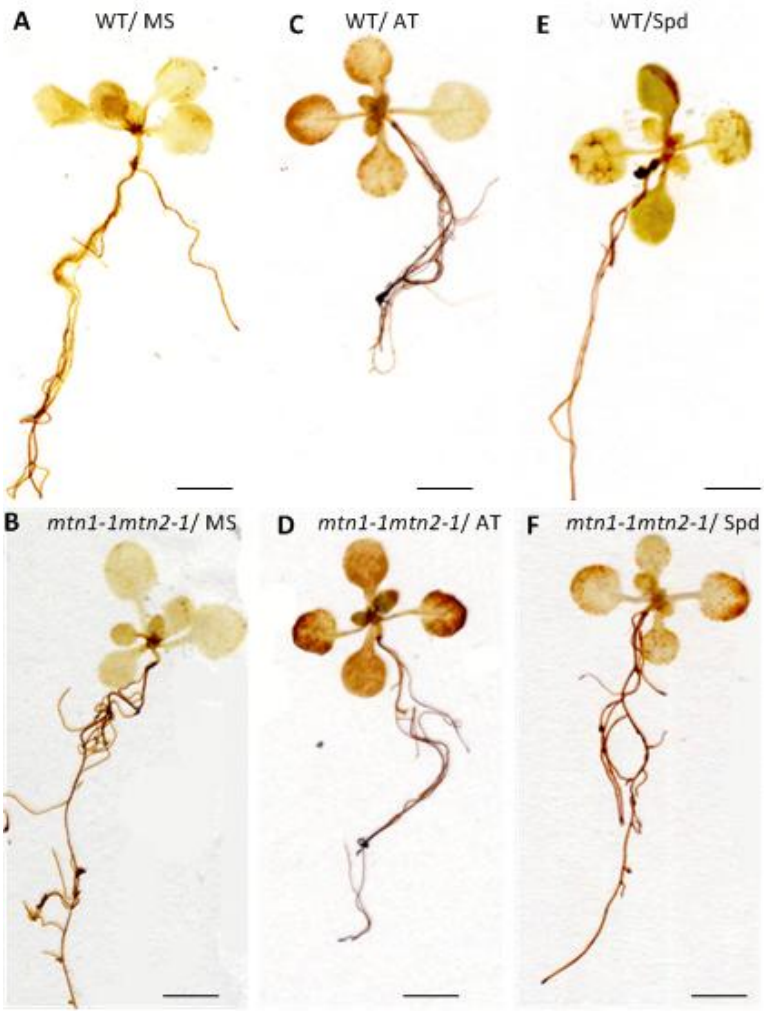

Figure 4.8: Histochemical DAB staining to detect H_2O_2 production

(A, B) *mtn1-1mtn2-1* and WT seedlings grown for 14 days in ½ MS did not show the distinct brown color in the leaves. However, the roots of both genotypes were stained.

(C, D) The seedling leaves and cotyledons of both genotypes are prominently stained with DAB when grown on oxidative-stress-inductive AT media for 2 days.

(E, F) When grown on media supplemented with Spd, the *mtn1-1mtn2-1* leaves were stained more intensely than those of the WT. Scale bars = 6 mm.

According to Takahashi et al. (2010) of the five PAOs of Arabidopsis, only PAO4 and PAO5 are present in 14-day-old Arabidopsis seedlings. Based on the microarray data obtained for the 14-day-old seedlings, no significant changes were detected in these genes with or without exogenous supplementation of Spd (Table S4.3). However, the CuAO (At4g12280) that was increased by 1.9 times in the *mtn1-1mtn2-1* seedlings grown on ½ MS compared to the levels in the WT was further increased 2.8 fold when the plants were supplemented with Spd.

4.4.8 Vasculature, embryos, and auxin distribution of restored branches

As mentioned, the *mtn1-1mtn2-1* generated from the seedlings that were grown on exogenous Spd for 14 days developed some siliques with viable seeds two-three weeks after bolting. This recovery of fertility occurred in random branches or at random times on sectors of one branch. The cross-sectional areas of the recovered branches show ~ eight vascular bundles compared to the increased number of vascular bundles (~ 12) in branches of untreated ("naïve"= never seen Spd) plants (Figure 4.9). The majority of the flowers on the fertile branches closer to the siliques were like those of the WT in appearance, with dehiscent anthers. The majority of ovules in the "recovered siliques" developed beyond the 2-V ovule stage into seeds with embryos (Figure 4.10C, F). In contrast to the fully developed mature embryos in WT seeds (Figure 4.10I), the restored siliques had seeds with embryos that spanned the stages between mature embryos and stage 2-V ovules. DR5*rev*::GFP expression reflected increased auxin distribution in stage 2-V *mtn1-1mtn2-1* ovules (Figure 4.10A, B). Using the GFP signal as an indicator of auxin distribution, the restored seeds had auxin maxima at the cotyledon tips and embryonic root tips similar to those found in WT embryos (Figure 4.10D, E). However, these *mtn1-1mtn2-1* embryos were different in morphology and had

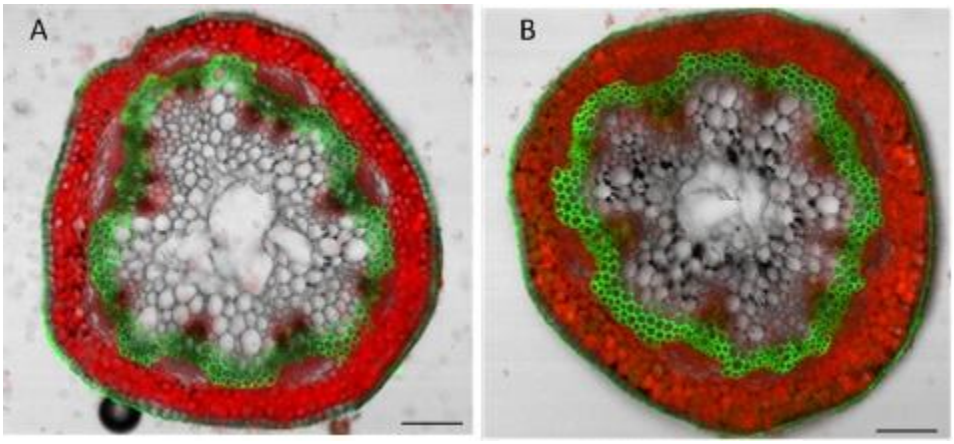

Figure 4.9: Confocal images of cross-sections of branches of a *mtn1-1mtn2-1* plant recovered after exogenous Spd feeding. Scale bars = 60 µm.

(A) Non-restored branch with no filled siliques

(B) Restored branch with seed-containing siliques

increased ectopically expressed auxin surrounding the embryo. This apparent improved auxin distribution may act as a signal for overcoming the barriers of *mtn1-1mtn2-1* mutants to generating viable embryos.

4.4.9 Transgenerational effects of Spd that give rise to WT-looking *mtn1-1mtn2-1* plants

The majority of seeds arising from Spd-treated plants germinated (Chapter 2). Preliminary analysis over two additional generations of Spd feeding (Figure S4.6, Table S4.16, Table S4.17) revealed that plants that were grown either twice (+ SpdG2) or three times (+ SpdG3) on exogenous Spd have variable vegetative phenotypes resembling those of *mtn1-1mtn2-1.* These included interveinal chlorosis, observed at 14 DAG (Table S4.16), and rosette leaf texture (Figure S4.7). Upon the transition to the reproductive phase, these plants appeared to adopt a moderate phenotype with more WT characteristics, including earlier bolting than in *mtn1-1mtn2-1*, although still later than in the WT (Table S4.4). These plants also had many closed buds, in contrast to the open buds of *mtn1-1mtn2-1* plants (Figure S4.7D-F). At maturity, both + SpdG2 and + SpdG3 plants were indistinguishable from the WT, with normal flowers, dehiscent anthers, and fertility (Figure S4.7G-H), despite being genotypically *mtn1-1mtn2-1* and having decreased MTN activity.

Amazingly, the generations that were exposed to only one (+ SpdG1–Spd G2) or two (+SpdG2–Spd G3) Spd treatments were indistinguishable from plants exposed to Spd: (+SpdG1, G2) and (+SpdG2, G3), respectively (Table S4.16). It was thus concluded that one Spd treatment triggers genotypically *mtn1-1mtn2-1* mutants to adopt a WT reproductive phase.

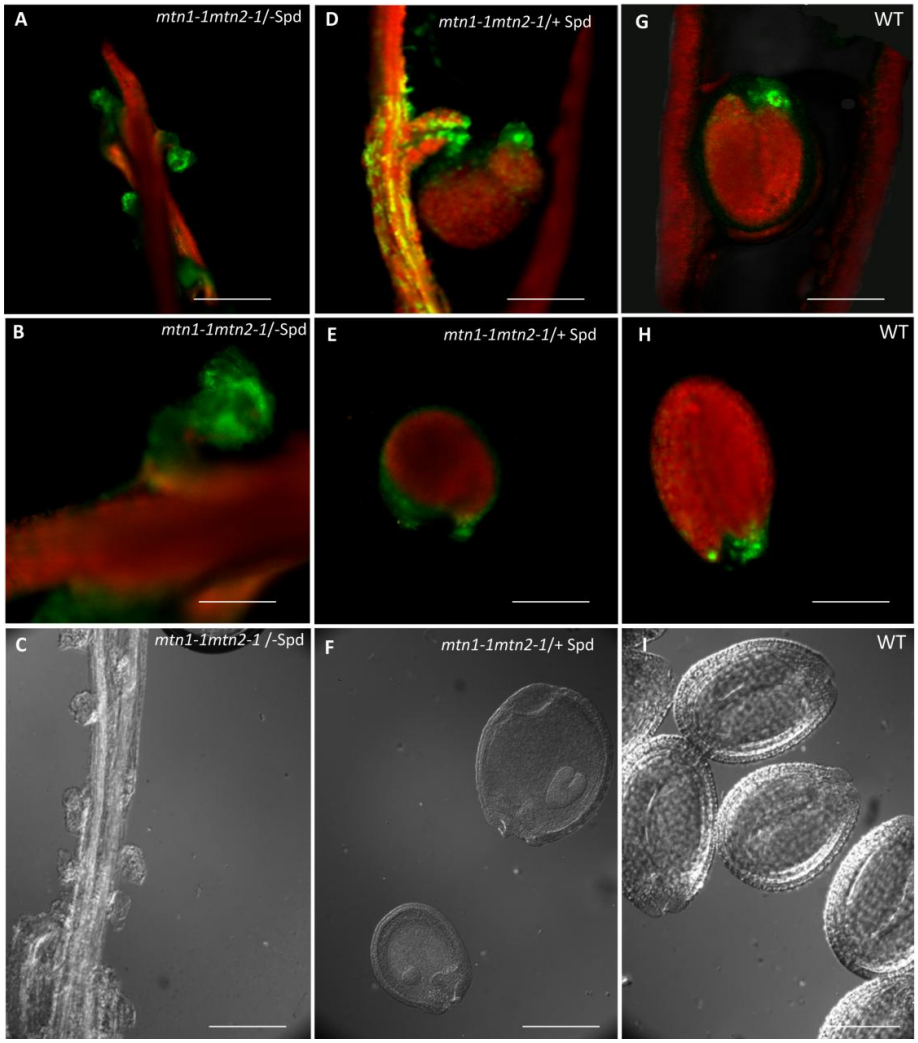

Figure 4.10: Seeds and embryos of restored plants

Compared to (A-B) underdeveloped ovules of *mtn1-1mtn2-1* grown on ½ MS, (D, E) restored seeds from exogenously fed Spd *mtn1-1mtn2-1* show close to (G, H) the WT Dr5*rev*::GFP distribution. The green florescence indicates the presence of auxin as reported by the auxin sensitive reporter Dr5. Yellow florescence indicates the co-localization of GFP florescence and autoflorescence (red). The restored siliques contained underdeveloped ovules similar to (C) *mtn1-1mtn2-1*, (F) different size seeds with embryos of different development stages, and (I) seeds with fully developed embryos similar to those of the WT. Scale bars = 25 µm.

4.5 Discussion

4.5.1 Spd and vascular development

PAs are known to affect vascular development by influencing processes such as cambium activity, the initiation of cell differentiation, and the induction of cell death (Vera-Sirera et al., 2010). These processes are thought to be mediated by interactions with (1) hormones including auxins, which affect cell division or (2) by the production of H_2O_2 during PA catabolism (Møller and McPherson, 1998). To our knowledge the only documented connection between PA, auxin, and xylem development is that auxin induces ACL5 transcription that encodes for Tspm synthase (Hanazawa et al., 1997) which is necessary for proper xylem differentiation. In *mtn1-1mtn2-1*, the low Tspm levels are speculated to be a result of accumulated MTA inhibiting ACL5 activity (Chapter 2). With Spd feeding, the Tspm levels would be expected to increase by either inducing ACL5 via recovered auxin or increasing *SAMDC* transcript levels. Since mutation of one of the SAMDC isoforms, *bud2*, showed severely deformed vascular development (Ge et al., 2006) it is possible that this increase in *SAMDC* transcript abundance may aid in producing normal vasculature by adjusting the PA homeostasis in *mtn1-1mtn2-1* mutants.

On the other hand, the increased H_2O_2 production detected by DAB staining in the 14-day-old seedlings that received the Spd exogenously suggests that the Spd-induced PA catabolism could also play a role in xylem differentiation and cell death in the *mtn1-1mtn2-1* plants, leading to improved fertility. In support of the possibility of a role played by H_2O_2, *CuAO* transcripts were up-regulated in *mtn1-1mtn2-1* compared to those in the WT when supplemented with Spd. However, a detailed analysis of the genes involved in PA catabolism, PA metabolism, and PA conjugation along with their anatomical changes will be necessary in order to narrow down the basis of the vascular changes in *mtn1-1mtn2-1* mutants when exposed to Spd. In any case, the

recovery of a normal vasculature may indirectly mediate the increased seed production of Spd-treated *mtn1-1mtn2-1* plants.

4.5.2 Spd and reproductive development

Several lines of evidence suggest that the effect of Spd on fertility involves auxin. First, Spd treatment led to the development of normal floral organogenesis with the proper number, spacing, and pattern of floral organs along with anthers that dehisce. Several mutants that were disrupted either in auxin biosynthesis, transport, or signaling also exhibit similar flowering defects related to organ number, spacing, and male and female reproductive structure morphology (Krizek et al., 2011). The *ett* mutant with a mutation in a gene that encodes the Auxin Response Factor, ETTIN (ETT)/ARF3, has an increased number of sepals, petals, and abnormal reproductive structures (Sessions, 1997). The *yuc1yuc4* mutant with defective auxin biosynthesis also has abnormal reproductive structures (Cheng et al., 2006). On the other hand, *pin* and *pid* mutants that have mutations in the genes that encode auxin transport system components exhibit fewer floral organs but more petals (Bennett et al., 1995). In addition, *ett* and *pid* mutants have alterations in the relative spacing and position of floral organ primordia (Bennett et al., 1995; Sessions, 1997). Taken together, these results suggest that recovered auxin homeostasis contributes to the proper development of floral organs in Spd-treated *mtn1-1mtn2-1* that would logically increase its fertilization efficiency. First, the fact that the “restored seeds” developed past the 2-V ovule stage and produced seeds with apparently normal embryos provides clear evidence that Spd-treated MTN mutant plants are partially fertile. Second, with Spd treatment, the auxin levels decreased to WT levels in the 14-day-old seedlings, unopened buds, and stage 14 flowers. Third, Spd treatment resulted in the recovery of the components of the endomembrane system the function of wfhich is essential for proper localization of membrane proteins, including PIN proteins and BR receptor proteins. PIN polarity is known to direct auxin flow in order to create the local gradients essential for pattern

formation (Friml et al., 2004). The auxin efflux transmembrane transporter PIN 7 (At1g23080) transcript was up-regulated 2.5-fold in the *mtn1-1mtn2-1* in response to Spd. Finally, the DR5*rev*::GFP expression of restored seeds in *mtn1-1mtn2-1* was distributed more closely to that of the WT expression (Figure 4.7) However, the partial recovery of fertility suggests the need for proper auxin distribution in the reproduction phase. A consideration of all of this evidence leads to the conclusion that auxin could be one of the key targets affected by Spd in the recovery of fertility of *mtn1-1mtn2-1.*

4.5.3 Spd effects on the Yang cycle and SAM utilization activities

The response to exogenous Spd was observed in both the transcripts and metabolites related to the Yang cycle and SAM utilization. The microarray data revealed that the transcript abundance associated with seven genes of this cycle was affected by exogenous Spd: *MTN1, MTN2, NAS2, NAS3, DCSAM, ACS6,* and *ACS11*. Exogenous Spd increased *MTN1* transcript abundance and decreased MTA content (20- and 13-fold, respectively). Irrespective of the MTN mutation of the *mtn1-1mtn2-1* knockdown mutant, the increase in *MTN* transcript abundance may result in higher MTN activity that leads to decreased MTA content. This reduction in MTA content should lower its inhibitory effects on MTA-producing enzyme activities (Chapter 2).

The mechanisms of handling the lower MTA inhibition are likely pathway-specific. The expression of *NAS* is up-regulated in *mtn1-1mtn2-1* compared to that in the WT, even when grown without Spd supplementation. The chlorotic phenotype of both *mtn1-1mtn2-1* plants grown on ½ MS or on ½ MS supplemented with Spd suggests that the mutants are experiencing low NAS activity and possibly lower NA content even after supplementation with Spd. The increases in *NAS 2* (3.6-fold) and *NAS 3* (2.6-fold) when grown on ½ MS may reflect a sensing of their low NA content (Chapter 2). On the other hand, *SAMDC* transcripts, which encode the enzyme activity needed to produce decarboxylated SAM, the essential cofactor for PA

biosynthesis, were up-regulated only as a response to Spd (2.8-fold). These results lead to the possibility of overriding the MTA inhibition of Spd and Tspm/Spm synthesis when treated with Spd. As with *SAMDC, ACS* transcripts were also detected when the seedlings were supplemented with exogenous Spd. These changes were isoform specific: ACS6 was up-regulated 2.6-fold and ACS11 was down regulated 4.7-fold. According to Tsuchisaka et al. (2009), individual ACS isoforms are non-essential, but specific combinations of ACS homo- and heterodimers mediate ethylene-associated processes. ACS6 and ACS11 generally form an inactive homodimer; upon Spd feeding, they may form other interactions with different activities. While these transcript changes have yet to be validated and their corresponding effects proven, it is evident that there are numerous potential effects of Spd on activities relating to the Yang cycle/SAM utilization.

However, the lower MTA and higher SAM content with Spd feeding in *mtn1-1mtn2-1* suggest that exogenous Spd effects occur at both the transcript and metabolite levels. The molecular mechanism and flux changes in its involvement merit further investigation.

4.5.4 Metabolic mechanism for Spd-dependent fertility recovery

The results presented in this chapter lead to a model for the partial improvement of fertility resulting from the feeding of exogenous Spd to *mtn1-1mtn2-1* (Figure 4.11). It is proposed that this improvement may occur via two distinct routes or by a combination of both: (1) recovery of proper auxin distribution and (2) development of normal vasculature. Analysis of all of the microarray data suggests that the exogenous Spd restored the endomembrane system. The recovery of the endomembrane system, which is needed for the proper localization of the auxin efflux protein PINs, may result in the recovery of normal auxin distribution in all organs, including both male and female reproductive structure, and their vasculature. It is proposed that the logical link between Spd and the endomembrane system is the Spd-dependent post-

translational activation of eIF5A. In addition to the potential link with eIF5A, formation of proper vasculature via auxin, increased Tspm produced from an exogenously supplied Spd precursor via SAMDC activity and/or from increased H_2O_2 production via CuAO may be partially responsible for the recovery of the *mtn1-1mtn2-1* vascular defects. Moreover, the possible involvement of hormone cross-talk especially with IAA, CK and BR cannot be ruled out.

4.5.5 Metabolic recovery versus epigenetic recovery

The evidence presented thus far suggests that the Spd-dependent recovery of fertility in *mtn1-1mtn2-1* is via a metabolic mechanism (Figure 4.11). However, three observations lead to the possible involvement of an epigenetic mechanism in this reversal: (1) the partial nature of the first reversal, with fertile siliques occurring only in some branches or sectors while retaining genotypic identity; (2) the transgenerational nature of the fertility reversal, whereby without further supplementation of Spd, the seeds from Spd-fed plants give rise to fertile plants in the subsequent generation, and (3) the proportion of fertile recovered plants in different Spd+ generations was inconsistent despite the plants being maintained at identical growth conditions.

However, based on the model presented, the partial recovery in some sectors could be due to altered auxin distribution in the meristem that gives rise to these branches. These initial stem cells, with variable properties based on the initial signals (auxin) they receive, will ultimately give rise to at least a few branches with altered auxin distribution. Branches with proper auxin gradients or locations with sufficient auxin content along the length of branches produce seeds.

The transgenerational effects may be due simply to the recovery of seeds with properly developed embryos (including embryonic vasculature) that are capable of giving rise to a

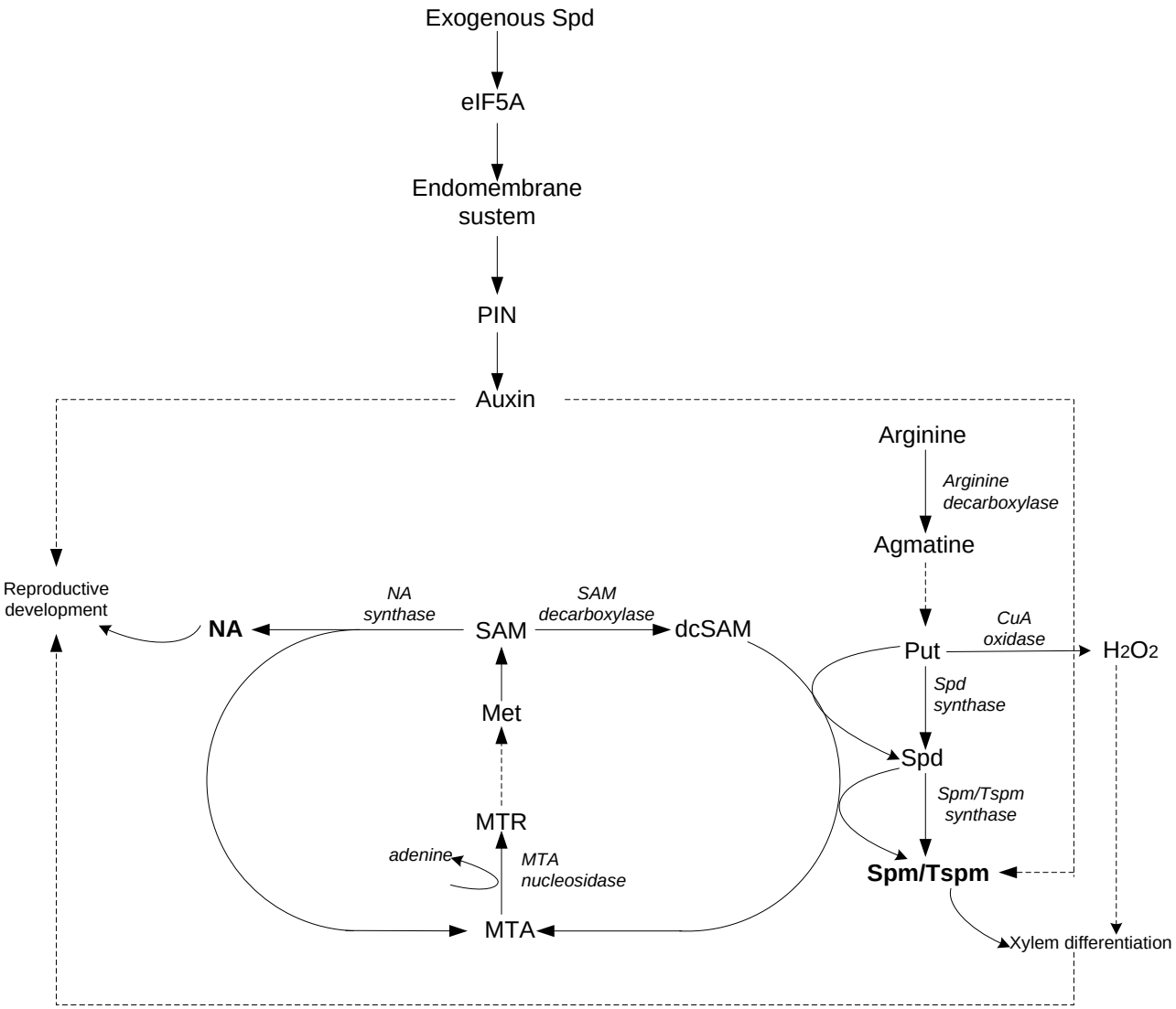

Figure 4.11: Model showing potential links resulting in the recovery of vasculature and reproduction for seed production after feeding with exogenous Spd

fertile plant that still holds the *mtn1-1mtn2-1* metabolism. However, what is questionable is how these next-generation plants remain fertile while being MTN deficient. This effect could result from a process that constitutively maintains either low MTA or high Spd levels. The methylation of target genes (epigenetic) could be one possibility. A logical and potential candidate could be the gene that encodes Spd sinapoyl CoA acyltransferase (Luo et al., 2009) which is required for the production of conjugated Spd in seeds. This conjugated Spd is proposed to serve as a PA reserve in seeds, which is released in order to fulfill the needs of the developing tissues (Luo et al., 2009). One such need of the embryonic tissues could be the activation of eIF5A. It is thus possible that methylation of this gene could release reserved PA and overcome the Spd deficiency in the *mtn1-1mtn2-1* mutant embryos.

4.6 Conclusion

Based on the results presented in this chapter, the key processes affected by exogenous Spd feeding are auxin distribution and/or vascular development, which either alone or together allow seed production in *mtn1-1mtn2-1*. The transgenerational effects observed as a result of exogenous Spd supplementation could be an epigenetic affect.

4.7 Technical assistance by others

Ishari Waduwara-Jayabahu (IWJ) designed the experiments; grew the plants; collected the samples; analyzed the reproductive organs using SEM, DIC, and confocal microscopes, except for the ovule observations presented in Figure 2 A-F, which were conducted by Sarah Schoor; IWJ also extracted and quantified the RNA for microarray analysis. The majority of this research was carried out in the research laboratory of Dr. H. Sakakibara, RIKEN, Japan, during the three-month period when IWJ joined his group on a JSPS-NSERC fellowship. The following laboratory members of RIKEN were involved in the project: Mikiko Kojima analyzed hormones, Yuji Sawada analyzed metabolites, and Nori Nakamichi analyzed microarray data and also extracted the list of transcripts that exhibited changes greater than two-fold.

4.8 Supplemental Material

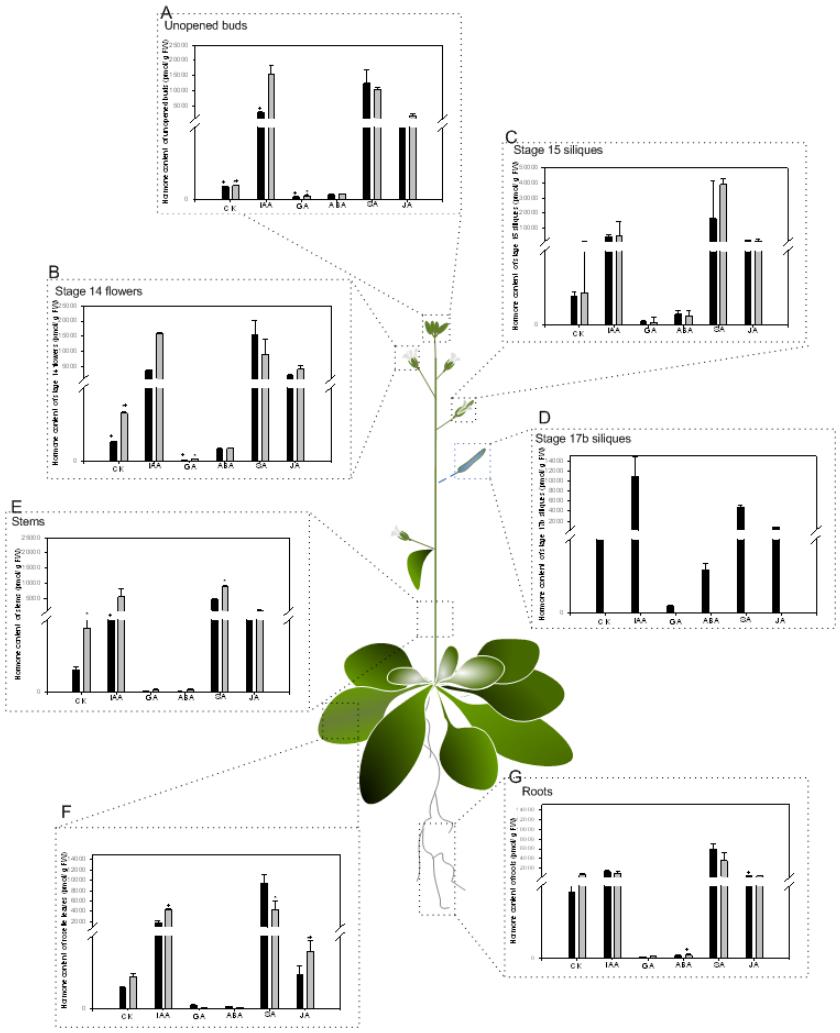

Figure S4.1: The hormone profiles of *mtn1-1mtn2-1* plants compared to WT grown on ½ MS.

Hormone profiles of seven organs (A) unopened buds, (B) stage 14 flowers, (C) stage 15 siliques, (D) stage 17b, (E) stems, (F) rosette leaves and (G) roots were compared between WT (black bars) and *mtn1-1mtn2-1* (grey bars). Note: the *mtn1-1mtn2-1* grown on ½ MS are sterile and will not have stage 17b siliques (G). Values are mean ± SD (N = 2-3).

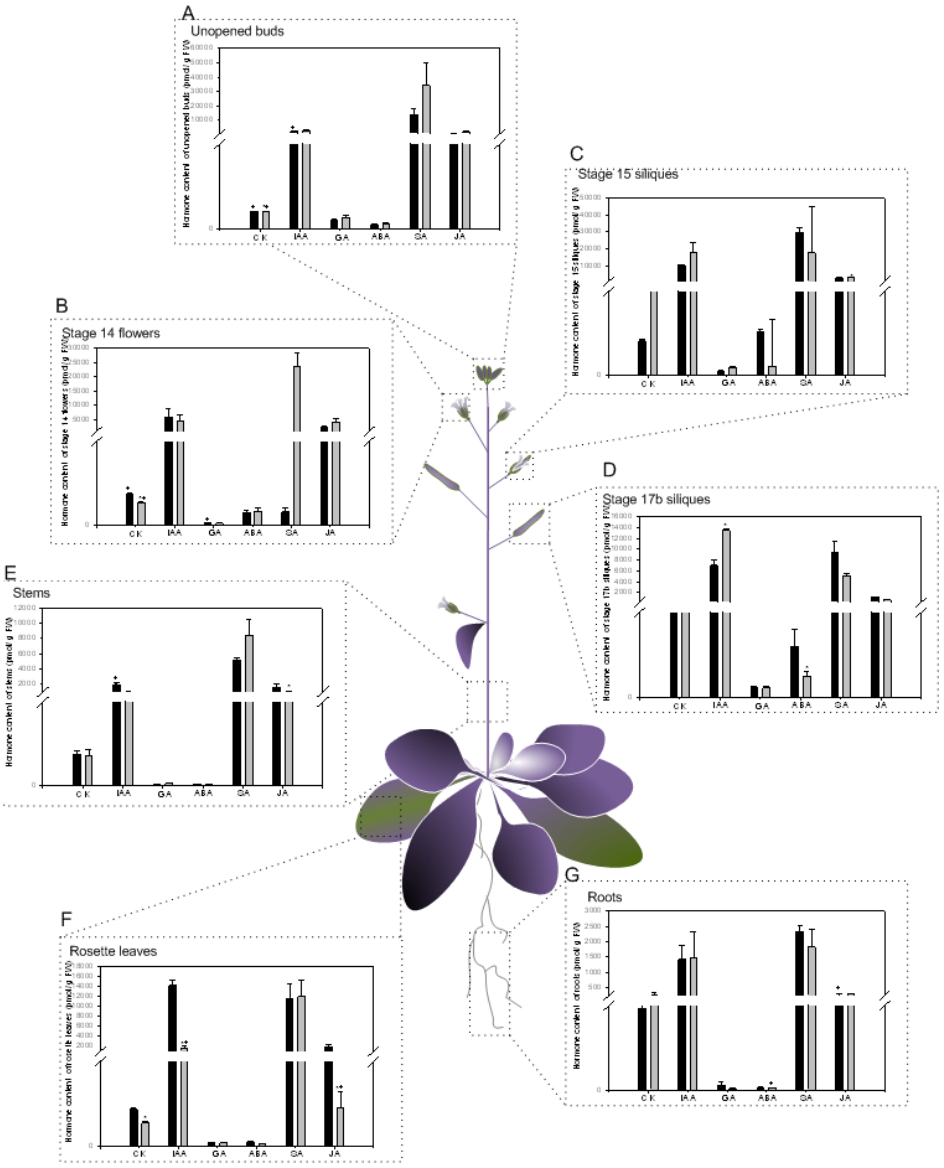

Figure S4.2: The profiles of *mtn1-1mtn2-1* plants compared to WT grown on ½ MS supplemented with Spd.

Hormone profiles of seven organs (A) unopened buds, (B)stage 14 flowers, (C) stage 15 siliques, (D) stage 17b, (E) stems, (F) rosette leaves and (G) roots were compared between WT (black bars) and *mtn1-1mtn2-1* (grey bars). Note the *mtn1-1mtn2-1* grown on ½ MS are sterile and will not have stage 17b siliques. Values are mean ± SD (N = 2-3). Purple color indicates that the plant was fed with exogenous Spd.

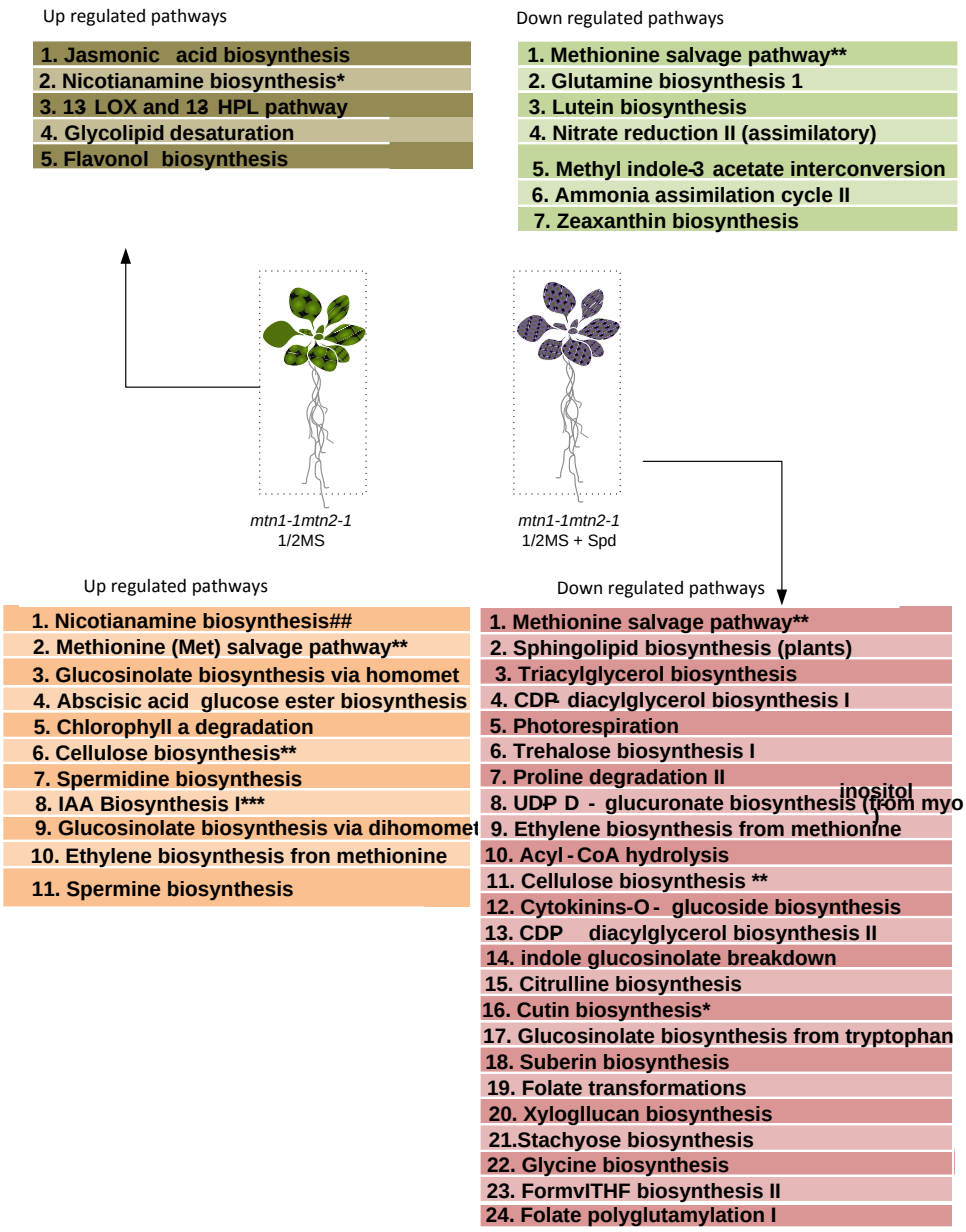

Figure S4.3: Pathways determined by genes that are affected as a response to Spd. Pathways in dark green and light green show -up and -down regulated pathways on ½ MS respectively. Similarly, pathways in orange and pink show -up and -down regulated pathways on ½ MS supplemented with Spd respectively. Asterics shows common pathways regulated among the four groups.

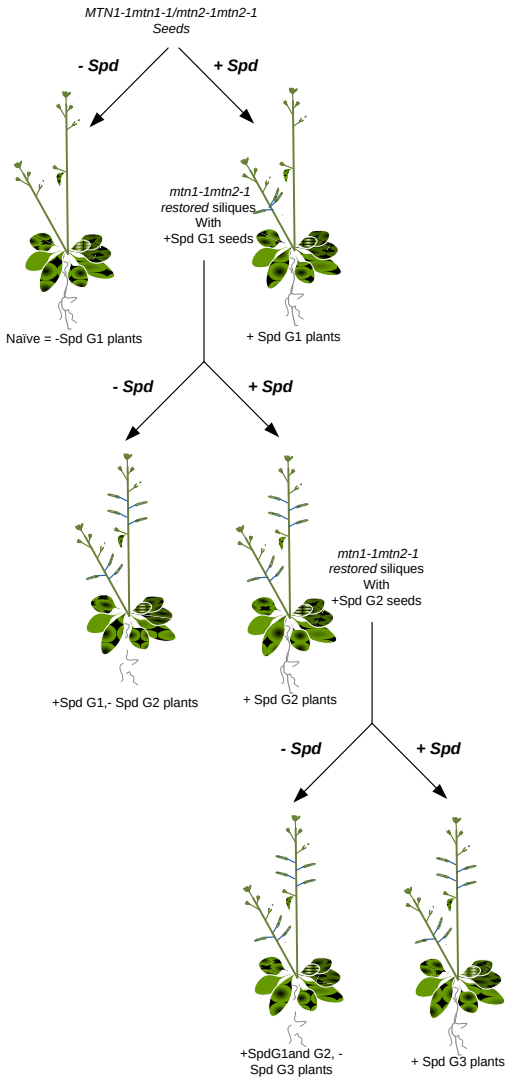

Figure S4.4: Nomenclature used to describe *mtn1-1mtn2-1* generations grown with or without Spd treatment

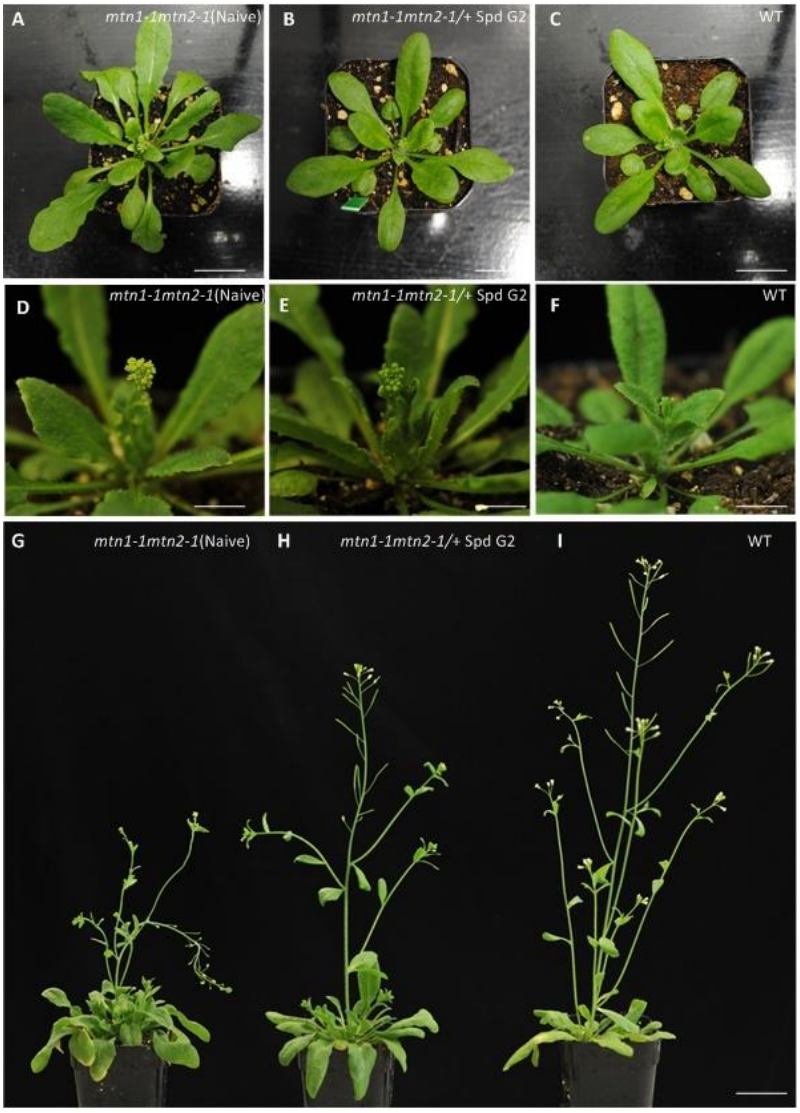

Figure S4.5: The phenotype of *mtn1-1mtn2-1* over two generations of Spd feeding

The plants at inflorescence emergence (A-C) with close up view of first buds (D-F) and 2-weeks after bolting (G-I).

(A, D, G) Naïve *mtn1-1mtn2-1*. Scale bar = 24 mm.

(B, E, H) The *mtn1-1mtn2-1* plants that were grown on exogenous Spd for two generations (+ Spd G2). Scale bar = 80 mm.

(C, F, I) WT. Scale bar = 30 mm.

Table S 4.1: Up regulated Gene Ontologies in the *mtn1-1mtn2-1* compared to WT when grown on ½ MS

GO#	GO annotation	Fisher's test p
GO:0009409	response to cold	1.52E-05
GO:0006952	defense response	2.73E-05
GO:0030418	nicotianamine biosynthesis	1.11E-04
GO:0009269	response to desiccation	1.17E-04
GO:0003700	transcription factor activity	1.17E-04
GO:0006355	regulation of transcription, DNA-dependent	2.91E-04
GO:0005618	cell wall	5.72E-04
GO:0042538	hyperosmotic salinity response	7.80E-04
GO:0009873	ethylene mediated signaling pathway	9.41E-04
GO:0004556	alpha-amylase activity	0.00100873
GO:0006879	iron ion homeostasis	0.00100873
GO:0042542	response to hydrogen peroxide	0.00100873
GO:0042752	regulation of circadian rhythm	0.00160161
GO:0005634	nucleus	0.00180821
GO:0009627	systemic acquired resistance	0.00194568
GO:0009737	response to abscisic acid stimulus	0.00213267
GO:0003677	DNA binding	0.00237656
GO:0009753	response to jasmonic acid stimulus	0.00289085
GO:0004568	chitinase activity	0.00316113
GO:0010266	response to vitamin B1	0.00613391
GO:0030275	LRR domain binding	0.00613391
GO:0048578	positive regulation of long-day photoperiodism, flowering	0.00613391
GO:0009695	jasmonic acid biosynthesis	0.00699144
GO:0016564	transcriptional repressor activity	0.00764403
GO:0009611	response to wounding	0.00856953
GO:0004121	cystathionine beta-lyase activity	0.0121931
GO:0004338	glucan 1,3-beta-glucosidase activity	0.0121931
GO:0004645	phosphorylase activity	0.0121931

GO:0010188	response to microbial phytotoxin	0.0121931
GO:0015086	cadmium ion transporter activity	0.0121931
GO:0016702	oxidoreductase activity,	0.0121931
GO:0046345	abscisic acid catabolism	0.0121931
GO:0009507	chloroplast	0.01433909
GO:0005506	iron ion binding	0.01456892
GO:0005509	calcium ion binding	0.01481291
GO:0006597	spermine biosynthesis	0.01817824
GO:0008898	homocysteine S-methyltransferase activity	0.01817824
GO:0009942	longitudinal axis specification	0.01817824
GO:0015691	cadmium ion transport	0.01817824
GO:0016566	specific transcriptional repressor activity	0.01817824
GO:0030410	nicotianamine synthase activity	0.01817824
GO:0031347	regulation of defense response	0.01817824
GO:0009908	flower development	0.01914803
GO:0004014	adenosylmethionine decarboxylase activity	0.02409001
GO:0005384	manganese ion transporter activity	0.02409001
GO:0006828	manganese ion transport	0.02409001
GO:0008199	ferric iron binding	0.02409001
GO:0009267	cellular response to starvation	0.02409001
GO:0046423	allene-oxide cyclase activity	0.02409001
GO:0005578	extracellular matrix (sensu Metazoa)	0.02992907
GO:0005654	nucleoplasm	0.02992907
GO:0006826	iron ion transport	0.02992907
GO:0008295	spermidine biosynthesis	0.02992907
GO:0008810	cellulase activity	0.02992907
GO:0009861	jasmonic acid and ethylene-dependent systemic resistance	0.02992907
GO:0042991	transcription factor import into nucleus	0.02992907
GO:0006596	polyamine biosynthesis	0.03569609
GO:0015976	carbon utilization	0.03569609
GO:0030304	trypsin inhibitor activity	0.03569609

GO:0043234	protein complex	0.03569609
GO:0048825	cotyledon development	0.03569609
GO:0009081	branched chain family amino acid metabolism	0.04139172
GO:0009625	response to insect	0.04139172
GO:0010039	response to iron ion	0.04139172
GO:0016165	lipoxygenase activity	0.04139172
GO:0040007	growth	0.04139172
GO:0016787	hydrolase activity	0.0448939
GO:0009651	response to salt stress	0.04628131
GO:0010017	red or far red light signaling pathway	0.04701661
GO:0010048	vernalization response	0.04701661
GO:0005375	copper ion transporter activity	0.05257142
GO:0009266	response to temperature stimulus	0.05257142
GO:0009698	phenylpropanoid metabolism	0.05257142
GO:0031012	extracellular matrix	0.05257142
GO:0005385	zinc ion transporter activity	0.05805678
GO:0005983	starch catabolism	0.05805678
GO:0007389	pattern specification	0.05805678
GO:0008283	cell proliferation	0.05805678
GO:0009817	defense response to fungus, incompatible interaction	0.05805678
GO:0016209	antioxidant activity	0.05805678
GO:0006829	zinc ion transport	0.06347332
GO:0009867	jasmonic acid mediated signaling pathway	0.06347332
GO:0009672	auxin:hydrogen symporter activity	0.06882168
GO:0010150	leaf senescence	0.06882168
GO:0016207	4-coumarate-CoA ligase activity	0.06882168
GO:0019761	glucosinolate biosynthesis	0.06882168
GO:0005554	molecular function unknown	0.07192527
GO:0008372	cellular component unknown	0.07286682
GO:0030528	transcription regulator activity	0.07771636
GO:0006869	lipid transport	0.08196074

GO:0009751	response to salicylic acid stimulus	0.08338001
GO:0006114	glycerol biosynthesis	0.08446388
GO:0009825	multidimensional cell growth	0.08446388
GO:0009414	response to water deprivation	0.08480117
GO:0016021	integral to membrane	0.08622134
GO:0009723	response to ethylene stimulus	0.08764828
GO:0008289	lipid binding	0.08907382
GO:0030154	cell differentiation	0.08954571
GO:0012505	endomembrane system	0.09364572
GO:0004089	carbonate dehydratase activity	0.09456243
GO:0009508	plastid chromosome	0.09456243
GO:0009887	organ morphogenesis	0.09456243
GO:0045941	positive regulation of transcription	0.09456243
GO:0008324	cation transporter activity	0.09951464
GO:0008483	transaminase activity	0.09951464
GO:0009631	cold acclimation	0.09951464
GO:0006520	amino acid metabolism	0.10440295
GO:0005488	binding	0.10763297
GO:0050832	defense response to fungus	0.11869029
GO:0009639	response to red or far red light	0.12332881
GO:0008757	S-adenosylmethionine-dependent methyltransferase activity	0.12790634
GO:0042742	defense response to bacterium	0.12790634
GO:0016887	ATPase activity	0.13153416
GO:0008080	N-acetyltransferase activity	0.13242342
GO:0005215	transporter activity	0.1349128
GO:0009744	response to sucrose stimulus	0.13688064
GO:0009910	negative regulation of flower development	0.13688064
GO:0048364	root development	0.13688064
GO:0007275	development	0.14110597
GO:0004222	metalloendopeptidase activity	0.14127854
GO:0005886	plasma membrane	0.15699221

GO:0030145	manganese ion binding	0.158288
GO:0009736	cytokinin mediated signaling	0.16239755
GO:0009926	auxin polar transport	0.16239755
GO:0000156	two-component response regulator activity	0.16645103
GO:0009735	response to cytokinin stimulus	0.17439193
GO:0005975	carbohydrate metabolism	0.18052686
GO:0048366	leaf development	0.18589587
GO:0009505	cell wall (sensu Magnoliophyta)	0.1962383
GO:0003993	acid phosphatase activity	0.19692315
GO:0006725	aromatic compound metabolism	0.20401651
GO:0007568	aging	0.20401651
GO:0004553	hydrolase activity, hydrolyzing O-glycosyl compounds	0.20861227
GO:0006970	response to osmotic stress	0.2109079
GO:0009617	response to bacterium	0.2109079
GO:0016706	oxidoreductase activity,	0.2109079
GO:0005737	cytoplasm	0.2129005
GO:0009733	response to auxin stimulus	0.22339416
GO:0003899	DNA-directed RNA polymerase activity	0.23040833
GO:0007165	signal transduction	0.23239402
GO:0016491	oxidoreductase activity	0.23834157
GO:0009793	embryonic development (sensu Magnoliophyta)	0.24507205
GO:0006633	fatty acid biosynthesis	0.24822548
GO:0048046	apoplast	0.24822548
GO:0006350	transcription	0.26185624
GO:0003824	catalytic activity	0.26188852
GO:0006857	oligopeptide transport	0.26445476
GO:0016563	transcriptional activator activity	0.26952748
GO:0045735	nutrient reservoir activity	0.26952748
GO:0008415	acyltransferase activity	0.2720025
GO:0009739	response to gibberellic acid stimulus	0.27683184
GO:0030599	pectinesterase activity	0.28150289

GO:0008026	ATP-dependent helicase activity	0.29664966
GO:0005576	extracellular region	0.30064628
GO:0005783	endoplasmic reticulum	0.30450114
GO:0046872	metal ion binding	0.31179687
GO:0006812	cation transport	0.31353658
GO:0009416	response to light stimulus	0.32016871
GO:0031072	heat shock protein binding	0.32629392
GO:0009058	biosynthesis	0.32917287
GO:0005507	copper ion binding	0.34182995
GO:0007046	ribosome biogenesis	0.35092028
GO:0004888	transmembrane receptor activity	0.35350265
GO:0005829	cytosol	0.36562
GO:0006979	response to oxidative stress	0.36933373
GO:0006629	lipid metabolism	0.37017032

Table S 4.2: Down regulated Gene Ontologies in *mtn1-1mtn2-1* compared to WT when the ½ MS media is supplemented with 100 µM Spd

GO#	GO annotation	Fisher's test p
GO:0012505	endomembrane system	7.11E-12
GO:0008289	lipid binding	6.28E-08
GO:0006869	lipid transport	5.50E-07
GO:0006629	lipid metabolism	6.29E-06
GO:0006118	electron transport	1.58E-04
GO:0016789	carboxylic ester hydrolase activity	3.51E-04
GO:0019825	oxygen binding	4.11E-04
GO:0004467	long-chain-fatty-acid-CoA ligase activity	9.93E-04
GO:0008393	fatty acid (omega-1)-hydroxylase activity	9.93E-04
GO:0009116	nucleoside metabolism	9.93E-04
GO:0006633	fatty acid biosynthesis	0.00117526
GO:0051707	response to other organism	0.001415697
GO:0016832	aldehyde-lyase activity	0.001823604
GO:0030508	thiol-disulfide exchange intermediate activity	0.002578186
GO:0006631	fatty acid metabolism	0.003494569
GO:0009807	lignan biosynthesis	0.004874878
GO:0004568	chitinase activity	0.005640654
GO:0006979	response to oxidative stress	0.006946893
GO:0001561	fatty acid alpha-oxidation	0.008293737
GO:0004038	allantoinase activity	0.008293737
GO:0010062	negative regulation of trichoblast fate	0.008293737
GO:0010143	cutin biosynthesis	0.008293737
GO:0018822	nitrile hydratase activity	0.008293737
GO:0046593	mandelonitrile lyase activity	0.008293737
GO:0047558	3-cyanoalanine hydratase activity	0.008293737
GO:0009911	positive regulation of flower development	0.009176
GO:0009626	hypersensitive response	0.010171293
GO:0045735	nutrient reservoir activity	0.014747574

GO:0008415	acyltransferase activity	0.01532335
GO:0004657	proline dehydrogenase activity	0.016450611
GO:0006562	proline catabolism	0.016450611
GO:0010136	ureide catabolism	0.016450611
GO:0016119	carotene metabolism	0.016450611
GO:0017057	6-phosphogluconolactonase activity	0.016450611
GO:0019499	cyanide metabolism	0.016450611
GO:0042411	beta-carotene hydroxylase activity	0.016450611
GO:0051410	detoxification of nitrogen compound	0.016450611
GO:0005618	cell wall	0.019544579
GO:0004601	peroxidase activity	0.023081291
GO:0009670	triose-phosphate transporter activity	0.02447231
GO:0010262	somatic embryogenesis	0.02447231
GO:0015717	triose phosphate transport	0.02447231
GO:0031304	intrinsic to mitochondrial inner membrane	0.02447231
GO:0030145	manganese ion binding	0.025051745
GO:0009751	response to salicylic acid stimulus	0.029863566
GO:0005615	extracellular space	0.032360499
GO:0006537	glutamate biosynthesis	0.032360499
GO:0009957	epidermal cell fate specification	0.032360499
GO:0015706	nitrate transport	0.032360499
GO:0050827	toxin receptor binding	0.032360499
GO:0051555	flavonol biosynthesis	0.032360499
GO:0000257	nitrilase activity	0.040116826
GO:0009725	response to hormone stimulus	0.040116826
GO:0005315	inorganic phosphate transporter activity	0.047742923
GO:0008519	ammonium transporter activity	0.047742923
GO:0009407	toxin catabolism	0.049266314
GO:0004364	glutathione transferase activity	0.052813643
GO:0003841	1-acylglycerol-3-phosphate O-acyltransferase activity	0.055240402
GO:0003954	NADH dehydrogenase activity	0.055240402

GO:0004356	glutamate-ammonia ligase activity	0.055240402
GO:0008429	phosphatidylethanolamine binding	0.055240402
GO:0009742	brassinosteroid mediated signaling	0.055240402
GO:0010167	response to nitrate	0.055240402
GO:0016165	lipoxygenase activity	0.055240402
GO:0042128	nitrate assimilation	0.055240402
GO:0010154	fruit development	0.062610858
GO:0010252	auxin homeostasis	0.062610858
GO:0031225	anchored to membrane	0.067529
GO:0048046	apoplast	0.06937214
GO:0009698	phenylpropanoid metabolism	0.06985587
GO:0009788	negative regulation of abscisic acid mediated signaling	0.06985587
GO:0010025	wax biosynthesis	0.06985587
GO:0015112	nitrate transporter activity	0.06985587
GO:0016161	beta-amylase activity	0.06985587
GO:0016740	transferase activity	0.071218532
GO:0016491	oxidoreductase activity	0.074197696
GO:0005385	zinc ion transporter activity	0.076976997
GO:0005983	starch catabolism	0.076976997
GO:0009585	red, far-red light phototransduction	0.076976997
GO:0015114	phosphate transporter activity	0.076976997
GO:0016787	hydrolase activity	0.08257815
GO:0006817	phosphate transport	0.083975782
GO:0006829	zinc ion transport	0.083975782
GO:0009051	pentose-phosphate shunt, oxidative branch	0.083975782
GO:0008889	glycerophosphodiester phosphodiesterase activity	0.090853754
GO:0009615	response to virus	0.090853754
GO:0009638	phototropism	0.090853754
GO:0016207	4-coumarate-CoA ligase activity	0.090853754
GO:0050660	FAD binding	0.090853754

GO:0009611	response to wounding	0.096212753
GO:0006730	one-carbon compound metabolism	0.09761242
GO:0008794	arsenate reductase (glutaredoxin) activity	0.09761242
GO:0016847	1-aminocyclopropane-1-carboxylate synthase activity	0.09761242
GO:0009408	response to heat	0.098146978
GO:0016020	membrane	0.102847532
GO:0005856	cytoskeleton	0.104253275
GO:0042335	cuticle biosynthesis	0.104253275
GO:0000038	very-long-chain fatty acid metabolism	0.110777795
GO:0006071	glycerol metabolism	0.110777795
GO:0007017	microtubule-based process	0.110777795
GO:0005576	extracellular region	0.111653471
GO:0005783	endoplasmic reticulum	0.115489512
GO:0004805	trehalose-phosphatase activity	0.117187441
GO:0009693	ethylene biosynthesis	0.117187441
GO:0003700	transcription factor activity	0.118560092
GO:0046872	metal ion binding	0.123111293
GO:0004089	carbonate dehydratase activity	0.123483657
GO:0015144	carbohydrate transporter activity	0.125004228
GO:0003677	DNA binding	0.125895785
GO:0005351	sugar porter activity	0.126891496
GO:0004867	serine-type endopeptidase inhibitor activity	0.135741499
GO:0006098	pentose-phosphate shunt	0.135741499
GO:0007267	cell-cell signaling	0.135741499
GO:0005992	trehalose biosynthesis	0.141705935
GO:0016998	cell wall catabolism	0.141705935
GO:0030076	light-harvesting complex	0.141705935
GO:0016021	integral to membrane	0.146165635
GO:0008194	UDP-glycosyltransferase activity	0.147192153
GO:0042626	ATPase activity, coupled to transmembrane movement of substances	0.147192153

GO:0009411	response to UV	0.147562562
GO:0006355	regulation of transcription, DNA-dependent	0.150824788
GO:0004872	receptor activity	0.153312747
GO:0005528	FK506 binding	0.153312747
GO:0009664	cell wall organization and biogenesis	0.164499182
GO:0009831	cell wall modification during multidimensional cell growth	0.16993809
GO:0016168	chlorophyll binding	0.16993809
GO:0030036	actin cytoskeleton organization and biogenesis	0.16993809
GO:0009744	response to sucrose stimulus	0.175275873
GO:0030570	pectate lyase activity	0.175275873
GO:0004693	cyclin-dependent protein kinase activity	0.18565322
GO:0008219	cell death	0.18565322
GO:0005200	structural constituent of cytoskeleton	0.190695327
GO:0009738	abscisic acid mediated signaling	0.195641394
GO:0005829	cytosol	0.210178658
GO:0009828	cell wall loosening (sensu Magnoliophyta)	0.214489783
GO:0009651	response to salt stress	0.216575063
GO:0005199	structural constituent of cell wall	0.218973922
GO:0016757	transferase activity, transferring glycosyl groups	0.221151557
GO:0006810	transport	0.222146013
GO:0005975	carbohydrate metabolism	0.222605128
GO:0006952	defense response	0.222825228
GO:0009737	response to abscisic acid stimulus	0.227188263
GO:0016759	cellulose synthase activity	0.227676876
GO:0015979	photosynthesis	0.236033707
GO:0016798	hydrolase activity, acting on glycosyl bonds	0.244053405
GO:0007568	aging	0.25174476
GO:0030246	carbohydrate binding	0.25174476
GO:0004553	hydrolase activity, hydrolyzing O-glycosyl compounds	0.256198872
GO:0009617	response to bacterium	0.259116363

GO:0046910	pectinesterase inhibitor activity	0.259116363
GO:0006457	protein folding	0.261498043
GO:0016298	lipase activity	0.262684891
GO:0009733	response to auxin stimulus	0.264890113
GO:0046686	response to cadmium ion	0.266176616
GO:0009793	embryonic development (sensu Magnoliophyta)	0.27266645
GO:0009624	response to nematode	0.276201125
GO:0003755	peptidyl-prolyl cis-trans isomerase activity	0.282518525
GO:0004194	pepsin A activity	0.282518525
GO:0015297	antiporter activity	0.282518525
GO:0004185	serine carboxypeptidase activity	0.288552517
GO:0005875	microtubule associated complex	0.299800436
GO:0016829	lyase activity	0.299800436
GO:0000074	regulation of progression through cell cycle	0.302446927
GO:0006857	oligopeptide transport	0.312397635
GO:0003777	microtubule motor activity	0.314730821
GO:0009739	response to gibberellic acid stimulus	0.323470812
GO:0009543	thylakoid lumen (sensu Viridiplantae)	0.325511701
GO:0009055	electron carrier activity	0.334891035
GO:0009826	unidimensional cell growth	0.339885953
GO:0009723	response to ethylene stimulus	0.356567403
GO:0009058	biosynthesis	0.361822218
GO:0009753	response to jasmonic acid stimulus	0.363931379
GO:0008234	cysteine-type peptidase activity	0.364561468

Table S4.3: Recovered phenotypes of *mtn1-1mtn2-1* over three generations of Spd supplementaion

Generational nomenclature is as shown in Figure S 4.6. (N = 8).

Phenotype	**Naïve / -Spd G1**	**+ Spd G1**	**+SpdG2**	**+SpdG3**	**WT**
Vegetative phase phenotypes					
Delayed first true leaf development	✓	✓	✓	✓/×	×
Interveinal chlorosis	✓	✓	✓	✓	×
Abnormal rosette leaves	✓	✓	✓	✓	×
Reproductive phase phenotypes					
Delayed bolting	✓	✓	×	×	×
Twisting	✓	✓	×	×	×
Bushy	✓	✓	×	×	×
Altered phyllotaxy	✓	✓	×	×	×
Fasciation	✓	✓	×	×	×
Altered stem vasculature	✓	✓	×	×	×
Abnormal flowers/ buds	✓	✓/×	×	×	×
Sterility	✓*	×**	×***	×***	×
Indehiscent anthers	✓	✓/×	×	×	×
Delayed senescence	✓	✓	×	×	×

***** Occasionally have around 5 seeds/ plant; develop few embryos but abort at globular stage;

** First flowers are sterile but some branches or sectors of branches develop siliques

*** First flowers develop siliques.

Table S4.4: Preliminary analysis of traits over multiple generations.

Delayed true leaf development, interveinal chlorosis, and bolting of *mtn1-1mtn2-1* over three generations. Generation nomenclature is as shown in Figure S4. 6**.**

Phenotype	**WT**	**Naïve**	**G1**		**G2**	**G3**	
		/-Spd G1	**+ Spd G1**	**+SpdG1, -Spd G2**	**+SpdG2**	**+SpdG1, G2, -Spd G3**	**+SpdG3**
First true leaf development (14DAG) N=32<	Bigger first true leaves.	1/10 of the segregating population showed delayed leaves (instead of 1/4).	1/8 of the segregating population showed delayed leaves.	Uniform phenotype. Small first true leaves.	Uniform phenotype. Comparatively bigger first true leaves than -Spd G1.	Segregating phenotype: (small 1, WT; 37 uniform looking) Uniform looking seedlings have bigger first true leaves than- Spd G1 but smaller than + Spd G1.	Segregating phenotype (1 14 small;16 WT) WT seedlings have bigger first true leaves that are the same as those of the WT.
Inerveinal chlorosis (14 DAG) N=32<	No interveinal chlorosis.	10 % of the segregating population shows interveinal chlorosis.	12 % of the segregating population shows interveinal chlorosis .	Uniform interveinal chlorosis in all plants.	Uniform interveinal chlorosis in all plants.	Segregating with 34 % of the poplulation showing interveinal chlorosis .	Segregating with 37 % of the population showing interveinal chlorosis .

Bolting (5 weeks AG) N=32	Bolted.	No bolting.	6 % of the population has bolted.	9 % of the population has bolted.	37 % of the population has bolted.	69 % of the population has bolted.	69 % of the population has bolted.
Appearance of rosettes and buds (5 weeks AG) N = 32	~ 8 leaves, rosettes with delicate leaves and closed buds.	Typical *mtn1-1mtn2-1* leaves	Typical *mtn1-1mtn2-1* rosettes and buds.	Typical *mtn1-1mtn2-1* rosettes with mixed open and closed buds.	Typical *mtn1-1mtn2-1* rosettes with mixed open and closed buds.	Majority of WT phenotype with mostly WT rosettes and closed buds.	All WT phenotype with WT rosettes and closed buds.

Chapter 5: Significant contributions and future directions

The complex nature of traits associated with the *mtn1-1mtn2-1* phenotype made determining the function of MTN extremely complicated. However, the research work presented in this thesis has provided directions to unravel the key targets and fundamental traits of MTN deficiency. My significant contributions to this project are as follows:

1. The identification of interveinal chlorosis in this *mtn1-1mtn2-1* was the first significant contribution, which led to the realization that this pleiotropic phenotype is due to disturbed MTA metabolism rather than solely to disrupted PA homeostasis, as was concluded by our German collaborators at that time.

2. Since *mtn1-1mtn2-1* is sterile, the homozygous mutants needed to be recovered from the segregation populations of *MTN1mtn1-1/mtn2-1mtn2-1,* or *mtn1-1mtn1-1/MTN2mtn2-1.* As a result, the type and number of experiments that could be conducted using this mutant were limited. I discovered a very simple and early development marker of *mtn1-1mtn2-1:* delayed development of the first true leaves. The use of this marker greatly facilitated the choice of the types of experiments in which these mutants could be used.

3. Meticulous analysis of the traits of the mutant allowed the delineation of the important traits that could be traced back to an individual pathway affected by inefficient MTA metabolism. Examples of these connections are interveinal chlorosis with NA-deficiency and xylem proliferation defects with Tspm deficiency.

4. The observations of the increased number of leaves, the bushy architecture, the altered phyllotaxy, the fasciation, and the altered vasculature led to the speculation that this mutant has auxin imbalances. Auxin transport assays showed that the *mtn1-1mtn2-1*

has a reduced ability to transport auxin. This conclusion was further supported by experiments conducted with an auxin sensitive reporter, DR5*rev*:: GFP, and by the hormone profiles of the organs.

5. Analysis of the series of *MTN*-deficient mutants developed in collaboration with other Moffatt lab members revealed that delayed bolting is a trait that is fundamental to MTN deficiency. In these mutants, a tight correlation was noted between the time of the bolting and the number of leaves at bolting. This increase in the number of leaves and the corresponding increase in the number of vascular bundles suggest changes in the auxin maxima as the most likely fundamental defect associated with disturbed MTA metabolism.

6. Most importantly, I discovered a means of making the sterile *mtn1-1mtn2-1* plants fertile, using a method in which exogenous Spd was applied daily. The seedlings that were grown for only 14 days on media supplemented with Spd could recover partial fertility three to four weeks after bolting. This finding has opened a whole new area of investigation of the possible links between Spd, eIF5A, and the endomembrane system.

7. During the period that I conducted research in Japan, it was discovered that the *mtn1-1mtn2-1* seeds generated by the exogenous Spd supply were able to generate phenotypically WT progeny that were genotypically *mtn1-1mtn2-1*. My supervisor, Prof. Barb Moffatt discovered the same effects independently at the same time, when she was on sabbatical in Germany.

Together with all the evidence gathered during the research for this thesis and the findings reported in the related literature, these significant findings support a holistic view of MTN functions in plant growth and development which is presented as a model in Figure 5.1

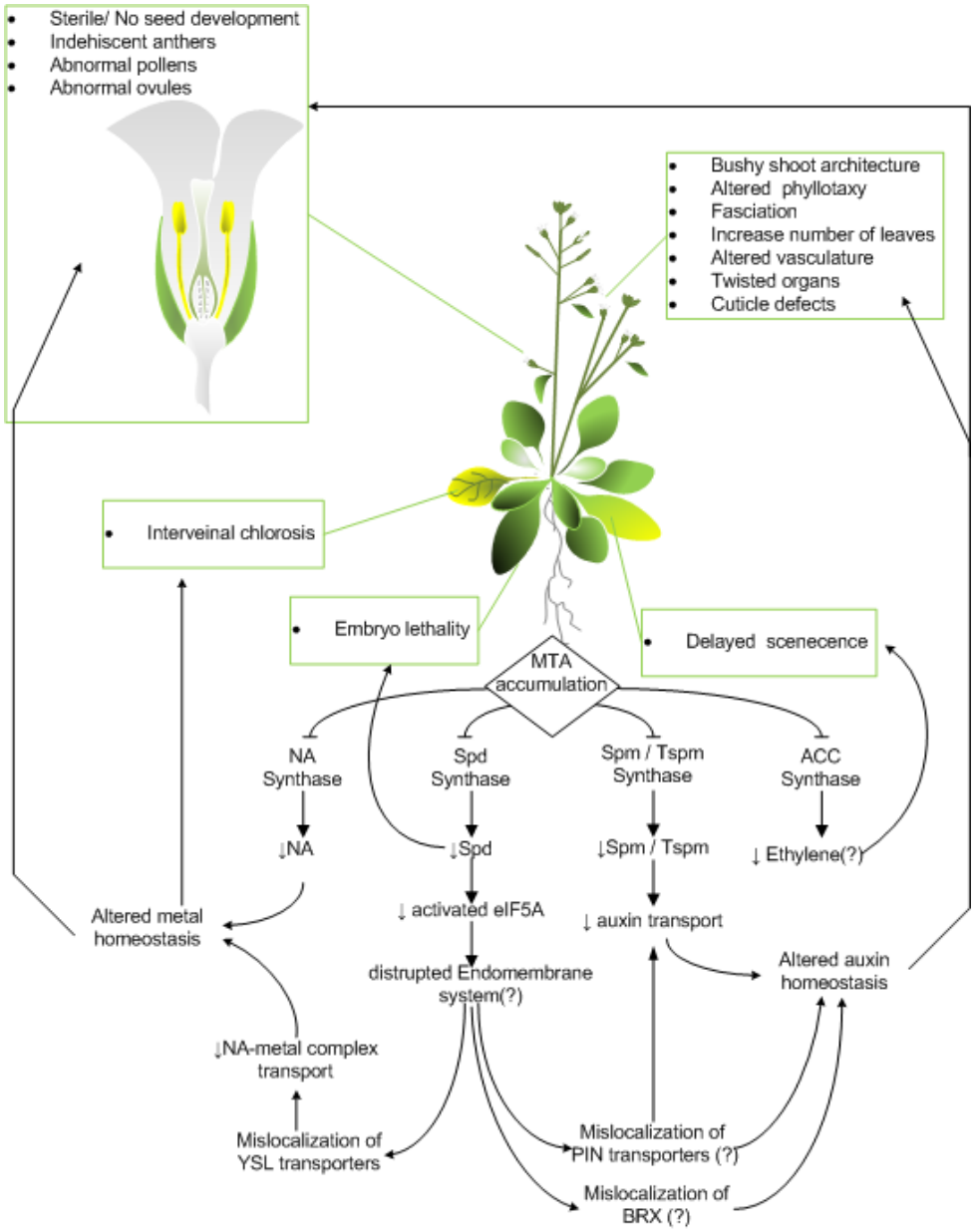

Figure 5.1: A model that explains the holistic view of MTN functions in plant growth and development

The *mtn1-1mtn2-1* double mutant with knocked down MTN1 and MTN2 resulted in a 14 % level of residual MTN activity and a two to five fold increase in the MTA content in the mutants. The accumulated MTA likely inhibits NA synthase, Spd synthase, Spm synthase, Tspm synthase, and ACC synthase activities. The result is a reduction in the levels of all the products of these enzymatic reactions, such as NA, Spd, Spm, Tspm, and ethylene. Reduced NA limits metal transport, which leads to interveinal chlorosis and low seed production. Reduced Tspm causes premature xylem differentiation. Finally, but most importantly, reduced Spd causes embryo lethality and reduced hypusination of eIF5A. Interestingly, *mtn1-1mtn2-1* mutants share sterility and delayed scenecence in common with suppression of DHS activity (the first step of hypusinating eIF5A; Wang et al., 2003, 2005) and increased xylogenesis with overexpression of eIF5A1 (Liu et al., 2008). Both these phenotypes are possibly due to accumulation of unhypusinated eIF5A as suggested by (Liu et al., 2008). Here I propose eIF5A as the possible link to auxin distribution via the disruption of the PIN proteins and the components of the endomembrane system. Current feedback models for polarized auxin transport have already incorporated the localization of PIN proteins at the plasma membranes to Tsvi Sachs theoretical canalization hypothesis (auxin flux directs the auxin transport (Wabnik et al., 2011). Thus a positive feedback between the auxin flux and PIN localization determines the rate and direction of the polar auxin transport. Thus in the *mtn1-1mtn2-1* mutant altered auxin gradients resulting from reduced PAT, either due to mislocalization of the PINs or due to altered vascular development, led to phenotypes such as short and bushy shoot architecture, altered phyllotaxy and fasciation, increased number of leaves, cuticle defects, and twisting. Reduction in ethylene may be the basis of the delayed senescence. Although the majority of this model is supported by the evidence presented in this thesis, further validation is necessary.

A comprehensive analysis of vascular development is necessary to narrow down the vascular defects caused either by (1) altered auxin distribution together with brassinosteroids, (2) H_2O_2

produced during PA catabolism, or (3) Tspm deficiency. The first step is to determine the most initial time point and development stage that is affected by MTN deficiency. This could be achieved by the study of a time course, including embryo sac formation, embryogenesis, and seed germination, until the seedlings are 14 days old. Utilizing vascular markers (ATHB8::YFP) will enable the detection of the vascular formation while the auxin responsive marker (DR5*rev*::GFP) will provide a visual representation of auxin distribution.

After the time and development stage of the first deformed vascular defect in *mtn1-1mtn2-1* have been established, it is necessary to determine the involvement of Tspm and H_2O_2 in these stages. To explore the involvement of H_2O_2 in xylem differentiation, H_2O_2 production could be visualized using the cell-permeable H_2O_2-specific dye dichlorofluorescein diacetate (DCFA-DA) or DAB. A parallel study could also be carried out using the Tspm-sensitive SAC51::GUS lines and Tspm-deficient *tkv* mutant along with the determination of the Tspm sensitive gene expression (*ACL5, ATHB8, PHB and SAC51*) levels. Once the potential cause is confirmed, it is necessary to determine which aspect of xylem differentiation is affected in these mutants and whether these aspects could be reversed through feeding with exogenous Spd.

To study the proposed involvement of eIF5A, that could link Spd to the endomembrane system, it is first necessary to determine whether the *mtn1-1mtn2-1* seedlings grown for 14 days on Spd have recovered WT levels of activated eIF5A. A parallel analysis of a mutant, with a mutation in the gene enording for deoxyhypusine synthase (*dhs*), which is incapable of activating the inactive eIF5A could also be beneficial, if such a mutant is available. Comparing this mutant phenotype to that of *mtn1-1mtn2-1* and studying whether the endomembrane system has been affected in these mutants, either directly using PIN-mEosFP (Dhonukshe et al., 2007) or indirectly using a lipid-binding, endocytic tracer (FM4-64; Vida and Emr, 1995), is vital in order to determine whether this link is a possibility. If the possibility is confirmed, then a yeast-two-

hybrid study can be conducted using eIF5A as bait in order to recover the potential candidates. If the model proposed in this thesis is accurate, it is expected that the PIN proteins and BR1 receptors would be among the potential candidates that interact with eIF5A. It would then be necessary to visualize the localization of the PIN proteins tagged with GFP and possibly the membrane localization of other proteins (BR1, brassinosteroid transporter or YSL1, Yellow strip-like NA transporter) in order to show whether the endomembrane system is affected in a PIN protein-specific or in a general manner.

The *MTN*-deficient mutant with the disrupted MTA metabolism, coupled with the current and proposed work described in this thesis has the potential to reveal the molecular basis of PA, NA, and auxin in the vascular development and transport of nutrients and signal molecules. This fundamental work has the potential to be applied in the engineering of crop plants so as to enhance the efficiency of nutrient use and increase yield. As a result, these findings will ultimately lead to decreased fertilizer use in crop cultivation, which will reduce costs and prevent environmental damage.

Appendix 1

A. MTN activity

Plant #, replicate #	WT	*mtn1-1mtn2-1*
1, 1	1.081	0.146
1, 2	0.769	0.136
1, 3	0.721	0.185
2, 1	1.198	0.185
2, 2	1.208	0.195
2, 3	1.052	0.107
3, 1	1.188	0.205
3, 2	1.276	0.205
3, 3	1.403	0.136
Mean	**1.1**	**0.167**
SD	**0.226**	**0.036**

B. MTA Content

Plant #	Leaves		Inflorescences	
	WT	***mtn1-1mtn2-1***	**WT**	***mtn1-1mtn2-2***
1	1.17	2.01	4.61	22.52
2	0.43	2.09	4.06	25.89
3	0.86	1.61	5.15	18.02
4	0.74	1.06	4.07	30.14
5	0.7	1.67	5.02	22.53
Mean	**0.8**	**1.7**	**4.6**	**23.8**
SD	**0.3**	**0.4**	**0.5**	**4.5**

C. NA Content

Plant #	Leaves		Inflorescences	
	WT	***mtn1-1mtn2-1***	**WT**	***mtn1-1mtn2-1***
1	32.86	0	273.87	78.15
2	89.35	0	211.26	107.04
3	105.05	0	318.3	91.44
4	157.53	0		
5	145.03	0		
	105.96	**0**	**267.81**	**92.21**
	49.51	**0**	**53.77**	**53.54**

D. Polyamine content

Polyamine	Plant #	Leaves		Inflorescences	
		WT	***mtn1-1mtn2-1***	**WT**	***mtn1-1mtn2-2***
PUT	1	21.06	71.55	70.64	96.50
	2	23.33	25.38	46.67	71.56
	3	5.77	11.17	26.36	57.48
	4	3.22	4.20	21.60	41.19
	Mean	**13.35**	**28.07**	**41.32**	**66.68**
	SD	**10.31**	**30.30**	**22.37**	**23.44**
SPD	1	336.42	188.74	431.23	140.96
	2	334.58	72.62	383.57	177.76
	3	53.45	25.53	183.54	123.83
	4	58.65	30.34	162.10	123.38
	Mean	**195.78**	**79.31**	**290.11**	**141.48**
	SD	**161.36**	**75.96**	**137.10**	**25.53**
SPM	1	22.03	13.45	65.67	33.50
	2	28.13	10.93	66.35	28.18
	3	21.35	20.27	33.82	31.79
	4		19.00	47.21	41.78
	Mean	**23.84**	**15.91**	**53.26**	**33.81**
	SD	**3.73**	**4.45**	**15.70**	**5.76**

E. Metal Content

	WT				*mtn1-1mtn2-1*			
Plant #	**Cu**	**Fe**	**Mn**	**Zn**	**Cu**	**Fe**	**Mn**	**Zn**
Leaves								
1	0.45	1.80	1.06	1.60	11.56	94.56	89.79	71.23
2	13.03	94.58	43.43	91.58	9.88	56.30	44.72	60.97
3	13.72	421.65	42.00	98.41	9.28	294.15	57.28	49.87
4	12.06	109.28	39.38	83.00	8.34	53.55	65.19	40.79
5	13.99	192.05	42.93	88.16	8.50	58.54	67.75	47.80
mean	**13.45**	**182.14**	**43.10**	**92.08**	**9.51**	**111.42**	**64.94**	**54.13**
SE	**0.42**	**62.59**	**1.36**	**3.08**	**0.58**	**46.29**	**7.39**	**5.36**
Inflorescences								
1	14.74	83.19	54.35	127.70	7.38	30.86	29.05	34.65
2	8.85	44.74	25.63	74.02	4.95	21.99	23.64	28.99
3	8.97	56.82	28.55	93.08	5.18	21.85	24.89	31.72
4	10.37	48.20	27.91	91.39	6.25	25.37	25.59	38.45
5	10.77	67.04	49.47	101.63	6.47	21.29	28.56	35.06
mean	**10.74**	**60.00**	**37.18**	**97.56**	**14.44**	**93.16**	**47.77**	**99.26**
SE	**1.07**	**6.96**	**6.08**	**8.77**	**6.05**	**24.27**	**26.35**	**33.77**

F. Vector Maps

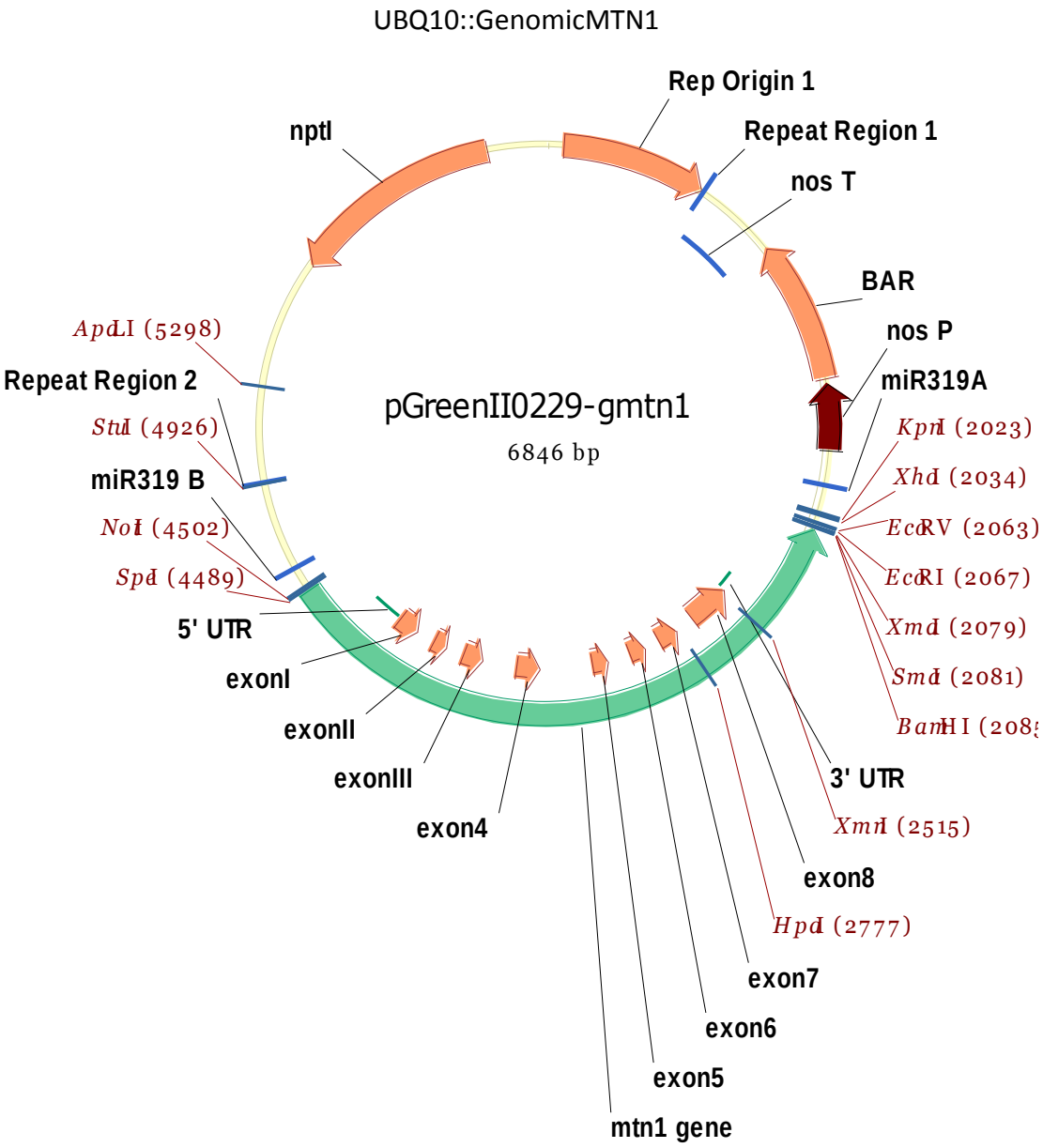

UBQ10::MTN1CDS

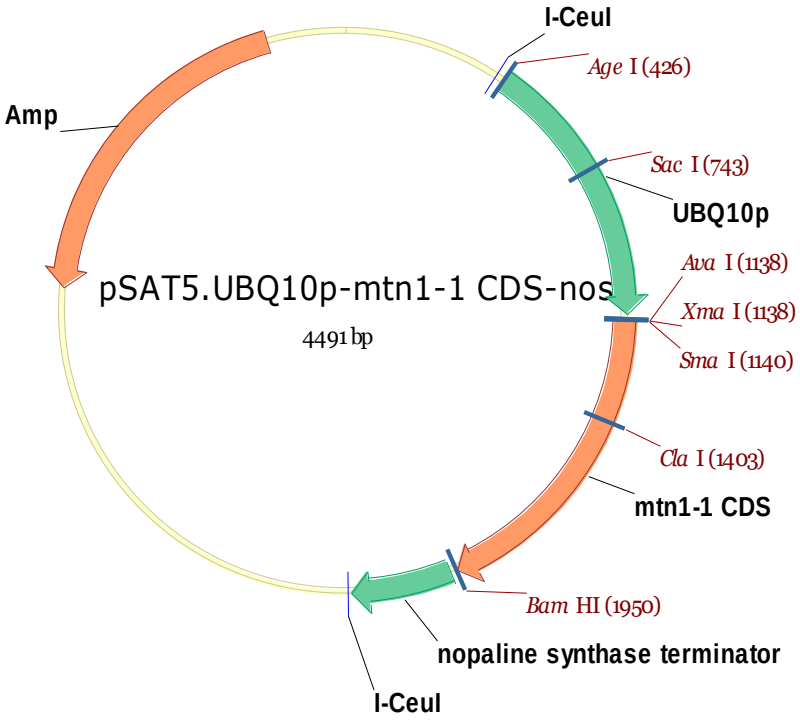

UBQ10::hMTAP

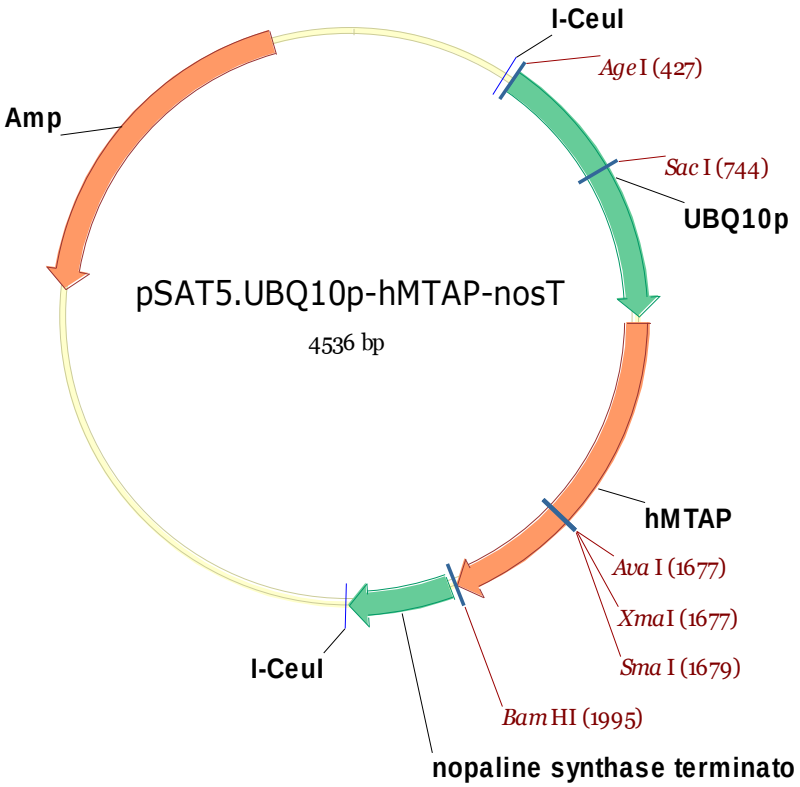
I-CeuI
AgeI (427)
SacI (744)
UBQ10p
Amp
pSAT5.UBQ10p-hMTAP-nosT
4536 bp
hMTAP
AvaI (1677)
XmaI (1677)
SmaI (1679)
I-CeuI
BamHI (1995)
nopaline synthase terminato

pSAT5.UBQ10p-nosT

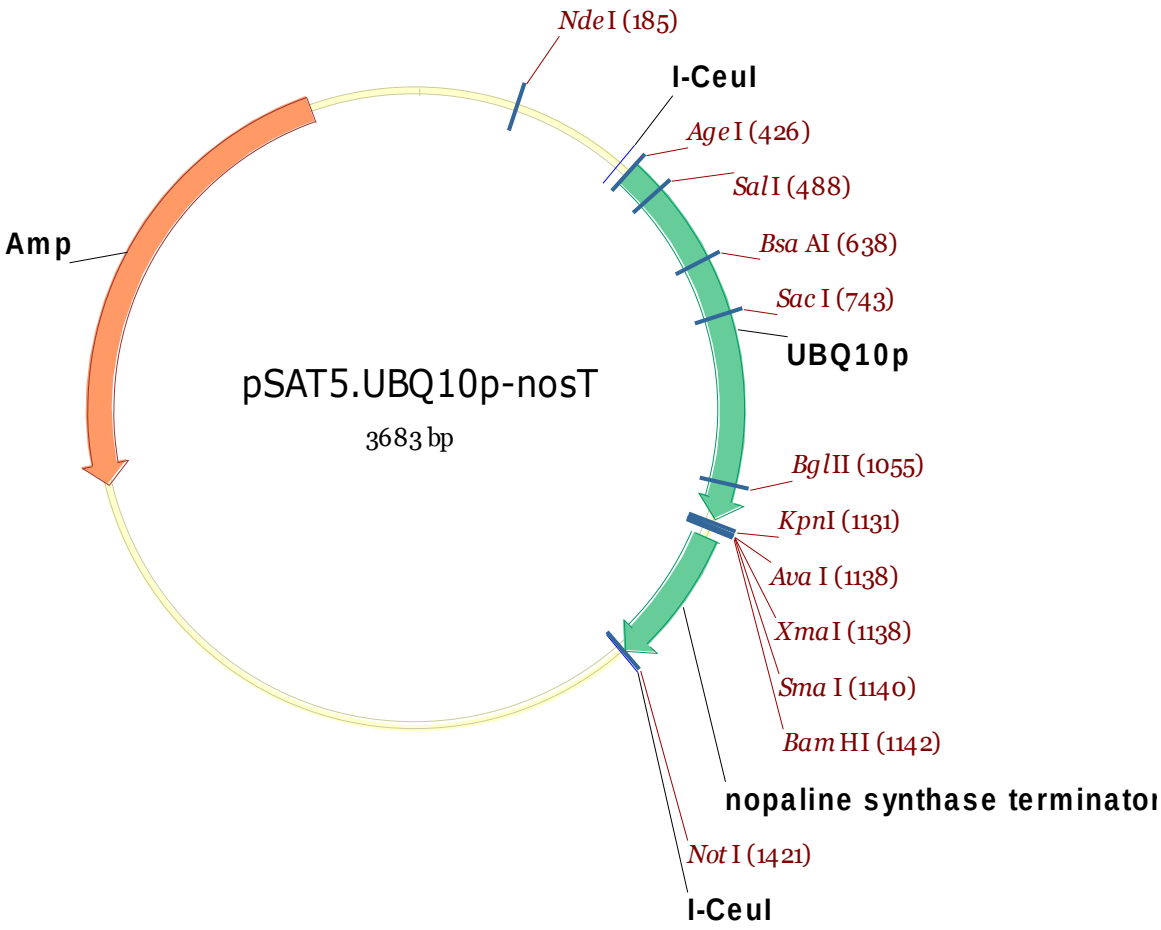

pSAT5.nosP.RNAi.nosT

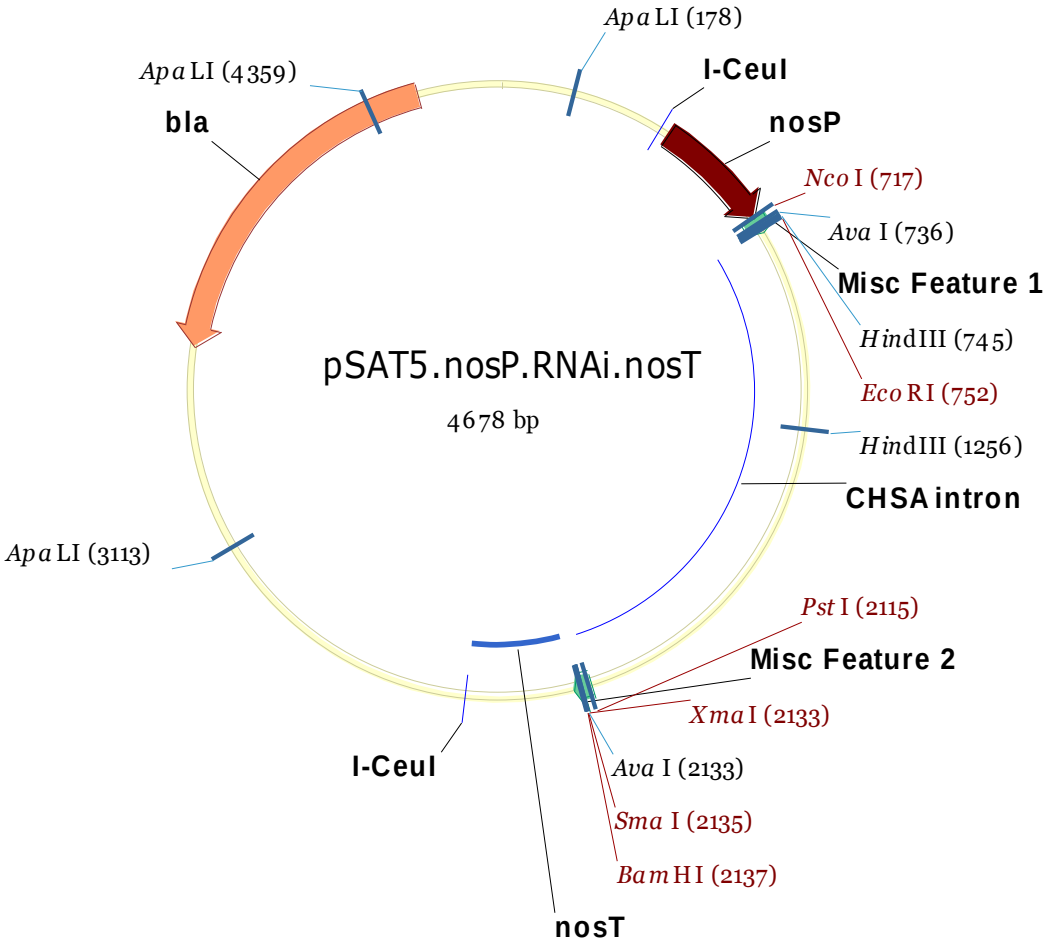

pPZP-RCS2-BAR (904)

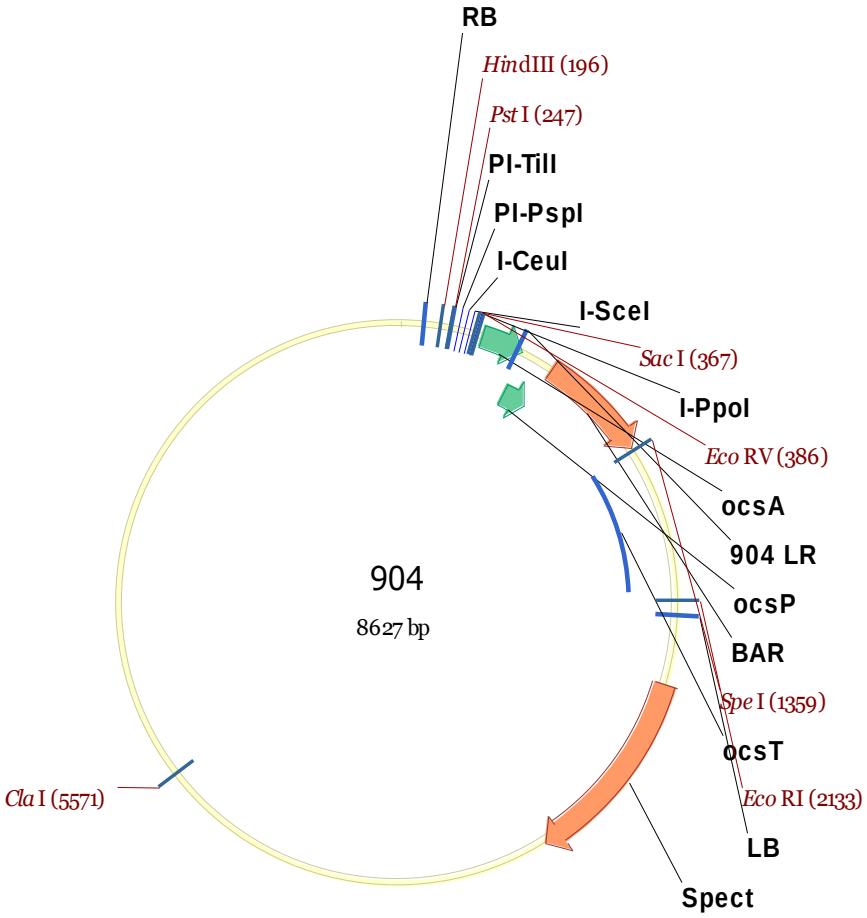

PGreen11 0229

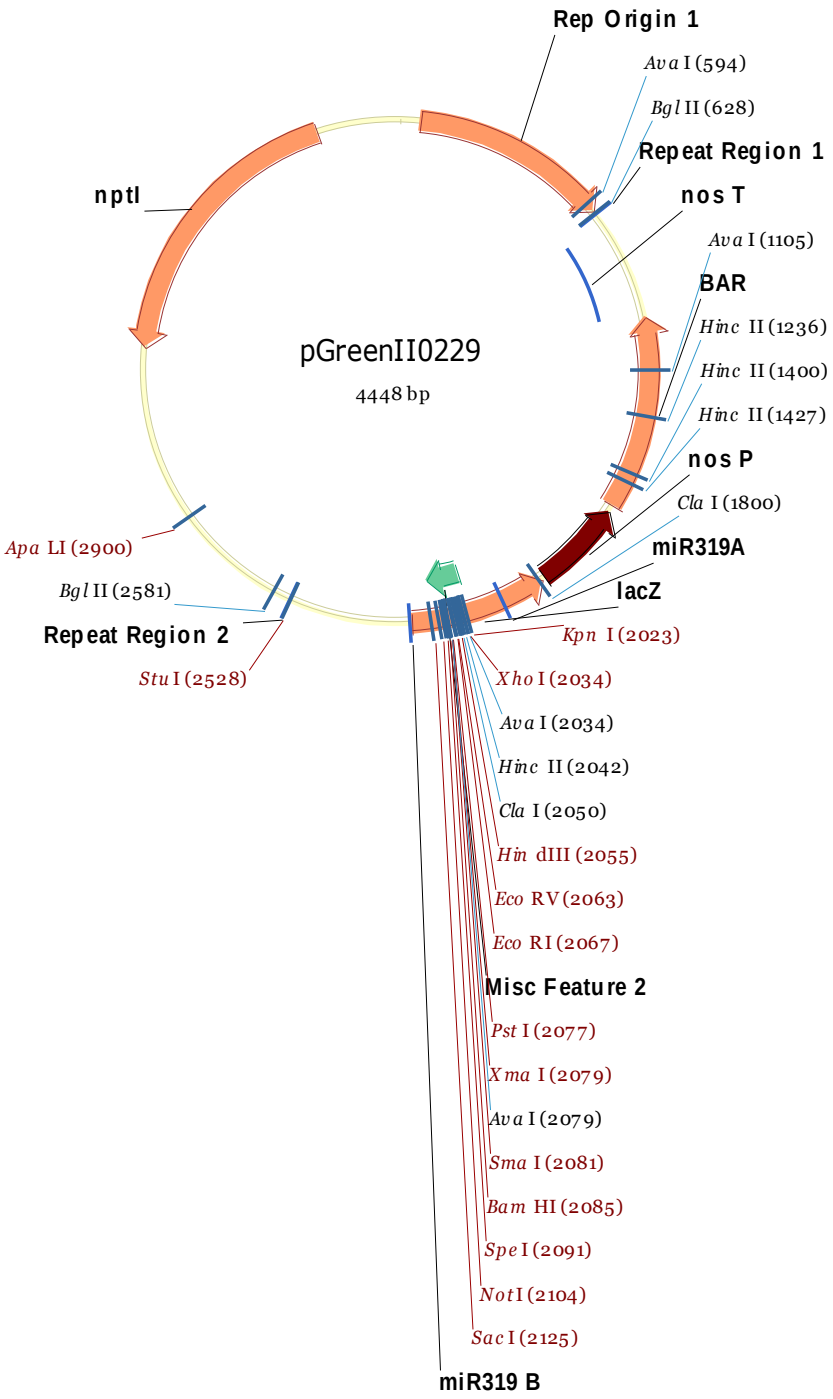

Appendix 2

A. MTN genes

Vector NTI diagrams of gene models

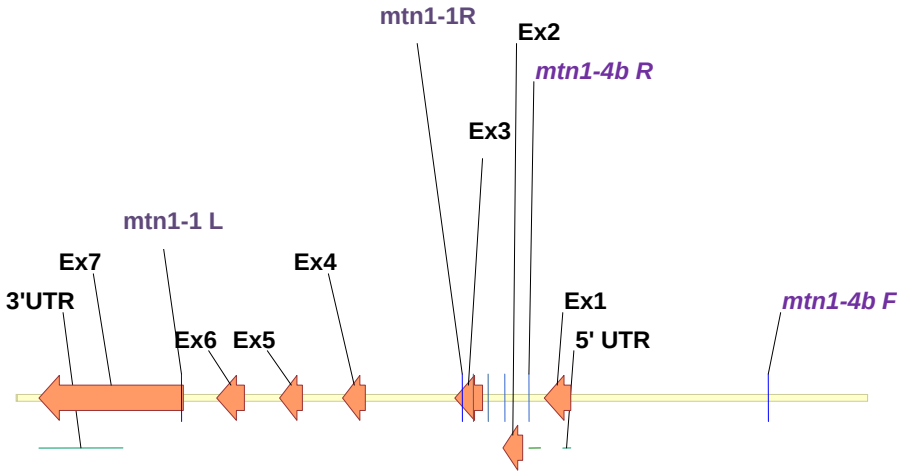

At4g38800 (MTN1)
2800 bp

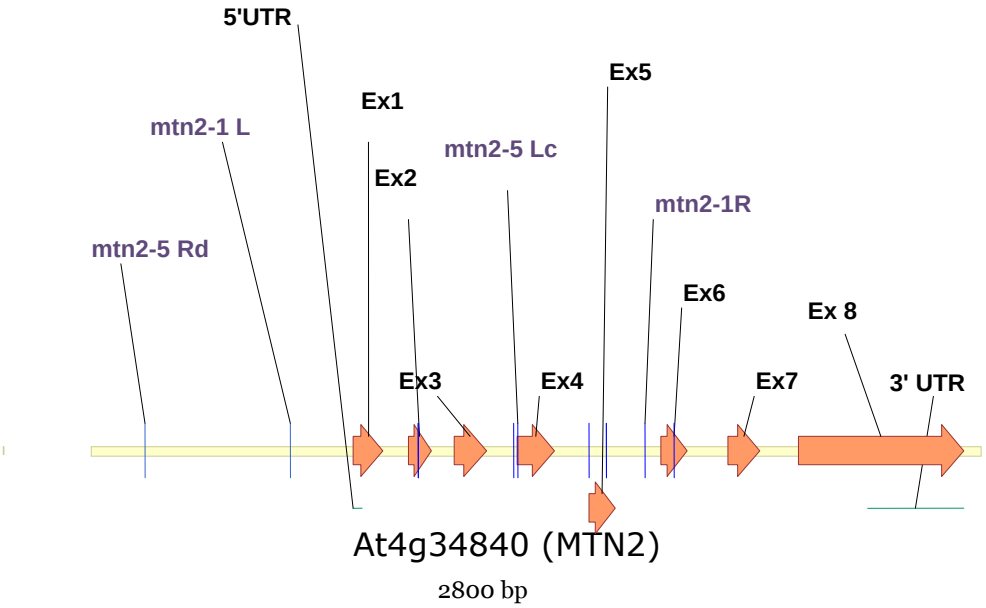

MTN1-Gene sequence and location of T-DNA inserts

```
ATG = Translational Start/Stop

atgc = UTR
ATGC = Exon
atgc = Intron
atgc = Annotation on other strand

atgctcgttg
|--====--> = T-DNA/Tn
| is end nearest insertion point
 === = sequence match
 --- = no sequence match
```

Sequence of AtMTN1 (Complement stand)

Aaaagaggaccaaaaggtccaaaaacgaataaactgtatctctcattcgccggagtttccagccgtttctt
tccgattctcggatttttcctgggaatcaaacgcatcgccgagaatcggaagagagggataaggtt
|==========SALK_088214==========
ATGGCTCCTCATGGAGATGGATTAAGTGACATCGAAGAACCTGAGGTCGATGCTCAATCGGAGATTCTTCG
ACCGATCTCCTCAGTCGTCTTCGTCATCG
gtactttatgatttatgaagtttccgattcgatcgatttcttcttcgtcttcttacttacttttgtgtgt
ttctgacggagctgcag
CTATGCAAGCGGAGGCTCTTCCTTTGGTCAACAAGTTCGGACTCTCTGAAACTACTGATTCGCCG
ttaagagctctccttttttcgattttgcttgtttggatttgatctccatgaatctctcacttcaaagttta
ctttttgcag
GCTTGGTAAAGGATTGCCCTGGGTTCTGTATCACGGCGTGCATAAAGATCTTCGAATCAATGTAGTTTGCC
CCGGAAGAGATGCAGCTTTAG
gtaagctttgcactcaatgctctcaaagatatgataattagcctgtgaatctctcagcattttagtata
gtagctttggtttctcaagtcgctgcattgtttggtatgagggaaaatgaatgcacttttttatgctact
===SALK_085385.47.75.X====|
aactgagatttctctccag
GGATCGATAGTGTTGGAACTGTTCCAGCTTCTCTCATAACTTTTGCTTCCATCCAAGCATTAAAACCTGAC
ATCATAATCAATGCCGGAACCTGCGGTGGCTTCAAG
gtacagttcttttacttctcgtgtgctctgtcttgacttccagcatccttgctaagaaccacgtcctctct
tctttctttacttgtggtttgggtttgattttgttactgctcgtttactcaactctgagatttgagttgca
tcataaaagatctctctctctctccatatctctatttttatgttgtgaaagttggtttattttcatgtaat
gaaagtgctgattggctgaacatttgcag
GTCAAAGGAGCCAACATAGGCGATGTATTCCTTGTATCTGATGTTGTGTTTCATGATAGAAGAATACCAAT
TCCGG
taggttcatcttcctttctttctttttccatctttagtgatgattccctttttgccagttcatcttgcaa
gttcctgagcaatgtttgtttatctctctag
ATGTTTGATCTGTATGGAGTTGGTCTCCGTCAGGCATTCTCGACACCCAATCTCCTCAAGGAACTCAATTT
GAAGG
tatttaatagactcaagatgctacttactcttttaactatttcaattttgacaaaattggggtggttcag
ATTGGCAGGTTATCTACTGGTGACTCGTTGGATATGTCCACGCAAGATGAAACATTGATCATTGCCAATGA
TGCTACGCTAAAGGACATGGAG
gtagtgtaatgttaacaattcttattactgaatctaaccagaaaatcaatgaaactgttgttttgaaactc
ttttggctctggattcttcag
GGTGCTGCCGTGGCGTATGTGGCTGATCTTCTGAAAATACCAGTCGTGTTCCTCAAAGCCGTGACCGATCT
AGTGGACGGAGATAAACCTACAGCAGAAGAGTTCTTGCAGAACTTGACAGTTGTGACCGCTGCATTAGAGG
GAACTGCTACTAAAGTGATCAACTTCATCAATGGGAGAAACCTTTCGGACCTT
TAActtctgttctcttccttttttatggagagtgatttttttaaaatgcgttcaacgtgcttgttgcagttt
cactgatttccagtgatcatatttctcgttaataaatttcaagttataagacgttctctccctagtgttgc
ttaaattttggtaaagaaacaatttcaaagataacttatcgacctgaaagacgttaaatcccttgataggc
aaaatatacaacactgtaaaattaattcgtaaccgagacacttggtgaaacctcaagacacataaacgatg
aaatcagaggtaaagaaaaattgagctatctttcccaattagaatttccgtcaagctcatcgcaggacatc
gttggggtatttctatcttttgaac

mtn1-1 (SALK_ 085385) sequence with LBb1.3

NNNNNNNNNNNCNNGGNNNNNNNGCGTGGNNCGCTTGCTGNNNTCTCTCAGGGCCAGGCGGTGAANNNNNNNNAGCTGTTGCCCGTCTCACTGGTGA
AAAGAAAAACCACCCCANTACATTAAAAACGTCCGCAATGTGTTATTAAGTTGCTAAGCGTCAATTTGTCCGCAGCGACTTGAGAAACCAAAG
CTACTATACTAAAATGCTGAGAGATTCACAGGCTAATTATCATATCTTTGAGAGCATTGAGTGCAAAGCTTACCTAAAGCTGCATCTCTTCCG
GGGCAAACTACATTGATTCGAAGATCTTTATGCACGCCGTGATACAGAACCCAGGGCAATCCTTTACCAAGCCTGCAAAAAAGTAAACTTTGA
AGTGAGAGATTCATGGAGATCAAATCCAAACAAGCAAAATCGAAAAAAGG

mtn1-4 (SALK_088214)sequence with LBb1.3

CMGGCATTTCGCTGCTGGGGCAACCAGCGTGGACCGCTTGCTGCAACTCTCTCAGGGCCAGGCGGTGAAGGGCAATCAGCTGTTGCCCGTCTCACTG
GTGAAAAGAAAAACCACCCCAGTACATTAAAAACGTCCGCAATGTGTTATTAAGTTGTCTAAGCGTCAATTTGTTTACACCACAATATGTGTT
ATTAAAAACGCATCGCCGAGAATCGGAAGAGAGGGATAARGTTAA

MTN2 sequence and location of T-DNA inserts

Sequence of AtMTN2
aaagcttcagagaaggaagtgaggatatgaaataacgaacgactctcttcttcgcattgtggacccccttgc
ttacgtggcataaacggccgtcaagtcgtcaacgttgtttatattaaaaaaaacatattttattaattatg
==========| SALK_022510.34.05.X
ctaaaattttattgggcctgggtccgagtagtggataggattcgggtcggatccgggtttttgttttccgg
gggaaatctagaaatttgatcttgacgaatcgc
cggcgacggattctcagacgctgct
ATGGAAGGTGTTATGGGTCAGGTAGAGAAACGGCCGATTTCTACCATCGTCTTCATCGTTGG
tactattttgtctttactatttctcgaattgtgatttttttttcttcttctaatgggtttgtgtattaaag
CTATGCAAAAGGAAGCTCAGCCTCTGATCAACAGATTACGCCTCGTTGAAGAAGTTAATACTCCG
tgagttctttgacctctttcaatttttttattttgattcgaaatcaaatgtgatagctttttttgtag
GTTTCCAAAAGAGGTGACTTGGATTATGTTTAAGGGAATGTATAAAGACTTGAACATCAATATAGTGTGTC
CTGGAAAAGATTCAACTCTTGG
tatgtgtatccatgtggttaagtgattgtaagtgaaatagtgtttcaagatgttttgtgaagttcttgatg
ttaattcgtttttcag
GGGTTGAGAGTGTTGGCACAGTTCCTGCATCACTCGTGACTTATGCTTCCATTCTAGCAATTCAACCAGAC
|=========SALK_071127========
TTAATCATTAATGCGGGAACCGCTGGTGGCTTTAAGG
tatcaacattacaaatttctctacatagttctcgtttcatgcctcttatgtgtcagaaataatgaacaccc
ttccttgtttttaaatggtcttttcag
GCCAAAGGAGCATGTATTAGCGATGTTTATGTTGTCTCTACTGTTGCTTTCCATGACAGAAGAATACCTGT
TCCTG
taagtgctcctttgtattgttcatgtatcagtatgagttgcaaagtaaacctgatgttcttgagtgttata
cttgcattctaattccatatatttttgccctttcctaaacatttttatactttctgcag
GTCCTTGATATATATGGTGTTGGTATGCGGAACACCTTCCCCACACCCAACCTTATAAAGGAGCTGAACCT
AAAG
gtgtatactttattagttgctctgagttcaccatttgatcctcatgcaagattttggttatttcttgatat
ggtttgcataagtggtagatttatgatttagttgcaatgttcccag
GTGGGAAGATTATCCACTGGCGATTCTATGGATATGTCTCCACATGACGAAGAATCCATCACAGCAAATGA
TGCTACAGTTAAAGATATGGAGG
tcaacaatccataagtttcctgtgttgatgtacctggctccatactatgtgtttgtctttgtgtctttatc
agttactacgacttatttacggattcttggcatttcag
GGAGCAGCAGTGGCCTATGTGGCTGATATCTTTAAAGTGCCTACGATTCTAATAAAAGGTGTGACTGATAT
TGTGGATGGCAATAGACCAACTTCTGAAGAATTTTTGGAGAACTTAGCTGCAGTCACTGCCAAACTTGATG
AGTCACTTACCAAAGTGATTGACTTCATCAGTGGGAAATGTCTCTCAGACCTCTAA
caagtcatacgtattaagtttcatctgttcagtatgtgcattgggcgaagaaagcatatgaagattcaagc
aaagggcgtaggtagggaataggtttgagcagaaatttcaactcttcacctttctcatttgttcctctat
ttctttttgctgtctttctattgatgatccatcatacatgtagaaactcagcaaatttgatacccaacaac
agagtcataattctttaatatcaatttcgaatgattgatgttaacagaagaaaaaatttagtt

mtn2-1 sequence with LBb1.3

NNNNNNNNNNNNNNCNGNNNCAANCAGCGTGGNCCGCTTGCTGCACTCTCTCAGGGCCAGGCGGNNANNNNNNNNNNNNNNTGCCCGTCTCACTGGTGAA
AAGAAAAACCNCNNNNNNNANATTAAAAACGTCCGCAATGTGTTATTAAGTTGTCTAAGCGTCAATTTGTCCGCAATATATCTTATGCTTCCATTCTAGCAA
TTCAACCAGACTTAATCATTAATGCGGGAACCGCTGGTGGCTTTAAGGTATCAACATTACAAATTTCTCTACATAGTTCTCGTTTCATGCCTCTTATGTGTCA
GAAATAATGAACACCCTTCCTTGTTTTTAAATGGTCTTTTCAGGCCAAAGGAGCATGTATTAGCGATGTTTATGTTGTCTCTACTGTTGCTTTCCATGACAG

AAGAATACCTGTTCCTGTAAGTGCTCCTTTGTATTGTTCATGTATCAGTATGAGTTGCAAAGTAAACCTGATGTTCTTGAGTGTTATACTTGCATTCTAATTC
CATATATTTTGCCCCTTTCCN

mtn2-5 sequence with LBb1.3

ATGATCGCTGCTGGGGCAACCAGCGTGGACCGCTTGCTGCAACTCTCTCAGGGCCAGGCGGTGAAGGGCAATCAGCTGTTGCCCGTCTCACTGGTGAAAAGAA
AAACCACCCCAGTACATTAAAAACGTCCGCAATGTGTTATTAAGTTGTCTAAGCGTCAATTTGTTTATGCCACGTAAGCAAGGGGTCCACAATGCGAAGAA
GAGAGTCGTTCGTTATTTCATATCCTCACTTCCTTCTCTGAAGCTTTATCCTCTAATCGTTTTCTCTCTAAGCCTCTCCAATGGAGGTTACCTCCACCACCTTC
ATCTCCACTACCAGATCTTCTAAATACCTTACCTTAACTTCGTACTCTCCGGTGATTCTTCCGGCTTCTACTCTCCGCCGTGATTTTCTTGGTTGTTGTCATAG
TCTCCGTCCTTCTCCTCATCTTCGAACTCGCGCCGGGAAACGCAATTCTCGTCGTTCTTCAATTCGATCGCCTCGTTTAGTTGTTAGAGCTTCTATCGATTCT
GGTTTGATTCTTATTGTTGTTGCTGTCACTGCGTTCTCTGCCATTGCTTTCGCTTATTGCCAAAGTACTTTCAGGAASGG

B. Number of rosette leaves

DAG	Plant #								Mean
WT	**1**	**2**	**3**	**4**	**5**	**6**	**7**	**8**	
21	10	12	11	10	11	12	10	11	**11**
35	18	25	25	14	18	16	20	20	**20**
42	20	26	28	16	19	17	22	25	**22**
mtn1-4mtn2-1	**1**	**2**	**3**	**4**	**5**	**6**	**7**	**8**	
21	12	10	9	10	12	10	12	11	
28	16	13	12	13	16	13	16	15	**14**
35	19	23	18	20	25	21	19	28	**22**
42	25	25	24	26	29	28	26	32	**27**
mtn1-1mtn2-5	**1**	**2**	**3**	**4**	**5**	**6**	**7**	**8**	
21	12	11	10	10	14	12	11	10	**11**
28	16	15	13	13	19	16	15	13	**15**
35	27	20	20	22	26	20	19	22	**22**
42	28	22	24	24	28	23	23	24	**25**
mtn1-1mtn2-1	**1**	**2**	**3**	**4**	**5**				
21	8	8	8	8	9				**8**
35	12	15	10	11	10				**12**
42	19	18	12	18	16				**17**
49	22	20	20	21	19				**20**
59	26	24	24	25	22				**24**
ami 5.3	**1**	**2**	**3**	**4**	**5**	**6**			
21	9	9	10	8	10	10			**9**
35	14	16	13	10	10	11			**12**
42	22	24	27	14	18	21			**21**
49	24	26	28	22	21	23			**24**
59	29	31	34	26	25	28			**29**
ami2.8	**1**	**2**	**3**	**4**	**5**	**6**	**7**	**8**	
21	11	12	10	9	12	10	9	8	**10**
28	15	16	13	12	16	13	12	11	**14**
35	20	27	20	15	21	22	25	18	**21**
42	22	31	28	18	25	28	31	26	**26**

C. Percent Bolting

DAG	WT	*mtn1-4 mtn2-1*	*mtn1-1 mtn2-5*	*mtn1-1 mtn2-1*	ami 5.3	ami 2.8
16	0	0	0	0	0	0
18	80	0	0	0	0	0
21	100	15	0	0	0	6
25	100	88	47	74	10	20
28	100	100	97	84	10	93
35	100	100	97	84	45	93
37	100	100	97	87	45	100
40	100	100	100	87	48	100
42	100	100	100	87	55	100
44	100	100	100	90	55	100
47	100	100	100	94	61	100
49	100	100	100	94	65	100
52	100	100	100	94	68	100
54	100	100	100	94	71	100
56	100	100	100	97	71	100
59	100	100	100	100	71	100
N	19	32	32	31	31	15

D. Number of leaves at bolting

# of days to bolt	21	28	28	59	59<	28
Plant #	**WT**	***mtn1-4 mtn2-1***	***mtn1-1 mtn2-5***	***mtn1-1 mtn2-1***	**ami5.3**	**ami 2.8**
1	10	16	16	26	29	14
2	12	13	15	24	31	15
3	11	12	13	24	34	16
4	10	13	13	25	26	13
5	11	16	19	22	25	12
6	12	13	16	.	28	16
7	10	16	15	.	.	13
8	11	15	13	.	.	12
Mean	**11**	**14**	**15**	**24**	**29**	**14**
SD	**1**	**2**	**2**	**1**	**3**	**2**

E. Percent senescence

DAG	WT	*mtn1-4 mtn2-1*	*mtn1-1 mtn2-5*	*mtn1-1 mtn2-1*	ami 5.3	ami 2.8
42	25	13	0	0	0	0
44	75	25	0	0	0	13
47	88	63	14	0	36	50
49	88	88	71	60	55	100
52	100	100	100	80	73	100
54	100	100	100	100	91	100
56	100	100	100	100	100	100
N	8	8	7	5	11	8

F. Bundles per unit area

	Plant #	Area (cm^2)	# of bundles	Bundles/ area	Bundles / area	
WT	1	6.38	8.00	1.25	Mean	SD
	2	6.62	6.00	0.91		
	3	7.61	6.00	0.79		
	4	5.51	8.00	1.45	1.10	0.31
mtn1-4mtn2-1	1	5.67	8.00	1.41		
	2	5.90	6.00	1.02		
	3	5.64	6.00	1.06		
	4	4.63	8.00	1.73	1.30*	0.33
mtn1-1mtn 2-5	1	10.94	10.00	0.91		
	2	7.69	7.00	0.91		
	3	8.35	7.00	0.84		
	4	11.29	10.00	0.89	0.89*	0.03
mtn1-1mtn2-1	1	11.40	11.00	0.96		
	2	10.69	12.00	1.12		
	3	9.65	10.00	1.04		
	4	10.23	14.00	1.37	1.12	0.18
ami5.8	1	8.78	8.00	0.91		
	2	7.57	9.00	1.19		
	3	7.14	8.00	1.12	1.07	0.14
ami2.8	1	6.68	11.00	1.65		
	2	5.50	6.00	1.09		
	3	5.41	7.00	1.30		
	4	6.06	11.00	1.81	1.46*	0.33

Paired Samples Test

		Paired Differences					t	df	Sig. (2-tailed)
		Mean	Std. Deviation	Std. Error Mean	95% Confidence Interval of the Difference Lower	Upper			
Pair 1	WT - MTN1421	-.2046	.08404	.04202	-.3383	-.0708	-4.868	3	.017
Pair 2	WT - AMI2.8	-.3609	.13331	.06666	-.5730	-.1487	-5.414	3	.012
Pair 3	WT - MTN1125	.2135	.29336	.14668	-.2533	.6803	1.456	3	.242
Pair 4	WT - MTN1121	-.0223	.25636	.12818	-.4302	.3856	-.174	3	.873
Pair 5	MTN1421 - AMI2.8	-.1563	.08931	.04465	-.2984	-.0142	-3.501	3	.039
Pair 6	MTN1421 - MTN1125	.4181	.32692	.16346	-.1021	.9383	2.558	3	.083
Pair 7	MTN1421 - AMI5.3	.0901	.35840	.20692	-.8002	.9804	.435	2	.706
Pair 8	MTN1421 - MTN1121	.1823	.26290	.13145	-.2361	.6006	1.387	3	.260
Pair 9	AMI2.8 - MTN1125	.5744	.32620	.16310	.0553	1.0934	3.522	3	.039
Pair 10	AMI2.8 - AMI5.3	.2702	.42463	.24516	-.7847	1.3250	1.102	2	.385
Pair 11	AMI2.8 - MTN1121	.3386	.30123	.15062	-.1408	.8179	2.248	3	.110
Pair 12	MTN1125 - AMI5.3	-.1862	.16327	.09426	-.5918	.2193	-1.976	2	.187
Pair 13	MTN1125 - MTN1121	-.2358	.17978	.08989	-.5219	.0503	-2.623	3	.079
Pair 14	AMI5.3 - MTN1121	.0327	.07490	.04324	-.1534	.2187	.755	2	.529

G. **Segregation analysis of *MTN1mtn1-4mtn2-1mtn2-1***

Plant #	Silique #	Total	Homo(-/-)	Het (-/+)	Homo(+/+)
1	1	38	9	17	12
	2	60	11	28	21
	3	59	17	29	13
		0			
2					
	1	45	19	23	3
	2	43	7	24	12
	3	21	6	9	6
		0			
3					
	1	52	20	22	10
	2	54	19	20	15
	3	48	7	27	14
	SUM	**420**	**115**	**199**	**106**

	Observed	**Expected**	**(Exp-Obs)^2/Exp**
Homo (-/-)	115	105	0.95
Het (+/-)	199	210	0.58
Homo(+/+)	106	105	0.01
SUM	420	420	
		Chi square	**1.54**
Number of doubles per / total			**4**

H. Segregation analysis of *mtn1-1mtn1-1MTN2mtn2-5(#1)* and *MTN1mtn1-1mtn2-5mtn2-5(#2)*

plant #	Silique #	Total	Homo (-/-)	Het (-/+)	2-5 (+/+)
1	1	52	13	21	18
	2	54	16	23	15
	3	50	12	36	2
2	1	24	6	14	4
	2	45	14	18	13

3	27	4	17	6
SUM	**252**	**65**	**129**	**58**

	Observed	**Expected**	**(Exp-Obs)^2/Exp**
Homo (-/-)	65	63	0.06
Het (+/-)	129	126	0.07
Homo(+/+)	58	63	0.40
SUM	252	252	0.53
		Chi square	**0.53175**
Number of doubles per / total			**4**

I. Segregation analysis of *mtn1-1mtn1-1MTN2mtn2-1*

Plant #	**Silique #**	**Total + aborted**	**2-1 Homo (-/-)**	**2-1 Het (-/+)**	**2-1 (+/+)**	**Aborted**	**total**
1	1	29	4	11	12	2	27
1	2	25	4	7	11	3	22
1	3	23	2	15	3	**3**	20
	Sums	**77**	**10**	**33**	**26**	**8**	**69**

	Observed	**Expected**	**(Exp-Obs)^2/Exp**
Homo (-/-)	10	17.25	3.05
Het (+/-)	33	34.5	0.07
Homo(+/+)	26	17.25	4.44
SUM	**69**	**69**	**7.55**
		Chi square	
Number of doubles per / total			**14**

J. Segregation based on silique observations

mtn 1-4 mtn2-1

Plant	Silique	Total	Mutants
1	1	59	0
	2	63	0
	3	58	0
	4	57	0
	5	61	0
	6	62	0
	7	64	0
	8	61	0
2	1	54	0
	2	43	0
	3	53	0
	4	59	0
	5	53	0
	6	46	0
	7	51	0
	8	59	0
3	1	59	0
	2	60	0
	3	63	0
	4	60	0
	5	50	0
	6	59	0
	7	63	0
	8	60	0
	9	59	0
TOTAL		1436	0

mtn 1-1 mtn2-5

Plant	Silique	Total	Mutants
1	1	56	0
	2	55	0
	3	54	0
	4	58	0
	5	55	0
	6	57	0
	7	42	0
	8	51	0
2	1	45	0
	2	53	0
	3	59	0
	4	42	0
	5	49	0
	6	48	0
	7	43	0
	8	49	0
	9	57	0
	10	49	0
	11	60	0
	12	44	0
3	1	41	0
	2	40	0
	3	42	0
	4	44	0
	5	38	0
TOTAL		**1231**	**0**

mtn1-1 mtn2-1

Plant	Silique	Total	Mutants
1	1	44	0
	2	47	0
	3	43	0
	4	48	0
	5	43	0
	6	51	0
	7	41	0
	8	47	0
2	1	52	0
	2	54	0
	3	47	0
	4	53	0
	5	55	0
	6	54	0
	7	52	0
	8	56	0
	9	49	0
	10	48	0
	11	59	0
3	1	52	0
	2	46	0
	3	50	0
	4	42	0
	5	48	0
	6	42	1
	7	44	0
4	1	41	0
	2	48	0
	3	45	0
	4	54	0
	5	40	0
	6	50	0
	7	44	0
	8	50	0
TOTAL		**1639**	**1**

K. MTN activity

Plant #	WT	*mtn1-1 mtn2-5*	*mtn1-1 mtn2-1*	ami 5.3
1	0.86	0.33	0.16	0.15
2	1.15	0.33	0.16	0.14
3	1.29	0.33	0.18	0.17
4	1.14	0.25	0.17	0.27
5	1.08	0.27	0.16	0.38
Mean	1.10	0.31	0.16	0.18
SD	0.09	0.04	0.01	0.07

Paired Samples Test

		Paired Differences					t	df	Sig. (2-tailed)
		Mean	Std. Deviation	Std. Error Mean	95% Confidence Interval of the Difference Lower	Upper			
Pair 1	WT - MTN5	.7995	.16363	.07318	.5963	1.0026	10.925	4	.000
Pair 2	WT - AMI5	.8802	.18671	.08350	.6483	1.1120	10.541	4	.000
Pair 3	WT - MTN2	.9383	.14884	.06656	.7535	1.1232	14.097	4	.000
Pair 4	MTN5 - AMI5	.0807	.13577	.06072	-.0879	.2493	1.329	4	.255
Pair 5	MTN5 - MTN2	.1389	.03938	.01761	.0900	.1878	7.887	4	.001

L. MTA content

	Leaves				**Inflorescences**			
Plant #	WT	*mtn1-1 mtn2-5*	*mtn1-1 mtn2-1*	ami 5.3	WT	*mtn1-1 mtn2-5*	*mtn1-1 mtn2-1*	ami 5.3
1	1	0.8	2.1	1.5	5.2	5.6		5.9
2	1	0.6	2.2	1.6	4.9	6.2	54.3	5.8
3	1	0.5	2.3	1.6	5.5	4.9	52.6	5.5
4	1	0.6	2.1	1.2	4.9	5.1	59.6	7.7
Mean	**0.9**	**0.6**	**2.2**	**1.5**	**5.1**	**5.4**	**55.5**	**6.2**
SD	**0.2**	**0.1**	**0.1**	**0.2**	**0.3**	**0.6**	**3.7**	**1.0**

Paired Samples Test

		Paired Differences					t	df	Sig. (2-tailed)
		Mean	Std. Deviation	Std. Error Mean	95% Confidence Interval of the Difference Lower	Upper			
Pair 1	LWT - LMTN15	.3750	.12583	.06292	.1748	.5752	5.960	3	.009
Pair 2	LWT - LAMI5.3	-.4750	.18930	.09465	-.7762	-.1738	-5.019	3	.015
Pair 3	LWT - LMTN12	-1.1750	.09574	.04787	-1.3273	-1.0227	-24.545	3	.000
Pair 4	LMTN15 - LAMI5.3	-.8500	.23805	.11902	-1.2288	-.4712	-7.141	3	.006
Pair 5	LMTN15 - LMTN12	-1.5500	.20817	.10408	-1.8812	-1.2188	-14.892	3	.001
Pair 6	LAMI5.3 - LMTN12	-.7000	.14142	.07071	-.9250	-.4750	-9.899	3	.002
Pair 7	FWT - FMTN15	-.3250	.78049	.39025	-1.5669	.9169	-.833	3	.466
Pair 8	FWT - FAMI5.3	-1.1000	1.19722	.59861	-3.0050	.8050	-1.838	3	.163
Pair 9	FWT - FMTN12	-50.3000	3.36452	1.94251	-58.6579	-41.9421	-25.894	2	.001
Pair 10	FMTN15 - FAMI5.3	-.7750	1.28679	.64340	-2.8226	1.2726	-1.205	3	.315
Pair 11	FMTN15 - FMTN12	-49.9333	4.28525	2.47409	-60.5785	-39.2882	-20.183	2	.002
Pair 12	FAMI5.3 - FMTN12	-49.7667	3.83710	2.21535	-59.2986	-40.2348	-22.464	2	.002

M. NA content

	Leaves				Inflorescences			
Plant #	WT	*mtn1-1 mtn2-5*	*mtn1-1 mtn2-1*	ami 5.3	WT	*mtn1-1 mtn2-5*	*mtn1-1 mtn2-1*	ami 5.3
1	51.71	51.71	19.39	10.98	770.66	468.83	11.63	671.41
2	43.83	43.83	24.01	32.44	536.37	568.06	131.61	540.38
3	43.36	43.36	14.97	54.18	741.06	639.92	132.45	414.69
4	29.14	29.14	13.57	51.03	603.7	550.77	87.04	596.3
Mean	**42**	**42**	**18**	**37**	**663**	**557**	**91**	**556**
SD	**9**	**9**	**5**	**20**	**111**	**70**	**57**	**108**

Paired Samples Test NA

L = leaves; F = inflorescences

		Paired Differences					t	df	Sig. (2-tailed)
		Mean	Std. Deviation	Std. Error Mean	95% Confidence Interval of the Difference Lower	Upper			
Pair 2	LNAWT - LNAMI5.3	.4167	16.38236	9.45836	-40.2794	41.1127	.044	2	.969
Pair 3	LNAWT - LNAMTN12	24.0250	7.68178	3.84089	11.8016	36.2484	6.255	3	.008
Pair 4	LNAMTN15 - LNAMI5.3	.4167	16.38236	9.45836	-40.2794	41.1127	.044	2	.969
Pair 5	LNAMI5.3 - LNAMTN12	26.4267	11.95301	6.90107	-3.2663	56.1196	3.829	2	.062
Pair 6	FNAWT - FNAMTN15	106.0525	141.59562	70.79781	-119.2577	331.3627	1.498	3	.231
Pair 7	FNAWT - FNAMI5.3	107.2525	153.21704	76.60852	-136.5500	351.0550	1.400	3	.256
Pair 8	FNAWT - FNAMTN12	565.6633	140.27368	80.98705	217.2042	914.1225	6.985	2	.020
Pair 9	FNAMTN15 - FNAMI5.3	1.2000	177.57685	88.78842	-281.3644	283.7644	.014	3	.990
Pair 10	FNAMTN15 - FNAMTN12	441.9033	107.96765	62.33515	173.6968	710.1098	7.089	2	.019
Pair 11	FNAMI5.3 - FNAMTN12	425.1267	107.11536	61.84308	159.0374	691.2160	6.874	2	.021

Appendix 3

A. Metabolite content

		Mean	N	Std. Deviation	Std. Error Mean
Pair 1	MTAWT	.0190	3	.00113	.00065
	MTADM	.6717	3	.14352	.08286
Pair 2	MTAWTSPD	.0114	3	.00067	.00039
	MTADMSPD	.2515	3	.02967	.01713
Pair 3	MTAWT	.0190	3	.00113	.00065
	MTAWTSPD	.0114	3	.00067	.00039
Pair 4	MTADM	.6717	3	.14352	.08286
	MTADMSPD	.2515	3	.02967	.01713
Pair 5	ADEWT	.0003	3	.00029	.00017
	ADEDM	.0003	3	.00053	.00030
Pair 6	ADEWTSPD	.0007	3	.00062	.00036
	ADEDMSPD	.0002	3	.00039	.00022
Pair 7	ADEWT	.0003	3	.00029	.00017
	ADEWTSPD	.0007	3	.00062	.00036
Pair 8	ADEDM	.0003	3	.00053	.00030
	ADEDMSPD	.0002	3	.00039	.00022
Pair 9	METWT	.0753	3	.00982	.00567
	METDM	.0695	3	.01357	.00784
Pair 10	METWTSPD	.0760	3	.00922	.00532
	METDMSPD	.0712	3	.00204	.00118
Pair 11	METWT	.0753	3	.00982	.00567
	METWTSPD	.0760	3	.00922	.00532
Pair 12	METDM	.0695	3	.01357	.00784
	METDMSPD	.0712	3	.00204	.00118
Pair 13	SAMWT	.0086	3	.00250	.00144
	SAMDM	.0089	3	.00220	.00127
Pair 14	SAMWTSPD	.0072	3	.00206	.00119
	SAMDMSPD	.0059	3	.00163	.00094
Pair 15	SAMWT	.0086	3	.00250	.00144
	SAMWTSPD	.0072	3	.00206	.00119
Pair 16	SAMDM	.0089	3	.00220	.00127
	SAMDMSPD	.0059	3	.00163	.00094
Pair 17	ADOWT	.0775	3	.01974	.01140
	ADODM	.0473	3	.00860	.00497

Pair 18	ADOWTSPD	.0800	3	.02133	.01232
	ADODMSPD	.1529	3	.11566	.06677
Pair 19	ADOWT	.0775	3	.01974	.01140
	ADOWTSPD	.0800	3	.02133	.01232
Pair 20	ADODM	.0473	3	.00860	.00497
	ADODMSPD	.1529	3	.11566	.06677
Pair 21	SAHWT	.0025	3	.00135	.00078
	SAHDM	.0026	3	.00207	.00120
Pair 22	SAHWTSPD	.0033	3	.00175	.00101
	SAHDMSPD	.0019	3	.00106	.00061
Pair 23	SAHWT	.0025	3	.00135	.00078
	SAHWTSPD	.0033	3	.00175	.00101
Pair 24	SAHDM	.0026	3	.00207	.00120
	SAHDMSPD	.0019	3	.00106	.00061
Pair 25	SMMWT	.0504	3	.00714	.00412
	SMMDM	.0328	3	.00867	.00501
Pair 26	SMMWTSPD	.0613	3	.00416	.00240
	SMMDMSPD	.0564	3	.00865	.00500
Pair 27	SMMWT	.0504	3	.00714	.00412
	SMMWTSPD	.0613	3	.00416	.00240
Pair 28	SMMDM	.0328	3	.00867	.00501
	SMMDMSPD	.0564	3	.00865	.00500

Paired Samples Test

		Paired Differences					t	df	Sig. (2-tailed)
		Mean	Std. Deviation	Std. Error Mean	95% Confidence Interval of the Difference				
					Lower	Upper			
Pair 1	MTAWT - MTADM	-.6527	.14251	.08228	-1.0067	-.2987	-7.933	2	.016
Pair 2	MTAWTSPD - MTADMSPD	-.2401	.02989	.01726	-.3144	-.1659	-13.915	2	.005
Pair 3	MTAWT - MTAWTSPD	.0077	.00167	.00097	.0035	.0118	7.969	2	.015
Pair 4	MTADM - MTADMSPD	.4202	.14618	.08440	.0571	.7833	4.979	2	.038
Pair 5	ADEWT - ADEDM	.0000	.00047	.00027	-.0011	.0012	.124	2	.913
Pair 6	ADEWTSPD - ADEDMSPD	.0005	.00050	.00029	-.0008	.0017	1.687	2	.234
Pair 7	ADEWT - ADEWTSPD	-.0004	.00033	.00019	-.0012	.0005	-1.933	2	.193
Pair 8	ADEDM - ADEDMSPD	.0001	.00014	.00008	-.0003	.0004	1.000	2	.423

Pair 9	METWT - METDM	.0059	.01234	.00713	-.0248	.0365	.823	2	.497
Pair 10	METWTSPD - METDMSPD	.0048	.00760	.00439	-.0141	.0237	1.094	2	.388
Pair 11	METWT - METWTSPD	-.0007	.00520	.00300	-.0136	.0123	-.221	2	.846
Pair 12	METDM - METDMSPD	-.0017	.01279	.00738	-.0335	.0300	-.234	2	.837
Pair 13	SAMWT - SAMDM	-.0003	.00147	.00085	-.0040	.0034	-.356	2	.756
Pair 14	SAMWTSPD - SAMDMSPD	.0013	.00369	.00213	-.0078	.0105	.628	2	.594
Pair 15	SAMWT - SAMWTSPD	.0014	.00456	.00263	-.0099	.0127	.536	2	.645
Pair 16	SAMDM - SAMDMSPD	.0031	.00114	.00066	.0002	.0059	4.617	2	.044
Pair 17	ADOWT - ADODM	.0302	.02046	.01181	-.0206	.0810	2.556	2	.125
Pair 18	ADOWTSPD - ADODMSPD	-.0729	.13496	.07792	-.4082	.2623	-.936	2	.448
Pair 19	ADOWT - ADOWTSPD	-.0024	.02699	.01558	-.0695	.0646	-.156	2	.890
Pair 20	ADODM - ADODMSPD	-.1056	.10725	.06192	-.3720	.1609	-1.705	2	.230
Pair 21	SAHWT - SAHDM	-.0001	.00325	.00188	-.0082	.0080	-.045	2	.968
Pair 22	SAHWTSPD - SAHDMSPD	.0014	.00275	.00159	-.0055	.0082	.875	2	.474
Pair 23	SAHWT - SAHWTSPD	-.0008	.00298	.00172	-.0082	.0066	-.451	2	.696
Pair 24	SAHDM - SAHDMSPD	.0007	.00305	.00176	-.0069	.0083	.397	2	.730
Pair 25	SMMWT - SMMDM	.0176	.01498	.00865	-.0196	.0548	2.033	2	.179
Pair 26	SMMWTSPD - SMMDMSPD	.0050	.00534	.00308	-.0083	.0182	1.616	2	.248
Pair 27	SMMWT - SMMWTSPD	-.0109	.00300	.00173	-.0184	-.0035	-6.299	2	.024
Pair 28	SMMDM - SMMDMSPD	-.0235	.01730	.00999	-.0665	.0194	-2.356	2	.143

B. Hormone content of organs

Hormone group	WT	*mtn1-1mtn2-1*
Unopened buds		
Total CKs	91.45 ± 0.76a	100.68 ± 0.96b
IAA	2860.20 ± 339.28	12897.22± 382.89
Total GA	23.25 ± 1.35a	29.87 ± 1.26b
ABA	36.70 ± 5.75	41.72 ± 2.94
SA	12465.87 ± 4380.40	10330.67 ± 931.81
JA	765.74 ± 220.01	1776.98 ± 854.27
Stage 14 flowers		
Total CKs	131.83 ± 2.69a	326.29 ± 8.37[b]
IAA	3936.98 ± 189.51a	16019.94 ± 303.57b
Total GA	8.10 ± 0.71a	14.31 ± 0.75[b]
ABA	81.65 ± 4.04	85.67 ± 16.37
SA	15382.22 ± 4802.22	9027.18 ± 4937.2378
JA	2301.32 ± 125.05	4170.19 ± 1365.15
Stage 15 siliques		
Total CKs	218.0865	1151.74
IAA	4709.08	17593. 1
Total GA	18.53	23.47
ABA	61.85157	258.69675
SA	38903.33	29847.858
JA	1621.60	2772.16
Stage 17b siliques		
Total CKs	211.52 ± 24.32	*
IAA	10920.09 ± 3931.29	*
Total GA	9.73 ± 1.55	*
ABA	58.52 ± 8.89	*
SA	4752.38 ± 433.60	*
JA	804.89 ± 109.60	*

C. Hormone content of seedlings

	1/2MS		1/2MS + Spd	
	WT	***mtn1-1mtn2-1***	**WT**	***mtn1-1mtn2-1***
Total CKs	8472.34 ± 3403.64 [a]	17557.34 ± 4227.45 [a]	11822.62 ± 2972.00	3142.66± 2609.9
IAA	1062.91 ± 239.91 [a]	3431.56 ± 2004.94 [a]	1354.24 ± 381.73*	194.01 ± 1.04*
Total GA	4.89 ± 0.65	10.48 ± 2.25 [c]	8.94 ± 3.49	1.75 ± 0.81 [c]
ABA	6.80 ± 0.65 [a]	16.33 ± 2.54 [a, c]	14.10 ± 6.19	2.41 ± 0.74 [c]
SA	4141.75 ± 1700.88 [a]	7187.36 ± 653.78 [a]	5724.58 ± 1534.16*	2124.87 ± 1187.44*
JA	82.95 ± 8.55[a]*	358.67 ± 100.51 [a]	171.12 ± 57.11*	20.39 ± 0.96*

D. Gene detection in the CEL files

Sample number	1	2	3	4	5	6
Sample	**Spd-WT-1**	**Spd-WT-2**	**Spd-WT-3**	**MS-WT-1**	**MS-WT-2**	**MS-WT-3**
Detection Call						
Absent	6900	6615	6531	6543	6405	6309
Marginal	202	211	232	228	200	214
Present	15644	15920	15983	15975	16141	16223
Total	**22746**	**22746**	**22746**	**22746**	**22746**	**22746**

Sample number	7	8	9	10	11	12
Sample	**Spd-mut-1**	**Spd-mut-2**	**Spd-mut-3**	**MS-mut-1**	**MS-mut-2**	**MS-mut-3**
Detection Call						
Absent	6377	6698	6239	6406	6361	6852
Marginal	194	229	212	224	219	250
Present	16175	15819	16295	16116	16166	15644
Total	**22746**	**22746**	**22746**	**22746**	**22746**	**22746**

Total Gene Number : 22746

E. Gene that significantly increased their expression as a result of MTN mutation.

AGI	TAIR-060104
At1g52040	[AT1G52030, myrosinase-binding protein, putative (F-ATMBP) identical to SP|Q9SAV1 Myrosinase binding protein-like f-AtMBP [Arabidopsis thaliana]; similar to myrosinase binding protein GI:1711295 from [Brassica napus]; contains Pfam PF01419: Jacalin-like
At1g53870	[AT1G53870, expressed protein contains Pfam profile PF04525: Protein of unknown function (DUF567)];[AT1G53890, expressed protein contains Pfam profile PF04525: Protein of unknown function (DUF567)]
At1g59930	[AT1G59930, hypothetical protein];[AT1G59920, hypothetical protein]
At1g60740	[AT1G60740, peroxiredoxin type 2, putative strong similarity to type 2 peroxiredoxin [Brassica rapa subsp. pekinensis] GI:4928472; contains Pfam profile: PF00578 AhpC/TSA (alkyl hydroperoxide reductase and thiol-specific antioxidant) family];[AT1G65970,
At3g28290	[AT3G28290, integrin-related protein 14a identical to At14a protein GI:11994573 [Arabidopsis thaliana] [Gene 230 (1), 33-40 (1999)], At14a protein [Arabidopsis thaliana] GI:4589123];[AT3G28300, integrin-related protein 14a identical to integrin-related
At4g16860	[AT4G16950, disease resistance protein (TIR-NBS-LRR class), putative domain signature TIR-NBS-LRR exists, suggestive of a disease resistance protein.; closest homolog in Col-0 to RPP5 of clutivar Landsberg erecta.];[AT4G16920, disease resistance protein
At4g23810	[AT4G23800, high mobility group (HMG1/2) family protein similar to HMG2B [Homo sapiens] GI:32335; contains Pfam profile PF00505: HMG (high mobility group) box];[AT4G23810, WRKY family transcription factor AR411 - Arabidopsis thaliana (thale cress), PID:
At5g08610	[AT5G08620, DEAD box RNA helicase (RH25) identical to RNA helicase [Arabidopsis thaliana] GI:3776023; contains Pfam profiles PF00270: DEAD/DEAH box helicase, PF00271: Helicase conserved C-terminal domain];[AT5G08610, DEAD box RNA helicase (RH26) strong
At5g39670	[AT5G39670, calcium-binding EF hand family protein contains INTERPRO:IPR002048 calcium-binding EF-hand domain];[AT5G39680, pentatricopeptide (PPR) repeat-containing protein contains INTERPRO:IPR002885 PPR repeats]
At3g49620	2-oxoacid-dependent oxidase, putative (DIN11) identical to partial cds of 2-oxoacid-dependent oxidase (din11) from GI:10834554 [Arabidopsis thaliana]; identical to cDNA 2-oxoacid-dependent oxidase (din11) GI:10834553; contains Pfam profile PF03171: oxidor

At4g03060	2-oxoglutarate-dependent dioxygenase, putative (AOP2) nearly identical to GI:16118891; contains Pfam profile PF03171: 2OG-Fe(II) oxygenase superfamily domain. The gene sequence is frameshifted, this could be a pseudogene or a sequencing error may exist;
At1g20510	4-coumarate--CoA ligase family protein / 4-coumaroyl-CoA synthase family protein similar to SP|P14912 and SP|P14913 from Petroselinum crispum; contains Pfam AMP-binding enzyme domain PF00501
At3g50930	AAA-type ATPase family protein contains Pfam profile: ATPase family PF00004
At3g28540	AAA-type ATPase family protein contains Pfam profile: ATPase family PF00004
At2g39920	acid phosphatase class B family protein weak similarity to pod storage protein [Phaseolus vulgaris GI:2627233 SP|P10743 STEM 31 kDa glycoprotein precursor (Vegetative storage protein B) {Glycine max}; contains Pfam profile PF03767: HAD superfamily (subfam
At5g15950	adenosylmethionine decarboxylase family protein contains Pfam profile: PF01536 adenosylmethionine decarboxylase
At1g69830	alpha-amylase, putative / 1,4-alpha-D-glucan glucanohydrolase, putative similar to SP|P17859 Alpha-amylase precursor (EC 3.2.1.1) (1,4-alpha-D-glucan glucanohydrolase) {Vigna mungo}, alpha-amylase [Malus x domestica] GI:7532799; contains Pfam profile PF00
At5g51190	AP2 domain-containing transcription factor, putative contains similarity to ethylene responsive element binding factor
At4g34410	AP2 domain-containing transcription factor, putative ethylene-responsive element binding protein homolog, Stylosanthes hamata, U91857
At1g74930	AP2 domain-containing transcription factor, putative similar to AP2 domain containing protein RAP2.1 GI:2281627 from [Arabidopsis thaliana]
At1g33760	AP2 domain-containing transcription factor, putative similar to TINY GB: CAA64359 GI:1246403 from [Arabidopsis thaliana]; contains Pfam profile PF00847: AP2 domain
At1g23080	auxin efflux carrier protein, putative similar to efflux carrier of polar auxin transport [Brassica juncea] gi|12331173|emb|CAC24691
At3g56980	basic helix-loop-helix (bHLH) family protein
At5g04150	basic helix-loop-helix (bHLH) family protein contains Pfam profile: PF00010 helix-loop-helix DNA-binding domain; PMID: 12679534
At1g32640	basic helix-loop-helix (bHLH) protein (RAP-1) identical to bHLH protein GB:CAA67885 GI:1465368 from [Arabidopsis thaliana]
At1g10070	branched-chain amino acid aminotransferase 2 / branched-chain amino acid transaminase 2 (BCAT2) identical to SP|Q9M439 Branched-chain amino acid aminotransferase 2, chloroplast precursor (EC 2.6.1.42) (Atbcat-2) {Arabidopsis thaliana}; contains Pfam profi

At1g62280	C4-dicarboxylate transporter/malic acid transport family protein contains Pfam profile PF03595: C4-dicarboxylate transporter/malic acid transport protein
At4g27280	calcium-binding EF hand family protein similar to EF-hand Ca2+-binding protein CCD1 [Triticum aestivum] GI:9255753; contains INTERPRO:IPR002048 calcium-binding EF-hand domain
At5g54490	calcium-binding EF-hand protein, putative similar to EF-hand Ca2+-binding protein CCD1 [Triticum aestivum] GI:9255753; contains INTERPRO:IPR002048 calcium-binding EF-hand domain
At2g33380	calcium-binding RD20 protein (RD20) induced by abscisic acid during dehydration PMID:10965948; putative transmembrane channel protein PMID:10965948; identical to GI:10862968 [Arabidopsis thaliana]; contains EF-hand domain
At1g23730	carbonic anhydrase, putative / carbonate dehydratase, putative similar to SP|P27140 Carbonic anhydrase, chloroplast precursor (EC 4.2.1.1) (Carbonate dehydratase) {Arabidopsis thaliana}; contains Pfam profile PF00484: Carbonic anhydrase
At2g43620	chitinase, putative similar to basic endochitinase CHB4 precursor SP:Q06209 from [Brassica napus]
At2g42530	cold-responsive protein / cold-regulated protein (cor15b) nearly identical to cold-regulated gene cor15b [Arabidopsis thaliana] GI:456016; contains Pfam profile PF02987: Late embryogenesis abundant protein
At1g07050	CONSTANS-like protein-related contains similarity to photoperiod sensitivity quantitative trait locus (Hd1) GI:11094203 from [Oryza sativa]; similar to Zinc finger protein constans-like 15 (SP:Q9FHH8) {Arabidopsis thaliana}
At4g12280	copper amine oxidase family protein contains Pfam domain, PF01179: Copper amine oxidase, enzyme domain
At4g23600	coronatine-responsive tyrosine aminotransferase / tyrosine transaminase similar to nicotianamine aminotransferase from Hordeum vulgare [GI:6498122, GI:6469087]; contains Pfam profile PF00155 aminotransferase, classes I and II; identical to cDNA coronatine
At5g45340	cytochrome P450 family protein similar to SP|Q42569|C901_ARATH Cytochrome P450 90A1 (SP:Q42569) [Arabidopsis thaliana]; contains Pfam profile: PF00067: Cytochrome P450
At1g06080	delta 9 desaturase (ADS1) identical to delta 9 acyl-lipid desaturase (ADS1) GB:BAA25180 GI:2970034 from [Arabidopsis thaliana]
At1g72920	disease resistance protein (TIR-NBS class), putative domain signature TIR-NBS exists, suggestive of a disease resistance protein.
At2g24120	DNA-directed RNA polymerase, chloroplast (RPOPT) identical to SP|O24600 DNA-directed RNA polymerase, chloroplast precursor (EC 2.7.7.6) {Arabidopsis

	thaliana}
At1g56300	DNAJ heat shock N-terminal domain-containing protein similar to SP|Q9QYI7 DnaJ homolog subfamily B member 8 Mus musculus; contains Pfam profile: PF00226: DnaJ domain
At3g25760	early-responsive to dehydration stress protein (ERD12) nearly identical to early-responsive to dehydration (ERD12) protein [GI:15320414]; similar to allene oxide cyclase GI:8977961 from [Lycopersicon esculentum]; identical to cDNA ERD12 partial cds GI:153
At4g19120	early-responsive to dehydration stress protein (ERD3) identical to ERD3 protein [Arabidopsis thaliana] GI:15320410; contains Pfam profile PF03141: Putative methyltransferase; identical to cDNA ERD3 GI:15320409
At1g28370	ERF domain protein 11 (ERF11) identical to ERF domain protein 11 (AtERF11) GI:15207789 from [Arabidopsis thaliana]
At1g53170	ethylene-responsive element-binding factor 8 / ERF transcription factor 8 (ERF8) identical to ERF transcription factor 8 GI:10567108 from [Arabidopsis thaliana]
At2g44840	ethylene-responsive element-binding protein, putative
At3g30720	expressed protein
At1g47400	expressed protein
At2g34600	expressed protein
At2g26530	expressed protein
At1g13470	expressed protein
At5g50335	expressed protein
At1g73120	expressed protein
At5g35480	expressed protein
At1g76960	expressed protein
At1g17380	expressed protein
At4g19430	expressed protein
At1g19180	expressed protein
At3g48500	expressed protein
At4g16146	expressed protein
At4g37290	expressed protein
At3g16670	expressed protein
At5g64870	expressed protein
At2g42870	expressed protein
At3g05730	expressed protein
At2g29920	expressed protein
At1g12845	expressed protein
At2g04460	expressed protein
At1g35210	expressed protein

At1g10522	expressed protein
At5g13220	expressed protein
At1g80130	expressed protein
At4g39675	expressed protein
At2g21640	expressed protein
At5g26270	expressed protein ; expression supported by MPSS
At2g15560	expressed protein contains Pfam profile PF04396: Protein of unknown function, DUF537
At5g01600	ferritin 1 (FER1) identical to ferritin [Arabidopsis thaliana] GI:1246401, GI:8163920
At2g39030	GCN5-related N-acetyltransferase (GNAT) family protein similar to SP|Q9SMB8 Tyramine N-feruloyltransferase 4/11 (EC 2.3.1.110) (Hydroxycinnamoyl- CoA: tyramine N-hydroxycinnamoyltransferase) {Nicotiana tabacum}; contains Pfam profile PF00583: acetyltransf
At3g05950	germin-like protein, putative similar to germin-like protein GLP6 [SP|P92997]; contains Pfam profile: PF01072 germin family
At1g22770	gigantea protein (GI) identical to gigantea protein SP:Q9SQI2 from [Arabidopsis thaliana]
At3g29320	glucan phosphorylase, putative similar to alpha-glucan phosphorylase, L isozyme 1 precursor GB:P04045 from [Solanum tuberosum] (J. Biochem. 106 (4), 691-695 (1989))
At5g07570	glycine/proline-rich protein contains similarity to flagelliform silk protein [Nephila clavipes] gi|7106224|gb|AAF36090
At3g20440	glycoside hydrolase family 13 protein similar to 1,4-alpha-glucan branching enzyme [Solanum tuberosum] GI:1621012, 1,4-alpha-glucan branching enzyme (EC 2.4.1.18) from [Homo sapiens] SP|Q04446, {Solanum tuberosum} SP|P30924; contains Pfam profiles: PF0012
At2g43610	glycoside hydrolase family 19 protein similar to chitinase GI:17799 from [Brassica napus]; contains Pfam profiles PF00182: Chitinase class I, PF00187: Chitin recognition protein
At3g18080	glycosyl hydrolase family 1 protein contains Pfam PF00232 : Glycosyl hydrolase family 1 domain; TIGRFAM TIGR01233: 6-phospho-beta-galactosidase; similar to beta-glucosidase BGQ60 precursor GB:A57512 [Hordeum vulgare]; similar to beta-mannosidase enzyme (G
At3g57260	glycosyl hydrolase family 17 protein similar to glucan endo-1,3-beta-glucosidase, acidic isoform precursor SP:P33157 from [Arabidopsis thaliana]
At1g67970	heat shock factor protein, putative (HSF5) / heat shock transcription factor, putative (HSTF5) identical to heat shock transcription factor 5 (HSF5) SP:Q9S7U5 from [Arabidopsis thaliana]; contains Pfam profile: PF00447 HSF-type DNA-

	binding domain
At3g22740	homocysteine S-methyltransferase 3 (HMT-3) identical to homocysteine S-methyltransferase HMT-3 [Arabidopsis thaliana] GI:9966515; similar to homocysteine S-methyltransferase AtHMT-2 (GI:6685163) [Arabidopsis thaliana]; similar to selenocysteine methyltran
At1g73480	hydrolase, alpha/beta fold family protein low similarity to monoglyceride lipase from [Homo sapiens] GI:14594904, [Mus musculus] GI:2632162; contains Pfam profile PF00561: hydrolase, alpha/beta fold family
At4g30660	hydrophobic protein, putative / low temperature and salt responsive protein, putative similar to SP|Q9ZNQ7 Hydrophobic protein RCI2A (Low temperature and salt responsive protein LTI6A) {Arabidopsis thaliana}; contains Pfam profile PF01679: Uncharacterized
At4g30650	hydrophobic protein, putative / low temperature and salt responsive protein, putative similar to SP|Q9ZNQ7 Hydrophobic protein RCI2A (Low temperature and salt responsive protein LTI6A) {Arabidopsis thaliana}; contains Pfam profile PF01679: Uncharacterized
At2g19850	hypothetical protein
At2g05950	hypothetical protein
At5g03090	hypothetical protein
At4g29200	hypothetical protein
At4g19690	iron-responsive transporter (IRT1) identical to Fe(II) transport protein [Arabidopsis thaliana] gi|1353266|gb|AAB01678; member of the Zinc (Zn2+)-Iron (Fe2+) permease (ZIP) family, PMID:11500563
At1g52000	jacalin lectin family protein similar to myrosinase binding protein [Brassica napus] GI:1711296, myrosinase-binding protein homolog [Arabidopsis thaliana] GI:2997767; contains Pfam profile: PF01419 jacalin-like lectin domain
At5g14180	lipase family protein similar to SP|Q64194 Lysosomal acid lipase/cholesteryl ester hydrolase precursor (EC 3.1.1.13) {Rattus norvegicus}; contains Pfam profile PF04083: ab-hydrolase associated lipase region
At1g72520	lipoxygenase, putative similar to lipoxygenase gi:1495804 [Solanum tuberosum], gi:1654140 [Lycopersicon esculentum], GB:CAB56692 [Arabidopsis thaliana]
At5g10140	MADS-box protein flowering locus F (FLF) identical to FLOWERING LOCUS C protein (MADS box protein FLOWERING LOCUS F) (Swiss-Prot:Q9S7Q7) [Arabidopsis thaliana]
At1g24140	matrixin family protein similar to matrix metalloproteinase [Cucumis sativus] GI:7159629; contains InterPro accession IPR001818: Matrixin
At1g10970	metal transporter, putative (ZIP4) similar to Zn and Cd transporter ZNT1 [Thlaspi caerulescens] gi|7381054|gb|AAF61374; member of the Zinc (Zn2+)-Iron (Fe2+)

	permease (ZIP) family, PMID:11500563
At5g47240	MutT/nudix family protein similar to SP|P53370 Nucleoside diphosphate-linked moiety X motif 6 {Homo sapiens}; contains Pfam profile PF00293: NUDIX domain
At1g18710	myb family transcription factor (MYB47) contains Pfam profile: PF00249 myb-like DNA-binding domain
At1g18570	myb family transcription factor (MYB51) contains PFAM profile: PF00249
At5g56080	nicotianamine synthase, putative similar to nicotianamine synthase [Lycopersicon esculentum][GI:4753801], nicotianamine synthase 2 [Hordeum vulgare][GI:4894912]
At1g09240	nicotianamine synthase, putative similar to nicotianamine synthase [Lycopersicon esculentum][GI:4753801], nicotianamine synthase 2 [Hordeum vulgare][GI:4894912]
At2g17040	no apical meristem (NAM) family protein contains Pfam PF02365: No apical meristem (NAM) domain; similar to petunia NAM (X92205) and A. thaliana sequences ATAF1 (X74755) and ATAF2 (X74756); probable DNA-binding protein
At1g69490	no apical meristem (NAM) family protein similar to N-term half of NAC domain protein NAM [Arabidopsis thaliana] GI:4325282
At2g16660	nodulin family protein similar to nodulin-like protein [Arabidopsis thaliana] GI:3329368, nodule-specific protein Nlj70 [Lotus japonicus] GI:3329366
At4g34950	nodulin family protein similar to nodulin-like protein [Arabidopsis thaliana] GI:3329368, nodule-specific protein Nlj70 [Lotus japonicus] GI:3329366
At5g50790	nodulin MtN3 family protein similar to MtN3 GI:1619602 (root nodule development) from [Medicago truncatula]
At1g14250	nucleoside phosphatase family protein / GDA1/CD39 family protein low similarity to SP|P97687 Ectonucleoside triphosphate diphosphohydrolase 1 (EC 3.6.1.5) (Ecto-apyrase) {Rattus norvegicus}; contains Pfam profile PF01150: GDA1/CD39 (nucleoside phosphatase
At2g14610	pathogenesis-related protein 1 (PR-1) identical to GB:M90508 SP|P33154
At1g31290	PAZ domain-containing protein / piwi domain-containing protein contains Pfam profiles PF02170: PAZ domain, PF02171: Piwi domain
At4g02330	pectinesterase family protein contains Pfam profile: PF01095 pectinesterase
At1g08610	pentatricopeptide (PPR) repeat-containing protein contains Pfam profile PF01535: PPR repeat
At3g17990	phosphoethanolamine N-methyltransferase 1 / PEAMT 1 (NMT1) identical to Phosphoethanolamine N-methyltransferase 1 (EC 2.1.1.103) (PEAMT 1) (AtNMT1) (SP:Q9FR44){Arabidopsis thaliana}; strong similarity to phosphoethanolamine N-methyltransferase from [Spina
At1g02390	phospholipid/glycerol acyltransferase family protein contains Pfam profile

	PF01553: Acyltransferase
At1g09530	phytochrome interacting factor 3 (PIF3) identical to phytochrome interacting factor 3 (PIF3) GI:3929585 from [Arabidopsis thaliana]
At2g22860	phytosulfokines 2 (PSK2) identical to phytosulfokines 2 (PSK2) from [Arabidopsis thaliana]
At5g44420	plant defensin protein, putative (PDF1.2a) plant defensin protein family member, personal communication, Bart Thomma (Bart.Thomma@agr.kuleuven.ac.be); similar to antifungal protein 1 preprotein [Raphanus sativus] gi|609322|gb|AAA69541
At2g26020	plant defensin-fusion protein, putative (PDF1.2b) plant defensin protein family member, personal communication, Bart Thomma (Bart.Thomma@agr.kuleuven.ac.be); similar to antifungal protein 1 preprotein [Raphanus sativus] gi|609322|gb|AAA69541
At1g19610	plant defensin-fusion protein, putative (PDF1.4) plant defensin protein family member, personal communication, Bart Thomma (Bart.Thomma@agr.kuleuven.ac.be); similar to SWISS-PROT:P30224, Cysteine-rich antifungal protein 1 precursor (AFP1)[Arabidopsis thal
At5g06870	polygalacturonase inhibiting protein 2 (PGIP2) identical to polygalacturonase inhibiting protein 2 (PGIP2) [Arabidopsis thaliana] gi|7800201|gb|AAF69828; contains leucine rich-repeat (LRR) domains Pfam:PF00560, INTERPRO:IPR001611
At4g22470	protease inhibitor/seed storage/lipid transfer protein (LTP) family protein similar to hydroxyproline-rich glycoprotein DZ-HRGP from Volvox carteri f. nagariensis GP|6523547; contains Pfam profile PF00234 Protease inhibitor/seed storage/LTP family
At4g12490	protease inhibitor/seed storage/lipid transfer protein (LTP) family protein similar to pEARLI 1 (Accession No. L43080): an Arabidopsis member of a conserved gene family (PGF95-099), Plant Physiol. 109 (4), 1497 (1995); contains Pfam protease inhibitor/see
At5g67080	protein kinase family protein contains protein kinase domain, Pfam:PF00069
At5g53450	protein kinase family protein contains protein kinase domain, Pfam:PF00069
At4g21680	proton-dependent oligopeptide transport (POT) family protein contains Pfam profile: PF00854 POT family
At3g17170	ribosomal protein S6 family protein (RFC3) annotation temporarily based on supporting cDNA gi|15620809|dbj|AB057424.1|; contains TIGRfam TIGR00166 and Pfam PF01250 profiles ribosomal protein S6.
At3g44860	S-adenosyl-L-methionine:carboxyl methyltransferase family protein similar to defense-related protein cjs1 [Brassica carinata][GI:14009292][Mol Plant Pathol (2001) 2(3):159-169]

At1g53885	senescence-associated protein-related similar to senescence-associated protein SAG102 (GI:22331931) [Arabidopsis thaliana];
At3g56710	sigA-binding protein identical to SigA binding protein [Arabidopsis thaliana] gi|6980074|gb|AAF34713; contains Pfam PF05678: VQ motif
At5g15960	stress-responsive protein (KIN1) / stress-induced protein (KIN1) identical to SP|P18612 Stress-induced KIN1 protein {Arabidopsis thaliana}
At5g61160	transferase family protein similar to anthocyanin 5-aromatic acyltransferase from Gentiana triflora GI:4185599, malonyl CoA:anthocyanin 5-O-glucoside-6'''-O-malonyltransferase from Perilla frutescens GI:17980232, Salvia splendens GI:17980234; contains Pfa
At2g43510	trypsin inhibitor, putative similar to SP|P26780 Trypsin inhibitor 2 precursor (MTI-2) {Sinapis alba}
At2g40670	two-component responsive regulator / response regulator 16 (ARR16) identical to response regulator 16 GI:11870067 from [Arabidopsis thaliana]
At2g38470	WRKY family transcription factor contains Pfam profile: PF03106 WRKY DNA -binding domain;
At1g80840	WRKY family transcription factor similar to WRKY transcription factor GB:BAA87058 GI:6472585 from [Nicotiana tabacum]
At3g01970	WRKY family transcription factor similar to WRKY1 GB:AAC49527 [Petroselinum crispum]
At5g46710	zinc-binding family protein similar zinc-binding protein [Pisum sativum] GI:16117799; contains Pfam profile PF04640 : Protein of unknown function, DUF597

F. Gene that significantly decreased their expression as a result of MTN mutation

AGI	TAIR-060104
At5g33370	GDSL-motif lipase/hydrolase family protein similar to family II lipase EXL3 (GI:15054386), EXL1 (GI:15054382), EXL2 (GI:15054384) [Arabidopsis thaliana]; contains Pfam profile PF00657: Lipase/Acylhydrolase with GDSL-like motif
At5g58310	hydrolase, alpha/beta fold family protein low similarity to SP|Q40708 PIR7A protein {Oryza sativa}, polyneuridine aldehyde esterase [Rauvolfia serpentina] GI:6651393, ethylene-induced esterase [Citrus sinensis] GI:14279437; contains Pfam profile PF00561:
At5g55450	protease inhibitor/seed storage/lipid transfer protein (LTP) family protein contains Pfam protease inhibitor/seed storage/LTP family domain PF00234
At5g52570	beta-carotene hydroxylase, putative similar to GI:1575296, beta-carotene hydroxylase
At5g23940	transferase family protein similar to anthranilate N-hydroxycinnamoyl/benzoyltransferase, Dianthus caryophyllus [gi:2239091]; contains Pfam transferase family domain PF002458
At5g15310	myb family transcription factor contains PFAM profile: myb DNA-binding domain PF00249
At5g01740	expressed protein wound-inducible protein wun1 protein - Solanum tuberosum, PIR:JQ0398
At3g44970	cytochrome P450 family protein similar to Cytochrome P450 85 (SP:Q43147) {Lycopersicon esculentum}; contains Pfam profile: PF00067 cytochrome P450
At4g38800	phosphorylase family protein contains weak similarity to Swiss-Prot:O51931 nucleosidase [Includes: 5'-methylthioadenosine nucleosidase (EC 3.2.2.16); S-adenosylhomocysteine nucleosidase [Buchnera aphidicola]
At4g38330	[AT4G38280, expressed protein unknown protein F4L23.24 Arabidopsis thaliana chromosome II BAC F4L23, PID:g2583136];[AT4G38330, expressed protein];[AT2G45250, expressed protein]
At4g34840	nucleosidase-related contains weak similarity to MTA/SAH nucleosidase (Swiss-Prot:O51931) [Buchnera aphidicola]
At4g11460	protein kinase family protein contains Pfam PF00069: Protein kinase domain
At4g08300	nodulin MtN21 family protein similar to MtN21 GI:2598575 (root nodule development) from [Medicago truncatula]
At1g52820	2-oxoglutarate-dependent dioxygenase, putative similar to AOP1 [Arabidopsis lyrata][GI:16118889]; contains Pfam profile PF03171: 2OG-Fe(II) oxygenase superfamily domain
At2g16005	MD-2-related lipid recognition domain-containing protein / ML domain-containing protein contains Pfam profile PF02221: ML domain
At1g10370	glutathione S-transferase, putative (ERD9) similar to glutathione S-transferase TSI-1 [Aegilops tauschii] gi:2190992 gb:AAD10129; similar to ESTs gb|R29860, emb|Z29757, and emb|Z29758; identical to cDNA ERD9 mRNA for glutathione S-transferase, GI:1537540
At2g40100	chlorophyll A-B binding protein (LHCB4.3) identical to Lhcb4:3 protein [Arabidopsis

	thaliana] GI:4741956; contains Pfam profile: PF00504 chlorophyll A-B binding protein
At2g39510	nodulin MtN21 family protein similar to MtN21 GI:2598575 (root nodule development) from [Medicago truncatula]
At2g42250	cytochrome P450 family protein similar to cytochrome P450 93A1 (SP:Q42798) [Glycine max]
At5g65730	xyloglucan:xyloglucosyl transferase, putative / xyloglucan endotransglycosylase, putative / endo-xyloglucan transferase, putative similar to endo-xyloglucan transferase GI:2244732 from [Gossypium hirsutum]
At4g30610	serine carboxypeptidase S10 family protein similar to Serine carboxypeptidase II chains A and B (SP:P08819) (EC 3.4.16.6) [Triticum aestivum (Wheat)];
At5g50260	cysteine proteinase, putative similar to cysteine endopeptidase precursor CysEP GI:2944446 from [Ricinus communis]
At4g01390	meprin and TRAF homology domain-containing protein / MATH domain-containing protein weak similarity to ubiquitin-specific protease 12 [Arabidopsis thaliana] GI:11993471; contains Pfam profile PF00917: MATH domain
At4g33720	pathogenesis-related protein, putative similar to SP|P33154 Pathogenesis-related protein 1 precursor (PR-1) {Arabidopsis thaliana}; contains Pfam profile PF00188: SCP-like extracellular protein
At1g78340	glutathione S-transferase, putative similar to glutathione transferase GI:2853219 from [Carica papaya]
At5g48850	male sterility MS5 family protein similar to male sterility MS5 [Arabidopsis thaliana] GI:3859112; contains Pfam profile PF00515 TPR Domain
At3g01420	pathogen-responsive alpha-dioxygenase, putative similar to pathogen-inducible alpha-dioxygenase [Nicotiana attenuata] GI:12539609; contains Pfam profile PF03098: Animal haem peroxidase
At1g23205	invertase/pectin methylesterase inhibitor family protein low similarity to pectinesterase from Phaseolus vulgaris SP|Q43111, Lycopersicon esculentum SP|Q43143; contains Pfam profile PF04043: Plant invertase/pectin methylesterase inhibitor
At3g50560	short-chain dehydrogenase/reductase (SDR) family protein contains INTERPRO family IPR002198 short-chain dehydrogenase/reductase (SDR) superfamily
At2g35380	peroxidase 20 (PER20) (P20) identical to SP|Q9SLH7 Peroxidase 20 precursor (EC 1.11.1.7) (Atperox P20) (ATP28a) {Arabidopsis thaliana}
At4g12500	protease inhibitor/seed storage/lipid transfer protein (LTP) family protein similar to pEARLI 1 (Accession No. L43080): an Arabidopsis member of a conserved gene family (PGF95-099), Plant Physiol. 109 (4), 1497 (1995); contains Pfam protease inhibitor/see
At5g16570	glutamine synthetase, putative similar to glutamine synthetase, cytosolic isozyme (glutamate-- ammonia ligase) [Alfalfa] SWISS-PROT:P04078
At1g44800	nodulin MtN21 family protein similar to MtN21 [Medicago truncatula] GI:2598575; contains Pfam profile PF00892: Integral membrane protein
At5g36910	thionin (THI2.2) identical to thionin [Arabidopsis thaliana] gi|1181533|gb|AAC41679
At5g22300	nitrilase 4 (NIT4) identical to SP|P46011 Nitrilase 4 (EC 3.5.5.1) {Arabidopsis thaliana}
At1g63710	cytochrome P450, putative similar to cytochrome P450 GB:O23066 [Arabidopsis

	thaliana]
At4g04955	amidohydrolase family protein similar to SP|P32375 Allantoinase (EC 3.5.2.5) {Saccharomyces cerevisiae}; contains Pfam profile PF01979: Amidohydrolase family
At5g47610	zinc finger (C3HC4-type RING finger) family protein contains Pfam profile: PF00097 zinc finger, C3HC4 type (RING finger)
At5g03350	legume lectin family protein contains Pfam domain, PF00139: Legume lectins beta domain
At1g68880	bZIP transcription factor family protein similar to common plant regulatory factor 6 GI:9650826 from [Petroselinum crispum]; contains Pfam profile: PF00170 bZIP transcription factor
At3g08770	lipid transfer protein 6 (LTP6) identical to GI:8571927
At1g65480	flowering locus T protein (FT) identical to SP|Q9SXZ2 FLOWERING LOCUS T protein {Arabidopsis thaliana}; contains Pfam profile PF01161: Phosphatidylethanolamine-binding protein
At1g49450	transducin family protein / WD-40 repeat family protein contains 7 WD-40 repeats (PF00400); similar to En/Spm-like transposon protein GI:2739374 from [Arabidopsis thaliana]; no characterized homologs
At5g18430	GDSL-motif lipase/hydrolase family protein similar to family II lipase EXL1 GI:15054382 from [Arabidopsis thaliana]; contains Pfam profile PF00657: GDSL-like Lipase/Acylhydrolase
At1g07180	pyridine nucleotide-disulphide oxidoreductase family protein contains similarity to alternative NADH-dehydrogenase GI:3718005 from [Yarrowia lipolytica], SP|P32340 Rotenone-insensitive NADH-ubiquinone oxidoreductase, mitochondrial precursor (EC 1.6.5.3) (
At3g50400	GDSL-motif lipase/hydrolase family protein similar to family II lipase EXL3 (GI:15054386), EXL1 (GI:15054382), EXL2 (GI:15054384) [Arabidopsis thaliana]; contains Pfam profile PF00657: Lipase/Acylhydrolase with GDSL-like motif
At3g25790	myb family transcription factor contains Pfam domain, PF00249: Myb-like DNA-binding domain
At2g21650	myb family transcription factor contains PFAM profile: PF00249 myb-like DNA-binding domain
At1g52690	late embryogenesis abundant protein, putative / LEA protein, putative similar to SP|P13934 Late embryogenesis abundant protein 76 (LEA 76) {Brassica napus}; contains Pfam profile PF02987: Late embryogenesis abundant protein
At5g24420	glucosamine/galactosamine-6-phosphate isomerase-related contains weak similarity to Swiss-Prot:O95336 6-phosphogluconolactonase (EC 3.1.1.31) (6PGL) [Homo sapiens]
At4g15620	integral membrane family protein contains TIGRFAM TIGR01569 : plant integral membrane protein TIGR01569; contains Pfam PF04535 : Domain of unknown function (DUF588)
At1g30530	UDP-glucoronosyl/UDP-glucosyl transferase family protein contains Pfam profile: PF00201 UDP-glucoronosyl and UDP-glucosyl transferase
At1g30700	FAD-binding domain-containing protein similar to SP|P30986 reticuline oxidase precursor (Berberine-bridge-forming enzyme) (BBE) (Tetrahydroprotoberberine

	synthase) [Eschscholzia californica]; contains PF01565 FAD binding domain
At1g16390	organic cation transporter-related low similarity to Organic cation/carnitine transporter 2 (Solute carrier family 22, member 5) (High-affinity sodium-dependent carnitine cotransporter) from {Homo sapiens} SP|O76082, {Rattus norvegicus} SP|O70594; contain
At3g22060	receptor protein kinase-related contains Pfam profile: PF01657 Domain of unknown function that is usually associated with protein kinase domain Pfam:PF00069
At4g16870	unknown
At3g02140	expressed protein
At5g50200	expressed protein similar to unknown protein (pir||T05562) isoform contains a non-consensus AT acceptor splice site at intron 1
At3g21870	cyclin family protein similar to cyclin 2 [Trypanosoma brucei] GI:7339572, cyclin 6 [Trypanosoma cruzi] GI:12005317; contains Pfam profile PF00134: Cyclin, N-terminal domain
At3g55710	[AT3G55700, UDP-glucoronosyl/UDP-glucosyl transferase family protein glucuronosyl transferase homolog, Lycopersicon esculentum, PIR:S39507 ;contains Pfam profile: PF00201 UDP-glucoronosyl and UDP-glucosyl transferase];[AT3G55710, UDP-glucoronosyl/UDP-gl
At5g01810	CBL-interacting protein kinase 15 (CIPK15) identical to CBL-interacting protein kinase 15 [Arabidopsis thaliana] gi|13249134|gb|AAK16692; identical to novel serine/threonine protein kinase [Arabidopsis thaliana] gi|1777312|dbj|BAA06311; contains Pfam prof
At1g26560	glycosyl hydrolase family 1 protein contains Pfam PF00232 : Glycosyl hydrolase family 1 domain; TIGRFAM TIGR01233: 6-phospho-beta-galactosidase; similar to amygdalin hydrolase isoform AH I precursor (GI:16757966) [Prunus serotina]
At2g47880	glutaredoxin family protein contains INTERPRO Domain IPR002109, Glutaredoxin (thioltransferase)
At3g28345	ABC transporter family protein similar to P-glycoprotein [Arabidopsis thaliana] GI:3849833; contains Pfam profiles PF00005: ABC transporter, PF00664: ABC transporter transmembrane region
At1g13650	expressed protein
At5g41080	glycerophosphoryl diester phosphodiesterase family protein weak similarity to SP|P37965 Glycerophosphoryl diester phosphodiesterase (EC 3.1.4.46) {Bacillus subtilis}; contains Pfam profile PF03009: Glycerophosphoryl diester phosphodiesterase family
At3g28740	[AT3G28730, structure-specific recognition protein 1 / high mobility group protein / HMG protein nearly identical to SP|Q05153 Structure-specific recognition protein 1 homolog (HMG protein) {Arabidopsis thaliana}; contains Pfam profile PF00505: HMG (high
At5g43370	[AT5G43370, inorganic phosphate transporter (PHT2) identical to inorganic phosphate transporter [Arabidopsis thaliana] GI:2780348];[AT5G43350, inorganic phosphate transporter (PHT1) (PT1) identical to inorganic phosphate transporter [Arabidopsis thalian
At4g23680	major latex protein-related / MLP-related low similarity to major latex protein {Papaver

	somniferum}[GI:294060] ; contains Pfam profile PF00407: Pathogenesis-related protein Bet v I family
At3g24290	ammonium transporter, putative similar to SP|Q9SQH9|AT13_ARATH Ammonium transporter 1, member 3 (AtAMT1;3) {Arabidopsis thaliana}; contains Pfam profile PF00909: Ammonium Transporter Family
At1g68440	expressed protein
At5g09520	hydroxyproline-rich glycoprotein family protein contains proline-rich extensin domains, INTERPRO:IPR002965
At2g48130	protease inhibitor/seed storage/lipid transfer protein (LTP) family protein contains Pfam protease inhibitor/seed storage/LTP family domain PF00234
At2g21045	senescence-associated family protein contains similarity to senescence-associated gene Ntdin from GI:7594903 [Nicotiana tabacum]; contains C2-domain profile. (PS50004;PF00168)
At3g30775	proline oxidase, mitochondrial / osmotic stress-responsive proline dehydrogenase (POX) (PRO1) (ERD5) nearly identical to SP|P92983 Proline oxidase, mitochondrial precursor (EC 1.5.3.-) (Osmotic stress- induced proline dehydrogenase) [Arabidopsis thaliana]
At4g28940	nucleosidase-related contains weak similarity to MTA/SAH nucleosidase (P46). (Swiss-Prot:P24247) [Shigella flexneri]
At2g43590	chitinase, putative similar to basic endochitinase CHB4 precursor SP:Q06209 from [Brassica napus]
At1g18810	phytochrome kinase substrate-related contains weak similarity to Swiss-Prot:Q9SWI1 phytochrome kinase substrate 1 [Arabidopsis thaliana]
At5g20270	expressed protein contains Pfam domain, PF03006: Uncharacterised protein family (Hly-III / UPF0073)
At1g79840	homeobox-leucine zipper protein 10 (HB-10) / HD-ZIP transcription factor 10 / homeobox protein (GLABRA2) identical to homeobox protein (GLABRA2) (homeobox-leucine zipper protein ATHB-10) (HD-ZIP protein ATHB-10) GB:P46607 [Arabidopsis thaliana]
At1g80320	oxidoreductase, 2OG-Fe(II) oxygenase family protein similar to GS-AOP loci [GI:16118889, GI:16118887, GI:16118891, GI:16118893]; contains PF03171 2OG-Fe(II) oxygenase superfamily domain
At5g64850	expressed protein
At5g55720	pectate lyase family protein similar to pectate lyase 1 GP:6606532 from [Musa acuminata]
At5g54720	ankyrin repeat family protein contains ankyrin repeats, Pfam:PF00023
At1g02200	CER1 protein identical to maize gl1 homolog (glossy1 locus) GI:1209703 and CER1 GI:1199467 from [Arabidopsis thaliana]
At1g22160	senescence-associated protein-related similar to senescence-associated protein SAG102 (GI:22331931) [Arabidopsis thaliana]
At3g21950	S-adenosyl-L-methionine:carboxyl methyltransferase family protein similar to SAM:salicylic acid carboxyl methyltransferase (SAMT) [GI:6002712][Clarkia breweri] and to SAM:benzoic acid carboxyl methyltransferase (BAMT)[GI:9789277][Antirrhinum

	majus]
At5g48490	protease inhibitor/seed storage/lipid transfer protein (LTP) family protein contains Pfam protease inhibitor/seed storage/LTP family domain PF00234
At3g50570	hydroxyproline-rich glycoprotein family protein contains proline-rich protein domains, INTERPRO:IPR000694
At1g55260	protease inhibitor/seed storage/lipid transfer protein (LTP) family protein contains Pfam protease inhibitor/seed storage/LTP family domain PF00234
At1g78170	expressed protein
At1g59500	[AT4G37390, auxin-responsive GH3 family protein similar to auxin-responsive GH3 product [Glycine max] GI:18591; contains Pfam profile PF03321: GH3 auxin-responsive promoter];[AT1G59500, auxin-responsive GH3 family protein similar to auxin-responsive GH3
At3g51350	aspartyl protease family protein contains Eukaryotic and viral aspartyl proteases active site, PROSITE:PS00141
At1g01600	cytochrome P450, putative similar to cytochrome P450 GI:10442763 from [Triticum aestivum]
At3g48720	transferase family protein similar to hypersensitivity-related hsr201 protein - Nicotiana tabacum,PIR2:T03274; contains Pfam transferase family domain PF00248
At4g15210	beta-amylase (BMY1) / 1,4-alpha-D-glucan maltohydrolase identical to Beta-amylase (EC 3.2.1.2) (1,4-alpha-D-glucan maltohydrolase) SP:P25853 [Arabidopsis thaliana]
At2g28305	expressed protein contains Pfam profile PF03641: decarboxylase family protein
At3g48920	myb family transcription factor (MYB45) similar to MybHv33 GI:456214 from [Hordeum vulgare]; contains PFAM profile: myb DNA binding domain PF00249
At3g12580	heat shock protein 70, putative / HSP70, putative strong similarity to heat shock protein GI:425194 [Spinacia oleracea]
At1g25450	very-long-chain fatty acid condensing enzyme, putative nearly identical to fatty acid condensing enzyme CUT1 GI:5001734 from [Arabidopsis thaliana]
At3g01140	myb family transcription factor (MYB106) similar to transforming protein (myb) homolog GB:S26605 from [Petunia x hybrida]
At2g35760	integral membrane family protein contains TIGRFAM TIGR01569 : plant integral membrane protein TIGR01569; contains Pfam PF04535 : Domain of unknown function (DUF588)
At3g01550	triose phosphate/phosphate translocator, putative similar to SWISS-PROT:P52178 triose phosphate/phosphate translocator [Cauliflower]{Brassica oleracea}
At2g02950	phytochrome kinase substrate 1 (PKS1) identical to Swiss-Prot:Q9SWI1 phytochrome kinase substrate 1 [Arabidopsis thaliana]
At1g06350	fatty acid desaturase family protein similar to delta 9 acyl-lipid desaturase (ADS1) GI:2970034 from [Arabidopsis thaliana]
At1g18980	germin-like protein, putative similar to germin-like protein subfamily T member 1 [SP|P92995]; contains PS00725 germin family signature
At4g13410	glycosyl transferase family 2 protein similar to beta-(1-3)-glucosyl transferase GB:AAC62210 GI:3687658 from [Bradyrhizobium japonicum], cellulose synthase from Agrobacterium tumeficiens [gi:710492] and Agrobacterium radiobacter [gi:710493];

	contains Pfam
At2g47200	expressed protein
At5g07680	no apical meristem (NAM) family protein contains Pfam PF02365 : No apical meristem (NAM) protein; similar to cup-shaped cotyledon CUC2 (GI:1944132) [Arabidopsis thaliana]
At1g13080	cytochrome P450 family protein identical to gb|D78605 cytochrome P450 monooxygenase from Arabidopsis thaliana and is a member of the PF|00067 Cytochrome P450 family. ESTs gb|Z18072, gb|Z35218 and gb|T43466 come from this gene
At3g17610	bZIP transcription factor family protein / HY5-like protein (HYH) nearly identical to HY5-like protein [Arabidopsis thaliana] GI:18042111; similar to TGACG-motif binding factor GI:2934884 from [Glycine max]; contains Pfam profile: PF00170 bZIP transcripti
At4g37010	caltractin, putative / centrin, putative similar to Caltractin (Centrin) SP:P41210 from [Atriplex nummularia]
At2g47240	long-chain-fatty-acid--CoA ligase family protein / long-chain acyl-CoA synthetase family protein similar to GI:1617270 (MF7P) and gi:1617628 (MF45P) from [Brassica napus] ; contains Pfam AMP-binding enzyme domain PF00501
At1g64500	glutaredoxin family protein
At4g28780	GDSL-motif lipase/hydrolase family protein similar to family II lipase EXL3 (GI:15054386), EXL1 (GI:15054382), EXL2 (GI:15054384) [Arabidopsis thaliana]; contains Pfam profile PF00657: Lipase/Acylhydrolase with GDSL-like motif
At3g10570	cytochrome P450, putative similar to cytochrome P450 77A3 GB:O48928 [Glycine max]
At1g15260	expressed protein EST gb|N65467 comes from this gene
At2g21100	disease resistance-responsive protein-related / dirigent protein-related similar to dirigent protein [Thuja plicata] gi|6694699|gb|AAF25360; similar to disease resistance response protein 206-d [Pisum sativum] gi|508844|gb|AAB18669
At5g51460	trehalose-6-phosphate phosphatase (TPPA) identical to trehalose-6-phosphate phosphatase (AtTPPA) [Arabidopsis thaliana] GI:2944178
At2g23540	GDSL-motif lipase/hydrolase family protein similar to family II lipase EXL1 GI:15054382 from [Arabidopsis thaliana]; contains Pfam profile PF00657: GDSL-like Lipase/Acylhydrolase
At4g29030	glycine-rich protein glycine-rich protein - Onobrychis viciifolia,PID:g2565429
At5g47600	heat shock protein-related contains weak similarity to Heat shock 22 kDa protein, mitochondrial precursor (Swiss-Prot:P46254) [Pisum sativum]
At2g48140	protease inhibitor/seed storage/lipid transfer protein (LTP) family protein similar to pEARLI 1 (Accession No. L43080): an Arabidopsis member of a conserved gene family (PGF95-099), Plant Physiol. 109 (4), 1497 (1995); contains Pfam protease inhibitor/see
At4g38080	hydroxyproline-rich glycoprotein family protein contains proline-rich extensin domains, INTERPRO:IPR002965; Common family member: At2g22510 [Arabidopsis thaliana]
At4g24140	hydrolase, alpha/beta fold family protein low similarity to 2-hydroxy-6-oxo-7-methylocta-2,4-dienoate hydrolase [Pseudomonas putida] GI:2822275, hydroxymuconic semialdehyde hydrolase, Pseudomonas stutzeri, AF039534; contains Pfam profile PF00561: hydrolas

At4g37980	mannitol dehydrogenase, putative (ELI3-1) identical to GI:16267
At5g13400	proton-dependent oligopeptide transport (POT) family protein contains Pfam profile: PF00854 POT family
At1g66230	myb family transcription factor (MYB20) similar to myb-related transcription factor GI:1430846 from [Lycopersicon esculentum]; contains PFAM profile: Myb DNA binding domain PF00249
At1g29660	GDSL-motif lipase/hydrolase family protein low similarity to family II lipase EXL1 [Arabidopsis thaliana] GI:15054382; contains InterPro Entry IPR001087 Lipolytic enzyme, G-D-S-L family
At1g04220	[AT1G04220, beta-ketoacyl-CoA synthase, putative Strong similarity to beta-keto-Coa synthase gb|U37088 from Simmondsia chinensis, GI:4091810];[AT1G04210, leucine-rich repeat family protein / protein kinase family protein contains Pfam domains PF00560: L
At1g68850	peroxidase, putative identical to peroxidase ATP23a GB:CAA70035 (Arabidopsis thaliana)
At1g65450	transferase family protein low similarity to anthranilate N-hydroxycinnamoyl/benzoyltransferase Dianthus caryophyllus GI:3288180, GI:2239091; contains Pfam profile PF02458 transferase family
At4g17215	expressed protein
At5g13900	protease inhibitor/seed storage/lipid transfer protein (LTP) family protein contains Pfam protease inhibitor/seed storage/LTP family domain PF00234
At2g17300	expressed protein
At2g38110	phospholipid/glycerol acyltransferase family protein low similarity to SP|O87707 CicA protein {Caulobacter crescentus}; contains Pfam profile PF01553: Acyltransferase
At2g32270	zinc transporter (ZIP3) identical to zinc transporter [Arabidopsis thaliana] gi|3252870|gb|AAC24199; member of the Zinc (Zn2+)-Iron (Fe2+) permease (ZIP) family, PMID:11500563
At3g61060	F-box family protein / lectin-related low similarity to PP2 lectin polypeptide [Cucurbita maxima] GI:410437; contains Pfam profile PF00646: F-box domain
At1g72970	glucose-methanol-choline (GMC) oxidoreductase family protein similar to mandelonitrile lyase from Prunus serotina [SP|P52706, SP|P52707]; contains Pfam profile PF00732 GMC oxidoreductase
At5g44550	integral membrane family protein similar to unknown protein (pir||T10581) This family of plant proteins contains a domain that may have a catalytic activity. It has a conserved arginine and aspartate that could form an active site. These proteins are pred
At2g03200	aspartyl protease family protein contains Pfam domain, PF00026: eukaryotic aspartyl protease
At1g64360	expressed protein
At3g13650	disease resistance response protein-related/ dirigent protein-related similar to dirigent protein [Thuja plicata] gi|6694699|gb|AAF25360; similar to pathogenesis-related protein [Pisum sativum] gi|4585273|gb|AAD25355
At3g52720	carbonic anhydrase family protein low similarity to storage protein (dioscorin)

	[Dioscorea cayenensis] GI:433463; contains Pfam profile PF00194: Eukaryotic-type carbonic anhydrase
At4g08040	1-aminocyclopropane-1-carboxylate synthase, putative / ACC synthase, putative similar to ACC synthase from Malus sylvestris [SP|P37821], Solanum tuberosum [GI:520914]
At1g75030	pathogenesis-related thaumatin family protein identical to thaumatin-like protein [Arabidopsis thaliana] GI:2435406; contains Pfam profile: PF00314 Thaumatin family
At3g23880	F-box family protein contains F-box domain Pfam:PF00646
At4g25760	expressed protein
At1g51840	protein kinase-related contains similarity to light repressible receptor protein kinase [Arabidopsis thaliana] gi|1321686|emb|CAA66376
At2g20870	cell wall protein precursor, putative identical to Putative cell wall protein precursor (Swiss-Prot:P47925) [Arabidopsis thaliana]; weak similarity to mu-protocadherin (GI:7861967) [Rattus norvegicus]
At1g29720	protein kinase family protein contains eukaryotic protein kinase domain, INTERPRO:IPR000719
At1g29600	zinc finger (CCCH-type) family protein contains Pfam domain, PF00642: Zinc finger C-x8-C-x5-C-x3-H type (and similar)
At1g65060	4-coumarate--CoA ligase 3 / 4-coumaroyl-CoA synthase 3 (4CL3) identical to SP|Q9S777 4-coumarate--CoA ligase 3 (EC 6.2.1.12) (4CL 3) (4-coumaroyl-CoA synthase 3) {Arabidopsis thaliana}
At1g06830	glutaredoxin family protein contains INTERPRO Domain IPR002109, Glutaredoxin (thioltransferase)
At1g26770	expansin, putative (EXP10) similar to expansin At-EXP1 GI:1041702 from [Arabidopsis thaliana]; alpha-expansin gene family, PMID:11641069
At5g09480	hydroxyproline-rich glycoprotein family protein contains proline-rich extensin domains, INTERPRO:IPR002965; Common family members At5g09530, At5g09520, At1g44222 [Arabidopsis thaliana]
At5g49350	unknown
At1g49430	long-chain-fatty-acid--CoA ligase / long-chain acyl-CoA synthetase nearly identical to acyl CoA synthetase (MF45P) GI:1617268 from [Brassica napus]
At5g59320	lipid transfer protein 3 (LTP3) identical to lipid transfer protein 3 from Arabidopsis thaliana [gi:8571921]; contains Pfam protease inhibitor/seed storage/LTP family domain PF00234
At1g31920	pentatricopeptide (PPR) repeat-containing protein contains Pfam profile PF01535: PPR repeat
At1g18970	germin-like protein (GLP1) (GLP4) identical to germin-like protein subfamily T member 1 [SP|P92995]
At4g21870	26.5 kDa class P-related heat shock protein (HSP26.5-P) contains Pfam profile: PF00011 Hsp20/alpha crystallin family: identified in Scharf, K-D., et al,Cell Stress & Chaperones (2001) 6: 225-237.
At5g42760	[AT5G42760, O-methyltransferase N-terminus domain-containing protein contains Pfam profile PF02409: O-methyltransferase N-terminus];[AT5G42765, expressed protein]

At2g34620	mitochondrial transcription termination factor-related / mTERF-related contains Pfam profile PF02536: mTERF
At3g25710	basic helix-loop-helix (bHLH) family protein contains Pfam profile: PF00010 helix-loop-helix DNA-binding domain
At4g00050	basic helix-loop-helix (bHLH) family protein contains Pfam profile: PF00010 helix-loop-helix DNA-binding domain
At1g12570	glucose-methanol-choline (GMC) oxidoreductase family protein similar to mandelonitrile lyase from Prunus serotina [SP|P52706, SP|P52707]; contains Pfam profile PF00732 GMC oxidoreductase
At5g37690	GDSL-motif lipase/hydrolase family protein similar to family II lipase EXL3 (GI:15054386), EXL1 (GI:15054382), EXL2 (GI:15054384) [Arabidopsis thaliana]
At3g10910	zinc finger (C3HC4-type RING finger) family protein contains Pfam domain, PF00097: Zinc finger, C3HC4 type (RING finger)
At2g38310	expressed protein low similarity to early flowering protein 1 [Asparagus officinalis] GI:1572683, SP|P80889 Ribonuclease 1 (EC 3.1.-.-) {Panax ginseng}
At4g38950	kinesin motor family protein similar to AtNACK1 kinesin-like protein (GI:19979627) [Arabidopsis thaliana]; similar to kinesin-like protein NACK1 (GI:19570247) [Nicotiana tabacum]
At5g26220	ChaC-like family protein contains Pfam profile: PF04752 ChaC-like protein
At1g06100	[AT1G06100, fatty acid desaturase family protein similar to delta 9 acyl-lipid desaturase (ADS1) GI:2970034 from [Arabidopsis thaliana]];[AT1G06120, fatty acid desaturase family protein similar to delta 9 acyl-lipid desaturase GB:BAA25180 GI:2970034 (AD
At1g65490	expressed protein
At2g22510	hydroxyproline-rich glycoprotein family protein similar to proline-rich cell wall protein [Gossypium barbadense] gi|451544|gb|AAA79364; contains proline-rich extensin domains, INTERPRO:IPR002965
At2g21140	hydroxyproline-rich glycoprotein family protein identical to proline-rich protein 2 [Arabidopsis thaliana] gi|7620011|gb|AAF64549
At5g14130	peroxidase, putative identical to peroxidase ATP20a [Arabidopsis thaliana] gi|1546694|emb|CAA67338
At1g11850	expressed protein
At5g13580	ABC transporter family protein
At4g37070	[AT4G37070, patatin, putative similar to patatin-like latex allergen [Hevea brasiliensis][PMID:10589016]; contains patatin domain PF01734];[AT4G37060, patatin, putative similar to patatin-like latex allergen [Hevea brasiliensis][PMID:10589016]; contains
At4g24510	eceriferum protein (CER2) identical to (CER2) [Arabidopsis thaliana] GI:1213594; contains Pfam profile PF02458: Transferase family
At5g15600	expressed protein
At5g23190	cytochrome P450 family protein contains Pfam profile: PF00067 cytochrome P450
At5g14070	glutaredoxin family protein contains INTERPRO Domain IPR002109, Glutaredoxin (thioltransferase)

At4g19830	immunophilin / FKBP-type peptidyl-prolyl cis-trans isomerase family protein similar to 70 kDa peptidylprolyl isomerase (Peptidylprolyl cis-trans isomerase) (PPiase) (Rotamase) (SP:Q43207) [Triticum aestivum]; FKBP-type peptidyl-prolyl cis-trans isomerase,
At2g44460	glycosyl hydrolase family 1 protein contains Pfam PF00232 : Glycosyl hydrolase family 1 domain; TIGRFAM TIGR01233: 6-phospho-beta-galactosidase; similar to beta-glucosidase 1 (GI:12043529) [Arabidopsis thaliana]
At5g43580	protease inhibitor, putative similar to SP|P19873 Inhibitor of trypsin and hageman factor (CMTI-V) {Cucurbita maxima}; contains Pfam profile PF00280: Potato inhibitor I family
At5g60910	agamous-like MADS box protein AGL8 / FRUITFULL (AGL8) NAP1-1, Nicotiana tabacum, EMBL:AF009126; identical to SP:Q38876 Agamous-like MADS box protein AGL8 (Floral homeotic protein AGL8) (FRUITFULL){Arabidopsis thaliana} PMID:9502732, PMID:10648231; identic
At5g47635	expressed protein
At4g28290	expressed protein
At3g54420	class IV chitinase (CHIV) almost identical to class IV chitinase from GI:2597826 [Arabidopsis thaliana]
At3g12110	actin 11 (ACT11) identical to SP|P53496 Actin 11 {Arabidopsis thaliana}

References

Albers E (2009) Metabolic characteristics and importance of the universal methionine salvage pathway recycling methionine from 5'-methylthioadenosine. IUBMB Life **61:** 1132-1142

Aloni R, Aloni E, Langhans M, Ullrich CI (2006) Role of auxin in regulating Arabidopsis flower development. Planta **223:** 315-328

Alonso JM, Stepanova AN, Leisse TJ, Kim CJ, Chen H, Shinn P, Stevenson DK, Zimmerman J, Barajas P, Cheuk R (2003) Genome-wide insertional mutagenesis of Arabidopsis thaliana. Science **301:** 653 - 657

Alvarez-Buylla ER, Benítez M, Corvera-Poiré A, Chaos Cador Á, de Folter S, Gamboa de Buen A, Garay-Arroyo A, García-Ponce B, Jaimes-Miranda F, Pérez-Ruiz RV (2010) Flower development. The Arabidopsis Book **8:** 1-57

Anderegg G, Ripperger H (1989) Correlation between metal complex formation and biological activity of nicotianamine analogues. J.Chem.Soc., Chem.Commun. 647-650

Arnold K, Bordoli L, Kopp J, Schwede T (2006) The SWISS-MODEL workspace: a web-based environment for protein structure homology modelling. Bioinformatics **22:** 195-201

Asami T, Nakano T, Nakashita H, Sekimata K, Shimada Y, Yoshida S (2003) The influence of chemical genetics on plant science: shedding light on functions and mechanism of action of brassinosteroids using biosynthesis inhibitors. J Plant Growth Regul **22:** 336-349

Baima S, Nobili F, Sessa G, Lucchetti S, Ruberti I, Morelli G (1995) The expression of the Athb-8 homeobox gene is restricted to provascular cells in *Arabidopsis thaliana*. Development **121:** 4171-4182

Bais PH, Ravishankar GA (2002) Role of polyamines in the ontogeny of plants and their biotechnological applications. Plant cell, tissue and organ culture **69:** 1-34

Baron K, Stasolla C (2008) The role of polyamines during *in vivo* and *in vitro* development. In Vitro Cell Dev-Pl **44:** 384-395

Benjamins R, Quint AB, Weijers D, Hooykaas P,Offringa R (2001) The PINOID protein kinase regulates organ development in Arabidopsis by enhancing polar auxin transport. Development **128:** 4057 - 4067

Benková E, Michniewicz M, Sauer M, Teichmann T, Seifertová D, Jürgens G, Friml J (2003) Local, efflux-dependent auxin gradients as a common module for plant organ formation. Cell **115:** 591-602

Bennett SRM, Alvarez J, Bossinger G, Smyth DR (1995) Morphogenesis in pinoid mutants of Arabidopsis thaliana. Plant J **8:** 505-520

Berger F, Grini PE, Schnittger A (2006) Endosperm: an integrator of seed growth and development. Curr Opin Plant Biol **9:** 664-670

Berleth T, Mattsson J, Hardtke CS (2000) Vascular continuity and auxin signals. Trends Plant Sci **5:** 387-393

Berleth T, Sachs T (2001) Plant morphogenesis: long-distance coordination and local patterning. Curr Opin Plant Biol **4:** 57-62

Bertino JR, Waud WR, Parker WB, Lubin M (2011) Targeting tumors that lack methylthioadenosine phosphorylase (MTAP) activity: current strategies. Cancer Biol Ther **11:** 627-32

Bleecker AB, Kende H (2000) Ethylene: a gaseous signal molecule in plants. Annu Rev Cell Dev Biol **16:** 1-18

Böhme H, Scholz G (1960) VersuchezurNormalisierung des Phänotyps Mutante Chloronerva von Lycopersicon esculentum Mill. Kulturpflanze **8:** 93-109

Bowman JL (1994) Arabidopsis: an atlas of morphology and development. Springer-Verlag NY 450pp.

Boyes DC, Zayed AM, Ascenzi R, McCaskill AJ, Hoffman NE, Davis KR, Gorlach J (2001) Growth stage-based phenotypic analysis of Arabidopsis: a model for high throughput functional genomics in plants. Plant Cell **13:** 1499-1510

Braybrook SA, Harada JJ (2008) LECs go crazy in embryo development. Trends Plant Sci **13:** 624-630

Bürstenbinder K, Rzewuski G, Wirtz M, Hell R, Sauter M (2007) The role of methionine recycling for ethylene synthesis in Arabidopsis. Plant J **49:** 238-249

Bürstenbinder K, Waduwara I, Schoor S, Moffatt BA, Wirtz M, Minocha SC, Oppermann Y, Bouchereau A, Hell R, Sauter M (2010) Inhibition of 5'-methylthioadenosine metabolism in the Yang cycle alters polyamine levels, and impairs seedling growth and reproduction in Arabidopsis. Plant J **62:** 977-988

Caño-Delgado A, Yin Y, Yu C, Vafeados D, Mora-García S, Cheng JC, Nam KH, Li J, Chory J (2004) BRL1 and BRL3 are novel brassinosteroid receptors that function in vascular differentiation in Arabidopsis. Development **131:** 5341

Carland FM, McHale NA (1996) LOP1: a gene involved in auxin transport and vascular patterning in Arabidopsis. Development **122:** 1811

Cecchetti V, Altamura MM, Falasca G, Costantino P, Cardarelli M (2008) Auxin regulates Arabidopsis anther dehiscence, pollen maturation, and filament elongation. Plant J **20:** 1760 -1774

Cheng Y, Dai X, Zhao Y (2006) Auxin biosynthesis by the YUCCA flavin monooxygenases controls the formation of floral organs and vascular tissues in Arabidopsis. Genes Dev **20:** 1790 - 1799

Choe S, Noguchi T, Fujioka S, Takatsuto S, Tissier CP, Gregory BD, Ross AS, Tanaka A, Yoshida S, Tax FE (1999) The Arabidopsis dw f 7/ste1 Mutant Is Defective in the δ7 Sterol C-5 Desaturation Step Leading to Brassinosteroid Biosynthesis. Plant Cell **11:** 207 - 222

Clay NK, Nelson T (2005) Arabidopsis *thick vein* Mutation Affects Vein Thickness and Organ Vascularization, and Resides in a Pro vascular Cell-Specific Spermine Synthase Involved in Vein Definition and in Polar Auxin Transport. Plant Physiol **138:** 767-777

Clough SJ, Bent AF (1998) Floral dip: a simplified method for Agrobacterium-mediated transformation ofArabidopsis thaliana. Plant J **16:** 735-743

Cnops G, Neyt P, Raes J, Petrarulo M, Nelissen H, Malenica N, Luschnig C, Tietz O, Ditengou F, Palme K (2006) The TORNADO1 and TORNADO2 genes function in several patterning processes during early leaf development in Arabidopsis thaliana. Plant Cell **18:** 852 - 866

Cona A, Rea G, Angelini R, Federico R, Tavladoraki P (2006) Functions of amine oxidases in plant development and defence. Trends Plant Sci **11:** 80-88

Cornell KA, Winter RW, Tower PA, Riscoe M (1996) Affinity purification of 5-methylthioribose kinase and 5-methylthioadenosine/S-adenosylhomocysteine nucleosidase from Klebsiella pneumoniae [corrected]. Biochem J **317:** 285 - 290

Costa LM, Gutierrez-Marcos JF, Dickinson HG (2004) More than a yolk: the short life and complex times of the plant endosperm. Trends Plant Sci **9:** 507-514

Curie C, Cassin G, Couch D, Divol F, Higuchi K, Le Jean M, Misson J, Schikora A, Czernic P, Mari S (2009) Metal movement within the plant: contribution of nicotianamine and yellow stripe 1-like transporters. Ann Bot **103:** 1-11

Demura T, Fukuda H (2007) Transcriptional regulation in wood formation. Trends Plant Sci **12:** 64-70

Dengler N, Kang J (2001) Vascular patterning and leaf shape. Curr Opin Plant Biol **4:** 50-56

Dengler NG (2006) The shoot apical meristem and development of vascular architecture. Can J Bot **84:** 1660-1671

Dhonukshe P, Aniento F, Hwang I, Robinson DG, Mravec J, Stierhof YD, Friml J (2007) Clathrin-mediated constitutive endocytosis of PIN auxin efflux carriers in Arabidopsis. Current Biol **17:** 520-527

Dhonukshe P, Grigoriev I, Fischer R, Tominaga M, Robinson DG, Hašek J, Paciorek T, Petrášek J, Seifertová D, Tejos R (2008) Auxin transport inhibitors impair vesicle motility and actin cytoskeleton dynamics in diverse eukaryotes. Pro Nat Acad Sci **105:** 4489 - 4494

Emsley P, Cowtan K (2004) Coot: model-building tools for molecular graphics. Acta Crystallogr D Biol Crystallogr **60** : 2126-2132

Ewing TJA, Makino S, Skillman AG, Kuntz ID (2001) DOCK 4.0: search strategies for automated molecular docking of flexible molecule databases. J Comput Aid Mol Des **15:** 411-428

Feng H, Chen Q, Feng J, Zhang J, Yang X, Zuo J (2007) Functional characterization of the Arabidopsis eukaryotic translation initiation factor 5A-2 that plays a crucial role in plant growth and development by regulating cell division, cell growth, and cell death. Plant Physiol **144:** 1531 - 1545

Friml J, Vieten A, Sauer M, Weijers D, Schwarz H, Hamann T, Offringa R, Jurgens G (2003) Efflux-dependent auxin gradients establish the apical-basal axis of Arabidopsis. Nature **426:** 147-153

Friml J, Yang X, Michniewicz M, Weijers D, Quint A, Tietz O, Benjamins R, Ouwerkerk PBF, Ljung K, Sandberg G (2004) A PINOID-dependent binary switch in apical-basal PIN polar targeting directs auxin efflux. Science **306:** 862 - 865

Fukuda H (1997) Tracheary element differentiation. Plant Cell **9:** 1147 - 1156

Fukuda H (2004) Signals that control plant vascular cell differentiation. Nature Reviews Molecular Cell Biol **5:** 379-391

Gadapati WR, Macfie SM (2006) Phytochelatins are only partially correlated with Cd-stress in two species of Brassica. Plant Sci **170:** 471-480

Gälweiler L, Guan C, Müller A, Wisman E, Mendgen K, Yephremov A, Palme K (1998) Regulation of polar auxin transport by AtPIN1 in Arabidopsis vascular tissue. Science **282:** 2226

Ge C, Cui X, Wang Y, Hu Y, Fu Z, Zhang D, Cheng Z, Li J (2006) BUD2, encoding an S-adenosylmethionine decarboxylase, is required for Arabidopsis growth and development. Cell Res **16:** 446-456

Gehring M, Choi Y, Fischer RL (2004) Imprinting and seed development. Plant Cell **16:** S203 – S213

Geldner N, Anders N, Wolters H, Keicher J, Kornberger W, Muller P, Delbarre A, Ueda T, Nakano A, Jürgens G (2003) The Arabidopsis GNOM ARF-GEF mediates endosomal recycling, auxin transport, and auxin-dependent plant growth. Cell **112:** 219-230

Goldberg RB, Beals TP, Sanders PM (1993) Anther development: basic principles and practical applications. Plant Cell **5:** 1217 - 1229

Grunewald W, Fimrl J (2010) The march of the PINs: developmental plasticity by dynamic polar targeting in plant cells. EMBO J **29:** 2700-2714

Guranowski A, Montgomery JA, Cantoni GL, Chiang PK (1981) Adenosine analogs as substrates and inhibitors of S-adenosylhomocysteine hydrolase. Biochemistry (N Y) **20:** 110-115

Ha HC, Sirisoma NS, Kuppusamy P, Zweier JL, Woster PM, Casero RA (1998) The natural polyamine spermine functions directly as a free radical scavenger. Proc Nat Acad Sci **95:** 11140 - 11147

Hamann T, Benkova E, Bäurle I, Kientz M, Jürgens G (2002) The Arabidopsis BODENLOS gene encodes an auxin response protein inhibiting MONOPTEROS-mediated embryo patterning. Genes Dev **16:** 1610 - 1615

Hamann T, Mayer U, Jurgens G (1999) The auxin-insensitive bodenlos mutation affects primary root formation and apical-basal patterning in the Arabidopsis embryo. Development **126:** 1387 - 1395

Hanfrey C, Sommer S, Mayer MJ, Burtin D, Michael AJ (2001) Arabidopsis polyamine biosynthesis: absence of ornithine decarboxylase and the mechanism of arginine decarboxylase activity. Plant J **27:** 551-560

Hanzawa Y, Takahashi T, Komeda Y (1997) *ACL5*: an Arabidopsis gene required for internodal elongation after flowering. Plant J **12:** 863-874

Hanzawa Y, Takahashi T, Michael AJ, Burtin D, Long D, Pineiro M, Coupland G, Komeda Y (2000) ACAULIS5, an Arabidopsis gene required for stem elongation, encodes a spermine synthase. EMBO J **19:** 4248-4256

Hardtke CS, Berleth T (1998) The Arabidopsis gene MONOPTEROS encodes a transcription factor mediating embryo axis formation and vascular development. EMBO J **17:** 1405-1411

Haughn G, Chaudhury A (2005) Genetic analysis of seed coat development in Arabidopsis. Trends Plant Sci **10:** 472-477

He Y, Fukushige H, Hildebrand DF, Gan S (2002) Evidence supporting a role of jasmonic acid in Arabidopsis leaf senescence. Plant Physiol **128:** 876 - 884

Herbik A (1997) Proteinchemische und molecular biologische Charakterisierung der Tomaten mutante chloronerva. PhD thesis. Humboldt-University, Berlin. pp 102.

Herbik A, Koch G, Mock HP, Dushkov D, Czihal A, Thielmann J, Stephan U (1999) Isolation, characterization and cDNA cloning of nicotianamine synthase from barley. Eur J Biochem **265:** 231-239

Hobbie L, McGovern M, Hurwitz LR, Pierro A, Liu NY, Bandyopadhyay A, Estelle M (2000) The axr6 mutants of Arabidopsis thaliana define a gene involved in auxin response and early development. Development **127:** 23 - 32

Huala E, Dickerman AW, Garcia-Hernandez M, Weems D, Reiser L, LaFond F, Hanley D, Kiphart D, Zhuang M, Huang W (2001) The Arabidopsis Information Resource (TAIR): a comprehensive database and web-based information retrieval, analysis, and visualization system for a model plant. Nucleic Acids Res **29:** 102 - 105

Huh JH, Bauer MJ, Hsieh TF, Fischer RL (2008) Cellular programming of plant gene imprinting. Cell **132:** 735-744

Hyodo H, Tanaka K (1986) Inhibition of 1-aminocyclopropane-l-carboxylic acid synthase activity by polyamines, their related compounds and metabolites of S-adenosylmethionine. Plant and cell physiol **27:** 391 - 398

Ibañes M, Fàbregas N, Chory J, Caño-Delgado AI (2009) Brassinosteroid signaling and auxin transport are required to establish the periodic pattern of Arabidopsis shoot vascular bundles. Proc Natl Acad Sci **106:** 13630-13635

Ibeñes M, Schreiber K, Ripperger H, Kircheiss A (1983) Metal complex formation by nicotianamine, a possibl e phytosiderophore. Cellular and Molecular Life Sci **39:** 261-262

Igarashi K, Kashiwagi K (2010) Modulation of cellular function by polyamines. Int J Biochem Cell Biol **42:** 39-51

Imai A, Akiyama T, Kato T, Sato S, Tabata S, Yamamoto KT, Takahashi T (2004a) Spermine is not essential for survival of Arabidopsis. FEBS Lett **556**: 148-152

Imai A, Hanzawa Y, Komura M, Yamamoto KT, Komeda Y, Takahashi T (2006) The dwarf phenotype of the Arabidopsis acl5 mutant is suppressed by a mutation in an upstream ORF of a bHLH gene. Development **133:** 3575 - 3585

Imai A, Matsuyama T, Hanzawa Y, Akiyama T, Tamaoki M, Saji H, Shirano Y, Kato T, Hayashi H, Shibata D (2004b) Spermidine synthase genes are essential for survival of Arabidopsis. Plant Physiol **135:** 1565 - 1573

Initiative AG (2000) Arabidopsis Genome Initiative, 2000. Analysis of the genome sequence of the flowering plant Arabidopsis thaliana. Nature **408:** 796–815

Irish VF (2010) The flowering of Arabidopsis flower development. Plant J **61:** 1014-1028

Irizarry RA, Warren D, Spencer F, Kim IF, Biswal S, Frank BC, Gabrielson E, Garcia JGN, Geoghegan J, Germino G (2005) Multiple-laboratory comparison of microarray platforms. Nature methods **2:** 345-350

Jaillais Y, Chory J (2010) Unraveling the paradoxes of plant hormone signaling integration. Nat Struct Mol Biol **17:** 642-645

Kakehi J, Kuwashiro Y, Niitsu M, Takahashi T (2008) Thermospermine is required for stem elongation in *Arabidopsis thaliana*. Plant Cell Physiol **49:** 1342-1349

Karim Sorefan TG, Sarah JL, Karin Ljung PR, Carlos S, Remko Offringa J (2009) A regulated auxin minimum is required for seed dispersal in Arabidopsis. Nature **459:** 583-586

Klatte M, Schuler M, Wirtz M, Fink-Straube C, Hell R, Bauer P (2009) The analysis of Arabidopsis nicotianamine synthase mutants reveals functions for nicotianamine in seed iron loading and iron deficiency responses. Plant Physiol **150:** 257-271

Kleine-Vehn J, Friml J (2008) Polar targeting and endocytic recycling in auxin-dependent plant development. Annu Rev Cell Dev Biol **24:** 447-473

Kojima M, Kamada-Nobusada T, Komatsu H, Takei K, Kuroha T, Mizutani M, Ashikari M, Ueguchi-Tanaka M, Matsuoka M, Suzuki K (2009) Highly sensitive and high-throughput analysis of plant hormones using MS-probe modification and liquid chromatography–tandem mass spectrometry: an application for hormone profiling in Oryza sativa. Plant and cell physiol **50:** 1201 - 1214

Koornneef M, Hanhart C, Veen JH (1991) A genetic and physiological analysis of late flowering mutants in Arabidopsis thaliana. Mol Genl Gen **229:** 57-66

Krizek BA (2011) Auxin regulation of Arabidopsis flower development involves members of the AINTEGUMENTA-LIKE/PLETHORA (AIL/PLT) family. J Exp Bot **62:** 3311 - 3319

Kumar A, Taylor M, Altabella T, Tiburcio AF (1997) Recent advances in polyamine research. Trends Plant Sci **2:** 124-130

Kusano T, Yamaguchi K, Berberich T, Takahashi Y (2007) Advances in polyamine research in 2007. J Plant Res **120:** 345-350

Kushad MM, Richardson DG, Ferro AJ (1985) 5'-Methylthioadenosine Nucleosidase and 5-Methylthioribose Kinase Activities and Ethylene Production during Tomato Fruit Development and Ripening. Plant Physiol **79:** 525-529

Laemmli UK (1970) Cleavage of structural proteins during the assembly of the head of bacteriophage T4. Nature **227:** 680-685

Lan P, Li W, Wen TN, Shiau JY, Wu YC, Lin W, Schmidt W (2011) iTRAQ Protein Profile Analysis of Arabidopsis Roots Reveals New Aspects Critical for Iron Homeostasis. Plant Physiol **155:** 821-834

Lancashire PD, Bleiholder H, Boom T, Langelüddeke P, Stauss R, Weber E, Witzenberger A (1991) A uniform decimal code for growth stages of crops and weeds. Ann App Biol **119:** 561-601

Lee JE, Luong W, Huang DJT, Kenneth A, Riscoe MK, Howell PL (2005) Mutational analysis of a nucleosidase involved in quorum-sensing autoinducer-2 biosynthesis. Biochem **44:** 11049-11057

Ling HQ, Koch G, Bäumlein H, Ganal MW (1999) Map-based cloning of chloronerva, a gene involved in iron uptake of higher plants encoding nicotianamine synthase. Pro Nat Acad Sci **96:** 7098 - 7103

Loenen W (2006) S-Adenosylmethionine: jack of all trades and master of everything? Biochem Soc Trans **34:** 330-333

Liu Z, Duguay J, Ma F, Wang T.W, Tshin R, Hopkins M, Nowack L, Thompson J.E. (2008) Modulation of eIF5A1 expression alters xylem abundance in *Arabidopsis thaliana* J Ex Bot **59:** 939–950.

Luo J, Fuell C, Parr A, Hill L, Bailey P, Elliott K, Fairhurst SA, Martin C, Michael AJ (2009) A novel polyamine acyltransferase responsible for the accumulation of spermidine conjugates in Arabidopsis seed. Plant Cell **21:** 318 – 333.

Mähönen AP, Bishopp A, Higuchi M, Nieminen KM, Kinoshita K, Törmäkangas K, Ikeda Y, Oka A, Kakimoto T, Helariutta Y (2006) Cytokinin signaling and its inhibitor AHP6 regulate cell fate during vascular development. Science **311:** 94 - 98

Mähönen AP, Bonke M, Kauppinen L, Riikonen M, Benfey PN, Helariutta Y (2000) A novel two-component hybrid molecule regulates vascular morphogenesis of the Arabidopsis root. Genes Dev **14:** 2938 - 2943

Mattsson J, Ckurshumova W, Berleth T (2003) Auxin signaling in Arabidopsis leaf vascular development. Plant Physiol **131:** 1327 - 1339

Mattsson J, Sung ZR, Berleth T (1999) Responses of plant vascular systems to auxin transport inhibition. Development **126:** 2979-2991

May MJ, and Leaver CJ (1993) Oxidative Stimulation of Glutathione Synthesis in *Arabidopsis thaliana* Suspension Cultures. Plant Physiol**103:** 621- 627

McCormick S (2004) Control of male gametophyte development. Plant Cell **16:** S142

Meinke DW (1994) seed development in *Arabidopsis* .*In* EM Meyerowitz, CR Somerville, eds, Arabidopsis. Cold Spring Harbor Laboratory Press, Cold Spring Harbor, NY, pp 253–295,

Michniewicz M, Zago MK, Abas L, Weijers D, Schweighofer A, Meskiene I, Heisler MG, Ohno C, Zhang J, Huang F (2007) Antagonistic regulation of PIN phosphorylation by PP2A and PINOID directs auxin flux. Cell **130:** 1044-1056

Minocha R, Shortle WC, Long SL, Minocha SC (1994) A rapid and reliable procedure for extraction of cellular polyamines and inorganic ions from plant tissues. J Plant Growth Regul **13:** 187-193

Minocha SC, Minocha R, Robie CA (1990) High-performance liquid chromatographic method for the determination of dansyl-polyamines. J Chromatogr A **511:** 177-183

Moffatt B, Somerville C (1988) Positive selection for male-sterile mutants of Arabidopsis lacking adenine phosphoribosyltransferase activity. Plant Physiol **86:** 1150-1154

Møller SG, McPherson MJ (1998) Developmental expression and biochemical analysis of the Arabidopsis atao1 gene encoding an H2O2-generating diamine oxidase. Plant J **13:** 781-791

Mori T, Kuroiwa H, Higashiyama H, Kuroiwa T (2006) GENERATIVE CELL SPECIFIC 1 is essential for angiosperm fertilization. Nature cell Biology **8**: 64 -71

Moschou PN, Paschalidis KA, Delis ID, Andriopoulou AH, Lagiotis GD, Yakoumakis DI, Roubelakis-Angelakis KA (2008) Spermidine exodus and oxidation in the apoplast induced by abiotic stress is responsible for H_2O_2 signatures that direct tolerance responses in tobacco. Plant Cell **20:** 1708 - 1728

Mueller LA, Zhang P, Rhee SY (2003) AraCyc: a biochemical pathway database for Arabidopsis. Plant Physiol **132:** 453 - 460

Muñiz L, Minguet EG, Singh SK, Pesquet E, Vera-Sirera F, Moreau-Courtois CL, Carbonell J, Blázquez MA, Tuominen H (2008) ACAULIS5 controls *Arabidopsis* xylem specification through the prevention of premature cell death. Development **135:** 2573-2582

Murashige T, Skoog F (1962) A revised medium for rapid growth and bio assays with tobacco tissue cultures. Physiol Plant **15:** 473-497

Mustroph A, Zanetti ME, Jang CJH, Holtan HE, Repetti PP, Galbraith DW, Girke T, Bailey-Serres J (2009) Profiling translatomes of discrete cell populations resolves altered cellular priorities during hypoxia in Arabidopsis. Proc Nat Acad Sci **106:** 18843

Naka Y, Watanabe K, Sagor G, Niitsu M, Pillai MA, Kusano T, Takahashi Y (2010) Quantitative analysis of plant polyamines including thermospermine during growth and salinity stress. Plant Physiol Bioch **48:** 527-533

Nakagami H, Soukupova H, Schikora A, Zarsky´ V, and Hirt H (2006) A Mitogen-activated Protein Kinase Mediates Reactive Oxygen Species Homeostasis in *Arabidopsis.* J BiolChem **281**: 38697-8704

Nakamichi N, Kusano M, Fukushima A, Kita M, Ito S, Yamashino T, Saito K, Sakakibara H, Mizuno T (2009) Transcript profiling of an Arabidopsis PSEUDO RESPONSE REGULATOR arrhythmic triple mutant reveals a role for the circadian clock in cold stress response. Plant and Cell Physiol **50:** 447

Nemhauser JL, Feldman LJ, Zambryski PC (2000) Auxin and ETTIN in Arabidopsis gynoecium morphogenesis. Development **127:** 3877 -3880

Nieminen KM, Kauppinen L, Helariutta Y (2004) A weed for wood? Arabidopsis as a genetic model for xylem development. Plant Physiol **135:** 653 - 657

Oh SI, Park J, Yoon S, Kim Y, Park S, Ryu M, Nam MJ, Ok SH, Kim JK, Shin JS (2008) The Arabidopsis Calcium Sensor Calcineurin B-Like 3 Inhibits the 5'-Methylthioadenosine Nucleosidase in a Calcium-Dependent Manner. Plant Physiol **148:** 1883-1896

Ohashi-Ito K, Fukuda H (2003) HD-zip III homeobox genes that include a novel member, ZeHB-13 (Zinnia)/ATHB-15 (Arabidopsis), are involved in procambium and xylem cell differentiation. Plant and cell physiol **44:** 1350

Ohnuma M, Ganbe T, Terui Y, Niitsu M, Sato T, Tanaka N, Tamakoshi M, Samejima K, Kumasaka T, Oshima T (2011) Crystal Structures and Enzymatic Properties of a Triamine/AgmatineAminopropyltransferase from *Thermusthermophilus*. J Mol Biol **408:** 971-986

Okada K, Ueda J, Komaki MK, Bell CJ, Shimura Y (1991) Requirement of the Auxin Polar Transport System in Early Stages of Arabidopsis Floral Bud Formation. Plant Cell **3:** 677-684

Orlando DA, Brady SM, Koch JD, Dinneny JR, Benfey PN (2009) Manipulating large-scale Arabidopsis microarray expression data: Identifying dominant expression patterns and biological process enrichment. Methods Mol Biol **553:** 57-77

Pagnussat GC, Yu HJ, Ngo QA, Rajani S, Mayalagu S, Johnson CS, Capron A, Xie LF, Ye D, Sundaresan V (2005) Genetic and molecular identification of genes required for female gametophyte development and function in Arabidopsis. Development **132:** 603 - 614

Pandey S, Ranade S, Nagar P, Kumar N (2000) Role of polyamines and ethylene as modulators of plant senescence. J Biosci **25:** 291-299

Park MH (2006) The post-translational synthesis of a polyamine-derived amino acid, hypusine, in the eukaryotic translation initiation factor 5A (eIF5A). J Biochem **139:** 161- 169

Park MH, Wolff EC, Folk JE (1993) Hypusine: its post-translational formation in eukaryotic initiation factor 5A and its potential role in cellular regulation. Biofactors **4:** 95-104

Pegg A, Shuttleworth K, Hibasami H (1981) Specificity of mammalian spermidine synthase and spermine synthase. Biochem J **197:** 315-320

Pegg AE, Casero RA (2011) Current status of the polyamine research field. Methods in MolBiol **720:** 3-35

Pianelli K, Mari S, Marques L, Lebrun M, Czernic P (2005) Nicotianamine over-accumulation confers resistance to nickel in *Arabidopsis thaliana*. Transgenic Res **14:** 739-748

Pierre T, Laurent C, Andrée H, Alexandra P, Emile K, Georges B, Claire P A novel high efficiency, low maintenance, hydroponic system for synchronous growth and flowering of *Arabidopsis thaliana.* BMC Plant Biol **3:**2-10

Pommerrenig B, Feussner K, Zierer W, Rabinovych V, Klebl F, Feussner I, Sauer N (2011) Phloem-Specific Expression of Yang Cycle Genes and Identification of Novel Yang Cycle Enzymes in *Plantago* and *Arabidopsis*. Plant Cell **23:** 1904-1919

Prado AM, Colaço R, Moreno N, Silva AC, Feijó JA (2008) Targeting of pollen tubes to ovules is dependent on nitric oxide (NO) signaling. Molecular plant **1:** 703 - 714

Raghavan V (2006) Double fertilization: embryo and endosperm development in flowering plants. Springer Verlag, Germany, pp 174-175

Rzewuski G, Cornell KA, Rooney L, Bürstenbinder K, Wirtz M, Hell R, Sauter M (2007) *OsMTN* encodes a 5'-methylthioadenosine nucleosidase that is up-regulated during submergence-induced ethylene synthesis in rice (*Oryzasativa* L.). J Exp Bot **58:** 1505-1514

Sanders PM, Bui AQ, Weterings K, McIntire K, Hsu YC, Lee PY, Truong MT, Beals T, Goldberg R (1999) Anther developmental defects in Arabidopsis thaliana male-sterile mutants. Sexual Plant Reproduction **11:** 297-322

Sauter M, Cornell KA, Beszteri S, Rzewuski G (2004) Functional analysis of methylthioribose kinase genes in plants. Plant Physiol **136:** 4061-4071

Sawada Y, Akiyama K, Sakata A, Kuwahara A, Otsuki H, Sakurai T, Saito K, Hirai MY (2009) Widely targeted metabolomics based on large-scale MS/MS data for elucidating metabolite accumulation patterns in plants. Plant and Cell Physiol **50:** 37 - 47

Scarpella E, Marcos D, Friml J, Berleth T (2006) Control of leaf vascular patterning by polar auxin transport. Genes Dev **20:** 1015 - 1027

Schneitz K, Hulskamp M, Kopczak SD, Pruitt RE (1997) Dissection of sexual organ ontogenesis: a genetic analysis of ovule development in Arabidopsis thaliana. Development **124:** 1367 - 1376

Schneitz K, Hülskamp M, Pruitt RE (1995) Wild-type ovule development in Arabidopsis thaliana: a light microscope study of cleared whole-mount tissue. Plant J **7:** 731-749

Schwab R, Ossowski S, Riester M, Warthmann N, Weigel D (2006) Highly specific gene silencing by artificial microRNAs in Arabidopsis. Plant Cell **18:** 1121 - 1133

Sessions R (1997) Arabidopsis (Brassicaceae) flower development and gynoecium patterning in wild type and ettin mutants. Am J Bot **84:** 1179 - 1183

Siu KKW, Asmus K, Zhang AN, Horvatin C, Li S, Liu T, Moffatt B, Woods Jr VL, Howell PL (2011) Mechanism of substrate specificity in 5'-methylthioadenosine/S-adenosylhomocysteine nucleosidases. J Struct Biol **173:** 86-98

Siu KKW, Lee JE, Sufrin JR, Moffatt BA, McMillan M, Cornell KA, Isom C, Howell PL (2008) Molecular Determinants of Substrate Specificity in Plant 5'-Methylthioadenosine Nucleosidases. J Mol Biol **378:** 112-128

Smyth DR, Bowman JL, Meyerowitz EM (1990) Early flower development in *Arabidopsis*. Plant Cell **2:** 755-767

Somerville C, Koornneef M (2002) A fortunate choice: the history of Arabidopsis as a model plant. Nat Rev Gen **3:** 883-889

Stevens AP, Spangler B, Wallner S, Kreutz M, Dettmer K, Oefner PJ, Bosserhoff AK (2009) Direct and tumor microenvironment mediated influences of 5’-deoxy-5’-(methylthio) adenosine on tumor progression of malignant melanoma. J Cell Biochem **106:** 210-219

Su YH, Liu YB, Zhang XS (2011) Auxin–Cytokinin Interaction Regulates Meristem Development. Molecular Plant **doi:10.1093/mp/ssr007**

Szekeres M, Németh K, Koncz-Kálmán Z, Mathur J, Kauschmann A, Altmann T, Rédei GP, Nagy F, Schell J, Koncz C (1996) Brassinosteroids rescue the deficiency of CYP90, a cytochrome P450, controlling cell elongation and de-etiolation in Arabidopsis. Cell **85:** 171-182

Takahashi M, Terada Y, Nakai I, Nakanishi H, Yoshimura E, Mori S, Nishizawa NK (2003) Role of nicotianamine in the intracellular delivery of metals and plant reproductive development. Plant Cell **15:** 1263-1280

Takahashi T, Kakehi JI (2010) Polyamines: ubiquitous polycations with unique roles in growth and stress responses. Ann Bot **105:** 1-6

Tanaka T, Tanaka H, Machida C, Watanabe M, Machida Y (2004) A new method for rapid visualization of defects in leaf cuticle reveals five intrinsic patterns of surface defects in Arabidopsis. Plant J **37:** 139-146

Tassoni A, van Buuren M, Franceschetti M, Fornalè S, Bagni N (2000) Polyamine content and metabolism in *Arabidopsis thaliana* and effect of spermidine on plant development. Plant Physiol Biochem **38:** 383-393

Tisi A, Federico R, Moreno S, Lucretti S, Moschou PN, Roubelakis-Angelakis KA, Angelini R, Cona A (2011) Perturbation of polyamine catabolism can strongly affect root development and xylem differentiation. Plant Physiol. **157:** 200–215

Toledo-Ortiz G, Huq E, Quail PH (2003) The Arabidopsis basic/helix-loop-helix transcription factor family. Plant Cell **15:** 1749 - 1770

Trampczynska A, Bottcher C, Clemens S (2006) The transition metal chelator nicotianamine is synthesized by filamentous fungi. FEBS Lett **580:** 3173-3178

Truernit E, Bauby H, Dubreucq B, Grandjean O, Runions J, Barthélémy J, Palauqui JC (2008) High-resolution whole-mount imaging of three-dimensional tissue organization and gene expression enables the study of phloem development and structure in Arabidopsis. Plant Cell **20:** 1494 - 1503

Tsuchisaka A, Theologis A (2004) Unique and overlapping expression patterns among the Arabidopsis 1-amino-cyclopropane-1-carboxylate synthase gene family members. Plant Physiol **136:** 2982 -2989

Tsuchisaka A, Yu G, Jin H, Alonso JM, Ecker JR, Zhang X, Gao S, Theologis A (2009) A combinatorial interplay among the 1-aminocyclopropane-1-carboxylate isoforms regulates ethylene biosynthesis in Arabidopsis thaliana. Genetics **183:** 979**-** 789

Urano K, Hobo T, Shinozaki K (2005) Arabidopsis ADC genes involved in polyamine biosynthesis are essential for seed development. FEBS Lett **579:** 1557-1564

Van Der Graaff E, Schwacke R, Schneider A, Desimone M, Flügge UI, Kunze R (2006) Transcription analysis of Arabidopsis membrane transporters and hormone pathways during developmental and induced leaf senescence. Plant Physiol **141:** 776- 792

Vera-Sirera F, Minguet EG, Singh SK, Ljung K, Tuominen H, Blázquez MA, Carbonell J (2010) Role of polyamines in plant vascular development. Plant Physiol Biochem **48:** 534-539

Vida TA, Emr SD (1995) A new vital stain for visualizing vacuolar membrane dynamics and endocytosis in yeast. J Cell Biol **128:** 779 - 792

Wabnik K, Govaerts W, Friml J, Kleine-Vehn J (2011) Feedback models for polarized auxin transport: an emerging trend. Mol.BioSyst. **7:** 2352-2359

Wang T.-W., Lu L., Zhang C.G., Taylor C. & Thompson J.E. (2003) Pleiotropic effects of suppressing deoxyhypusine synthase expression in Arabidopsis thaliana. Plant Mol Biol **52** 1223–1235

Wang T.-W., Zhang C.G., Wu W., Nowack L.M., Madey E. & Thompson J.E. (2005) Antisense suppression of deoxyhypusine synthase in tomato delays fruit softening and alters growth anddevelopment. Plant Physiol **138** 1372–1382

Wang YH (2008) How effective is T-DNA insertional mutagenesis in Arabidopsis? Journal of Biochem Tech **1:** 11-20

Wimalasekera R, Villar C, Begum T, Scherer GFE (2011) COPPER AMINE OXIDASE1 (CuAO1) of Arabidopsis thaliana Contributes to Abscisic Acid-and Polyamine-Induced Nitric Oxide Biosynthesis and Abscisic Acid Signal Transduction. Molecular Plant 4: 663 - 678

Wortman JR, Haas BJ, Hannick LI, Smith RK, Maiti R, Ronning CM, Chan AP, Yu C, Ayele M, Whitelaw CA (2003) Annotation of the Arabidopsis genome. Plant Physiol **132:** 461 -470

Wu H, Min J, Zeng H, McCloskey DE, Ikeguchi Y, Loppnau P, Michael AJ, Pegg AE, Plotnikov AN (2008) Crystal Structure of Human Spermine Synthase. J Biol Chem **283:** 16135-16146

Wu J, Shang Z, Wu J, Jiang X, Moschou PN, Sun W, Roubelakis-Angelakis KA, Zhang S (2010) Spermidine oxidase-derived H_2O_2 regulates pollen plasma membrane hyperpolarization-activated Ca^{2} ˉpermeable channels and pollen tube growth. Plant J **63:** 1042-1053

Yamagami T, Tsuchisaka A, Yamada K, Haddon WF, Harden LA, Theologis A (2003) Biochemical diversity among the 1-amino-cyclopropane-1-carboxylate synthase isozymes encoded by the Arabidopsis gene family. J Biol Chem **278:** 49102 - 49112

Yamakawa H, Kamada H, Satoh M, Ohashi Y (1998) Spermine is a salicylate-independent endogenous inducer for both tobacco acidic pathogenesis-related proteins and resistance against tobacco mosaic virus infection. Plant Physiol **118:** 1213 - 1222

Yamamoto R, Demura T, Fukuda H (1997) Brassinosteroids induce entry into the final stage of tracheary element differentiation in cultured Zinnia cells. Plant and cell physiol**38:** 980 - 983

Yamamoto R, Fujioka S, Iwamoto K, Demura T, Takatsuto S, Yoshida S, Fukuda H (2007) Co-regulation of brassinosteroid biosynthesis-related genes during xylem cell differentiation. Plant and cell physiol **48:** 74 - 83

Yang SF, Hoffman NE (1984) Ethylene biosynthesis and its regulation in higher plants. Annual Review of Plant Physiol **35:** 155-189

Zheng Q, Song J, Doncaster K, Rowland E, Byers DM (2007) Qualitative and quantitative evaluation of protein extraction protocols for apple and strawberry fruit suitable for two-dimensional electrophoresis and mass spectrometry analysis. J Agric Food Chem **55:** 1663-1673

Zhou J, Sebastian J, Lee JY (2011) Signaling and gene regulatory programs in plant vascular stem cells. Genesis doi10.1002/dvg.20795

Zimmermann P, Hirsch-Hoffmann M, Hennig L, Gruissem W (2004) GENEVESTIGATOR. Arabidopsis microarray database and analysis toolbox. Plant Physiol **136:** 2621- 2632